



ANP-10268NP  
Revision 0

**U.S. EPR Severe Accident Evaluation  
Topical Report**

**October 2006**

AREVA NP Inc.

---

Non-Proprietary

(c) 2006 AREVA NP Inc.

**Copyright © 2006**

**AREVA NP Inc.**

**All Rights Reserved**

The design, engineering and other information contained in this document have been prepared by or on behalf of AREVA NP Inc., a jointly owned subsidiary of AREVA and Siemens, in connection with its request to the U.S. Nuclear Regulatory Commission for a pre-application review of the U.S. EPR nuclear power plant design. No use of or right to copy any of this information, other than by the NRC and its contractors in support of AREVA NP's pre-application review, is authorized.

The information provided in this document is a subset of a much larger set of know-how, technology and intellectual property pertaining to an evolutionary pressurized water reactor designed by AREVA NP and referred to as the U.S. EPR. Without access and a grant of rights to that larger set of know-how, technology and intellectual property rights, this document is not practically or rightfully usable by others, except by the NRC as set forth in the previous paragraph.

For information address: AREVA NP Inc.

An AREVA and Siemens Company

3315 Old Forest Road

Lynchburg, VA 24506

## **U.S. Nuclear Regulatory Commission**

### **Disclaimer**

#### **Important Notice Concerning the Contents and Application of This Report**

##### ***Please Read Carefully***

This report was developed based on research and development funded and conducted by AREVA NP, Inc., and is being submitted by AREVA NP to the U.S. Nuclear Regulatory Commission (NRC) to facilitate future licensing processes that may be pursued by licensees or applicants that are customers of AREVA NP. The information contained in this report may be used by the NRC and, under the terms of applicable agreements with AREVA NP, those customers seeking licenses or license amendments to assist in demonstrating compliance with NRC regulations. The information provided in this report is true and correct to the best of AREVA NP's knowledge, information, and belief.

AREVA NP's warranties and representations concerning the content of this report are set forth in agreements between AREVA NP and individual customers. Except as otherwise expressly provided in such agreements with its customers, neither AREVA NP nor any person acting on behalf of AREVA NP:

- Makes any warranty or representation, expressed or implied, with respect to the accuracy, completeness, or usefulness of the information contained in this report, nor the use of any information, apparatus, method, or process disclosed in this report.
- Assumes any liability with respect to the use of or for damages resulting from the use of any information, apparatus, method, or process disclosed in this report.

---

**Nature of Changes**

Item	Section(s) or Page(s)	Description and Justification
1.	All	This is a new document

## Contents

	<u>Page</u>
<b>ABSTRACT .....</b>	<b>xiii</b>
<b>EXECUTIVE SUMMARY .....</b>	<b>xiv</b>
<b>1.0 INTRODUCTION .....</b>	<b>1-1</b>
1.1 Regulatory Requirements and Guidance .....	1-3
1.1.1 Governing Documents .....	1-3
1.1.2 Acceptance Criteria .....	1-4
1.1.3 Analysis Requirements .....	1-6
1.2 Definitions .....	1-7
<b>2.0 DESIGN DESCRIPTION OF U.S. EPR SEVERE ACCIDENT MANAGEMENT SYSTEMS .....</b>	<b>2-1</b>
2.1 General Plant Description .....	2-1
2.1.1 Reactor Vessel .....	2-1
2.1.2 Reactor Coolant System .....	2-4
2.1.3 Safety Systems for Design Basis Events .....	2-6
2.1.4 Electric Power .....	2-11
2.2 Description of Dedicated Severe Accident Plant Features .....	2-12
2.2.1 Severe Accident Depressurization Valves .....	2-14
2.2.2 Combustible Gas Control System .....	2-16
2.2.3 Core Melt Stabilization System .....	2-20
2.2.4 Severe Accident Heat Removal System .....	2-32
2.2.5 Severe Accident Instrumentation and Control .....	2-39
2.2.6 Severe Accident Uninterruptible Power Supply System .....	2-44
<b>3.0 SAFETY ISSUE RESOLUTION EVALUATION METHODOLOGY .....</b>	<b>3-1</b>
3.1 Risk Oriented Accident Analysis Methodology .....	3-2
3.2 Integrated Structure for Technical Issue Resolution Methodology .....	3-3
3.3 AREVA NP's Adaptation .....	3-4
3.4 Methodology Objectives .....	3-7
<b>4.0 DESCRIPTION OF SEVERE ACCIDENT SAFETY ISSUES .....</b>	<b>4-1</b>
4.1 Identification of Safety Goals .....	4-1
4.2 Identification of Processes and Phenomena .....	4-3
4.2.1 A Hypothetical Phenomenologically-Bounding Severe Accident ..	4-3
4.2.2 Presentation of Severe Accident Processes and Phenomena .....	4-6
4.2.3 Scaling Analysis for Phenomenological Importance .....	4-8
<b>5.0 RESEARCH AND DEVELOPMENT RELATED TO THE U.S. EPR SEVERE ACCIDENT CONCEPT .....</b>	<b>5-1</b>
5.1 Hydrogen Mitigation .....	5-2
5.1.1 Hydrogen Production .....	5-3
5.1.2 Hydrogen Distribution .....	5-7

5.1.3	Hydrogen Combustion .....	5-12
5.1.4	Hydrogen Recombiners .....	5-19
5.1.5	Conclusion on Hydrogen Mitigation.....	5-24
5.2	Core Debris Coolability .....	5-25
5.2.1	Reactor Vessel Failure Modes .....	5-27
5.2.2	Molten Core-Concrete Interactions .....	5-32
5.2.3	Temporary Melt Retention in the Reactor Cavity.....	5-42
5.2.4	Melt Spreading, Flooding and Stabilization .....	5-57
5.2.5	Core Debris Coolability Conclusions .....	5-70
5.3	High Pressure Melt Ejection.....	5-71
5.3.1	High Pressure Melt Ejection Phenomenology .....	5-72
5.3.2	High Pressure Melt Ejection Experimental Programs.....	5-75
5.3.3	High Pressure Melt Ejection Conclusions .....	5-78
5.4	Containment Performance .....	5-79
5.4.1	General Overpressurization .....	5-79
5.4.2	Fuel-Coolant Interactions .....	5-81
5.5	Equipment Survivability.....	5-89
5.5.1	In-core / In-RCS .....	5-90
5.5.2	Inside Containment .....	5-90
5.5.3	SAHRS-Compartment.....	5-93
5.5.4	Annulus .....	5-94
<b>6.0</b>	<b>ANALYSIS METHODS .....</b>	<b>6-1</b>
6.1	Overview of U.S. EPR Analytical Methodology .....	6-1
6.1.1	MAAP4.07 .....	6-2
6.1.2	MELTSPREAD-1.4.....	6-13
6.1.3	WALTER .....	6-15
6.2	Code Applicability .....	6-17
6.2.1	MAAP4.07 .....	6-17
6.2.2	MELTSPREAD-1.4.....	6-26
6.2.3	WALTER .....	6-27
6.3	Validation of Analytical Tools .....	6-29
6.3.1	MAAP4.07 .....	6-29
6.3.2	MELTSPREAD-1.4.....	6-48
6.3.3	WALTER .....	6-51
6.4	Description of U.S. EPR Analytical Models.....	6-53
6.4.1	MAAP4.07 .....	6-53
6.4.2	MELTSPREAD-1.4.....	6-63
6.4.3	WALTER .....	6-64
6.5	Calculation Matrix for Safety Issue Resolution.....	6-66
6.5.1	Best-Estimate Analysis .....	6-66
6.5.2	Uncertainty Analysis.....	6-71
6.5.3	Supplemental Deterministic Studies.....	6-71
<b>7.0</b>	<b>SAMPLE PROBLEM ANALYSES .....</b>	<b>7-1</b>
7.1	Introduction .....	7-1
7.2	Scenario Description.....	7-2

---

7.2.1	Integral Analysis Scenarios .....	7-2
7.2.2	Separate Effect Analyses .....	7-4
7.3	Results of Integral Analyses .....	7-9
7.3.1	Large Break Loss of Coolant Accident (LBLOCA).....	7-9
7.3.2	Loss of Off-site Power .....	7-33
7.3.3	Small Break Loss of Coolant Accident (SBLOCA) .....	7-57
7.3.4	Large Break Loss of Coolant Accident Crossover (LBLOCA Crossover) .....	7-81
<b>8.0</b>	<b>CONCLUSION .....</b>	<b>8-1</b>
<b>9.0</b>	<b>REFERENCES .....</b>	<b>9-1</b>
<b>Appendix A Basic Data and Calculations.....</b>		<b>A-1</b>
<b>Appendix B Supporting Information on Sacrificial Concrete.....</b>		<b>B-1</b>
<b>Appendix C MELCOR 1.8.6 Model of the U.S. EPR.....</b>		<b>C-1</b>

## List of Tables

Table 2-1	Composition Reactor Cavity Concrete (FeSi/PZ15/8) .....	2-23
Table 2-2	Composition Spreading Room Concrete (Siliceous) .....	2-30
Table 4-1	Chronology of a Bounding Severe Accident Through RPV Failure .....	4-6
Table 4-2	Identification of Severe Accident Processes and Phenomena for the U.S. EPR.....	4-7
Table 5-1	Experimental Work Addressing Hydrogen Production.....	5-7
Table 5-2	Test Programs for Assessing Hydrogen Distribution .....	5-11
Table 5-3	Hydrogen Combustion Experiments .....	5-17
Table 5-4	Hydrogen Recombiner Experiments.....	5-23
Table 5-5	Experiment Programs Related to Reactor Vessel Failure .....	5-29
Table 5-6	MCCI Experimental Programs .....	5-36
Table 5-7	Melt Interaction with Refractory Material .....	5-51
Table 5-8	Melt Gate Experiment Programs .....	5-56
Table 5-9	Melt Spreading Experimental Programs .....	5-61
Table 5-10	Melt Flooding and Stabilization Experimental Programs .....	5-69
Table 5-11	Survey of Dch-Relevant Experiments.....	5-78
Table 5-12	Fuel-Coolant Interactions Experiment Programs.....	5-87
Table 6-1	MAAP4.07 Severe Accident Phenomena Modeling Capability.....	6-18
Table 6-2	Severe Accident Phenomena Modeling Capability.....	6-26
Table 6-3	Severe Accident Phenomena Modeling Capability.....	6-28
Table 6-4	Concrete Compositions for the Ace Experiments .....	6-31
Table 6-5	Corium Compositions for the Ace Experiments .....	6-32
Table 6-6	U.S. EPR MAAP4.07 Containment Nodes .....	6-61
Table 6-7	Number and Location of AREVA NP PAR Units.....	6-63
Table 6-8	Postulated Initiating Events .....	6-67
Table 6-9	Possible Representative and Bounding Scenarios Identified to Address Key Severe Accident Issues .....	6-70
Table 7-1	Events of Concern for the Representative Model .....	7-6
Table 7-2	Event Progression of a LBLOCA .....	7-9
Table 7-3	Key Results From a LBLOCA .....	7-9
Table 7-4	Event Progression of a SBO .....	7-33
Table 7-5	Key Results From a SBO.....	7-33
Table 7-6	Event Progression of a SBLOCA.....	7-57
Table 7-7	Key Results From a SBLOCA.....	7-57
Table 7-8	Event Progression of a LBLOCA Crossover.....	7-81
Table 7-9	Key Results From A Lbloca Crossover.....	7-81

## List of Figures

Figure 2-1 U.S. EPR Reactor Internals .....	2-2
Figure 2-2 Heavy Reflector .....	2-3
Figure 2-3 Reactor Coolant System.....	2-4
Figure 2-4 Containment Layout .....	2-7
Figure 2-5 Annulus Ventilation System.....	2-8
Figure 2-6 Safety Injection Systems .....	2-9
Figure 2-7 Dedicated Severe Accident Design Features .....	2-14
Figure 2-8 Severe Accident Depressurization Valves.....	2-15
Figure 2-9 Pressurizer Relief Tank .....	2-16
Figure 2-10 Passive Autocatalytic Recombiner .....	2-17
Figure 2-11 Hydrogen Mixing Damper .....	2-19
Figure 2-12 Pressure Equalization Ceiling.....	2-20
Figure 2-13 Core Melt Stabilization System.....	2-21
Figure 2-14 Reactor Cavity .....	2-22
Figure 2-15 Melt Plug And Gate Support Frame .....	2-26
Figure 2-17 Melt Discharge Channel .....	2-27
Figure 2-18 Spreading Compartment .....	2-28
Figure 2-19 Spreading Compartment Isolation .....	2-29
Figure 2-20 Cooling Structure Elements .....	2-30
Figure 2-21 Cooling Structure.....	2-31
Figure 2-22 Flooding Valve Actuation.....	2-32
Figure 2-23 Severe Accident Heat Removal System.....	2-34
Figure 2-24 Passive Cooling of Molten Core Debris.....	2-35
Figure 2-25 Active Melt Retention System Cooling .....	2-38
Figure 3-1 Process for Severe Accident Safety Issue Resolution .....	3-5
Figure 4-1 Postulated Containment Failure Mechanisms .....	4-1
Figure 5-1 Common Reactor Vessel Failure Modes Considered for the U.S. EPR.....	5-28
Figure 5-2 Reactor Vessel Failure Modes Examined in the LHF Program .....	5-31
Figure 5-3 Schematic Presenting Oxide-Metal Layer-Flip Phenomenon.....	5-34
Figure 5-4 Solidus-Liquidus Temperatures for Uo <sub>2</sub> -Zro <sub>2</sub> -Concrete Mixtures.....	5-38
Figure 5-5 Steam Explosion Stages .....	5-83
Figure 5-6 Geometry Of Steam Explosion Facilities Testing with Prototypic Materials .....	5-88
Figure 6-1 Overview of U.S. EPR Severe Accident Analytical Methodology .....	6-2
Figure 6-2 Pressurized Relief Tank Model.....	6-13
Figure 6-3 ACE L2 Melt Temperature Predictions .....	6-33
Figure 6-4 ACE L2 Ablation Depth Predictions.....	6-33
Figure 6-5 ACE L6 Melt Temperature Predictions .....	6-34
Figure 6-6 ACE L6 Ablation Depth Predictions.....	6-35
Figure 6-7 ACE L7 Melt Temperature Predictions .....	6-36
Figure 6-8 ACE L7 Ablation Depth Predictions.....	6-36

Figure 6-9 BETA V5.1 Melt Temperature Predictions.....	6-39
Figure 6-10 BETA V5.1 Ablation Depth Predictions .....	6-39
Figure 6-11 BETA V5.2 Melt Temperature Predictions.....	6-40
Figure 6-12 BETA V5.2 Ablation Depth Predictions .....	6-41
Figure 6-13 MAAP4.07 Predicted Erosion Rates vs. CCI-2 Data .....	6-44
Figure 6-14 MAAP4.07 Predicted Average Melt Temperatures vs. CCI-2 Data .....	6-45
Figure 6-15 MAAP4.07 Predicted Erosion Rates vs. CCI-3 Data .....	6-47
Figure 6-16 MAAP4.07 Predicted Average Melt Temperatures vs. CCI-3 Data .....	6-47
Figure 6-17 U.S. EPR MAAP4 Containment Model.....	6-60
Figure 6-18 Representative User-Defined Nodalization Scheme Used In MELTSPREAD-1.4.....	6-64
Figure 7-1 Aluminum Gate Temperature Profile with Oxidic Melt.....	7-5
Figure 7-2 Aluminum Gate Temperature Profile with Metallic Melt.....	7-6
Figure 7-3 Cooling Structure Temperature Profile .....	7-8
Figure 7-4 Melt And Structure Temperature Profile .....	7-8
Figure 7-5 Core Outlet Temperature (LBLOCA).....	7-10
Figure 7-6 Two-Phase Water Level In Core (LBLOCA).....	7-11
Figure 7-7 RCS Pressure (LBLOCA).....	7-12
Figure 7-8 RCS Water Inventory (LBLOCA).....	7-13
Figure 7-9 In-Vessel Hydrogen Production (LBLOCA) .....	7-14
Figure 7-10 Hydrogen Release Rate (LBLOCA).....	7-15
Figure 7-11 Mass of Corium in Lower Head (LBLOCA).....	7-16
Figure 7-12 Mass of Material in Core (LBLOCA) .....	7-17
Figure 7-13 Mass of Material in Lower Head and Core (LBLOCA).....	7-18
Figure 7-14 Containment Pressure (LBLOCA) .....	7-19
Figure 7-15 Average Hydrogen Mole Fraction In Containment (LBLOCA).....	7-20
Figure 7-16 Average Mole Fraction of Air in Containment (LBLOCA) .....	7-21
Figure 7-17 Average Mole Fraction of Steam in Containment (LBLOCA) .....	7-22
Figure 7-18 Hydrogen Mass in Containment (LBLOCA).....	7-23
Figure 7-19 Mass of Corium in Reactor Pit (LBLOCA) .....	7-24
Figure 7-20 Mass of Corium in Spreading Compartment (LBLOCA).....	7-25
Figure 7-21 Spreading Room Ablation (LBLOCA) .....	7-26
Figure 7-22 Reactor Cavity Ablation (LBLOCA) .....	7-27
Figure 7-23 Spreading Room Water Level (LBLOCA).....	7-28
Figure 7-24 IRWST Water Level (LBLOCA) .....	7-29
Figure 7-25 Corium Temperature In Reactor Pit (LBLOCA) .....	7-30
Figure 7-26 Containment Spray Flow (LBLOCA).....	7-31
Figure 7-27 SAHRS Suction Temperature (LBLOCA) .....	7-32
Figure 7-28 Core Outlet Temperature (SBO).....	7-34
Figure 7-29 RCS Pressure (SBO).....	7-35
Figure 7-30 RCS Water Inventory (SBO).....	7-36
Figure 7-31 Two-Phase Water Level in Core (SBO).....	7-37
Figure 7-32 In-Vessel Hydrogen Production (SBO).....	7-38

Figure 7-33 Hydrogen Release Rate (SBO) .....	7-39
Figure 7-34 Mass of Corium in Lower Head (SBO) .....	7-40
Figure 7-35 Mass of Material in Core (SBO).....	7-41
Figure 7-36 Mass of Material in Lower Head and Core (SBO) .....	7-42
Figure 7-37 Containment Pressure (SBO).....	7-43
Figure 7-38 Average Hydrogen Mole Fraction in Containment (SBO).....	7-44
Figure 7-39 Average Mole Fraction of Air in Containment (SBO).....	7-45
Figure 7-40 Average Mole Fraction of Steam in Containment (SBO).....	7-46
Figure 7-41 Hydrogen Mass in Containment (SBO) .....	7-47
Figure 7-42 Mass of Corium In Reactor Pit (SBO).....	7-48
Figure 7-43 Mass of Corium in Spreading Compartment (SBO) .....	7-49
Figure 7-44 Spreading Room Ablation (SBO).....	7-50
Figure 7-45 Reactor Pit Ablation (SBO).....	7-51
Figure 7-46 Spreading Room Water Level (SBO) .....	7-52
Figure 7-47 IRWST Water Level (SBO).....	7-53
Figure 7-48 Corium Temperature In Reactor Pit (SBO).....	7-54
Figure 7-49 Containment Spray Flow (SBO) .....	7-55
Figure 7-50 SAHRS Suction Temperature (SBO).....	7-56
Figure 7-51 Core Outlet Temperature (SBLOCA).....	7-58
Figure 7-52 RCS Pressure (SBLOCA).....	7-59
Figure 7-53 RCS Water Inventory (SBLOCA).....	7-60
Figure 7-54 Two-Phase Water Level in Core (SBLOCA).....	7-61
Figure 7-55 In-Vessel Hydrogen Production (SBLOCA).....	7-62
Figure 7-56 Hydrogen Release Rate (SBLOCA) .....	7-63
Figure 7-57 Mass of Corium in Lower Head (SBLOCA) .....	7-64
Figure 7-58 Mass of Material in Core (SBLOCA).....	7-65
Figure 7-59 Mass of Material in Lower Head And Core (SBLOCA) .....	7-66
Figure 7-60 Containment Pressure (SBLOCA).....	7-67
Figure 7-61 Average Hydrogen Mole Fraction in Containment (SBLOCA).....	7-68
Figure 7-62 Average Mole Fraction of Air in Containment (SBLOCA).....	7-69
Figure 7-63 Average Mole Fraction of Steam in Containment (SBLOCA).....	7-70
Figure 7-64 Hydrogen Mass in Containment (SBLOCA) .....	7-71
Figure 7-65 Mass of Corium in Reactor Pit (SBLOCA).....	7-72
Figure 7-66 Mass of Corium in Spreading Compartment (SBLOCA).....	7-73
Figure 7-67 Spreading Room Ablation (SBLOCA).....	7-74
Figure 7-68 Reactor Pit Ablation (SBLOCA).....	7-75
Figure 7-69 Spreading Compartment Water Level (SBLOCA) .....	7-76
Figure 7-70 IRWST Water Level (SBLOCA).....	7-77
Figure 7-71 Corium Temperature in Reactor Pit (SBLOCA).....	7-78
Figure 7-72 Containment Spray Flow (SBLOCA) .....	7-79
Figure 7-73 SAHRS Suction Temperature (SBLOCA).....	7-80
Figure 7-74 Core Outlet Temperature (LBLOCA Crossover).....	7-82
Figure 7-75 RCS Pressure (LBLOCA Crossover).....	7-83

Figure 7-76 RCS Water Inventory (LBLOCA Crossover).....	7-84
Figure 7-77 Two-Phase Water Level in Core (LBLOCA Crossover).....	7-85
Figure 7-78 In-Vessel Hydrogen Production (LBLOCA Crossover).....	7-86
Figure 7-79 Hydrogen Release Rate (LBLOCA Crossover).....	7-87
Figure 7-80 Mass of Corium in Lower Head (LBLOCA Crossover).....	7-88
Figure 7-81 Mass of Material in Core (LBLOCA Crossover).....	7-89
Figure 7-82 Mass of Material in Lower Head And Core (LBLOCA Crossover).....	7-90
Figure 7-83 Containment Pressure (LBLOCA Crossover).....	7-91
Figure 7-84 Average Hydrogen Mole Fraction in Containment (LBLOCA Crossover).....	7-92
Figure 7-85 Average Mole Fraction of Air in Containment (LBLOCA Crossover).....	7-93
Figure 7-86 Average Mole Fraction of Steam In Containment (LBLOCA Crossover).....	7-94
Figure 7-87 Hydrogen Mass in Containment (LBLOCA Crossover).....	7-95
Figure 7-88 Mass of Corium in Reactor Pit (LBLOCA Crossover).....	7-96
Figure 7-89 Mass of Corium in Spreading Compartment (LBLOCA Crossover).....	7-97
Figure 7-90 Spreading Room Ablation (LBLOCA Crossover).....	7-98
Figure 7-91 Reactor Pit Ablation (LBLOCA Crossover).....	7-99
Figure 7-92 Spreading Compartment Water Level (LBLOCA Crossover).....	7-100
Figure 7-93 IRWST Water Level (LBLOCA Crossover).....	7-101
Figure 7-94 Corium Temperature In Reactor Pit (LBLOCA Crossover).....	7-102
Figure 7-95 Containment Spray Flow (LBLOCA Crossover).....	7-103
Figure 7-96 SAHRS Suction Temperature (LBLOCA Crossover).....	7-104

**Nomenclature**Acronym/InitialismDefinition

<b>AC</b>	<b>Alternating Current</b>
<b>AICC</b>	<b>Adiabatic Isochoric Complete Combustion</b>
<b>ANL</b>	<b>Argonne National Laboratory</b>
<b>ATWS</b>	<b>Anticipated Transient Without Scram</b>
<b>AVS</b>	<b>Annulus Ventilation System</b>
<b>CEA</b>	<b>Commissariat à l'Energie Atomique</b>
<b>CCVS</b>	<b>Chemical and Volume Control System</b>
<b>CCW</b>	<b>Component Cooling Water</b>
<b>CDF</b>	<b>Core Damage Frequency</b>
<b>CFR</b>	<b>Code of Federal Regulations</b>
<b>CGCS</b>	<b>Combustible Gas Control System</b>
<b>CHF</b>	<b>Critical Heat Flux</b>
<b>CMSS</b>	<b>Core Melt Stabilization System</b>
<b>CRDM</b>	<b>Control Rod Drive Mechanism</b>
<b>CWTI</b>	<b>Corium-Water Thermal Interaction</b>
<b>DC</b>	<b>Direct Current</b>
<b>DCA</b>	<b>Design Certification Application</b>
<b>DCD</b>	<b>Design Control Document</b>
<b>DCH</b>	<b>Direct Containment Heating</b>
<b>DDT</b>	<b>Deflagration-to-Detonation Transition</b>
<b>EBS</b>	<b>Emergency Borated System</b>
<b>EDG</b>	<b>Emergency Diesel Generator</b>
<b>EFW</b>	<b>Emergency Feedwater</b>
<b>EOP</b>	<b>Emergency Operating Procedures</b>
<b>EPRI</b>	<b>Electric Power Research Institute</b>
<b>ESW</b>	<b>Essential Service Water</b>
<b>FAI</b>	<b>Fauske and Associates, Inc.</b>
<b>FCI</b>	<b>Fuel-Coolant Interactions</b>

---

<b>FzK</b>	<b>Forschungszentrum Karlsruhe</b>
<b>GCM</b>	<b>Generalized Containment Model</b>
<b>HDR</b>	<b>Heißdampf-Reaktor</b>
<b>HIPS</b>	<b>High-Pressure Melt Streaming</b>
<b>HPME</b>	<b>High-Pressure Melt Ejection</b>
<b>I&amp;C</b>	<b>Instrumentation and Control</b>
<b>INL</b>	<b>Idaho National Laboratory</b>
<b>IRWST</b>	<b>In-containment Refueling Water Storage Tank</b>
<b>ISP</b>	<b>International Standard Problem</b>
<b>ISTIR</b>	<b>Integrated Structure for Technical Issue Resolution</b>
<b>LCS</b>	<b>Limestone Common Sand</b>
<b>LERF</b>	<b>Large Early Release Frequency</b>
<b>LHSI</b>	<b>Low Head Safety Injection</b>
<b>LOCA</b>	<b>Loss-Of-Coolant Accident</b>
<b>LOOP</b>	<b>Loss Of Offsite Power</b>
<b>LWR</b>	<b>Light Water Reactor</b>
<b>MAAP</b>	<b>Modular Accident Analysis Program</b>
<b>MCCI</b>	<b>Molten Corium-Concrete Interaction</b>
<b>MFW</b>	<b>Main Feedwater</b>
<b>MHSI</b>	<b>Medium Head Safety Injection</b>
<b>MSSV</b>	<b>Main Steam Safety Valve</b>
<b>NUPEC</b>	<b>Nuclear Power Engineering Corporation</b>
<b>NRC</b>	<b>Nuclear Regulatory Commission</b>
<b>OECD</b>	<b>Organization for Economic Cooperation and Development</b>
<b>OSSA</b>	<b>Operating Strategies for Severe Accidents</b>
<b>PAR</b>	<b>Passive Autocatalytic Recombiner</b>
<b>PDS</b>	<b>Primary Depressurization System</b>
<b>PRA</b>	<b>Probabilistic Risk Assessment</b>
<b>PRT</b>	<b>Pressurizer Relief Tank</b>
<b>PSV</b>	<b>Pressurizer Safety Valves</b>
<b>PWR</b>	<b>Pressurized Water Reactor</b>

---

<b>RCCA</b>	<b>Rod Cluster Control Assemblies</b>
<b>RCP</b>	<b>Reactor Coolant Pump</b>
<b>RCS</b>	<b>Reactor Coolant System</b>
<b>RHR</b>	<b>Residual Heat Removal</b>
<b>ROAAM</b>	<b>Risk-Oriented Accident Analysis Methodology</b>
<b>RPV</b>	<b>Reactor Pressure Vessel</b>
<b>RSG</b>	<b>Recirculating Steam Generators</b>
<b>RSS</b>	<b>Reactor Safety Study</b>
<b>SAHRS</b>	<b>Severe Accident Heat Removal System</b>
<b>SBO</b>	<b>Station Blackout</b>
<b>SERG</b>	<b>Steam Explosion Review Group</b>
<b>SGTR</b>	<b>Steam Generator Tube Rupture</b>
<b>SIS</b>	<b>Safety Injection System</b>
<b>SNL</b>	<b>Sandia National Laboratory</b>
<b>SRM</b>	<b>Staff Requirements Memorandum</b>
<b>TMI</b>	<b>Three Mile Island</b>
<b>UPS</b>	<b>Uninterruptible Power Supply</b>

---

**ABSTRACT**

This report has been provided to the NRC to support the discussion of severe accident response features that will be presented in the U.S. EPR Design Control Document (DCD). The information in this report will support the evaluation of the U.S. EPR against the SECY-93-087 guidance on severe accident safety issue resolution and will support the success criteria for probabilistic risk assessment (PRA). The primary topics include the U.S. EPR severe accident design philosophy, key processes and phenomena, the experimental bases for the severe accident design features and for the analytical techniques and tools used to assess hypothetical severe accident sequences, the major computer code models, and examples of severe accident analyses. The conclusion is that the approach for demonstrating the performance of the U.S. EPR during a severe accident is systematic, complete, and comprehensive and will provide sufficient insight for resolution of severe accident safety issues for the U.S. EPR. Results of this approach will appear in the U.S. EPR DCD, including quantification of the performance ranges and limits of U.S. EPR severe accident response features.

## EXECUTIVE SUMMARY

In accordance with NRC policy statements on severe accidents and advanced and evolutionary reactors, new reactor designs should demonstrate improved severe accident characteristics compared to the current fleet of operating reactors. The improvements are generally considered in two distinct ways related to prevention and mitigation:

- New reactors will have a lower probability of occurrence of severe accidents, as measured by Core Damage Frequency (CDF) in a full-scope Level 1 Probabilistic Risk Assessment (PRA).
- New reactors will have improved capabilities of mitigating the consequences of postulated severe accidents, as measured by standard containment performance metrics in a Level 2 PRA.

While regulatory expectations indicate that both prevention and mitigation are to be assessed using PRA techniques, certain specific severe accident precursors and phenomena must be addressed directly by demonstrating either that the plant is designed to address them or that they have been rendered irrelevant by the plant design. These process studies are referred to as “deterministic” evaluations, and are specified in SECY-93-087, “Policy, Technical, and Licensing Issues Pertaining to Evolutionary and Advanced Light-Water Reactor Designs.”

The objective of this report is to support the content on severe accident evaluation that will be in the U.S. EPR DCD. This report has been prepared with specific attention to supporting the evaluation of the U.S. EPR against the SECY-93-087 guidance on severe accident safety issue resolution and to support success criteria for PRA. The primary topics include the U.S. EPR severe accident design philosophy, key processes and phenomena, the experimental bases for the severe accident design features and analytical techniques and tools used to assess hypothetical severe accident sequences (through both individual process studies and PRA), the major computer code models,

and examples of severe accident analyses. The required PRA scope and methods will be discussed in a separate report.

The regulatory guidance set forth in SECY-93-087 identifies several severe accident mitigative features expected for new plant designs:

- Hydrogen control
- Core debris coolability
- High-pressure core melt ejection
- Containment performance
- Equipment survivability.

Drawing on industry experience, the U.S. EPR includes design and operational features that specifically address these issues. Section 2 provides a description of the U.S. EPR with an emphasis on severe accident response features. To address the severe accident safety issues related to the performance of these features, a methodology is presented in Section 3 that draws on elements from industry-recognized methodologies used to assess severe accident issues. The remainder of the report implements the methodology by:

- Identifying relevant severe accidents for consideration (Section 4)
- Identifying important severe accident processes and phenomena (Section 4)
- Assessing severe accident phenomena applicable to the U.S. EPR severe accident response features (Section 5)
- Providing applicable test program information and insights (Section 5)
- Presenting analytical methods based on the MAAP4.07 code, and related validation and verification (Section 6)

- 
- Identifying a calculation matrix to complete the severe accident safety issue resolution activities (Section 6)
  - Demonstrating analysis methods through the presentation of sample problems (Section 7).

The conclusion is that the approach for demonstrating the performance of the U.S. EPR during a severe accident is systematic, complete, and comprehensive and will provide sufficient insight for resolution of severe accident safety issues for the U.S. EPR. Results of this approach will appear in the U.S. EPR DCD, including quantification of the performance ranges and limits of U.S. EPR severe accident response features.

## 1.0 INTRODUCTION

The U.S. EPR is an evolutionary pressurized water reactor (PWR) that incorporates proven technology within an optimized configuration to enhance safety. The U.S. EPR has been designed both for the prevention and mitigation of design basis accidents as well as beyond design basis (severe) accidents. The ultimate design objective is to restrict the radiological consequences to the immediate vicinity of the plant and reduce the likelihood of stringent countermeasures such as evacuation or relocation of the neighboring population. This will be accomplished by evaluating potential containment failure mechanisms to demonstrate that the likelihood of postulated hazardous outcomes is remote. The U.S. EPR takes full advantage of the insights gained from operating experience (e.g., Individual Plant Examinations), PRA, severe accident research, and accident analysis by incorporating features to reduce the likelihood of severe accidents, and, in the unlikely occurrence of a severe accident, to minimize and/or mitigate the consequences of such an accident.

The objective of this report is to support the discussion of severe accident response features to appear in the U.S. EPR Design Control Document (DCD). This topical report includes the U.S. EPR severe accident design philosophy, phenomenological assessment, the experimental bases for the severe accident design features and analytical techniques and tools used to assess hypothetical severe accident sequences (through both individual process studies and PRA), the major computer code models, and examples of severe accident analyses. With regard to PRA, this objective extends to analytical methods used to support PRA per the Standard Review Plan, NUREG-0800, Section 19.1 expectation that “the elements of [an analytical] model used to generate those results are of sufficient technical quality” (Reference 1). A presentation of PRA methods used to assess the U.S. EPR design will be provided in a separate report.

NRC regulations and regulatory guidance do not prescribe specific techniques or analytical methods for addressing severe accident phenomenology. In addition, the uniqueness of the U.S. EPR severe accident response features has necessitated first-

of-a-kind experimental testing programs and, likewise, supporting analytical methods have undergone similar first-of-a-kind innovation. Methods employed during design engineering have evolved from the state-of-the-art development activities within the international severe accidents community. This includes participation in international research and development programs related to experimental programs that specifically address the U.S. EPR severe accidents response features and to computer analysis tools, such as MAAP4 (Reference 2) and MELCOR (Reference 3).

AREVA NP has adopted “public” domain tools, such as MAAP4 for production analyses and, where applicable, MELCOR as a self-audit tool. The primary code documentation for these tools has been developed by the associated code sponsors and their contractors. The code documentation typically includes a description of models and correlations, user instructions and guidelines, code structure and/or programming guidelines, and developmental assessment. Code applicability to the analysis of severe accidents in the U.S. EPR is addressed in this document and builds on previous work performed by code vendors. Supplemental code verification and validation reported in this topical or in the U.S. EPR DCD are developed to reinforce or extend a code’s applicability to model the relevant severe accident phenomena. Such validation activities either specifically address uncertainties associated with the range of potential conditions during a severe accident or simply examine a realistic situation to confirm that sufficient physical modeling methods have been incorporated in the analysis tools.

This report provides a description of U.S. EPR severe accident response features and presents the related phenomenology, test program activities, analytical methods defining the basis for its design, and sample problem analyses demonstrating application of the analytical methods to the U.S. EPR. An analytical methodology is presented incorporating specific process studies designed for the purpose of addressing the safety issues associated with severe accident response in nuclear power plants. These analyses are distinct from a complete PRA (which will be provided in a separate report). Nonetheless, PRA is used to identify relevant scenarios demonstrating U.S. EPR severe accident response features. Collectively, this approach integrates risk

considerations, phenomenological identification, experimental insight, code development, analysis, and uncertainty quantification for the purpose of providing a complete and comprehensive presentation of severe accident safety issues and the systematic approach to resolution.

## **1.1 *Regulatory Requirements and Guidance***

### **1.1.1 *Governing Documents***

The principal regulatory requirements related to severe accidents as specified in the Code of Federal Regulations (CFR) (Reference 4) are as follows:

- 10 CFR Part 20 Standards for Protection against Radiation
- 10 CFR 50.34(b) Final safety analysis report
- 10 CFR 50.34(f) Additional Three Mile Island (TMI)-related requirements
- 10 CFR 50.34(g) Combustible gas control
- 10 CFR 50.34(h) Conformance with the Standard Review Plan
- 10 CFR 50.44 Standards for combustible gas control system in light-water-cooled power reactors
- 10 CFR 50.48 Fire protection

For advanced nuclear power plants, including both the evolutionary and passive designs, the NRC concluded that vendors should address severe accidents during the design stage (Reference 5). Designers can take full advantage of the insights gained from such input as PRA, operating experience, severe accident research, and accident analysis by including features to reduce the likelihood that severe accidents will occur and, in the unlikely occurrence of a severe accident, to mitigate the consequences of such an accident.

The NRC has issued guidance for addressing severe accidents in the following documents:

- NRC Policy Statement, Severe Reactor Accidents Regarding Future Designs and Existing Plants (Reference 5)
- NRC Policy Statement, "Safety Goals for the Operations of Nuclear Power Plants" (Reference 6)
- NRC Policy Statement, "Nuclear Power Plant Standardization" (Reference 7)
- NRC Policy Statement, "The Use of Probabilistic Risk Assessment Methods in Nuclear Regulatory Activities" (Reference 8)
- SECY-90-016, "Evolutionary Light-Water Reactor (LWR) Certification Issues and Their Relationship to Current Regulatory Requirements," (Reference 9)
- SECY-93-087, "Policy, Technical, and Licensing Issues Pertaining to Evolutionary and Advanced Light-Water Reactor Designs," (Reference 10)

The first four documents provide guidance for implementing the NRC's policies regarding nuclear power plant safety performance, the treatment of severe accidents, and the use of PRA. SECY-90-016, SECY-93-087, and the accompanying Staff Requirements Memoranda (SRMs) provide Commission-approved guidance for implementing features in new designs to prevent and mitigate severe accidents and for evaluating certain severe accident safety issues through deterministic analyses.

### **1.1.2 Acceptance Criteria**

The NRC's Policy Statement on Severe Reactor Accidents Regarding Future Designs and Existing Plants states the NRC expectation that future and existing nuclear power plants perform a PRA and consider severe accident vulnerabilities. With regard to severe accidents, 10 CFR Parts 50 and 52 codify regulations developed from this Policy Statement, research and development, TMI-2 lessons learned, and plant risk

assessments. Specifically, with respect to severe accidents, the Design Certification Application (DCA) must contain the following:

- Demonstration of compliance with all explicit regulatory requirements, as they apply to plant severe accident response features, including the TMI requirements for new plants, as reflected in 10 CFR 50.34(f)
- Demonstration of technical resolution of all applicable unresolved safety issues (USI) and the medium- and high-priority generic safety issues (GSI), including a special focus on assuring the reliability of decay heat removal systems and the reliability of both alternating current (AC) and direct current (DC) electrical supply systems
- Completion of a PRA and consideration of the severe accident vulnerabilities, along with the insights that it may add to providing assurance of no undue risk to public health and safety

As a final step in the process, the NRC's regulations specify that a DCA must address compliance with certain technical requirements for Final Safety Analysis Reports (FSARs), as discussed in 10 CFR 50.34. Specifically, 10 CFR 50.34(f)(1)(i) requires that the plant-specific PRA include an evaluation of "improvements in the reliability of core and containment heat removal systems as are significant and practical and do not impact excessively on the plant." To satisfy these requirements, additional design alternatives must be proposed that have the potential of improving plant severe accident performance, and a cost-benefit analysis must be performed to determine if each alternative is justified by the reduced consequences of severe accidents. For these assessments, the impacts are interpreted as primarily those affecting the surrounding population (i.e., offsite consequences), so that a Level 3 PRA is required to perform the cost-benefit analysis.

These rules and related policy statements were prompted by the NRC's judgment that severe accidents, which are beyond the traditional design-basis events, constitute the

major remaining risk to the public associated with radioactive releases from nuclear power plant accidents. The fundamental objective is to take all reasonable steps to reduce the chances that a severe accident involving substantial damage to the reactor core will occur and to mitigate the consequences of such an accident, should one occur.

### **1.1.3 Analysis Requirements**

As identified in the previous section, regulations related to severe accidents require the following:

- Compliance with any technically-relevant TMI requirements in 10CFR 50.34(f)
- Resolutions of USI and GSI, and
- Completion of a design-specific PRA.

While a final severe accident safety issue resolution and a PRA will be included in the U.S. EPR design certification application, this report supports these requirements through the identification of technical bases related to design choices and analytical methods.

Guidance in SECY-90-016 and SECY-93-087 and their corresponding SRMs provide the Commission-approved guidance for implementing features in new designs to prevent severe accidents and to mitigate their effects, should they occur.

As discussed in SECY-90-016, based on:

- NRC reviews of current-generation reactor designs and advanced light water reactors (ALWRs)
- Consideration of operating experience, including the TMI-2 accident
- Results of PRAs of current-generation reactor designs and ALWRs
- Early efforts conducted in support of severe accident rulemaking

- 
- Research to address previously identified severe accident safety issues

the NRC identified for advanced passive and evolutionary plants the following preventive feature issues (SECY-93-087):

- anticipated transient without scram (ATWS)
- midloop operation
- station blackout (SBO)
- fire protection
- interfacing loss-of-coolant accident

In addition, SECY-93-087 identifies the following mitigative feature issues:

- hydrogen control
- core debris coolability
- high-pressure core melt ejection
- containment performance
- equipment survivability

The U.S. EPR has been designed to address these issues. This topical report has been prepared specifically to present the technical bases for the U.S. EPR approach and methods applied to resolve these safety issues as will be documented in the U.S. EPR DCD.

## **1.2      *Definitions***

Several technical terms appear throughout this report. Those that frequently occur have been compiled in this section along with appropriate definitions and explanations.

**Adiabatic Isochoric Complete Combustion (AICC):** An ideal combustion event describing flammable reactants, configured such that a combustion event results in the consumption of all original reactants and retains energy released from the exothermic reaction within the original space of reactants only, without heat transfer to walls or other volumes. The resultant pressure in the gas space is the theoretical maximum from the combustion process.

**Accident Progression Bin:** A group of postulated accidents that has similar characteristics with respect to (for this summary report) the timing of containment building failure and other factors that determine the amount of radioactive material released (see Plant Damage State). These are analogous to containment failure modes used in previous PRAs.

**Core Uncovery:** The water mixture level in the reactor vessel falls below the top of the active fuel.

**Core Damage:** Uncovery and heat up of the reactor core to the point at which prolonged mechanical fracturing, oxidation and/or melting involving a large fraction of the core is anticipated.

**Core Damage Frequency:** The sum of frequencies of severe accident sequences in a PRA that result in core damage (as defined above).

**Cumulative Distribution Function:** The function that gives the probability of a parameter being less than or equal to a specified value. The complementary cumulative distribution function gives the probability of a parameter value being equal to or greater than a specified value.

**Decay Heat:** Residual heat generation in nuclear fuel resulting from the decay of fission products.

**Degraded Core:** An advanced state of core damage in which the original fuel bundle geometry has been substantially lost.

**Direct Containment Heating:** A postulated containment failure scenario in which a large quantity of molten core material, appearing as fine particles or an aerosol, rapidly transfers sensible heat to the containment atmosphere raising both containment pressure and temperature.

**Early Phase:** Refers to the initial stages of core damage, including clad oxidation and the melting and relocation of mainly metallic material. A rod-like geometry is maintained.

**Fuel-Coolant Interactions:** A process by which molten fuel transfers its thermal energy to the surrounding coolant, leading to the break up of corium with possible formation of a coolable debris bed or potential evolution to an energetic steam explosion

**High Pressure Melt Ejection:** A reactor vessel failure mode in which molten core materials are ejected from the reactor vessel at high pressure and are dispersed into the containment as fine particles or aerosols.

**Late Phase:** Refers to the stages of core degradation involving substantial melting and relocation of fuel material, including the transfer of materials to the lower vessel plenum and, possibly, the containment.

**Molten Core-Concrete Interaction:** The combination of thermal attack and chemical reactions contributing to the degradation of concrete in the containment caused by contact with molten materials from a reactor core.

**Offsite Consequences:** The effects of a release of radioactive material from the power plant site measured (for this summary report) as the number of early fatalities in the area surrounding the site and within one mile of the site boundary. It is also measured as the number of latent cancer fatalities in the area surrounding the site and within 10 miles of the power plant, and the integrated population dose in the area surrounding the site and within 50 miles of the power plant.

**Probability Density Function:** The derivative of the cumulative distribution function. A function used to calculate the probability that a random variable (e.g., amount of

---

hydrogen generated in a severe accident) will fall in a given interval. That probability is proportional to the height of the distribution function in the given interval.

**Plant Damage State:** A group of accident sequences that has similar characteristics with respect to accident progression and containment engineered safety feature operability.

**Reactor Coolant System/Reactor Pressure Vessel Failure Modes:** Any process in which the reactor coolant system or reactor pressure vessel boundary weakens and ultimately fails, allowing its contents, including hydrogen, fission products, and molten core debris, to be transferred to the containment.

**Severe Accident:** A severe accident is a category of beyond design basis accidents which result in catastrophic fuel rod failure, degradation of the structural integrity of the reactor core, and release of radioactive fission products into the reactor coolant system (RCS). Such an event can only occur as a result of a sustained loss of adequate core cooling, which leads to a build up of fission product decay heat and elevated core temperatures. The resulting consequence of melting the reactor core (and internals) may lead to the breaching of the reactor pressure vessel (RPV) and, through the relocation of molten core material into the containment, may potentially compromise the ability of the containment to perform its radionuclide retention function.

Given the potential consequences, nuclear power plants are designed with the “defense-in-depth” strategy, that is, multiple layers of defense mechanisms, so that in combination a severe accident is considered highly unlikely as quantified through PRA.

**Source Term:** The fractions defining the portion of the radionuclide inventory in the reactor fuel at the start of an accident that is released to the environment. Also included in the source term are the initial elevation, energy, and timing of the release.

## **2.0 DESIGN DESCRIPTION OF U.S. EPR SEVERE ACCIDENT MANAGEMENT SYSTEMS**

The purpose of this section is to introduce the U.S. EPR design features, particularly as they relate to severe accident performance. Section 2.1 provides an overview of the general plant configuration and safety systems. Section 2.2 focuses on systems and components dedicated to severe accident response. Design features and/or parameters are subject to modest changes up until the time of submittal of the DCA.

### **2.1 *General Plant Description***

The U.S. EPR is a 4590 MWth evolutionary PWR that incorporates proven technology with innovative system configuration to enhance safety. The U.S. EPR was originally developed through a joint effort between AREVA NP and Siemens in the 1990s by incorporating key technological and safety features from the French and German reactor fleets. This section provides a general overview of plant features.

#### **2.1.1 *Reactor Vessel***

The RPV of the U.S. EPR is a cylindrical vessel with a welded hemispherical bottom head and a removable, flanged hemispherical upper head. Reactor coolant enters the RPV via four cold leg inlet nozzles near the vessel flange and flows down through the annular space between the core barrel and the RPV wall, turns at the bottom, and flows up through the core to the outlet nozzles, which guide it to the four hot legs. There are no penetrations in the bottom of the RPV.

##### **2.1.1.1 *Reactor Internals and Core***

The U.S. EPR is an optimized thermal-fission reactor capable of converting heat generated from nuclear fission into electricity for commercial distribution. The U.S. EPR core consists of 241 fuel assemblies. The assemblies, containing various fissile enrichments, are configured into an arrangement supported by the reactor internals. These internals also direct the coolant flow past the fuel rods. The coolant and moderator are light water at a normal operating pressure of approximately 2250 psia.

The fuel, internals, and coolant are contained within a heavy walled RPV. The vessel internals of the U.S. EPR are similar to those of conventional PWRs with the exception of a dedicated heavy reflector and a thicker lower core support plate (LCSP). Figure 2-1 shows the configuration of the U.S. EPR reactor internals.

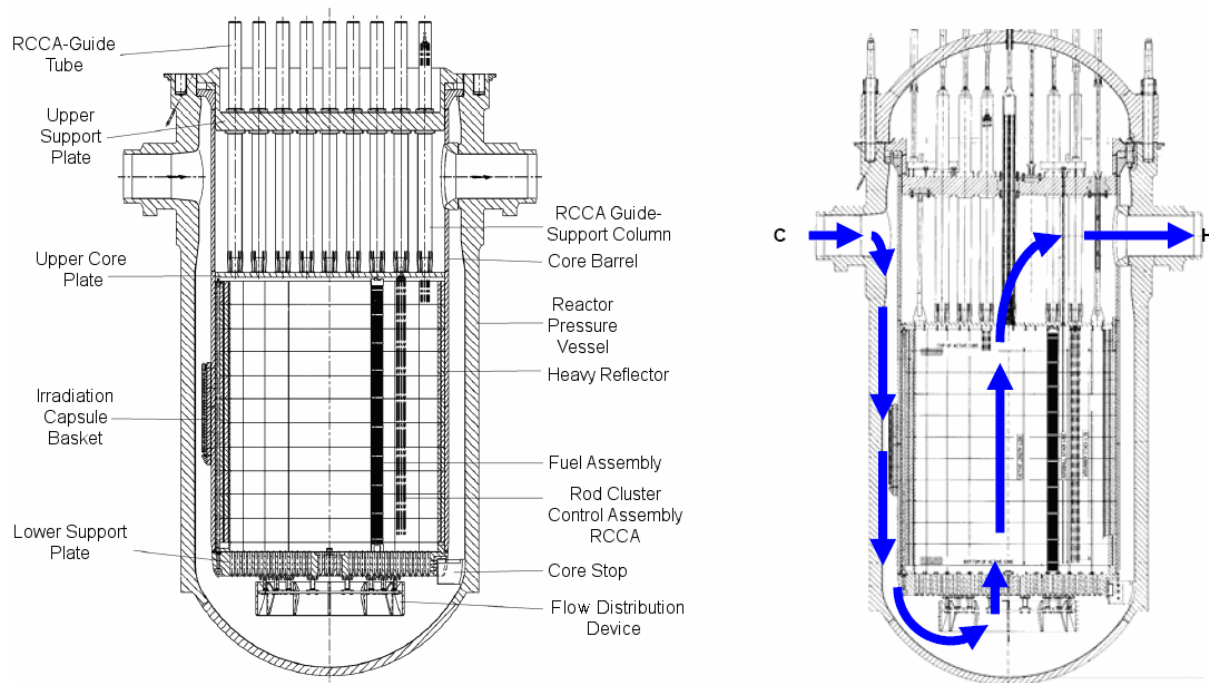


**Figure 2-1 U.S. EPR Reactor Internals**

The heavy reflector replaces the baffle plates and formers around the core of a conventional PWR to improve neutron economy. The heavy reflector consists of a series of concentric stacked rings of forged stainless steel with machined flow holes. The heavy reflector is removable and geometrically varies in thickness from approximately 4 to 10 inches. The configuration of the heavy reflector is depicted in Figure 2-2.

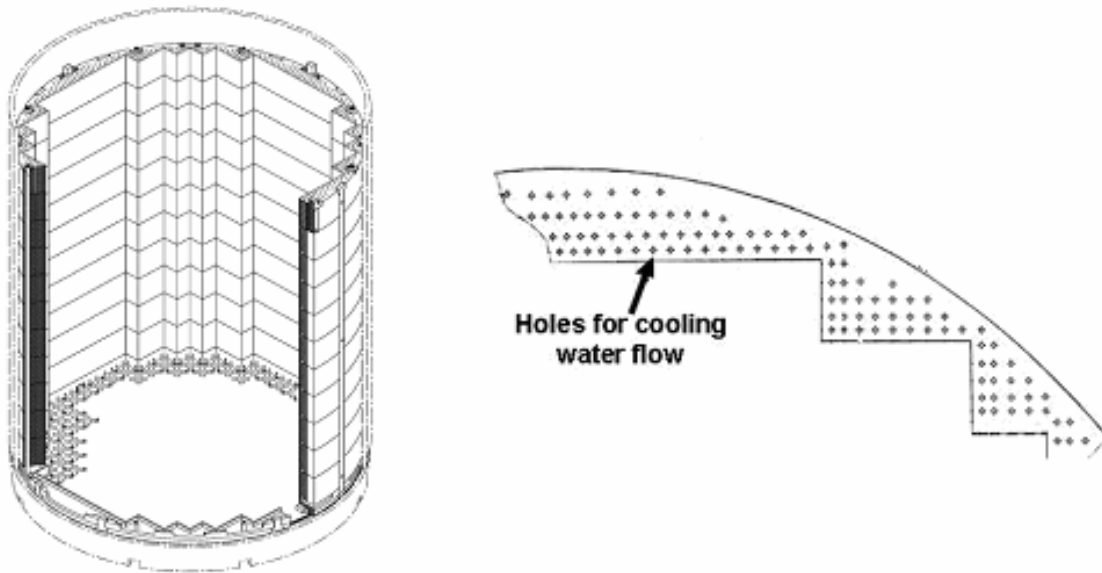


**Figure 2-2 Heavy Reflector**

A U.S. EPR fuel assembly consists of 265 fuel rods in a 17x17 square array. The remaining fuel assembly positions have guide thimbles joined to the top and bottom nozzles of the fuel assembly to provide the supporting structure of the fuel grids. Depending on the position of the assembly in the core, the guide thimbles are used for rod cluster control assemblies (RCCAs) or neutron source rods. The fuel rods consist of enriched  $\text{UO}_2$ , contained in zirconium alloy tubing. Other types of fuel rods are burnable absorbers containing gadolinia within the  $\text{UO}_2$  fuel pellets to provide a burnable absorber integral to the fuel. During irradiation the burnable absorber is depleted and reactivity is gained partly to offset the negative reactivity effect from fuel depletion and fission product build-up. In addition, the burnable absorbers can be used for optimizing the radial power distribution within the core.

#### **2.1.1.2 Reactivity Control Systems**

The U.S. EPR uses multiple means to control reactivity. For controlling relatively slow reactivity changes, such as the effects of fuel burnup, soluble boron concentration in the coolant is varied. Neutron absorbers (gadolinia), in the form of burnable absorber bearing fuel rods, are used to establish the desired initial reactivity and power

distribution. The core reactivity and power distribution can also be controlled by movable control rods consisting of absorber rods. The RCCAs are used to control rapid changes in reactivity. Each RCCA consists of a group of individual absorber rods fastened at the top end to a common hub. Each absorber rod is clad with stainless steel and contains Ag-In-Cd. The RCCAs are split into several groups with control rod drive mechanisms (CRDM) enabling the RCCAs to be inserted, held in position or withdrawn. The CRDMs consist of electromechanical devices fixed to the RPV closure head. They are used to control the RCCA positions and ensure reactor trip by insertion under the force of gravity, which is effected by de-energizing the CRDM power supplies.

### 2.1.2 *Reactor Coolant System*

The U.S. EPR uses a proven 4-loop RCS design that is similar to those in commercial PWRs throughout the world. A major enhancement to the RCS is an increase in size and free volume of primary system components. The 4-loop RCS includes an RPV, a pressurizer (with a surge line and two spray lines), 4 steam generators, 4 reactor coolant pumps (RCPs), 4 hot legs, 4 cross-over legs, and 4 cold legs. The configuration of the U.S. EPR primary system is shown in Figure 2-3.

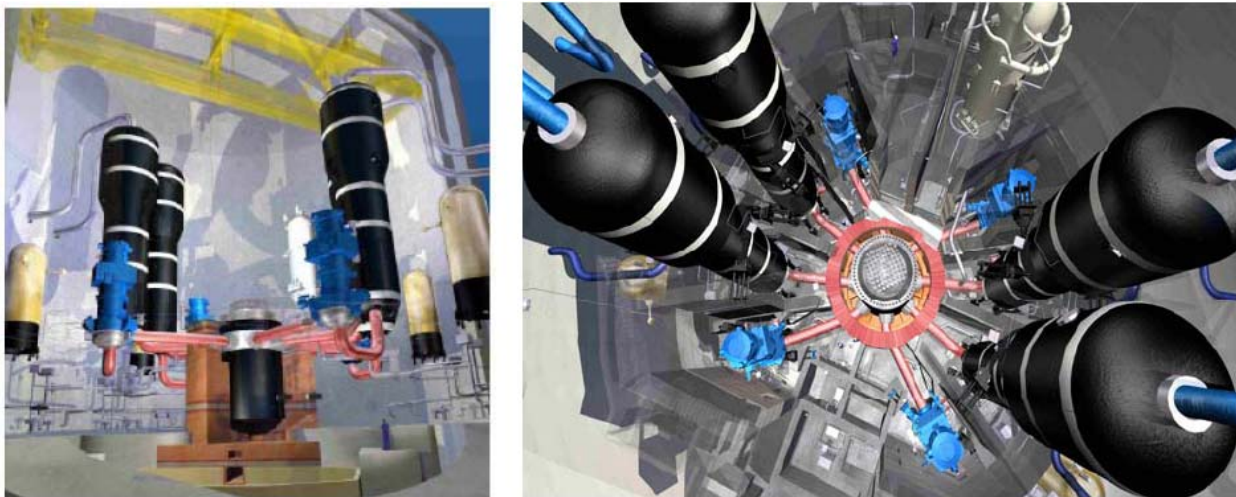


**Figure 2-3 Reactor Coolant System**

### **2.1.2.1 Steam Generator**

The U.S. EPR uses recirculating steam generators (RSGs) with an axial economizer to produce saturated steam. The use of an axial economizer is an optimized difference between the U.S. EPR RSGs and those of a traditional plant. With the axial economizer, feedwater entering the generator is forced to the cold leg of the tube bundle to obtain a preheating effect. The feedwater is preheated to saturation temperature in the lower portion of the tube bundle without mixing. The higher temperature difference between the primary fluid and the feedwater increases the heat transfer over the tube region. Entrained water in the steam-water mixture leaving the tube bundle and flowing into the steam drum is separated out by steam separators and dryers before the dry steam exits the steam outlet nozzle to drive the turbine-generator of the plant. The water separated out in the steam drum falls back into the tube bundle region; however, the economizer forces most of the saturated water into the hot leg side of the tube bundle, thereby increasing the efficiency of heat transfer during the steam generation process.

### **2.1.2.2 Pressurizer**

The pressurizer is the principal component of the RCS pressure control for the U.S. EPR. Similar to pressurizers in the current-generation plants, the pressurizer is a vertical, cylindrical vessel with hemispherical top and bottom heads, where liquid and vapor are maintained in equilibrium at saturated conditions. With approximately 2,650 ft<sup>3</sup> the U.S. EPR pressurizer includes an increased water volume compared to current 4-loop plants. Spray lines are connected to two of the cold legs at the discharge of the RCPs, each feeding a separate spray nozzles within the pressurizer. Relief valves for both design-basis events and severe accidents are attached to the top of the pressurizer.

### **2.1.2.3 Reactor Coolant Pumps**

The U.S. EPR RCPs are vertical, single stage, mixed-flow pumps designed to deliver a large flow of reactor coolant at high temperature and pressure. The RCS contains four

RCPs located between the cross-over and cold legs associated with each steam generator. The RCPs are high head pumps consisting of three major components; the pump, the shaft seals, and the motor. The RCPs use a mechanical shaft seal system that consists of three seals arranged in series with a standstill seal. During normal operation, the shaft seal system provides a pressure breakdown from RCS pressure to ambient conditions. The number one seal ensures the majority of the pressure breakdown with controlled leakage to the chemical and volume control system (CVCS), while the number two and three seals ensure the remaining pressure breakdown with low leakage to the Vent and Drain System (VDS). Seal cooling system is maintained by the emergency power systems of the plant.

### **2.1.3 Safety Systems for Design Basis Events**

As the U.S. EPR is an evolutionary design based on proven technology, the plant safety scheme relies on the use of active systems powered by AC power systems.

#### **2.1.3.1 Reactor Building**

The U.S. EPR Reactor Building is composed of a containment building and a shield building separated by an annular region. A depiction of the U.S. EPR Reactor Building is provided in Figure 2-4.

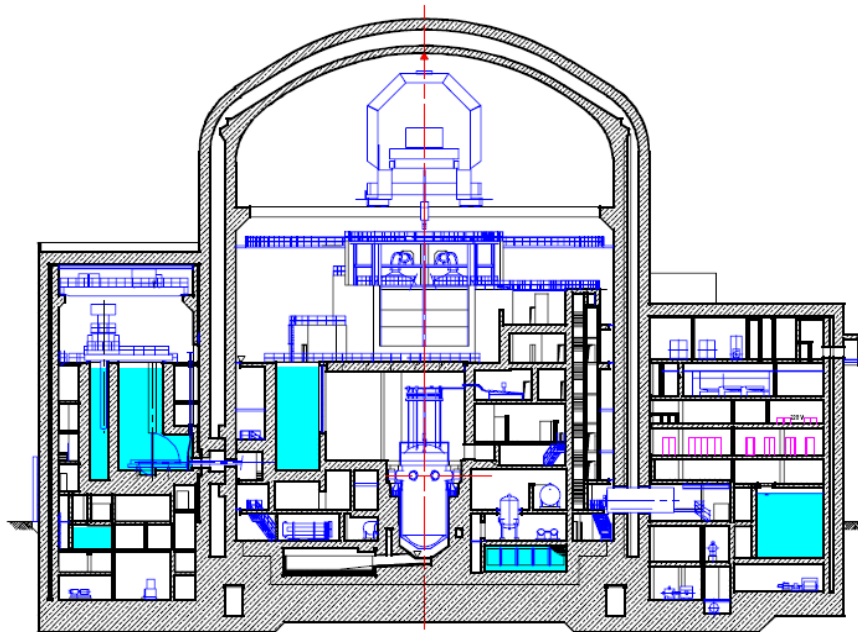


**Figure 2-4 Containment Layout**

#### ***2.1.3.1.1 Containment and Shield Building***

The containment is a pre-stressed concrete shell with steel liner on its inner surface (including the basemat). Within containment are the RCS, the In-containment Refueling Water Storage Tank (IRWST), and parts of the main steam and feedwater lines. The containment includes a large free volume of approximately  $2.8 \times 10^6$  ft<sup>3</sup> and a design pressure of 62 psig.

The shield building surrounds the containment. It is a reinforced concrete structure designed to provide protection against external hazards.

#### ***2.1.3.1.2 Annulus Ventilation System***

The containment building and shield building are physically independent from one another except at the basemat. These structures are separated by an annular space that is maintained at sub-atmospheric pressure by the Annulus Ventilation System (AVS). The AVS is a safety-related system used to filter any leakage through the

primary containment, in the event of both design basis and severe accidents, prior to releasing it from the plant stack. The AVS ensures 2x100% extraction capability and consists of a high efficiency particulate air (HEPA) filters and charcoal absorbers in series with air handling equipment. The configuration of the AVS is depicted as Figure 2-5.

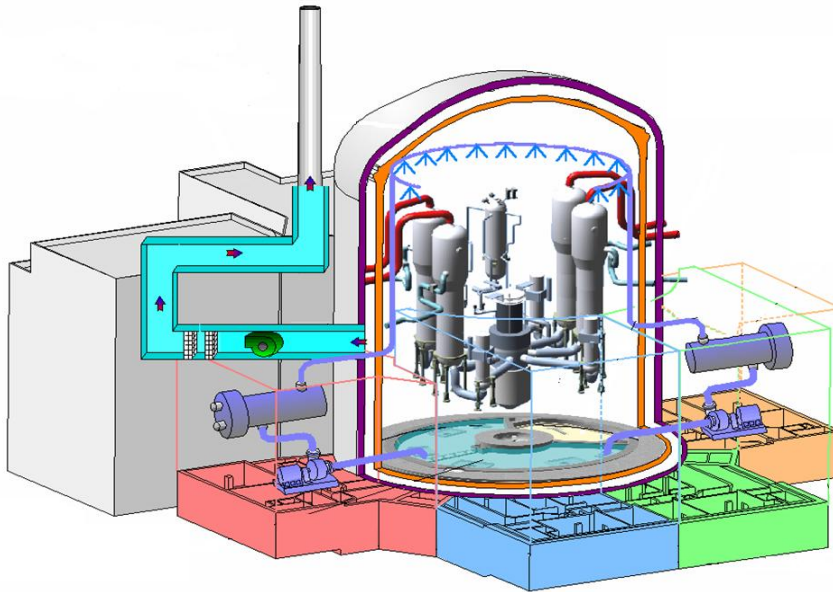


**Figure 2-5 Annulus Ventilation System**

### **2.1.3.2 Containment Cooling Systems**

Containment heat removal in the U.S. EPR is ensured through use of active systems. During normal operation or hot shutdown conditions, the containment cooling ventilation system (CCVS) removes heat released by the operation of plant components. The CCVS is not a safety-related system but is designed with sufficient redundancy to ensure reliable operation.

In response to design-basis events, the U.S. EPR does not require active containment heat removal systems to ensure short-term pressure and temperature control due to the large free volume and heat capacity of the containment and internal structures. Containment heat removal is ensured by the Low Head Safety Injection (LHSI) /

Residual Heat Removal (RHR) heat exchanger outside containment. For example, under a design-basis loss-of-coolant accident (LOCA), LHSI draws water from the IRWST and rejects the containment heat to the plant cooling water systems through the LHSI/RHR heat exchanger before being injected back into the RCS where it may escape back to the IRWST to complete the cooling loop. The configuration of the LHSI system is depicted in Figure 2-6.

The U.S. EPR also includes a dedicated severe accident heat removal system (SAHRS) to ensure containment cooling in response to severe accidents. This system is described in detail in Section 2.2.4.

**2.1.3.3 Core Cooling Systems**

Core cooling is provided by a series of independent cooling systems that draw borated water from a dedicated source within the containment. The systems that comprise the safety injection system (SIS) of the U.S. EPR include the IRWST, Medium Head Safety Injection (MHSI), and LHSI/RHR systems. The orientation of these systems is depicted in Figure 2-6.

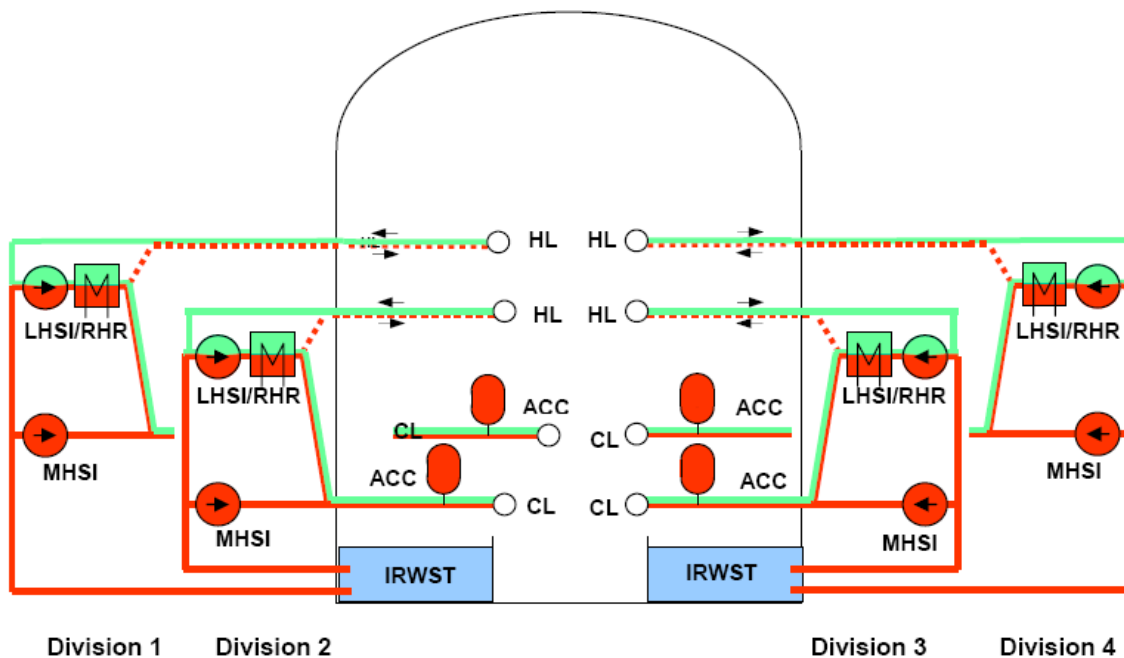


**Figure 2-6 Safety Injection Systems**

### ***2.1.3.3.1 In-Containment Refueling Water Storage Tank***

The function of the IRWST is to maintain a large reserve of borated water at a homogeneous concentration and temperature. The borated water is used to flood the refueling cavity for normal refueling. It is also the safety-related source of water for emergency core cooling in the event of a LOCA and is a source of water for containment cooling and for core melt cooling in the event of a severe accident. The IRWST represents the lowest point in the containment and communicates with the remainder of the containment such that any water discharged from the RCS will drain back into the IRWST.

Each of the four SIS (safety-related) and two SAHRS (non-safety-related) trains is provided with a separate sump suction connection to the IRWST. To prevent RCS thermal insulation and other debris from reducing the suction head of the SIS and SAHRS pumps, a series of barriers is used to minimize the amount of debris which can reach the sumps, including a back-flushing function provided by the SAHRS.

### ***2.1.3.3.2 Safety Injection***

Safety injection within the U.S. EPR is performed by an MHSI system, an LHSI system, and four accumulators. These safety-related systems consist of 4x100% independent trains that are physically separated and protected within the safeguard buildings. The MHSI system draws borated water from the IRWST and injects it into the cold leg at a pressure lower than the main steam safety valve (MSSV) setpoints to ensure that in the event of a steam generator tube rupture (SGTR), primary inventory cannot be released directly to the environment. The four accumulators are connected to the RCS cold legs and provide injection when the RCS pressure falls below the corresponding setpoint.

### ***2.1.3.3.3 Residual Heat Removal***

The RHR system is combined with the LHSI system; however, different operating configuration is used to transfer residual heat to the plant cooling water systems. The RHR system of each plant safety train includes suction on the hot leg of each RCS loop

where it draws heated water and pumps it through a heat exchanger in the safeguards building before being injected back into the cold leg of that same RCS loop. This is an active system with emergency power provided by diesel generators.

#### **2.1.3.3.4 Emergency Boration System**

The U.S. EPR includes an Emergency Boration System (EBS) that can be used to provide borated water at high pressure to shut down the reactor following accidents. The EBS consists of 2x100% trains that can be used as a safety-related means of maintaining the reactor in a shutdown state at any temperature in case of unavailability of the CVCS. The EBS is also a means to mitigate the effects of an ATWS by bringing the reactor into a sub-critical state.

#### **2.1.3.4 Reactor Coolant System Depressurization System**

To prevent RCS overpressure, the U.S. EPR includes three pressurizer safety valves (PSVs) at the top of the pressurizer. These PSVs discharge to a common header connected to the pressurizer relief tank (PRT). The PRT is protected against over-pressurization by use of rupture disks. If the PRT pressure exceeds a specified upper value, the rupture disks will burst, allowing fluid to exit the PRT and relieve the pressure. The outlets of the rupture disks are connected to a piping system that distributes the fluid to the RCP rooms.

The depressurization system also includes dedicated valves to ensure that the RCS can be depressurized in the event of a severe accident. These dedicated valves are discussed in detail in Section 2.2.1.

#### **2.1.4 Electric Power**

The electric power systems of the U.S. EPR are similar to those of conventional plants only with increased reliability, which is attained through redundancy, diversity and independence.

### **2.1.4.1 Off-site Electrical System**

The U.S. EPR uses redundant offsite power supplies similar to those used in the current-generation PWRs. The transmission lines and their associated structures are designed to withstand site-specific environmental conditions.

### **2.1.4.2 On-site Electrical System**

On-site electrical power systems include dedicated features to ensure that plant loads can be provided, if necessary, with both AC and DC power.

#### **2.1.4.2.1 AC Power Systems**

In the event of a loss-of-offsite-power (LOOP), the U.S. EPR includes 4x100% safety-related emergency diesel generators (EDG), each designed to provide sufficient power supply to plant systems to shut down the reactor and maintain it in a stable condition until offsite power can be restored. Each EDG is associated with an independent safety train. In addition to these EDGs, the U.S. EPR also includes two smaller diesel generators that are not safety-related to provide power to critical plant loads in a SBO.

#### **2.1.4.2.2 DC Power System**

The main DC power system of the U.S. EPR is similar to that of conventional operating plants. The U.S. EPR uses safety-related station batteries with redundant trains of battery chargers to power critical loads until the EDGs can be started. The batteries are designed for a discharge of two hours based on the necessary loading of the batteries.

The U.S. EPR also includes a non-class 1E Uninterruptible Power Supply (UPS) for severe accident management. The non-class 1E UPS is discussed in Section 2.2.6.

## **2.2 Description of Dedicated Severe Accident Plant Features**

The U.S. EPR includes dedicated features to mitigate the effects of beyond-design basis, severe accidents. The plant design philosophy is based on a deterministic consideration of defense-in-depth comprising four levels:

1. A combination of conservative design, quality assurance, and surveillance activities to prevent departures from normal operation
2. Detection of deviations from normal operation and protection devices and control systems to prevent escalation into accidents
3. Engineered safety features and protective systems that are provided to mitigate accidents and thus prevent their evolution into severe accidents
4. Measures to preserve the integrity of the containment and enable control of severe accidents.

The implementation of this design philosophy has resulted in the inclusion of innovative features to minimize the risk of energetic scenarios that could lead to containment failure. Some examples of these dedicated, risk-reducing design provisions include:

- Prevention of high pressure RCS failure through the use of dedicated severe accident depressurization valves
- A dedicated Core Melt Stabilization System (CMSS) used to stabilize molten core debris resulting from hypothetical core melt scenarios
- A dedicated Combustible Gas Control System (CGCS) to prevent hydrogen detonation by reducing the post-accident hydrogen concentration within the containment
- Control of the environmental conditions within the containment following a severe accident through the use of the SAHRS.

The combined effect of each of these systems plus the robust and leak-tight design containment of the U.S. EPR provides assurances that the offsite dose following a severe accident is minimal.

Figure 2-7 depicts some of these important plant features. Each of these severe accident features is described in the following subsections and supplemental data are provided in Appendix A.

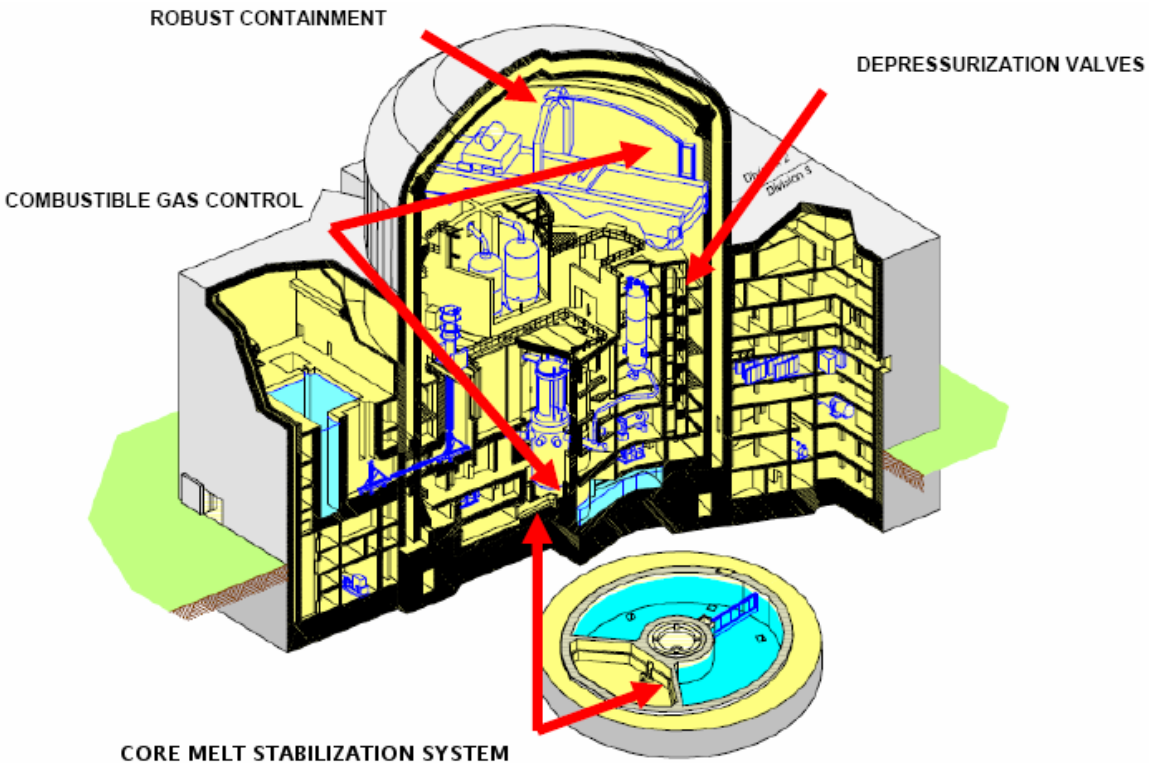


**Figure 2-7 Dedicated Severe Accident Design Features**

### **2.2.1 Severe Accident Depressurization Valves**

RPV failure under high internal pressure is of importance to severe accident risk from high pressure melt ejection (HPME) resulting in direct containment heating (DCH). Even though such a failure is physically unlikely, an objective of the U.S. EPR severe accident response strategy is to convert high pressure core melt sequences into low pressure sequences with high reliability so that a high pressure vessel breach can be practically excluded. For the U.S. EPR, this is achieved through two dedicated severe accident depressurization valve trains that are part of the Primary Depressurization System (PDS). Each of these valve trains consists of a DC-powered depressurization valve (globe valve) in series with an isolation valve (gate valve) as shown in Figure 2-8.

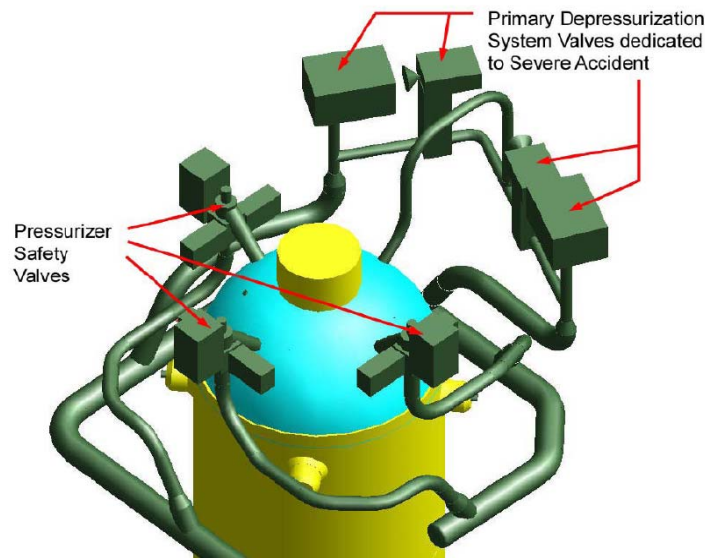


**Figure 2-8 Severe Accident Depressurization Valves**

Each depressurization train has a discharge capacity of approximately 550 lb/s of saturated steam at design pressure. Even though these valve trains are used exclusively for severe accident mitigation, a 2x100% design philosophy is followed to provide a performance margin.

The severe accident depressurization valves are independent of the PSVs, a safety-grade system that provides RCS relief for an overpressurization event (see Section 2.1.3.4). Both the severe accident depressurization valves and the PSVs discharge to the PRT. The PRT is protected by rupture disks and connected to two of the four RCP rooms as shown in Figure 2-9.

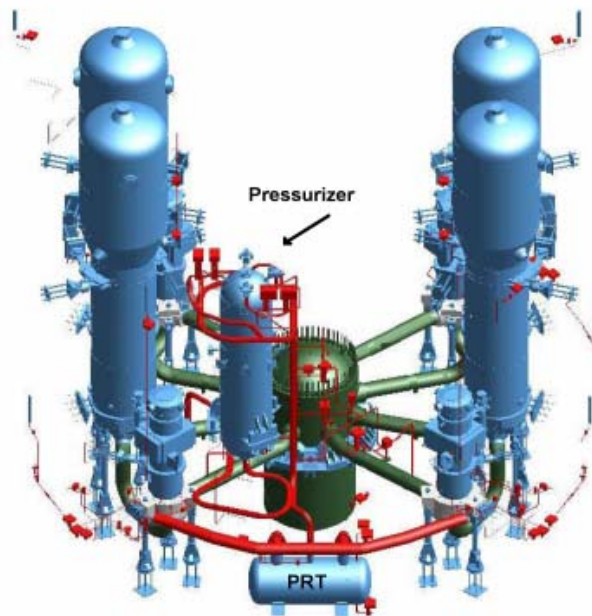


**Figure 2-9 Pressurizer Relief Tank**

Failure of the PRT rupture disks encourages the mixture of non-condensable gases residing in the pump rooms to prevent the preferential accumulation of hydrogen in the containment rooms. Hydrogen distribution is further discussed in Section 5.1.2.

### **2.2.2 Combustible Gas Control System**

Combustible gas control in the containment is necessary to avoid the risk of containment failure due to fast deflagration or from accidental ignition of a critical gas mixture. The U.S. EPR includes a dedicated CGCS to minimize the post-accident hydrogen combustion risk within containment. The CGCS system is divided into two subsystems corresponding to their operational functions:

- Hydrogen Reduction System
- Hydrogen Mixing and Distribution System

### 2.2.2.1 Hydrogen Reduction System

The Hydrogen Reduction System (HRS) consists of 41 large and 6 small passive autocatalytic recombiners (PARs) installed in various parts of the containment. Both models of PARs used in the U.S. EPR design have been developed by AREVA NP and are currently used in some European operating plants. Each PAR consists of a metal housing designed to promote natural convection with a gas inlet at the bottom and a lateral gas outlet at the top. The horizontal cover of the housing at the top of the recombiner protects the catalyst against direct water spray and aerosol deposition. Numerous parallel plates with a catalytically active coating (Pt/Pd substrate) are arranged vertically in the bottom of the housing. Accessibility to the catalytic plates is provided by the use of a removable inspection drawer. A rendering of a PAR is provided in Figure 2-10.

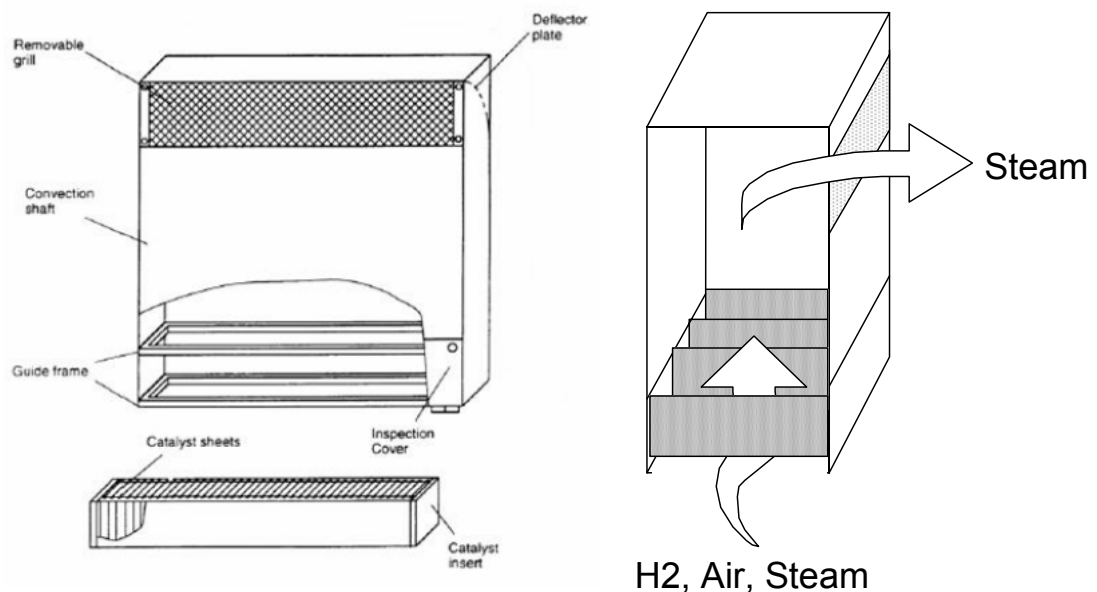


**Figure 2-10 Passive Autocatalytic Recombiner**

Hydrogen and oxygen in containment gas mixtures are recombined upon contact with the catalyst in the lower part of the housing. The heat from this reaction in the lower part of the recombiner causes a reduction in gas density in this area promoting natural circulation through the PAR and ensuring high efficiency of recombination.

In the presence of oxygen, the PARs will automatically start if the threshold hydrogen concentration is reached at the catalytic surfaces. The recombination rate depends mainly on the hydrogen density seen by the PAR. An increasing hydrogen concentration enhances the removal rate up to a type-specific upper limit.

The PARs are arranged inside the equipment rooms to support global convection within the containment, and thereby homogenize the atmosphere and reduce local peak hydrogen concentrations. Recombiners are also included in the containment dome to cope with stratification and to improve depletion after atmospheric homogenization. The PARs are installed above the floor to provide unobstructed inflow and easy access to facilitate maintenance. The PARs are also arranged to avoid direct contact with spray water (despite their qualification to operate in the presence of water).

The PARs are designed and located to ensure that the global concentration of hydrogen in the containment atmosphere is maintained below 10% by volume during phases of an accident resulting in oxidation up to 100% of the zirconium surrounding the reactor core fuel. The PARs also minimize the potential for hydrogen detonation and ensure that the global hydrogen concentration can be maintained below the lower flammability limit of 4% by volume of the containment atmosphere in the long term.

#### **2.2.2.2 Hydrogen Mixing and Distribution System**

The hydrogen mixing and distribution system is designed to ensure that adequate communication exists throughout the containment to facilitate atmospheric mixing. Several of the equipment rooms surrounding the RCS are isolated from the rest of the containment during normal operation. In the event of an accident, communication is established between these equipment rooms, thereby eliminating any potential dead-end compartments where non-condensable gases could accumulate. This ability to transform the containment into a single convective volume is supported by a series of mixing dampers and blowout panels.

The mixing dampers are stainless steel flaps similar in design to traditional fire dampers. The mixing dampers are held closed during normal plant operation by an

electric motor that stretches a spring actuator. If the power is lost to the motor, the mixing dampers are opened passively. These mixing dampers can also be opened manually from the control room as well as by a pressure differential between compartments or the exceedence of a certain absolute pressure. Figure 2-11 provides a view of a hydrogen mixing damper.

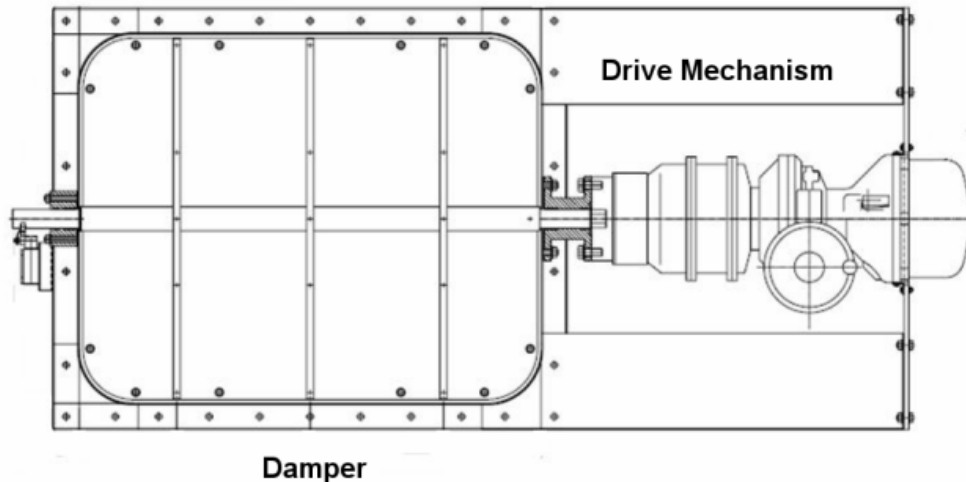


**Figure 2-11 Hydrogen Mixing Damper**

There are eight mixing dampers within the annular rooms at the bottom of the containment towards the air space of the IRWST. The blowout panels are located at the top of the steam generator compartments and comprise what is referred to as the pressure equalization ceiling. The blowout panels are standard rupture and convection foils that become dislodged and create an open flow path when subjected to a differential pressure. The configuration of the pressure equalization ceiling is depicted in Figure 2-12.

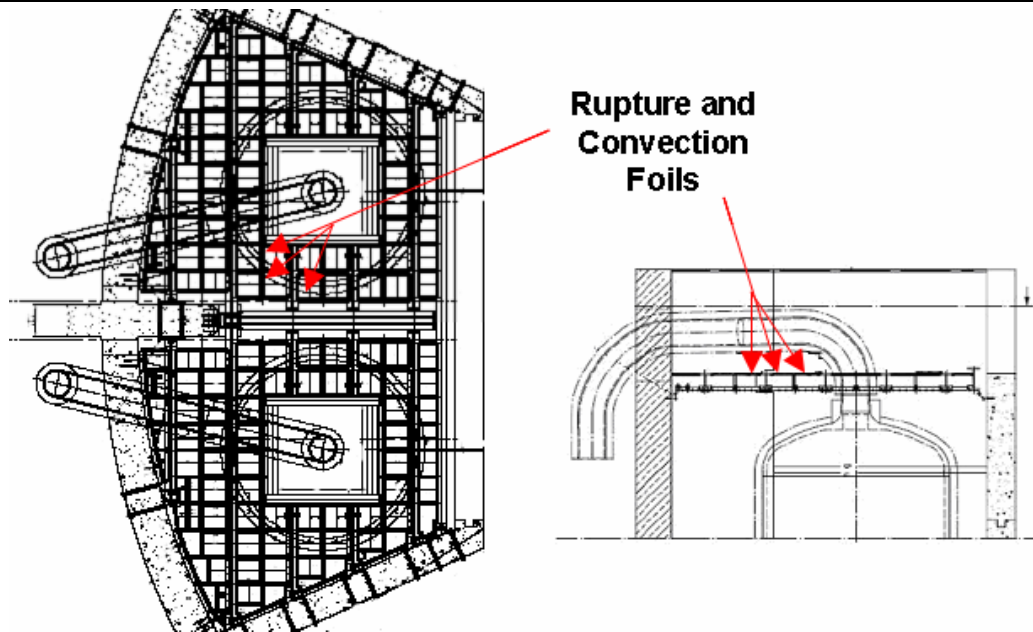


**Figure 2-12 Pressure Equalization Ceiling**

### **2.2.3 Core Melt Stabilization System**

Melt retention within the RPV was not a design goal for the U.S. EPR. Rather, the U.S. EPR is equipped with a dedicated ex-vessel system to accommodate molten core debris, including the entire core inventory and reactor internals, which penetrates the RPV. The goal of this system is to stabilize molten core debris before it can challenge the integrity of the containment. It is attained through the combined effects of the following portions of the CMSS:

- Reactor Cavity
- Melt Plug
- Melt Discharge Channel
- Spreading Area and Cooling Structure

The reactor cavity utilizes a combination of sacrificial concrete and a protective layer of refractory material to provide a stage of temporary melt retention. The melt plug and

gate are located in the reactor cavity and support the melt retention concept by providing a pre-defined failure location. The melt discharge channel utilizes a steel duct lined with refractory material to direct the conditioned melt from the reactor cavity to the lateral spreading compartment. The spreading area consists of a dedicated cooling structure lined with sacrificial concrete to promote stabilization of molten core debris. The general configuration of the CMSS is provided as Figure 2-13.

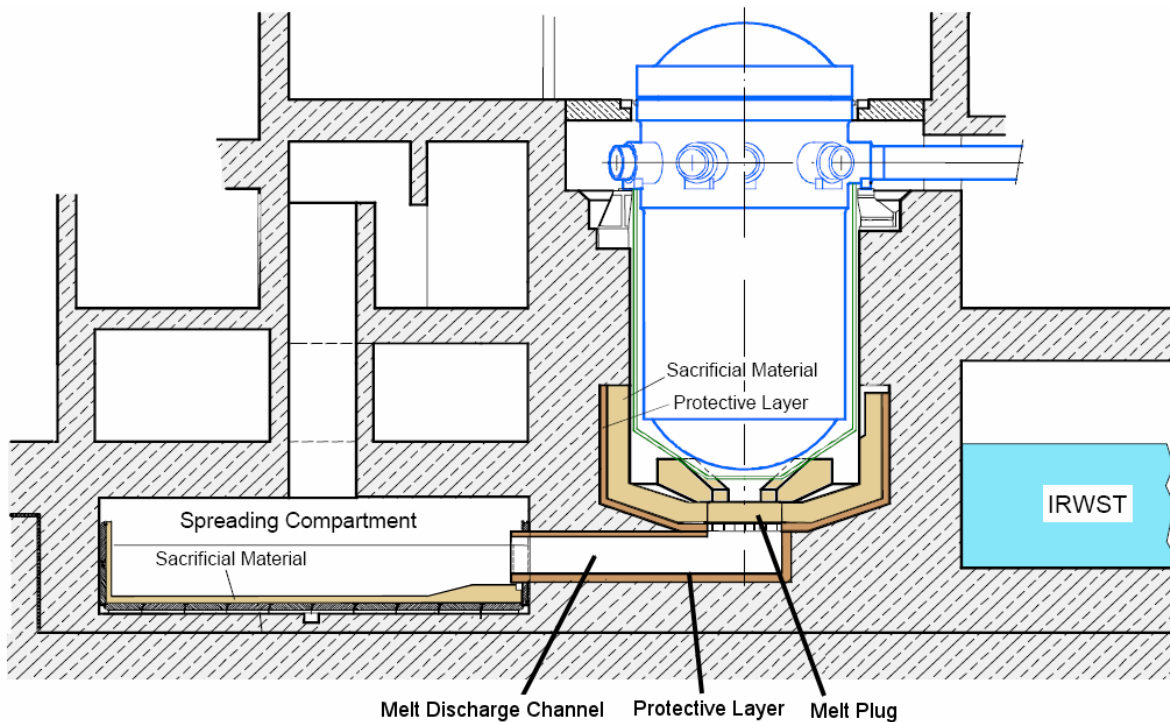


**Figure 2-13 Core Melt Stabilization System**

### 2.2.3.1 Reactor Cavity

The reactor cavity refers to the region between the RPV and the surrounding structural concrete closest to the lower head. Between the RPV and cavity is a layer of insulation limiting heat loss from the vessel and four walls aligned radially from the melt plug effectively creating four 90° azimuthal sectors. These walls are designed to limit the downward expansion of the lower head resulting from contact with a molten pool and provide protection for the reactor cavity integrity in the event of an abrupt vessel failure

that results in a large section of the lower head falling into the reactor cavity. These features ensure that the reactor cavity can withstand the loads resulting from a failure of the RPV under an internal pressure of up to approximately [ .] The reactor cavity region is highlighted in blue in Figure 2-14.

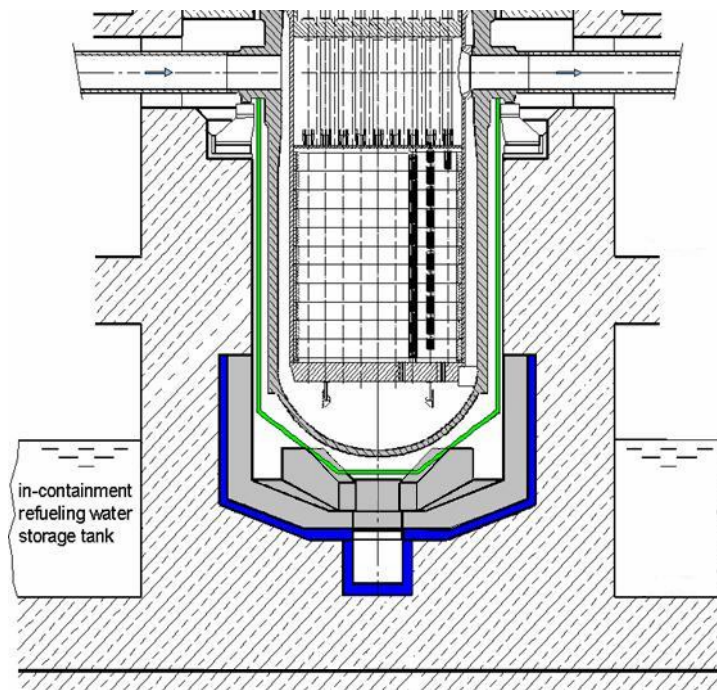


**Figure 2-14 Reactor Cavity**

The reactor cavity provides many functions that support both the operation of the plant and the melt stabilization concept of the U.S. EPR. Similar to existing PWRs, during normal operation, the reactor cavity is designed to support the RPV and act as a biological shield. This “primary shield” isolates adjacent steel structures (primary loops, heat exchangers, etc.) from excessive radiation during reactor operation and provides biological protection for the personnel inside the reactor building. The RPV support is anchored in the reactor cavity wall. This space is sealed at the top by a flexible metallic ring welded to the RPV flange and to the cavity liner.

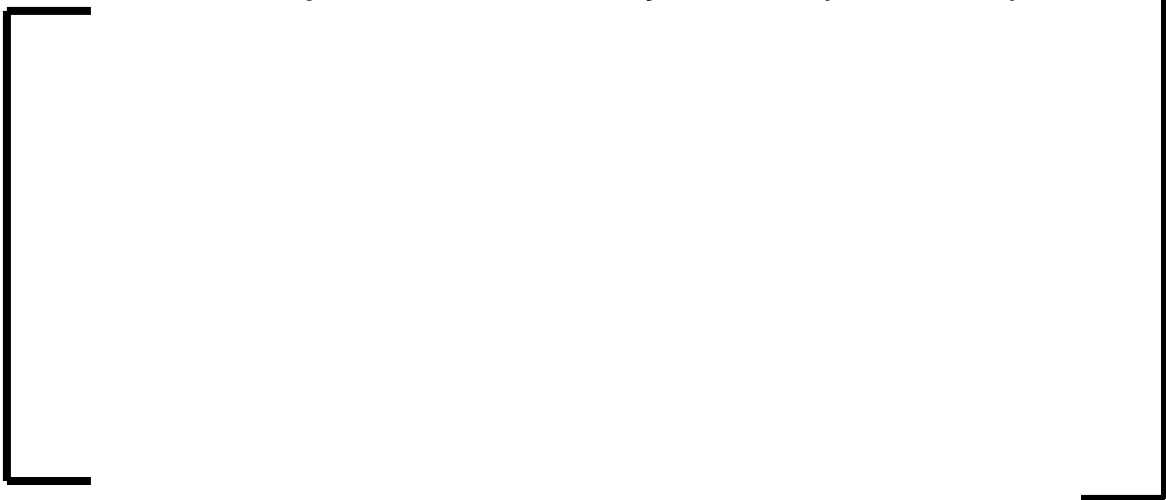
The initial conditions for melt stabilization are determined by the course of in-vessel core degradation, relocation and quenching, and finally by the sequence of melt release

after failure of the lower head. All of these processes involve a degree of uncertainty. To make the U.S. EPR melt stabilization concept tolerant of such uncertainties, the reactor cavity is used to provide a period of temporary melt retention. This period of temporary retention addresses the fact that the predicted release of molten material from the vessel will, most likely, not occur in one pour, but over a period of time.

Temporary retention is provided by a layer of sacrificial material that must be penetrated by the melt before it can escape from the cavity. The corresponding delay, which is determined by the time needed to penetrate the sacrificial layer and to destroy the metallic gate described in Section 2.2.3.2, ensures that even in case of an incomplete first release of melt from the RPV, practically the entire core inventory will be collected in the cavity prior to spreading and stabilization.

The sacrificial layer consists of a 19.7 in (50 cm) layer of siliceous concrete with high iron-oxide content. The sacrificial concrete within the reactor cavity has the following approximate composition:

**Table 2-1 Composition Reactor Cavity Concrete (FeSi/PZ15/8)**



The sacrificial concrete within the reactor cavity also serves to equalize the spectrum of potential melt states by homogenizing the thermo-chemical conditions of the melt release from the vessel. Therefore, the retention phase serves to condition the melt to ensure that the spreading process and subsequent measures are independent of the uncertainties associated with in-vessel melt progression and RPV failure mode. The

advantages of the high iron-oxide content of the reactor cavity concrete are that it oxidizes remaining zirconium and uranium within the melt that can attack the zirconium bricks protecting the structural concrete of the cavity, and it ensures a low melt temperature and viscosity for spreading. The high SiO<sub>2</sub> composition helps the conditioning process through the formation of silicates that lower the radionuclide release from the corium pool.

The sacrificial concrete layer is backed with a refractory material that confines the melt and insulates the RPV support structure in case of a local penetration of the sacrificial concrete. The refractory material consists of zirconia bricks, which have a low thermal conductivity and a mechanical strength greater than concrete. This protective layer “guides” the melt towards the metallic gate of the melt plug, described in Section 2.2.3.2.

Located in the cavity above the level of the protective layer are a number of ventilation inlet nozzles connected by a cylindrical ventilation channel. The channels are extended into the lower region of the cavity by means of rectangular channels embedded in the sacrificial concrete. This ventilation system is used to cool the concrete wall of the reactor cavity during normal operation.

### **2.2.3.2 Melt Plug and Gate**

As previously discussed, the U.S. EPR melt stabilization concept involves a phase of temporary melt retention in the reactor cavity. The melt plug and gate support this concept by acting as a predefined failure location in the reactor cavity through which melt will flow to the spreading compartment. During outages the melt plug can be removed to support maintenance activities in the cavity.

The upper part of the melt plug is essentially a layer of sacrificial concrete with the same composition as the sacrificial layer within the cavity. However, this layer of concrete is not backed by refractory blocks but by an approximately [

.] At the end of the retention phase the

melt plug and gate are designed to fail open with sufficient cross-section to achieve a complete and rapid relocation of the accumulated melt into the lateral discharge channel leading to the spreading compartment. The configuration of the melt plug and gate is shown in Figure 2-15.



**Figure 2-15 Melt Plug and Gate**

The concrete cover of the plug is an integral part of the sacrificial layer in the cavity [ .] Due to the large diameter of the cavity, the ablation front is expected to be relatively even and the entire surface of the gate is expected to be fully uncovered within a short time.

Once the molten core debris comes into contact with the gate, the intensity of the convection within the molten pool is expected to almost instantaneously destroy the aluminum gate. The outflow of melt is limited by the residual concrete layer. The resulting rate of melt discharge after opening the full cross-section of the residual melt plug is substantially greater than that necessary to ensure adequate spreading in the spreading compartment. If the gate initially failed over less than its full cross-section, the diameter of the generated hole would steadily increase due to the heat transfer from the flowing melt. Hole-widening effects make the discharge process self-adjusting: for a small initial opening, the duration of the discharge and the time of interaction will be correspondingly longer.

Figure 2-16 shows the configuration of the gate support frame. [

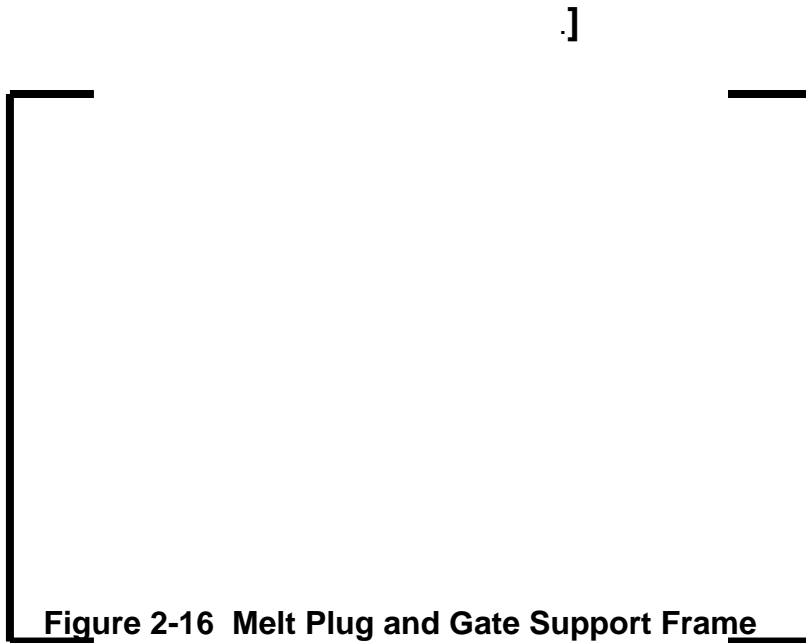


**Figure 2-16 Melt Plug and Gate Support Frame**

### **2.2.3.3 Melt Discharge Channel**

Following the failure of the cavity retention gate, the melt will progress through the transfer channel in a single pour. After passing the outlet of the melt discharge channel, the melt flows over the surface of the spreading compartment.

The melt discharge channel is a welded design with a large rectangular cross section and a length of 24 ft (7.3 m). The channel consists of a steel structure that is embedded within the structural concrete of the containment. The bottom, side walls and top of this structure are layered with refractory material. This protective layer consists of zirconia bricks which have a low thermal conductivity and greater mechanical strength than concrete. The configuration of the discharge channel is depicted in Figure 2-17.

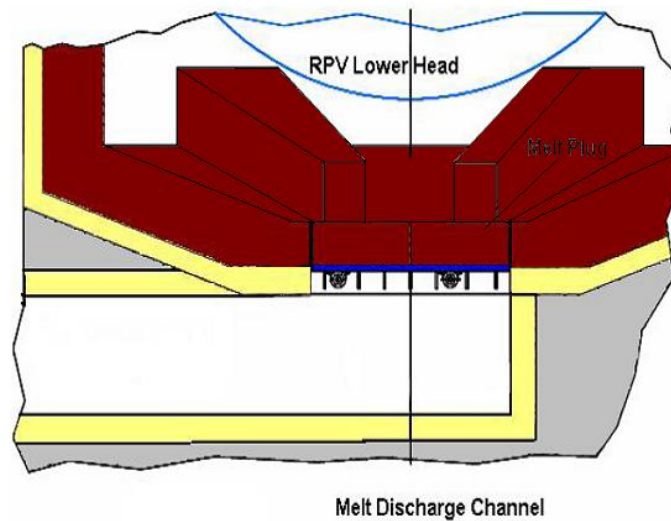


**Figure 2-17 Melt Discharge Channel**

#### **2.2.3.4 Spreading Area and Cooling Structure**

As previously discussed, the CMSS is designed to ensure passive transport of molten core debris through the discharge channel and into the spreading compartment. The spreading area consists of an approximately 1872 ft<sup>2</sup> (170 m<sup>2</sup>) horizontal concrete surface over which the molten core debris can be dispersed. Spreading increases the surface-to-volume ratio of the molten core debris to ensure fast and effective stabilization via subsequent cooling. The spreading area is located in the lower portion of the containment and is surrounded by the IRWST. The configuration of the spreading area surface is provided as Figure 2-18.

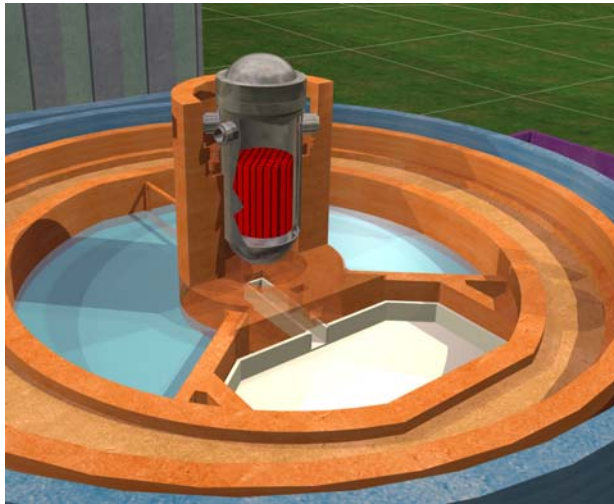


**Figure 2-18 Spreading Compartment**

The design of the spreading compartment prevents accumulation of any large amount of water and ensures that molten core debris will be spread under dry conditions. The spreading compartment is a dead-end room and is isolated from the rest of containment by flood and splash walls. These features prevent the direct inflow of water from sprays, leaks or pipe breaks. Only a limited amount of condensate may form inside the room. Though dry conditions are not required for successful spreading, they make the distribution more predictable and reduce the potential for fuel coolant interactions. The relationship of the spreading compartment to the remainder of the containment is shown in Figure 2-19.

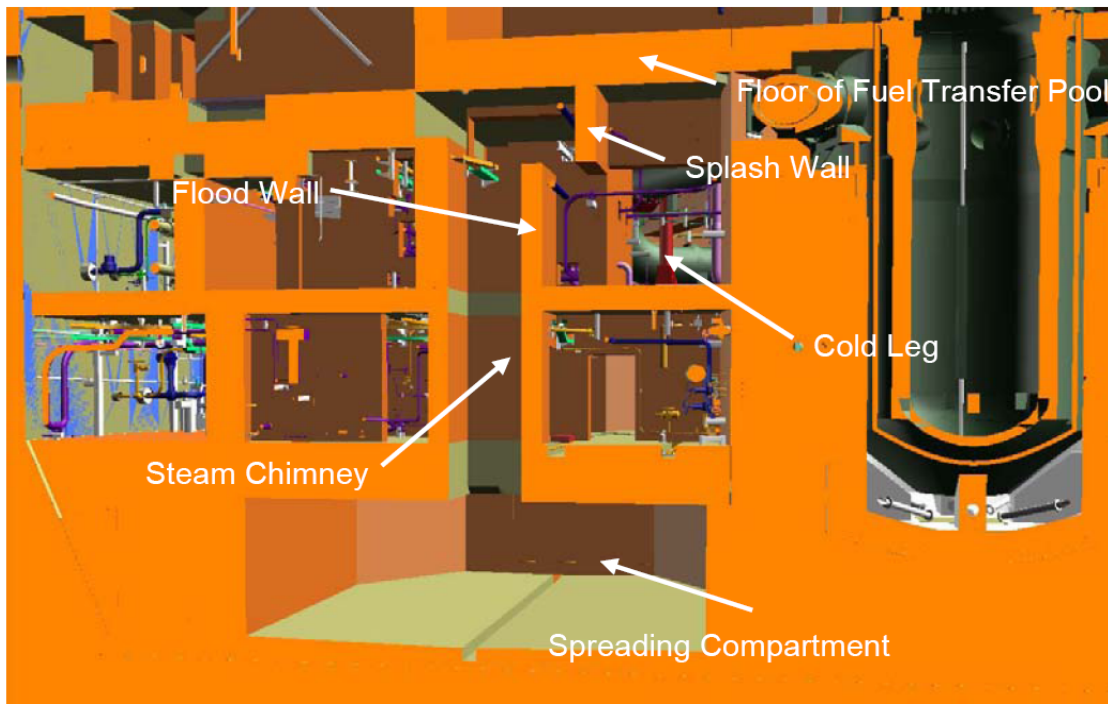


**Figure 2-19 Spreading Compartment Isolation**

The spreading area is essentially a shallow crucible within which molten core debris can be stabilized. The concrete of the spreading compartment covers a dedicated cooling structure used to cool the molten core debris on all sides with water from the IRWST. This dedicated cooling structure consists of a number of cast iron cooling elements that line the floor and side walls of the spreading compartment. To enhance heat transfer, the horizontal and vertical plates have fins that form rectangular cooling channels. The sacrificial concrete layer protects the cooling structure against thermal loads resulting from melt spreading. It also delays melt contact with the metallic cooling structure to ensure that the cooling elements will be flooded with water from the IRWST prior to the initial contact between them and the molten core debris. The structural elements are joined using flexible connections to ensure that the cooling structure is insensitive to expansion and deformation. An example of a cooling element is shown in Figure 2-20.

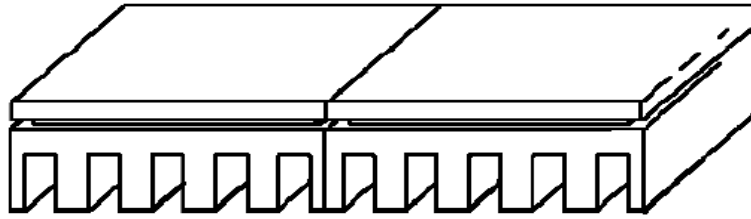


**Figure 2-20 Cooling Structure Elements**

The siliceous sacrificial concrete of the cooling structure is different from that used in the reactor cavity. Its approximate composition is given in Table 2-2. Once it has been ablated by the molten core debris, the molten pool will rest on top of the cooling structure. The combined cooling elements will form a series of parallel cooling channels which provides a flow path for water from the IRWST to flow under the melt, along the side walls and onto the top of the molten core debris, cooling and stabilizing the melt. An example of a cooling structure is given in Figure 2-21.

**Table 2-2 Composition Spreading Room Concrete (Siliceous)**

--	--

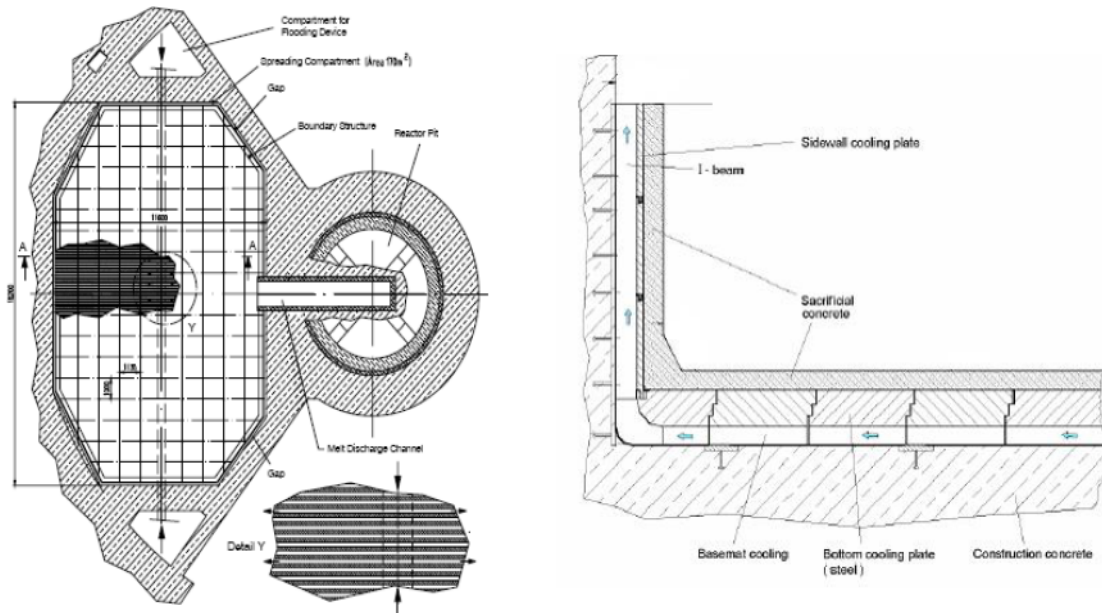


**Figure 2-21 Cooling Structure**

The upper portions of the sidewall elements have a smaller thickness than those at the bottom. Both are stacked inside vertical beams. Flexible connections are ensured by a technique similar to that used for the bottom plate. The outlet of the steam vent at the top is protected to prevent the entry of core debris that could have potentially been splashed.

The arrival of the melt into the spreading compartment triggers the opening of spring loaded valves that initiate the gravity-driven flow of water from the IRWST into the spreading compartment. Initially, as shown in Figure 2-22, a cable holds a spring loaded valve closed. Within the spreading compartment the cable is attached to a thermally sensitive initiator, consisting of a material of low melting point. When the initiator is destroyed during contact with molten core debris, the cable will allow the spring-loaded actuator to open the flooding valve and allow water to flow from the IRWST.

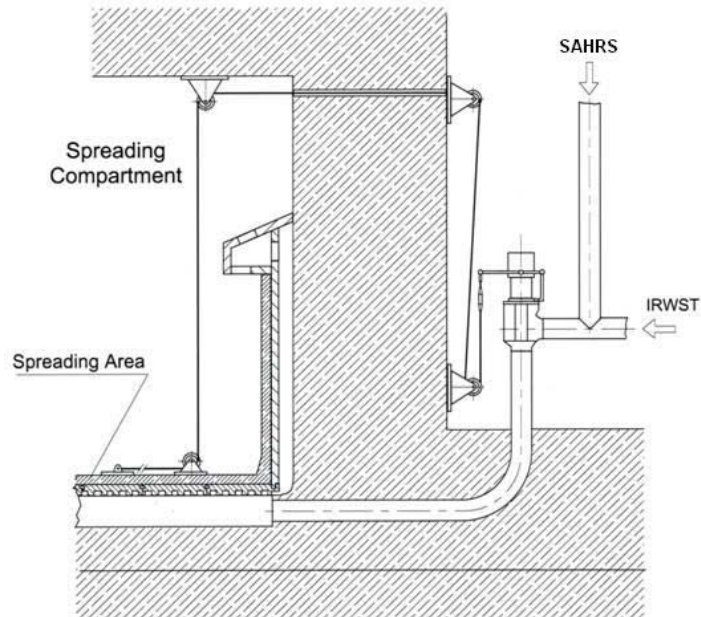


**Figure 2-22 Flooding Valve Actuation**

The water first fills the central supply duct underneath the spreading area. From there, it enters the horizontal cooling channels and then fills the space behind the sidewall cooling structure. Finally the water pours onto the surface of the melt and overflow will continue until the hydrostatic pressure in the IRWST and the spreading room is equal. In parallel with the inflow of water, the spread melt interacts with the sacrificial concrete covering the horizontal and vertical cooling plates. The resulting delay ensures that the walls of the cooling structure will always be cooled on the outside prior to the first contact with the molten corium.

#### **2.2.4 Severe Accident Heat Removal System**

The SAHRS is a dedicated thermal-fluid system used to control the environmental conditions within the containment following a severe accident. As a result, the SAHRS is a non-safety-related system and is not required to meet traditional safety-related design criteria such as consideration of a single failure or seismic events within the design basis. Nonetheless, certain conservative principles and guidelines are

considered within the system. To ensure substantial margin in containment pressure control the SAHRS is designed with 2x100% trains.

The SAHRS has four primary modes of operation, each playing a role in controlling the environmental conditions within the containment so that its fission product retention function is maintained. These modes of SAHRS operation include:

- Passive cooling of molten core debris
- Active spray for environmental control of the containment atmosphere
- Active recirculation cooling of the molten core debris and containment atmosphere
- Active back-flush of the IRWST.

Each of the two identical SAHRS trains is located in dedicated, radiologically-controlled rooms within two of the four plant safeguard buildings. Each SAHRS train includes:

- A dedicated suction line from the IRWST
- Containment isolation valves
- A pump to support active recirculation
- A heat exchanger for containment heat rejection
- Discharge lines to a containment spray header, the spreading room, and sump screen
- Support from a dedicated cooling chain via plant auxiliary systems.

The SAHRS heat exchangers transfer the residual heat from the containment to the ultimate heat sink via dedicated portions of Component Cooling Water (CCW) and Essential Service Water (ESW) trains. During operation, the three possible flow paths downstream of the pump and the heat exchanger are:

1. To a containment spray system with a ring header and spray nozzles
2. To the spreading area of the CMSS
3. To a sump screen flushing device which is used to remove accumulated debris.

The general configuration of a single SAHRS train is provided in Figure 2-23.

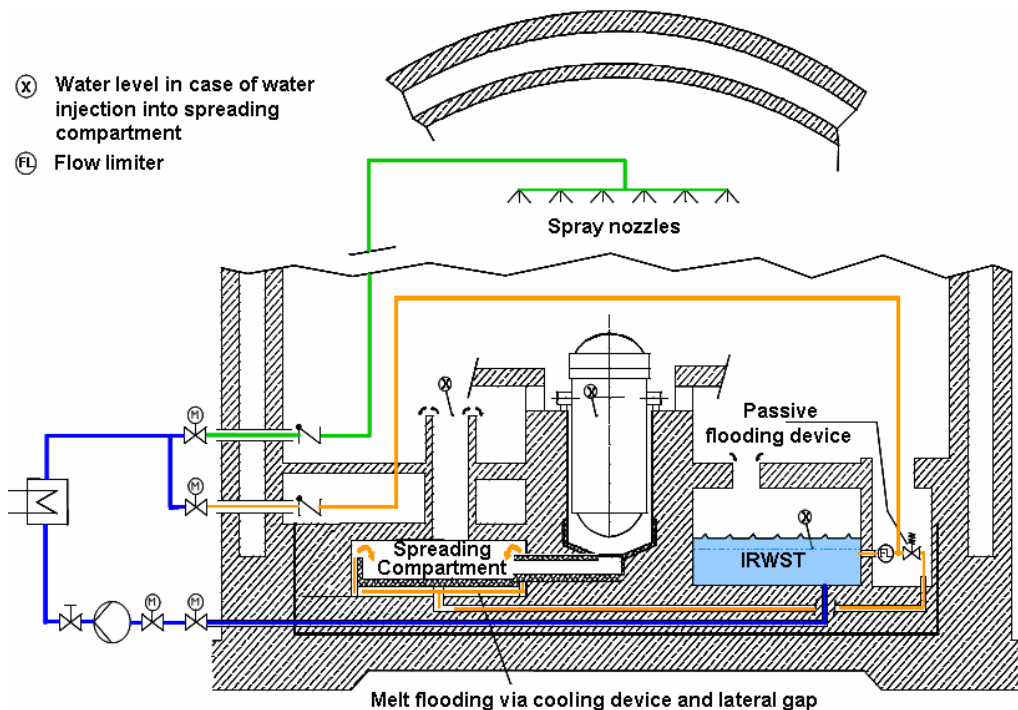


**Figure 2-23 Severe Accident Heat Removal System**

#### 2.2.4.1 *Passive Cooling of Core Debris*

As discussed in Section 2.2.3, the U.S. EPR includes a CMSS to stabilize molten core debris resulting from a severe accident. The SAHRS provides the cooling water to the cooling structure used for melt stabilization as described in Section 2.2.3.4. Once molten core debris is within the spreading compartment, water from the IRWST will passively start to fill the cooling structure. This dedicated flooding line is equipped with a flow limiter downstream of the IRWST outlet, which limits the flow to around 13,000 lb/min. This expected flow rate fills the cooling structure within five minutes. Water then

overflows into the spreading compartment until it is hydrostatically balanced with water from the IRWST. This flooding is expected to result in submersion of the spreading area and transfer channel, as well as a portion of the reactor cavity, thereby stabilizing any residual core debris in those areas.

Operating in this passive mode, IRWST water supplied by the SAHRS will be boiled-off as steam and released into the free volume of the containment through the steam chimney directly above the spreading compartment as shown in Figure 2-24. As this process continues, the temperature and pressure within the containment will steadily increase; however, the U.S. EPR containment is designed with sufficient free volume and structural heat sinks that atmospheric conditions of the containment will not approach design limits for several hours following the onset of core damage.

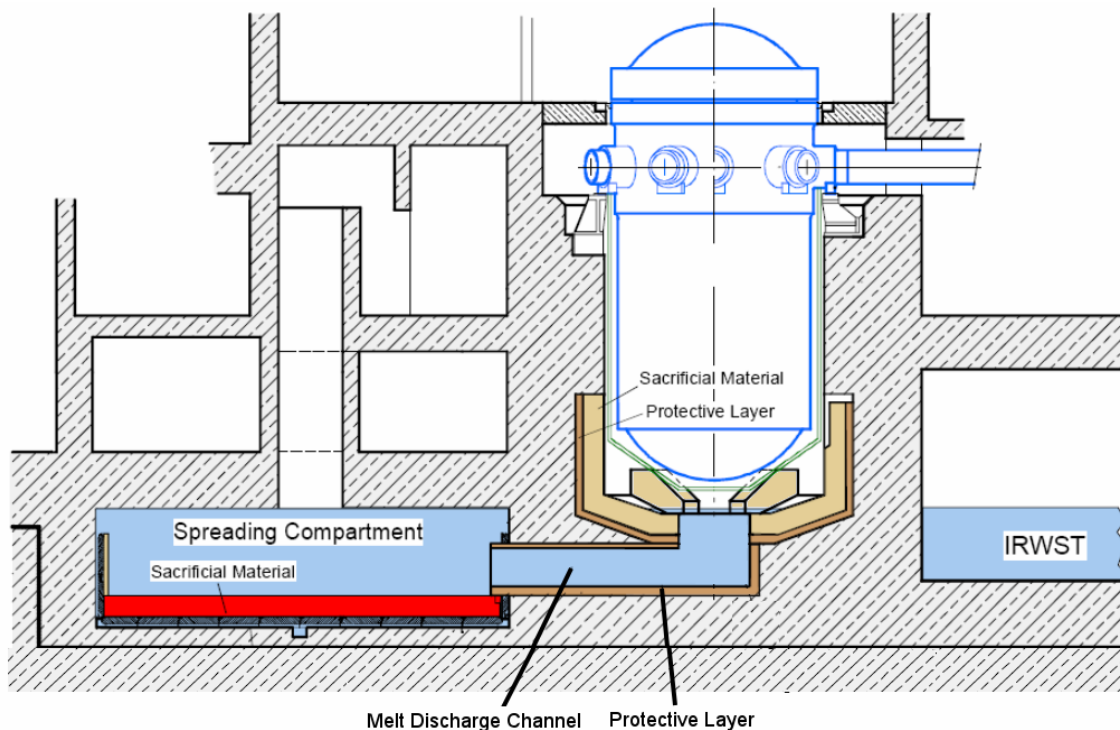


**Figure 2-24 Passive Cooling of Molten Core Debris**

#### **2.2.4.2 Active Containment Spray**

As was previously discussed, the U.S. EPR containment has sufficient capacity to allow a grace period of several hours before operator action is needed to prevent the environmental conditions within the containment from exceeding design values following a beyond design basis accident. When activated, the SAHRS is configured to first operate in the containment spray mode.

When operating in the containment spray mode, the SAHRS takes suction from the IRWST; coolant then flows through a heat exchanger outside containment prior to being routed back to the spray headers located in the upper volume of the containment. The spray water condenses atmospheric steam as the water droplets fall through the containment atmosphere. The resulting condensate then flows along the structural elements of the containment before being routed back into the IRWST for continued recirculation.

The U.S. EPR containment spray is smaller in capacity than containment spray systems of conventional plants and other evolutionary designs. For example, the U.S. EPR containment spray system is an approximately 1600 gpm system compared to around 5000 gpm for other evolutionary PWR designs. The difference in capacities is a direct function of intended use. The containment spray system in the conventional operating fleet and other evolutionary plants has been used for environmental control of the containment atmosphere following design basis events, whereas the spray in the U.S. EPR is strictly for severe accident mitigation.

The SAHRS also provides a defense-in-depth function by scrubbing fission products from the containment atmosphere. While this function is not needed to meet relevant dose requirements for design basis events, it further demonstrates a consistent approach in regard to protecting the health and safety of the public through a robust defense-in-depth philosophy.

---

### **2.2.4.3 Active Recirculation Cooling**

As a core melt accident progresses, it can become necessary to use the recirculation function of the SAHRS to further control the environmental conditions within the containment. As previously discussed, the containment spray can be used to condense atmospheric steam with the condensate returning to the IRWST where it can be used as additional inventory for continued passive cooling of the molten core debris. Once the containment spray has sufficiently reduced containment pressure, the SAHRS can be switched to a long-term recirculation mode where the SAHRS feeds water directly into the spreading area. As a result, the water pool in the cooling channels and on top of the melt will become subcooled. Decay heat will now be removed from the spread melt by single-phase flow, instead of by evaporation into the containment atmosphere. This way an ambient pressure level can be maintained in the containment in the long-term, thereby further reducing the potential for the release of activity.

In this mode of operation, the water level in the spreading compartment will rise to the top of the steam outlet chimney, overflow onto the containment floor and drain back into the IRWST where it can be recirculated back into the spreading area cooling system. Because the spreading compartment and the reactor cavity are connected through the now open gate and transfer channel, water will also enter the reactor cavity and submerge the vessel up to the level of the RCS piping. This establishes long-term cooling of any debris that has remained within the transfer channel, the reactor cavity, or the vessel itself. Operation in this mode is depicted as Figure 2-25.

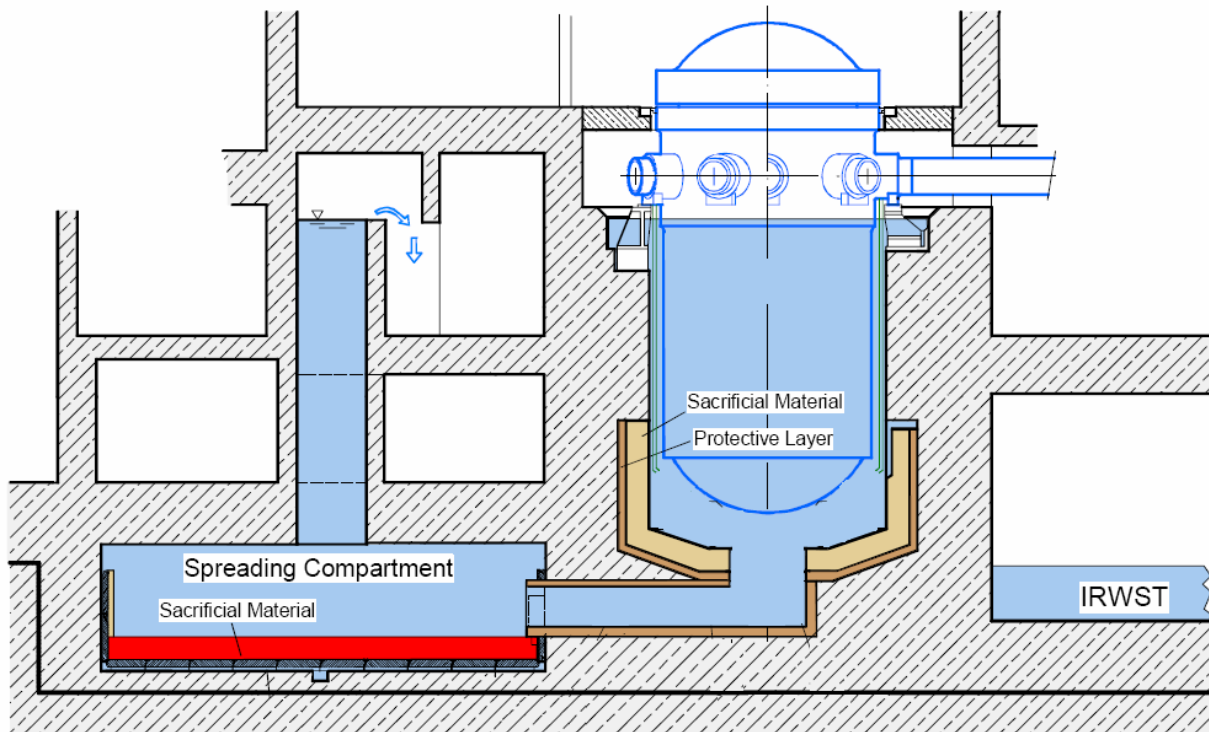


**Figure 2-25 Active Melt Retention System Cooling**

#### **2.2.4.4 IRWST Backflush**

The final mode of operation of the SAHRS is to provide a back-flushing function within the IRWST. Operation in this mode serves to dislodge any debris from the sump strainers that might compromise the ability of the SAHRS to draw water from the IRWST. Only a fraction of the SAHRS is used for back-flushing; therefore, the system can operate in this mode while continuing operation in another containment cooling mode.

#### **2.2.4.5 SAHRS Dedicated Cooling Chain**

To support the active heat removal modes of the SAHRS, dedicated portions of the CCW and ESW systems are used to form a dedicated cooling chain to transfer heat to the ultimate heat sink. These dedicated cooling trains are composed of a non-safety CCW and ESW train for each SAHRS train. This cooling chain is dedicated to severe accident operation and is not used to support normal plant operations or mitigate the

effects of a design basis event. Both the CCW and ESW are designed to receive power for either EDGs or SBO diesels.

Each of the CCW trains consist of a pump located upstream of a dedicated heat exchanger, a surge tank connected to the pump suction line and a demineralized water supply line with a pressurizing pump. This portion of the cooling chain feeds water to the shell side of the SAHRS heat exchanger where containment heat is removed and discharged through the tube side of the CCW heat exchanger interfacing with ESW. The pressurizing pump ensures the demineralize water supply to this CCW train and pressurization of the surge tank. The surge tank allows for pressurization of the dedicated CCW trains to ensure an outflow of the system cooling medium in the event of a rupture in the SAHRS heat exchanger. This is necessary to prevent a contamination of the cooling chain by leakage of radioactive water at the SAHRS heat exchanger.

The ESW train essentially consists of a pump whose inlet is separated from the ultimate heat sink by a strainer. This ESW train supplies water to the shell side of the CCW heat exchanger where it removes transferred heat and rejects it back into the ultimate heat sink.

### **2.2.5 Severe Accident Instrumentation and Control**

The U.S. EPR includes dedicated instrumentation and controls (I&C) that are part of the overall severe accident management concept. These I&C functions can be categorized as (1) those necessary to perform operator action, and (2) those necessary to closely monitor the progression of a severe accident. Specific I&C can be further identified by association with those severe accident features utilized to mitigate the effect of a severe accident as follows:

1. Support of RCS depressurization
2. Monitoring of melt progression

3. Monitoring of hydrogen mitigation
4. Monitoring of containment heat removal
5. Monitoring of overall plant behavior

While other I&C may be necessary to support the ultimate strategies for severe accident management, the functionality of the primary plant I&C facilitating severe accident management is described in the following sections.

#### **2.2.5.1 Support of RCS Depressurization**

As discussed in Section 2.2.1, the U.S. EPR includes dedicated depressurization valves to ensure that a core melt does not progress ex-vessel under high pressure conditions. The system is actuated manually based on a defined core outlet temperature. The U.S. EPR includes the following provisions to support reliable RCS depressurization:

- *Measurement of Core Outlet Temperature.* Provided to allow the operator to anticipate the onset of core damage
- *Manual Actuation of Severe Accident Depressurization Valves.* Provides the ability to depressurize the RCS during a severe accident
- *Position Indication for Severe Accident Depressurization Valves.* Provides the ability to monitor the state of the depressurization valves
- *Measurement of RCS Pressure.* Provides the ability to monitor the effectiveness of RCS depressurization prior to failure of the RPV.

#### **2.2.5.2 Monitoring of Melt Progression**

As previously discussed, the U.S. EPR uses a dedicated CMSS to bring molten core debris released from the RPV into a safe, stable condition. While this process is entirely passive, dedicated measurements are provided within the plant to monitor the progression of the core melt, including:

- *Monitoring of RPV Failure.* Thermocouples in the RPV insulation are used to measure the outside temperature of the RPV lower head. The temperature evolution of the RPV lower head allows the operator to predict the onset of RPV failure. Failure of the thermocouples in the RPV insulation provides the operator indication that the RPV has failed.
- *Monitoring of Corium in the Spreading Compartment.* The arrival of molten core debris within the spreading compartment triggers the actuation of the passive flooding valves of the SAHRS. Position indication of these valves allows the operator to determine that the conditioned core melt has flowed into the spreading compartment. IRWST level indication provides redundant information relative to passive flooding initiated by molten core debris in the spreading compartment.
- *Monitoring of Basemat Failure Threat.* Thermocouples located in the central cooling water supply duct of the CMSS cooling structure allows the operator to determine if molten core debris has entered the cooling channels either through increasing temperature readings or a loss of function.

### **2.2.5.3 Support of Hydrogen Mitigation**

As discussed in Section 2.2.2, the U.S. EPR uses a CGCS to control post-accident hydrogen within the containment. While this hydrogen mitigation process is entirely passive, dedicated measurements are provided within the plant to monitor the progression of its effectiveness.

- *Measurement of Hydrogen Concentration.* Hydrogen concentration is monitored in various parts of the containment including the upper dome and the steam generator, pressurizer, and pressurizer valve compartments. Hydrogen concentration measurements allow the effectiveness of recombination to be monitored as well as the potential for combustion within the containment.

- *Actuation of Hydrogen Mixing Dampers.* Provides the ability to open the mixing dampers either automatically on measured containment pressure or manually from the control room.
- *Position Indication of Hydrogen Mixing Dampers.* Provides the ability to monitor the state of the mixing dampers.

#### **2.2.5.4 Monitoring of Containment Heat Removal**

As discussed in Section 2.2.4, the U.S. EPR uses a SAHRS to control the long-term, post-accident, environmental conditions within the containment. To control containment pressure, the system is operated in an active mode with either a containment spray or long-term recirculation. This system is manually started on a defined containment pressure and supported by the dedicated cooling chain as described in 2.2.4.5. The U.S. EPR includes the following provisions to monitor containment heat removal:

- *Measurement of Containment Pressure.* Provided to identify the need for active containment cooling.
- *Measurement of IRWST Temperature.* Provided to monitor system performance during operation.
- *Measurement of SAHRS Heat Exchanger Inlet Temperature.* Provided to monitor system performance during operation.
- *Measurement of SAHRS Heat Exchanger Outlet Temperature.* Provided to monitor system performance during operation.
- *Measurement of SAHRS Flow Rate.* Provided to monitor system performance during operation.
- *Measurement of SAHRS Sump Level.* Provided to identify fluid leakage from SAHRS trains.

- *Measurement of IRWST Water Level.* Provided to monitor remaining water level available and measure system performance during operation.
- *Measurement of SAHRS Pump Inlet Pressure.* Provided to identify sump strainer clogging and need to align the system for operation in back flush mode.
- *Measurement of CCW Heat Exchanger Inlet Temperature.* Provided to monitor system performance during operation.
- *Measurement of CCW Heat Exchanger Outlet Temperature.* Provided to monitor system performance during operation.
- *Measurement of CCW Flow Rate.* Provided to monitor system performance during operation.

#### **2.2.5.5 Monitoring of Overall Plant Behavior**

To support the overall severe accident performance of the plant, the U.S. EPR includes a number of additional I&C indications. The U.S. EPR includes the following provisions to monitor overall plant behavior during a severe accident:

- *Position Indication of Containment Isolation Valves.* Provides the ability to monitor the status of the outboard containment isolation valves.
- *Measurement of Containment Radiation Level.* Provides the ability to measure fission product concentration within the containment following a severe accident.
- *Measurement of Annulus Radiation Level.* Provides the ability to measure the fission product concentration in the annulus region resulting from leakage from the primary containment.
- *Measurement of Annulus Pressure.* Provides the ability to measure the post-accident annulus pressure and detect leakage into the annulus.

- *Measurement of Safeguard Radiation Level.* Provides the ability to evaluate the environmental conditions and measure the dose in safeguard buildings 1 & 4.
- *Measurement of Radioactive Release from the Plant.* Redundant gamma detectors are located downstream of the AVS filters to measure activity release to the environment.

### **2.2.6 Severe Accident Uninterruptible Power Supply System**

The UPS system for severe accident management is a non-class 1E system. In a severe accident with loss of all AC power sources, this dedicated UPS supplies necessary equipment and process instrumentation needed for severe accident management for up to 12 hours.

During normal operation (AC power available) the UPS is fed via the rectifiers and DC/AC inverter. In these operation modes the battery is kept charged by the rectifier in floating charge mode. The rectifier is able to charge the battery and to feed, at the same time, the highest loads.

During a loss of all AC power (offsite power, all EDGs and SBO diesels), necessary plant features are fed from the 12 hour battery until an AC power source can be recovered. Therefore, in a severe accident with loss of all AC power, necessary equipment used to manage the effect of a severe accident will be available for 12 hours, which is expected to be sufficient until an AC power source can be restored.

### **3.0 SAFETY ISSUE RESOLUTION EVALUATION METHODOLOGY**

Associated with rare, hazardous events, such as nuclear power plant severe accidents, is a degree of uncertainty that provides a significant challenge to the evaluation and resolution of related design and analysis methods issues. For events occurring at some sufficiently observable frequency, design improvements can evolve through the understanding gained from such events, leading to long-term acceptance. This is not an option for severe accident design. The U.S. EPR severe accident response design features and analytical methods have evolved following a process of:

- Establishment of aggressive safety goals
- Identification of processes and phenomena
- Iterative design processes focused on risk reduction
- Collaborative international testing programs
- Expert elicitation on important severe accident safety issues.

Consistent with current U.S. regulatory requirements and guidance, final acceptance and resolution of relevant beyond-design-basis events is demonstrated through detailed process studies and probabilistic analyses. The unique characteristic of this process for severe accidents is the consideration of risk in the resolution of severe accident safety issues. For the U.S. EPR, design features have been incorporated which have significantly reduced risk relative to current-generation PWRs. Practical consideration of this reduced risk requires that this information be incorporated into measures not only of acceptable performance, but also of relevance.

One objective of any severe accident safety issue resolution methodology is the determination of the calculation matrix necessary to demonstrate the performance of a plant's severe accident response features. The performance figure of merit in all cases is the demonstration that the containment is preserved as a leak-tight barrier for at least 24 hours (Reference 10). By virtue of the inherent low probability of severe accidents,

there is broad diversity in postulated mechanisms that can lead to containment failure.

In light of this divergent situation, priority must be established so that meaningful conclusions can be drawn from analysis.

AREVA NP's approach to safety issue resolution for severe accidents draws on aspects and ideas incorporated in two previously-published methodologies:

- the Risk Oriented Accident Analysis Methodology (ROAAM) (Appendix A of Reference 12, Reference 13, Reference 14), and
- the Integrated Structure for Technical Issue Resolution (ISTIR) (Reference 15, Reference 16).

These two methods approach the issue of priority and importance on the path towards issue resolution uniquely, with the ROAAM emphasizing risk and expert elicitation and ISTIR emphasizing phenomenology and scaling. These two approaches are briefly described in this section followed by a description of AREVA NP's approach.

### **3.1 *Risk Oriented Accident Analysis Methodology***

ROAAM is specifically aimed at key containment integrity (or even vessel integrity) issues. As such, it has to be used in the context of the whole realm of severe accident scenarios. This includes their respective plant damage states, as all severe accidents, by definition, challenge containment integrity. A crucial aspect of ROAAM is that the "physical consistency" that permeates the quantification is carried over to a similar consistency with what is "physically possible." This "consistency" is found by applying a screening-out level of frequency on major contributing classes of plant damage states and by ensuring that the Level 1 PRA quantifications examined for such screening are in themselves sufficiently robust. This provides the initial context of selecting the enveloping scenarios within the ROAAM. In practical terms this consistent approach addresses core melt frequency goals in the "frequency" domain, and containment integrity goals (but only for severe accident sequences above the screening level) in the "qualitative probabilistic" domain; that is, physically-based probability scale representing

judgmental degrees of belief. Since the emphasis is on high-confidence assessments (i.e., in removing the intangible factors), accident management becomes a natural integral part of ROAAM.

Decision making with ROAAM requires identification of a threshold of importance, described, for example, by the conditional containment failure probability. This evaluation is defined by expert elicitation. Outside this threshold, events are considered “remote and speculative.” The essential element of the ROAAM methodology is, therefore, to define a severe accident “defense-in-depth” concept obtained by requiring that containment failure is “physically unreasonable” for all accidents that are not “remote and speculative.” The quantification of probabilistic elements in ROAAM are derived such that one can explicitly recognize, and accept, that at certain high levels of reliability, system failures as a whole can be considered “remote and speculative.” As such, they can be ignored. It follows, therefore, that the treatment of deterministic elements is based on identification of dominant and quantifiable physics. Acceptance is established when it can be shown that containment failure for postulated events is “physically unreasonable.”

### **3.2      *Integrated Structure for Technical Issue Resolution Methodology***

The ISTIR is a physically-based methodology that integrates experiments, analyses, and uncertainty quantifications. This integrated experimental and analytical program structure for solving safety issues is achieved by five components:

- Component I - Identification of safety issues and phenomena evaluation
- Component II - Characterization of these in terms of scaling parameters from experimental programs
- Component III - Development and qualification of models and correlations
- Component IV - Development of computational codes for integral analyses
- Component V - Quantification of total uncertainty

To provide sufficiency and efficiency, both experiments and analyses include features of the inductive (top-down) approach that considers the whole system, and of the deductive (bottom-up) approach that focuses on the parts. The top-down approach ensures that the experimental and analytical methods used to resolve issues are comprehensive, systematic, auditable, and traceable. The bottom-up approach ensures that all important features of an issue are fully addressed.

The ISTIR methodology evaluates importance based on the outcome of scaling analyses, rather than the broader evaluation of all phenomena contributing to a particular phenomenological outcome. The identification of scaling parameters provides the necessary phenomenological insight on the important aspects of a particular scenario or process; thus, bypassing unnecessary sensitivity analyses normally required to determine importance.

Final resolution is achieved through analyses following the Code Scaling, Applicability, and Uncertainty methodology (Reference 17). The uncertainty quantifications determined for special models and correlations are convolved for integral analyses and margin to limit. The margin to limit is evaluated with total uncertainty quantified.

### **3.3      *AREVA NP's Adaptation***

AREVA NP's evaluation methodology for severe accident safety issue resolution departs from the original treatments of the ROAAM and ISTIR methods. AREVA NP recognizes that each methodology, taken individually, serves a specific role in addressing the most demanding examples of issue resolution (i.e., of low frequency, high consequence), including DCH (References 12 and 15) and lower head failure from in-vessel steam explosion (Reference 18). This appears to be the ideal application for these methods as they provide the rigorous approach necessary for such highly uncertain containment failure challenges, characterized by phenomena on a very short time scale.

For the broader objective of complete and comprehensive design validation, AREVA NP recognizes that severe accident safety issues are resolved by demonstrating

comprehensive severe-accident-related engineering through applicable testing programs, process studies demonstrating certain deterministic elements, and PRA. Therefore, AREVA NP’s evaluation methodology begins with the identification of safety goals, documentation of severe accident engineering activities addressing related issues, derivation of a calculation matrix, and presentation of analysis results based on the derived calculation matrix. This is detailed in Figure 3-1. While the major components of severe accident engineering are the credited test programs (Section 5.0) and corresponding analytical methods (Section 6.0), the identification of the necessary analyses involves engineering insights that combine regulation, industry experience, fundamental understanding of thermal-hydraulic and severe accident phenomena, and risk/consequence factors. It is this element of AREVA NP’s safety issue resolution evaluation methodology that incorporates some of the seminal ideas of both the ROAAM and ISTIR methodologies.

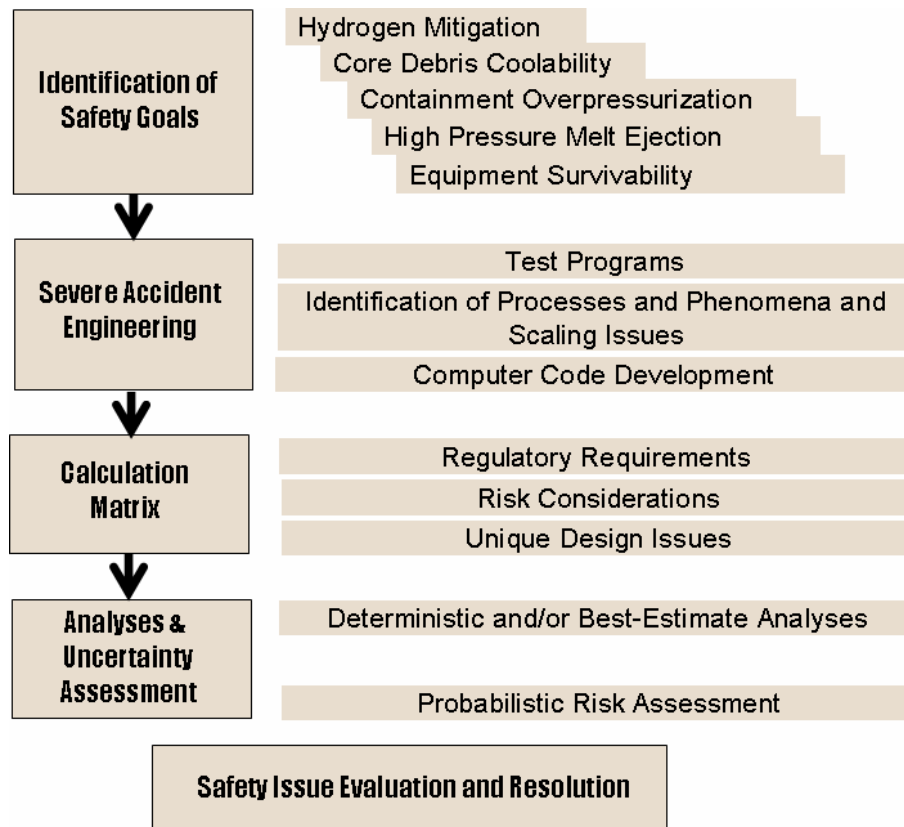


**Figure 3-1 Process for Severe Accident Safety Issue Resolution**

The goal of both ROAAM and ISTIR is to clearly formulate a safety issue in terms of its fundamentals, both from a risk/consequence position and a phenomenological position. From the ROAAM approach, the AREVA NP approach incorporates risk/consequence information from PRA to identify the “relevant” events that could challenge containment integrity. From the ISTIR approach, the AREVA NP approach categorizes event classes based on dominant phenomena, identified through testing programs and related scaling analyses. This list is then reduced by eliminating improbable single-failure considerations that are not required for beyond design basis events. The list is further refined by applying engineering judgment to define a threshold of relevance based on CDF, combined with additional applicable probabilistic failure rate data, if available. This step declares that the remote nature of such events or event classes does not merit detailed assessment. This filtering of events and event classes is done exclusively to identify the specific process studies on containment integrity for the purpose of deterministic safety issue evaluation associated with severe accident phenomenology. All originally identified events and event classes are expected to be retained for PRA.

The U.S. EPR severe accident response features have been designed to reduce or eliminate many of the uncertainties associated with severe accident progression. Low probability events with multiple failures and coincident occurrences up to the total loss of safety-grade systems are necessary assumptions to reach the threshold for a severe accident. For PRA, many scenarios will be exercised to evaluate the likelihood of core damage (Level 1) and containment failure (Level 2) in order to demonstrate the acceptable performance of severe accident response features of the U.S. EPR. In deriving a calculation matrix for process studies of the U.S. EPR severe accident response features, for the purpose of deterministic safety issue evaluation, it is expected that the characterization of relevant events and event classes of severe accidents identified by PRA will credit:

- isolated containment (no bypass issue)
- full RCS depressurization

- 
- passive protection of the containment liner
  - available, active SAHRS
  - well-mixed containment atmosphere
  - reliable hydrogen recombiner performance.

Wherever possible, subsequent process studies will apply deterministic analyses with bounding assumptions to demonstrate acceptable containment response. As needed, best-estimate analysis with uncertainty quantification can be performed. In such cases, phenomenological insights gained from experiments and/or analytical models would be convolved into the task of quantifying uncertainty. Reference 19 provides an example best-estimate plus uncertainty analysis used to address risk-informed assessment of hydrogen control measures.

Section 6.5 provides further discussion on how this methodology for deriving the calculation matrix will proceed.

Specific to DCH and lower head failure from in-vessel steam explosion, applicable previously-published analyses using ROAAM and ISTIR will be credited (as discussed in the respective subsections of Section 6).

### **3.4 Methodology Objectives**

The results of AREVA NP's Safety Issue Resolution Evaluation Methodology will appear in the U.S. EPR DCD. Application of the described approach provides a list of relevant severe accident scenarios that 1) provide insight into plant-specific severe accident processes and phenomena and 2) form the basis for a calculation matrix. Processes and phenomena can be characterized in terms of parametric performance ranges (i.e., an uncertainty measure) from applicable test program results and incorporated into computational analysis tools, such as MAAP4 for production analyses and MELCOR for self-audits. These tools are used to establish the limits of these processes and

---

phenomena through the demonstration of the U.S. EPR's severe accident response capability to the relevant severe accident events.

The remainder of this report presents the elements of this severe accident evaluation methodology for issue resolution. Specifically,

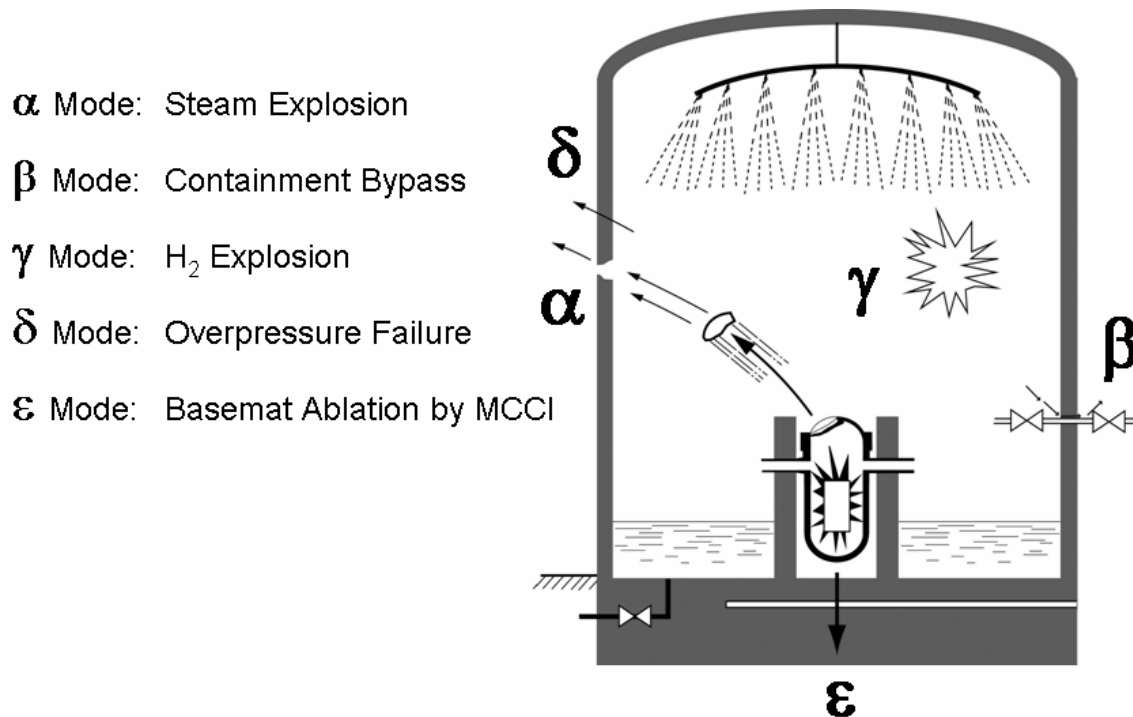
- Identification of Safety Goals, Section 4.1
- Identification of Processes and Phenomena, Section 4.2
  - A Hypothetical Phenomenologically-Bounding Severe Accident, Section 4.2.1
  - Presentation of Severe Accident Processes and Phenomena, Section 4.2.2
  - Scaling Analysis for Phenomenological Importance, Section 4.2.3
- Assessment of applicable research and development programs, Section 5.0
- Analysis Methods, Section 6.0
  - Overview of the U.S. EPR Analytical Methodology, Section 6.1
  - Code Applicability, Section 6.2
  - Validation of Analytical Tools, Section 6.3
  - Description of U.S. EPR Analytical Models, Section 6.4
  - Calculation Matrix for Safety Issue Resolution, Section 6.5
- Sample Problem Analyses, Section 6.0.

#### 4.0 DESCRIPTION OF SEVERE ACCIDENT SAFETY ISSUES

The description of severe accident safety issues provide the initial framework for applying AREVA NP's evaluation methodology for severe accident safety issue resolution through the identification of safety goals and processes, and phenomena for one of the more challenging severe accidents in the U.S. EPR: the large-break LOCA without active safety injection.

#### 4.1 *Identification of Safety Goals*

The ultimate safety goal of any nuclear power plant is the protection of the public from uncontrolled release of fission products through a breach in containment following a severe accident. As outlined in WASH-1400 (Reference 20), the commonly recognized modes of containment failure following a postulated severe accident are shown in Figure 4-1.



- $\alpha$  Mode: Steam Explosion
- $\beta$  Mode: Containment Bypass
- $\gamma$  Mode: H<sub>2</sub> Explosion
- $\delta$  Mode: Overpressure Failure
- $\epsilon$  Mode: Basemat Ablation by MCCI

**Figure 4-1 Postulated Containment Failure Mechanisms**

With the exception of containment bypass, these containment failure mechanisms are expected to be mitigated through design features. The containment bypass mode is addressed through preventive features and demonstrated in Level 2 PRA. To benchmark plant safety for new LWR designs, the NRC has outlined in SECY-93-087 the following general criteria.

#### Hydrogen Mitigation

- accommodate hydrogen generation equivalent to a 100% metal-water reaction of the fuel cladding
- limit containment hydrogen concentration to no greater than 10%
- provide containment-wide hydrogen control for severe accidents.

#### Core Debris Coolability

- provide reactor cavity floor space to enhance debris spreading
- provide a means to flood the reactor cavity to assist in the cooling process
- protect the containment liner and other structural members with concrete, if necessary
- ensure that the best-estimate environmental conditions (pressure and temperature) resulting from core-concrete interactions do not exceed Service Level C for steel containments or Factored Load Category for concrete containments, for approximately 24 hours. Also ensure that the containment capability has margin to accommodate uncertainties in the environmental conditions from core-concrete interactions.

#### High Pressure Melt Ejection (HPME)

- provide a reliable depressurization system

- provide cavity design features to decrease the amount of ejected core debris that reaches the upper containment.

### Containment Performance

- The containment should maintain its role as a reliable, leak-tight barrier for approximately 24 hours following the onset of core damage under the more likely severe accident challenges. Following this period, the containment should continue to provide a barrier against the uncontrolled release of fission products.

### Equipment Survivability

- Maintain reliability of functions during relevant severe accident scenarios.

## **4.2 Identification of Processes and Phenomena**

The derivation of the dominant processes and phenomena associated with relevant U.S. EPR severe accident scenarios has considered the body of severe accident research and development, identification of analysis objectives, and expert opinion. Also considered is the robust severe accident mitigation features included in the U.S. EPR design, meaning that certain uncertainties normally associated with severe accident processes and phenomena that can be either bounded or eliminated. To illustrate the procedure for identifying these severe accident processes and phenomena, a process is demonstrated for identifying a hypothetical phenomenologically-bounding severe accident for a sequence of events proceeding to RPV failure. A table identifying the severe accident processes and phenomena is then presented to chronologically map the accident description.

### **4.2.1 A Hypothetical Phenomenologically-Bounding Severe Accident**

As previously discussed, the primary depressurization system for severe accidents is designed as a highly reliable mitigation feature for severe accidents in the U.S. EPR. The rapid depressurization of the RCS removes a degree of uncertainty associated with

postulated scenarios since many such events become very similar to a large-break LOCA (LBLOCA). Therefore, for purposes of identifying important processes and phenomena challenging the U.S. EPR severe accident response strategy, a hypothetical phenomenologically-bounding severe accident for challenging the U.S. EPR melt retention measures is an initiating large primary system pipe rupture followed by scram and subsequent accumulator injection. The result is a configuration in which the core is completely flooded.

Typical of a station blackout, a complete failure of all active safety systems is assumed, which results in a progressive dry-out of the core and a disintegration of the fuel assemblies. Exothermic chemical reactions primary between zirconium and residual water and steam results in significant hydrogen generation. In certain configurations this hydrogen may be vulnerable to combustion, which causes pressure spikes in the containment. Eventually, a molten corium pool will form inside the core; the pool then expands towards the heavy reflector and the heavy support plate. As the event progresses, intact fuel elements surrounding the core will eventually be destroyed.

Since the melt is primarily oxidic, its contact with the heavy reflector will not lead to instant failure but to a slow, crust-limited heat-up. Due to its high mass and correspondingly high heat capacity, the heavy reflector plus lower support plate will act as a temporary internal crucible retaining the core within its boundary. As a consequence, it is expected that this intermediate molten pool will already contain a large fraction of the core. Melt-through of the heavy reflector is expected to occur in the upper region of the molten pool. During relocation into the lower plenum the out-flowing melt will steadily widen the initial hole.

As a result of the contact with the residual water in the lower head, the released melt may either form a partially fragmented debris bed and/or an encrusted molten pool. After evaporation of the residual water, a secondary molten pool will form within the lower plenum. The lower support plate will then be heated from both sides, by convection from above and by thermal radiation from below.

---

The two pools will evolve independently. Within the upper pool, remaining fuel and solid debris will heat-up. Newly created melt will exit through the existing hole in the heavy reflector and become incorporated into the lower pool. During this process the average temperature of the lower head will steadily increase, which leads to its deformation by thermal expansion and creep. Downward expansion of the lower head is ultimately limited by the concrete support structures provided at the bottom of the reactor cavity. These structures preserve sufficient space for the outflow of melt and the later formation of a molten pool in the reactor cavity.

At some point, the RPV lower head will fail thermally. This will most likely occur as a local failure at a location in the upper part of the melt-contacted region. Therefore, it is expected that only part of the contained melt will be released with the first pour. After this first relocation, further outflow into the reactor cavity will depend on the development of the melt configuration within the RPV.

Under the expected dry conditions, the lower head will be subject to radiant heating from the surface of the molten pool and/or the surrounding aerosol-rich gas. This heat flux will accelerate the global failure of lower head and lower internals of the RPV. The chronology of events of this hypothetical severe accident is summarized in Table 4-1.

**Table 4-1 Chronology of a Bounding Severe Accident through RPV Failure**

<b>Event</b>	<b>Comment</b>
Safety Injection Refills Core	Large amount of water is bounding for hydrogen generation
Injection Fails	Complete failure necessary for maximum fuel melt
Fuel Heat up, Failure, and Melting	N/A
Contact with Core Support Structure and Heavy Reflector	Slow melt of heavy reflector retains heat in the core region, enhancing transition to liquid phase
Melt Progression towards the Lower Head	Convective heat transfer enhances destruction of core and supports
Debris Formation from Contact with Water in the Lower Head	Crust/Debris formation insulates molten pool from vessel wall, retention allows separation of oxide and metal
Molten Pool Formation	
Lower Head Failure	Flow of metallic melt from the RPV further degrades the RPV, spilling the entire core into the reactor cavity

#### **4.2.2 Presentation of Severe Accident Processes and Phenomena**

As presented in Section 2, the U.S. EPR has incorporated design features to specifically address the major severe accident safety issues. Associated with each of these issues are processes and phenomena arising from a particular severe accident. Table 4-2 identifies, for the U.S. EPR severe accident response features, the credible processes and phenomena that need to be characterized and understood to make an informed judgment on the merits of the integral design. This supports the technical quality of the subsequent process studies and the PRA, which relies on the completeness of analytical methods developed for the simulation and analysis of severe accidents.

**Table 4-2 Identification of Severe Accident Processes and Phenomena for the U.S. EPR**

<b>Phenomena</b>	<b>Safety Issue</b>
1. Thermal-hydraulics and fuel rod degradation	Hydrogen Control/Core Debris Coolability/Equipment Survivability
2. Core melt progression (degradation of core structure)	Hydrogen Control/Core Debris Coolability
3. Core melt relocation to lower head	Hydrogen Control/Core Debris Coolability
4. In-vessel fuel-coolant interaction	Containment Performance/High Pressure Melt Ejection
5. Oxide/metal separation	Hydrogen Control/Core Debris Coolability
6. Crust formation and failure	Core Debris Coolability
7. In-vessel debris formation	Core Debris Coolability
8. RPV failure modes	Containment Performance/High Pressure Melt Ejection
9. Melt conditioning in reactor cavity/MCCI*/oxide-metal stratification/integrity of ex-vessel protective structure	Hydrogen Control/Core Debris Coolability/Containment Performance
10. Melt spreading in spreading compartment	Core Debris Coolability
11. MCCI* in spreading compartment/oxide-metal stratification	Hydrogen Control/Core Debris Coolability/Containment Performance
12. Spreading compartment flooding and basemat cooling	Core Debris Coolability/Containment Performance/Equipment Survivability

Phenomena	Safety Issue
13. Steam/hydrogen transport	Containment Performance/Equipment Survivability
14. Hydrogen recombination	Containment Performance/Equipment Survivability
15. Hydrogen combustion	Containment Performance/Equipment Survivability
16. Long-term containment heat removal	Containment Performance/Equipment Survivability
17. Fission product transport	Containment Performance/Equipment Survivability

\*Molten Corium-Concrete Interactions (MCCI)

#### 4.2.3 **Scaling Analysis for Phenomenological Importance**

Severe accident processes and phenomena can be further characterized based on scaling analyses. The magnitude of nondimensional groups appearing in equations derived from scaling analysis determines the relative importance of various nondimensional parameters related to the particular phenomena. While multiple scaling treatments exist, the method of hierarchical, two-tier system decomposition was used in Reference 15 to investigate scaling in complex systems, in general, and for a severe accident problem, in particular. For that approach, the following identify the ingredients of the scaling analysis approach at each hierarchical level:

1. *System*: The entire system that must be analyzed for the proposed application (i.e., U.S. EPR)
2. *Subsystems*: Major components that must be considered in the analysis (primary system, secondary system, and containment)

3. *Modules*: Physical components within the subsystem (i.e., reactor vessel, steam generator, pressurizer, piping run, reactor cavity, spreading compartment, etc.)
4. *Constituents*: Chemical form of substance (e.g., water, hydrogen, air, boron, concrete, Zr, UO<sub>2</sub>, etc.)
5. *Phases*: Solid, liquid, or vapor
6. *Geometrical Configurations (phase topology or flow regime)*: The geometrical shape defined for a given transfer process (e.g., pool, drop, bubble, film, etc.)
7. *Fields*: The properties that are being transported (i.e., mass, momentum, and energy)
8. *Transport Processes*: Mechanisms that determine the transport of and interactions between constituent phases throughout the system (pumps, flow resistances, heat transfer, decay heat, chemical processes like oxidation, etc.).

By carefully defining the number and type of each ingredient at each level, the basic characteristics of a process or phenomenon can be characterized. Several applicable scaling analyses have been published in the areas of heat transfer (Reference 21 and 22), containment dynamics (Reference 23), and melt spreading (Reference 24). These results, supplemented as needed by new analyses, will be used for identifying the adequacy of code models, the calculation matrix, and test programs.

## **5.0 RESEARCH AND DEVELOPMENT RELATED TO THE U.S. EPR SEVERE ACCIDENT CONCEPT**

The research and development activities supporting the U.S. EPR severe accident concept are described in this section. These supporting activities, identified as general severe accident safety issues, are in the areas of:

- Hydrogen Mitigation
- Core Debris Coolability
- High Pressure Melt Ejection
- Containment Performance
- Equipment Survivability.

AREVA NP has inherited a rich database of research and development from participation in international programs, many of which have been explicitly designed with U.S. EPR features. In addition, many testing programs providing insights into severe accident phenomena are available in various technical reports and code manuals, which are identified in this section. In general, these references provide a good compilation and discussion of key programs and conclusions drawn from those tests. Specific to the objectives of this topical is an assessment of the applicability of these tests relative to system scaling and ranges of key measurable variables.

The research and development work performed in parallel with the various U.S. EPR development phases has helped to achieve a better understanding of the underlying phenomena, improve available codes, models and data bases, and provide more realistic assumptions regarding initial and boundary conditions. Specifically, these programs are being used to:

1. define applicability and uncertainty ranges to be considered in characterizing analyses

2. provide a degree of authority resolving an issue, in the case of DCH and fuel-coolant interactions (FCI) (further discussed in this Section)
3. validate computational tools for production analysis (e.g., MAAP4, etc.).

Items 1 and 2 are addressed in this section. Validation of analytical methods is addressed in Section 6.0.

Units of measure presented in the remainder of this report are given in metric. The purpose is to be consistent with the body of experimental work, which has been predominantly reported in the general literature in metric units.

## 5.1 *Hydrogen Mitigation*

The U.S. EPR hydrogen mitigation concept aims at 1) preventing flammable configurations of combustible gases capable of breaching the containment, and 2) removing hydrogen in order to achieve global hydrogen concentrations below the ignition limit under dry condition when the time containment sprays are needed for long-term depressurization.

The system consists of recombiners, rupture and convection foils, and mixing dampers. Hydrogen mitigation is supported by the fact that depressurization of the RCS occurs directly into the containment atmosphere, via a relief tank with a rupture disc at two low locations near the elevation of the steam generator supports. This guarantees a large amount of well-mixed steam in the containment for nearly all scenarios.

To maintain containment integrity, in particular in the early phase of an accident, the following must safely be avoided:

- Any deflagration with Adiabatic Isochoric Complete Combustion (AICC) pressure above design pressure
- Fast deflagration with the potential to initiate a detonation
- Local temperatures that pose a threat to the containment shell.

The justification of this concept is based on the application of experimentally founded criteria to determine the potential combustion mode with the goal of excluding flame acceleration and, in particular, Deflagration-to-Detonation Transition (DDT).

Despite recent progress worldwide, some uncertainties still exist in the field of:

- Prediction of transient hydrogen production (e.g. reflood of a molten core)
- Refined application of combustion criteria to exclude fast deflagration and DDT to real containments (degree of confinement, potential of venting)
- Conditions for the development and stability of a standing flame (e.g., resulting from ex-vessel release at high temperature).

#### **5.1.1 Hydrogen Production**

Hydrogen production during the risk-dominant core heat-up phase of a severe accident is characterized by the following phenomena:

- cladding ballooning and failure due to the increase of inner pin pressure (gas release)
- oxidation of fuel rod surfaces
- rupture
- oxidation of inner surfaces following cladding rupture
- melting and relocation of fuel rod materials
- oxidation of core support material

Hydrogen production is also a byproduct of the molten-core concrete interaction (see Section 5.2.2).

### **5.1.1.1 Hydrogen Production Phenomenology**

Reference 25 provides a thorough discussion on both in-vessel and ex-vessel hydrogen sources.

#### **5.1.1.1.1 In-vessel Hydrogen Production**

Hydrogen in-vessel production is due to zirconium or steel oxidation. The zirconium oxidation is limited by the availability of steam and zirconium, and by the steam diffusion process to clad surface. Steel oxidation in the primary circuit will impact the core barrel, internals, core support plate and upper core plate, and the metallic phase in the corium.

Fuel and component melting does not intrinsically enhance hydrogen production. It brings to the melt surface previously unexposed metal to a corrosive environment, bringing about more oxidation. The material in the control rods (Ag-In-Cd) is the first released in the primary circuit. Melting occurs over a range of 1050 K - 1100 K, but their relocation awaits failure of the steel sheath around 1500 K. For the fuel rods, several chemical interactions are considered in the heating phase of fuel, resulting in the formation of eutectic solids at metal interfaces, thus, advancing the core degradation.

Materials on the outer face of cladding flow down as soon as the melting point is reached. Relocation and solidification of molten materials on fuel pins or control rods may reduce oxidation since the flow area for steam through channels may decrease. Thus, H<sub>2</sub> production may be curbed due to the lack of steam in some part of core.

Uncertainties related to reflood (around onset of core melting) and late phase core melt still exist. Without the addition of water, late phase phenomena that occur at the time of core slumping or later do not significantly contribute to the hydrogen risk. Uncertainty is, therefore, focused on reflood that may result from intentional action (re-establishment of safety injection) or unintentional flooding by accumulators.

Because of large uncertainties associated with hydrogen production due to reflood, bounding assumptions for oxidation rates, hence, hydrogen production, are necessary to address the potential impact from hydrogen combustion.

#### **5.1.1.1.2 Ex-vessel Hydrogen Production**

The process of hydrogen and carbon monoxide production during MCCI is well understood and characterized. It is essentially the result of the oxidation of metals by gases ( $H_2O$  and  $CO_2$ ) that are released during the interaction. The metals Zr, Si, Cr, and Fe will oxidize. Zr, Cr, and Fe come from the molten core, molten parts of the RPV and the concrete rebar. Si (and some  $SiO$ ) is produced by initial reduction of  $SiO_2$  present in the concrete by Zr. The main effect of  $SiO_2$  is to delay the hydrogen production. A significant amount of hydrogen is produced during the early phase of the core-concrete interaction while Zr is being oxidized. The uncertainty here is essentially due to the initial amount of Zr to be taken into account, which differs for different accident sequences. However, this quantity is clearly dependent on the level of oxidation during the in-vessel phase of the accident. Overall, it can be assumed that the remaining mass of Zr, which is the major source of early hydrogen production, will be oxidized during the early phase of the MCCI. The corresponding amount of  $H_2$  released into the containment by complete oxidation of all Zr is on the order of 1000 kg for a typical PWR. However, for those plants equipped with mitigation systems, such as PARs, hydrogen production during MCCI would occur at a time that the hydrogen concentration in the containment would have already been depleted to a certain extent, thus limiting the associated threat to the containment. After depletion of Zr and its follow-on products,  $H_2$  release continues at a much lower rate during MCCI, governed by Fe oxidation, which would continue over several days. This release is, however, accompanied by a larger rate of steam flow, which reduces its flammability.

#### **5.1.1.2 Experimental Work on Hydrogen Production**

Several experiments examining the degradation of fuel with the generation of hydrogen have been performed, including at the CORA (Forschungszentrum Karlsruhe (FzK)),

---

Reference 26), PBF (Idaho National Laboratory (INL), Reference 27), LOFT (Organization for Economic Cooperation and Development (OECD) sponsored at the INL, Reference 28), PHEBUS (Commissariat à l'Energie Atomique (CEA), Reference 29 and 30), and QUENCH (FzK, Reference 31 and 32) facilities. These are identified in Table 5-1. The focus of these experiments at these facilities has been to:

- examine the physico-chemical behavior of overheated fuel
- provide an understanding of the effects of water/steam injection
- determine the hydrogen source term.

Among the tests performed at these facilities, a few were chosen as part of the International Standard Problem (ISP) program. Those of particular interest are also identified in Table 5-1.

**Table 5-1 Experimental Work Addressing Hydrogen Production**

<b>Program (Organization)</b>	<b>Description and Phenomena</b>
CORA (FzK)	PWR fuel assembly with electrical heater rods. Flow of steam and argon through assembly, parametric studies on reflooding conditions. Measurements of temperatures and damage of fuel rods and H <sub>2</sub> production. CORA-13 was the subject of ISP-31.
PBF SFD Tests (INL)	Nuclear heatup of PWR fuel assembly. Steam (with and without argon) flow through assembly. Measurements of temperatures and damage of fuel rods and H <sub>2</sub> production.
PHEBUS (CEA)	Nuclear heatup of PWR fuel assembly. Flow of steam through assembly. Measurements of temperatures and damage of fuel rods and H <sub>2</sub> production. Analyses completed and documented for MAAP4. PHEBUS SFD was the subject of ISP-28.
QUENCH (FzK)	PWR fuel assembly with electrical heater rods. Flow of steam through assembly, parametric studies on reflooding conditions. Measurements of temperatures and damage of fuel rods and H <sub>2</sub> production. Also addressed oxidation of control rods containing B <sub>4</sub> C. QUENCH-06 was the subject of ISP-45.
LOFT (OECD)	Actual PWR fuel assembly destroyed to measure temperatures and damage of fuel rods and H <sub>2</sub> production.

### 5.1.1.3 *Conclusion on Hydrogen Production*

While the phenomena related to hydrogen production are well understood, uncertainties in the total amount of metal that can be oxidized (considering realistic limits to this process) must be considered. For severe accident safety assessments, hydrogen production must be addressed as a bounding initial condition.

### 5.1.2 *Hydrogen Distribution*

The issue of hydrogen distribution is associated with the transport of hydrogen from production sources (i.e., the reactor core and MCCI) to locations in which

concentrations can result in combustible configurations. Hydrogen, a very light element, easily diffuses through heavier gaseous substances. In spaces without inherent convection currents, hydrogen may stratify, consolidating in high concentrations that pose a combustion risk. An inherent mitigating consideration is that steam either from a large break or the primary relief valves contributes to the reduction of combustion potential in two ways; enhancing the homogenization of hydrogen reduces peak hydrogen concentrations, and higher steam volume concentration reduces the flammability.

#### **5.1.2.1 *Hydrogen Distribution Phenomenology***

Hydrogen transport is influenced by both natural and forced circulation phenomena. Hydrogen will passively distribute through the containment as a result of diffusion, and thermal and buoyancy forces through the current complex geometry. The situation is complicated by the presence of other constituents in the containment, including air, steam, aerosols and CO, among others. In addition, a system break or compartment vent, heat transfer to surfaces, and sprays will drive the circulation of all air-borne constituents in the containment. As such, the homogenization of hydrogen over the long term is very likely.

Control of the threat from hydrogen combustion begins with an understanding of how hydrogen is expected to distribute within the U.S. EPR containment during a severe accident. Coupled with the expected high steam concentration, hydrogen concentration sufficient for deflagration is not likely as long as it remains in a homogenous state. As such, the period of interest, meaning the period for which risk from hydrogen combustion is the highest, is restricted to the time where hydrogen distribution is strongly inhomogeneous. During this time the hydrogen distribution is expected to appear as one or two narrow rising plumes releasing from the RCS. Compartment venting and hydrogen recombiners ensure that the containment behaves as a single convective volume resulting in the homogenization of hydrogen in the containment. In this configuration, the risk from fast combustion then strongly decreases.

Local regions of high hydrogen concentration susceptible to ignition are anticipated for the bounding severe accident described in Section 4.2.1. The two most probable locations of high hydrogen concentration are equipment rooms (via a pipe break) or the reactor cavity (via vessel failure). In the event that combustion should occur in an equipment room, the effects of detonation could be locally significant, but the containment would be shielded from the internal compartment event and only minimally affected. Combustion in the reactor cavity will be the result of auto-ignition at the time of reactor vessel failure when the very hot corium and hydrogen are reintroduced to an oxygen-rich environment. Hydrogen generated during MCCI reactions is expected to burn above the corium layer; however, full combustion is unlikely. As with the postulated combustion event in an equipment room, such local events are not expected to threaten containment leaktightness.

The most vulnerable locations in the containment are those in close proximity to the containment shell. High local pressure peaks near the interior surface of the containment shell are unlikely because to get to the containment shell, hydrogen must travel through several compartments before exiting the steam generator compartment radially through vents and then be decelerated in the dome. During the early periods of a severe accident when hydrogen concentrations are the highest (but the amount generated is still only a fraction of the total potential), the distribution is seen to be inhomogeneous with decreasing concentrations along the common pathways from hydrogen production source to the containment. Specifically, regions of high concentration might be expected in the equipment rooms but little hydrogen is in the dome. Later, when the concentration in the dome rises, the overall gas distribution is quite homogeneous. This effect is mainly due to overall convection but is also supported by the recombiners.

### **5.1.2.2 *Experimental Work on Hydrogen Distribution***

The present status of containment thermal-hydraulics and hydrogen distribution research and development is described in an OECD state of the art report (Reference 33). The content of this report includes descriptions of the major experimental facilities

(size, shape and relevant instrumentation) that exist worldwide and the experiments performed highlighting the major phenomena investigated.

Relevant to hydrogen distribution the central issues are:

- Vapor, gas, aerosol distribution in a containment (mass transfer: stratification, accumulation or dissolution of concentrations)
- Pressurization/depressurization (governs vapor and gas properties)
- Behavior of global convection (mixing)
- Local heat transfer
- Distribution of energy in the containment.

Large-scale experiments, incorporating multiple compartments approaching the scale of the U.S. EPR provide the most valuable insights to the expected behavior of effluents in the containment. Among those programs, tests performed at the HDR (Heißdampf-Reaktor, cited in Reference 33), NUPEC Large Scale Test Facility (Nuclear Power Engineering Corporation (NUPEC), Reference 34), and Battelle Model Containment (Reference 35) facilities have been extensively evaluated for the central issues of interest. Tests from these facilities have also served the methods development community through the ISP program. These tests are summarized in Table 5-2 (presented with a comparison to U.S. EPR). In general, the transport of gases is reasonably well understood. These programs have been designed primarily for the specific purpose of validating containment performance codes (both lumped parameter and finite volume/computational fluid dynamics codes).

**Table 5-2 Test Programs for Assessing Hydrogen Distribution**

Program (Organization)	Specification	Description and Phenomena
HDR (Germany)	Full height, cylindrical steel vessel, large-scale (H = 60 m; V = 11300 m <sup>3</sup> , 62 compartments; hemispherical dome). Included spraying on the outer steel shell to induce inner condensation to enrich hydrogen as a result of the condensation process; S/V* ≈ 0.88; Max. Pressure = 600 kPa;	Full-scale containment to study mixing and distribution of steam and hydrogen in containment. Test E11 subject of ISP-29. Concentrated on containment internal natural convection flows, heat absorption processes by structure and gas distribution.
NUPEC Large Scale Test Facility (MITI, Japan)	Cylindrical steel vessel, mid-scale (height = 17.4 m; volume = 1300 m <sup>3</sup> , 28 compartments; hemispherical dome); S/V ≈ 1.1; Max. Pressure = 150 kPa	Mixing and distribution of hydrogen in containment with high steam concentration and sprays. Tests M-7-1 subject of ISP-35: concentrated on containment internal natural convection flows, heat absorption processes by structure and gas distribution.
Battelle Model Containment (USA)	Cylindrical reinforced concrete vessel, (H = 9 m; V = 626 m <sup>3</sup> , 9 compartments, flat ceiling); compartments interconnected by vent openings, thus forming a geometry similar to that of a PWR containment; S/V ≈ 1.75; Max. Pressure = 250 kPa	Mixing and distribution of hydrogen in containment. Measurements of gas concentration, temperature, and velocity; and structure temperature and heat transfer. VANAM-3 subject of ISP-37.

\* Surface/Volume (S/V)

None of these tests explicitly consider the introduction of hydrogen resulting from MCCI. In a postulated U.S. EPR severe accident, much of the hydrogen produced from MCCI is expected to auto-ignite. Later when the melt has progressed to the spreading compartment, much of the unburned hydrogen released from the MCCI process is

expected to move from the spreading compartment directly to the containment atmosphere and not produce local areas with a high concentration of hydrogen.

### **5.1.2.3 Conclusion on Hydrogen Distribution**

In general, the transport of vapor and gases is well understood from experimental programs and is captured in validated analytical methods. For application to the U.S. EPR, the containment integrity under combustion loads is the safety issue. As such, the uncertainties related to hydrogen distribution are related to whether a global accumulation or a local accumulation near the containment shell can occur at concentrations considered to be a combustion threat. Experimental programs have provided valuable information for assessing both global and local gas transport phenomena in a system similar to the U.S. EPR. While the probable gas transport processes expected during a severe accident in the U.S. EPR do not exclude the possibility of local accumulations of hydrogen resulting in combustible configurations, the dynamics of hydrogen transport and distribution in U.S. EPR containment are expected to show the following:

1. hydrogen concentration during the early phase of a severe accident is initially low and is progressively lower with distance from the generation sources
2. hydrogen concentration becomes more homogenized with time as a result of diffusion and inherent convection fields, with reduction driven by recombiners, decreasing the overall likelihood of critical concentrations of hydrogen.

These inherent preventive and mitigative measures considerably reduce those uncertainties related to hydrogen distribution in the U.S. EPR containment.

### **5.1.3 Hydrogen Combustion**

The combustion mechanism for hydrogen can be classified into two regimes, deflagration and detonation. Deflagrations are combustion waves in which unburned gases are heated by thermal conduction to temperatures high enough for chemical

reactions to occur. A deflagration is a combustion process where the flame speed, or the combustion front, is subsonic. This regime can be further divided into slow deflagration and fast deflagration. Slow deflagrations are typically classified with a maximum flame speed between 100 - 200 m/s which decelerates to a velocity close to the laminar burning velocity. Fast deflagration is produced as a result of flame acceleration, which is also the driving mechanism for detonation. Detonations are combustion waves in which heating of the unburned gases is caused by compression from shock waves. This is a combustion process where the flame speed is sonic or supersonic and is capable of producing large impulsive loads in containment. A detonation can be initiated in one of two ways: direct detonation, such as a large ignition force, or DDT. Direct detonation of hydrogen is not possible within the containment environment due to the high activation energy that is required to initiate such an event. DDT can result from flame acceleration. Hydrogen detonation can only occur in the containment as a result of flame acceleration.

#### **5.1.3.1 *Hydrogen Combustion Phenomenology***

Hydrogen combustion can have two damaging effects on a containment structure: those resulting from (1) pressure and (2) temperature. During the course of a severe accident equipment is expected to function for the purpose of mitigation. This equipment must survive the harsh environment of the event. In order for the equipment and containment structure to survive this event, the pressure and temperature resulting from hydrogen combustion should not exceed certain limits.

The pressure resulting from slow deflagration comes in the form of a thermodynamic change of energy. The combustion front itself has a dynamic component of pressure associated with it; however, because the wave is subsonic, it is bounded by the adiabatic isochoric complete combustion (AICC) pressure. The AICC pressure is one that would result if the combustible material were to undergo complete combustion in a constant volume (isochoric) and there was no heat transfer to the outside volume (adiabatic). However, this pressure is unlikely to be reached in a realistic containment due to the following:

- As flame velocity is low, heat can be transferred to the structures, inertants, steam, and droplets (departure from adiabatic condition).
- If hydrogen concentration is below 8% by volume, combustion is not complete. Also the complex structure of the large containment leads to incomplete combustion in case of a deflagration (departure from the completeness condition).

The pressure loads from a detonation are the results of dynamic pressure due to the supersonic wave front. These values can be greater than the AICC pressure by a factor of two or more. While in deflagration, the pressure distribution is uniform because the combustion front moves slower than the pressure wave; during detonation the pressure can vary significantly in the combustion front. In a detonation the peak pressure has a very short duration; thus, if the dynamic impact is not excessive, structures may be able to withstand a detonation.

The mode of combustion is largely dependent on the atmospheric mixture of the reactants (oxygen and hydrogen), the location of ignition, and the geometry containing the combustion process. The atmospheric mixture of the reactants not only influences the concentration of the fuel, it also affects the combustion process by the presence of inertants. An inertant is any substance that either hinders or is not involved in the combustion process. Steam concentrations at or above 55% by volume create an inert atmospheric environment. During such conditions the stoichiometric mixture of hydrogen is approximately 13% by volume. A stoichiometric mixture is one in which the ratio of products (the ratio of hydrogen to oxygen) is as combustion will consume all of the products. A mixture with too little hydrogen for combustion is called 'lean', whereas a mixture with too little oxygen for combustion is called 'rich'. As the concentration of the inertant increases, the threshold concentration of lean hydrogen combustion increases. Extensive research has been performed for numerous combinations of hydrogen, oxygen, and inertants to map out the hydrogen and oxygen concentrations that are combustible. The key inertants for hydrogen combustion in containment are

nitrogen (in air) and steam (which is also a product of combustion). Some key atmospheric conditions include:

- Hydrogen concentrations must be above 8%, by volume, in order for complete combustion to occur.
- In dry atmospheric conditions concentration of hydrogen above 4% by volume can lead to combustion.
- For inert atmospheric conditions (steam concentrations  $\geq 55\%$ ) the hydrogen concentration must be above 10% for combustion.

### **5.1.3.2 *Experimental Work on Hydrogen Combustion***

The factors that determine the type of combustion reaction and the resulting pressures are concentrations of fuel (hydrogen and carbon monoxide), oxidant (oxygen in air) and inertant (nitrogen in air, carbon dioxide, and steam), initial ambient conditions (i.e., thermodynamic state), geometry, turbulence, and ignition. Composition and the initial thermodynamic state impose limits to both flammability and detonability, while geometry and turbulence can determine the potential for detonation.

The current state of the art, including the major test facilities appearing in Table 5-3, is described in an OECD state-of-the-art report on flame acceleration and DDT (Reference 36). It concludes that the database available for flame acceleration is quite large and covers all relevant phenomena, but that unsolved topics still exist concerning ignition, quenching and flame acceleration at elevated pressure. Two different criteria, derived from the many experiments performed in the past in tubes or tube-like arrangements, have been established to determine the conditions under which flame acceleration and DDT, respectively, cannot occur:

- the sigma criterion, which relates the expansion ratio sigma to a limit value identified for many experiments (mainly those performed in tube-like geometry)

- the 7-lambda criterion, which uses the detonation cell size and a characteristic length and which can be used to exclude DDT.

Each criterion is a necessary, but not sufficient, condition for the occurrence of the corresponding phenomenon. The violation of the sigma criterion is necessary for DDT, as flame acceleration is a precondition. Correction factors for the sigma criterion have been derived to account for radial venting. These factors are important when experiments from closed tubes are applied to a containment-like structure. Provided fast deflagration cannot be excluded, the 7-lambda criterion assesses the non-occurrence of DDT by comparing the mixture quality, in terms of the detonation cell width lambda, with a characteristic length of the compartment or of a group of compartments. The detonation cell width can be determined by interpolation of experimentally determined cell widths with hydrogen and steam concentration, temperature, and pressure as parameters.

The database for the assessment of the combustion mode, which includes laminar combustion, flame acceleration to sonic velocity in the burned gas (fast deflagration) and DDT, is described in the flame acceleration and DDT state-of-the art report. The hydrogen combustion experiments from that report, which are considered applicable to the U.S. EPR design in terms of geometry and mixture properties, are provided in Table 5-3. The U.S. EPR is also described in this table for comparison. The results from these tests have shown reasonable support for the applicability of the two flammability criteria and, while none of these facilities is full scale, the sensitivity to scale has been demonstrated to be minimal with regard to the flammability criteria. This database is considered good up to very high pressures, temperatures, and steam concentration with regard to the limit value of sigma. With respect to the U.S. EPR and its direct depressurization of the RCS, the region with high steam concentration (above 40 vol. %) is important.

Experiments in vented facilities have resulted in deceleration in the vents by releasing gas (Reference 37). Based on such results, DDT can be clearly avoided in conditions where DDT otherwise would have occurred when vents are available.

**Table 5-3 Hydrogen Combustion Experiments**

<b>Program (Organization)</b>	<b>Specification</b>	<b>Mixture</b>	<b>Description and Phenomena</b>
Large View (University of Pisa)	670x670 mm, L=3.2m; (F)	8.5% - 10% H <sub>2</sub>	Two chambers; examined ignition and opening location, jet ignition, turbulence
AECL Interconnected Vessels (Canada/AECL)	V <sub>sphere</sub> =2.3m <sup>3</sup> , V <sub>cyl</sub> =10.7 m <sup>3</sup> ; (S)	6-20 vol % H <sub>2</sub>	Two chambers – cylinder to sphere; examined jet ignition, independent hydrogen chamber concentration
Large Scale Vented Containment Test Facility(Canada/AECL)	10x4x3 m; V = 120 m <sup>3</sup> ; (S)	8% - 14% H <sub>2</sub> , Steam	Single chamber (cylinder) with vented combustion with different vent areas
Battelle Model Containment (BMC) (Germany/Battelle)	D= 10 m, H = 10 m, V 40 – 200 m <sup>3</sup> ; (H)	7-14% H <sub>2</sub> , 0% - 50% Steam, (CO <sub>2</sub> )	Both single and multi-chamber studies of slow and fast combustion, vented combustion, jet ignition, realistic obstacles
PHDR (Germany/FZK)	L = ~10 m, V = 535 m <sup>3</sup> ; (H)	8% - 12% H <sub>2</sub> , 34% - 30% Steam	Examined slow and fast combustion, vented combustion, jet ignition, realistic obstacles with expected high steam concentration. Scaling to BMC
NUPEC Large Scale Test Facility (Japan)	L = ~10 m, V = 270 m <sup>3</sup> ; (H)	8-15% Hydrogen, 0-60% Steam	Mixing/distribution, ignition location, spray, elevated initial pressure, transient behavior
RUT (Russian Research Centre “Kurchatov Institute”)	Channel: L = 34.6 m, W = 2.5 m, H = 2.3m, “Canyon” L = 10.55 m, H = 6.3 m, W = 2.5 m, V=480 m <sup>3</sup>	H <sub>2</sub> - Air - H <sub>2</sub> O- Mixtures	Influence of mixtures sensitivity to detonation and DDT [Also, HYCOM program for Scaling, H <sub>2</sub> concentration gradients (9 – 13%), and venting experiments using the RUT and other facilities]

\* Dome shape key: F – Flat; S – Sphere; H - Hemisphere

In addition, the stability of standing flames has been investigated at AECL Whiteshell (Reference 38) for horizontal and at Sandia National Laboratory (SNL) for vertical flames. Standing flames are expected in the U.S. EPR after vessel failure when hydrogen is released at high temperature due to core concrete interaction; however, they are not expected to trigger a damaging combustion event. In this scenario, the combustion phenomenon is driven by high temperature (auto-ignition) and limited by the available reactants (hydrogen and oxygen), which will appear as a product of the MCCI.

### **5.1.3.3 Conclusion on Hydrogen Combustion**

Based on the extensive work to date, it is now possible to assess the potential combustion mode based solely on the gas distribution and temperature. However, important uncertainties still exist with respect to:

- Limit values for sigma in case of high steam concentration and high temperature
- Characterization of cloud size, in particular characteristic length
- Consideration of venting.

Given the existing uncertainties, the conservative flammability criteria that have been experimentally verified currently provide the strongest basis for assessing hydrogen combustion risk in the U.S. EPR. In a practical sense the conservatism means that the combustion process has to be calculated for situations (violation of the criteria) where the outcome is no fast deflagration.

As a consequence, the combustion process has to be considered for situations where the criteria are violated but which realistically do not lead to flame acceleration.

Combustion behavior in subcompartments is uncertain and depends on geometry, hydrogen and steam concentration and availability (and location) of ignition sources. Depending on geometry and gas concentrations, turbulent deflagration, accelerated flames and transition to a detonation (DDT) cannot be excluded in all cases.

Nonetheless, two phenomenological considerations contribute to prevent hydrogen combustion in the U.S. EPR. The containment atmosphere during a severe accident will contain a high fraction of steam as a result of either a LOCA or the primary depressurization. Steam concentrations during a severe accident are expected to be between approximately 40 – 50%. In addition, rupture and convection foils provide vent paths for the steam and hydrogen. In combination with mixing dampers, convection paths are established. The distribution of steam in the containment leads to an improvement of the flammability limits while the reduction of peak hydrogen concentrations reduces the risk of flame acceleration and DDT. These inherent phenomena are expected to reduce the combustion threat and, hence, those related uncertainties applicable to hydrogen combustion in the U.S. EPR containment.

#### **5.1.4 *Hydrogen Recombiners***

Various hydrogen countermeasure strategies exist, including using igniters (plug/catalytic), pre/post inertization, and hydrogen recombiners (active or passive, thermal or catalytic). These various options have been evaluated and compared by several investigators (Reference 39) and, as a result, the PAR design provides the greatest benefit with the least amount of uncertainty related to performance and impact on regular plant maintenance, relative to the other options. These systems have been designed to meet the following characteristics:

- high functional reliability, such as resistance to poisoning;
- highly efficient, exhibiting H<sub>2</sub> reduction rates of greater than 110 lb/hr (50 kg/h);
- simple design;
- integrated passive equipment;
- cost-effective; and
- easy to integrate into existing plant designs.

Given these advantages, the U.S. EPR design incorporates 47 PARs as the primary hydrogen mitigation feature. While not explicitly discussed in this report, these PARs also function to recombine CO.

#### **5.1.4.1 *Hydrogen Recombiner Phenomenology***

PARs are simple devices, consisting of catalyst surfaces arranged in an open-ended enclosure. In the presence of hydrogen (with available oxygen), a catalytic reaction occurs spontaneously at the catalyst surfaces and the heat of reaction produces natural convection flow through the enclosure, exhausting the warm, humid hydrogen-depleted air and drawing fresh gas from below. Thus, PARs do not need external power or operator action. The performance of recombiner units has been shown to be insensitive to the location within a particular room because of quite vigorous natural mixing produced by their operation. PAR capacities are ultimately subject to mass transfer limitations and may not keep up with high hydrogen release rates in small volumes, for example, as could exist in the immediate vicinity of the hydrogen release

PARs work both individually, as a remover of free hydrogen in the containment, and collectively, to drive atmospheric circulation in the containment, thus, encouraging the homogenization of hydrogen. PARs use catalytic coatings to transform molecular hydrogen and oxygen into water vapor. They are self-starting and self-feeding, even under cold and wet conditions. The buoyancy of the hot gases expelled at the top of the PAR vertical flow channels sets up natural convective flow currents that promote mixing of combustible gases in the containment. Recombination of these gases commences as soon as hydrogen is released into containment as a result of a design-basis or severe accident. Hydrogen and oxygen in the containment atmosphere are recombined upon contact with the catalyst contained within a metal housing designed to promote flow with gas entering on the bottom and gas exiting at the top.

The aim of the recombiner is not to prevent hydrogen combustion but to limit the consequences, in particular to avoid containment failure. This is achieved by providing good atmospheric convection conditions in order to limit peak hydrogen concentration in

time and space and to quickly remove sufficient amount of hydrogen at time of vessel failure, when ignition conditions exist as a consequence of the ex-vessel melt release, so that no fast deflagration will occur. During the period of in-vessel hydrogen release, a strongly non-uniform hydrogen concentration (rising plume) exists for some time, dependent on the characteristics of the initiating event. A major target of the justification process is to show that this situation is limited in time so that random ignition would not lead to flame acceleration up to sonic speed, and thus DDT is unlikely.

With the application of PARs, a broad spectrum of operating environments and situations must be considered. These include

- local accumulation of H<sub>2</sub>;
- other environmental conditions (pressure/temperature/steam (up to ~60%)/rich-lean oxygen content);
- other gases including CO, inertants, etc.;
- poisons/aerosols/fission products;
- incidents such as nearby combustion and sprays;
- ignition sources including the recombiner itself

The performance and efficiency of the PARs during a severe accident must also consider the arrangement of the recombiners. In general, this involves the identification of those locations of greatest likelihood of high concentration of hydrogen (which contributes to the overall efficiency of hydrogen removal during a severe accident) balanced with an appreciation for operational and maintenance constraints.

#### **5.1.4.2 *Experimental Programs with Hydrogen Recombiners***

The objective of previous experiment programs has been to analyze the interaction between hydrogen depletion of the individual recombiners and the induced convection under a broad range of potential operational conditions. Qualification tests for recombiners under enhanced H<sub>2</sub> concentration, poisoning, realistic flow conditions have been performed at KALI, a 16 m<sup>3</sup> test facility erected by CEA (Reference 40), the Battelle Model Containment (Reference 41), AECL Whiteshell laboratories' Large Scale Vented Containment Test Facility (Reference 42) and at CEA's H2PAR facility (Reference 43). These are summarized in Table 5-4 below. The recombiners used in these experiments were manufactured by multiple suppliers. Among these tests, the AREVA NP design (appearing as the Framatome-ANP and Siemens design in literature) has been specifically studied.

The AREVA NP recombiner consists of a metal housing designed to promote natural convection with a gas inlet at the bottom and a lateral gas outlet at the top. The horizontal cover of the housing at the top of the recombiner protects the catalyst against direct spray of water and aerosol deposition. Numerous parallel plates with a catalytically active coating are arranged vertically in the bottom of the housing. Good accessibility to the catalytic plates is guaranteed through the provision of a removable inspection drawer. This ensures easy maintenance and inservice inspection of the recombiner. The qualification and development of AREVA NP recombiners is described in (Reference 40 and Reference 44). Based on the magnitude of experiments to test and qualify recombiners the component is considered sufficiently qualified for application in nuclear power plants.

**Table 5-4 Hydrogen Recombiner Experiments**

<b>Program (Organization)</b>	<b>Specification</b>	<b>Description and Phenomena</b>
Large Scale Vented Containment Test Facility (Canada/AECL)	Single H <sub>2</sub> recombiner in containment (V = 120 m <sup>3</sup> , 10x4x3 m); P <sub>max</sub> = 1 bar	Catalytic recombiners with accelerated thermal ageing, prolonged operation in hydrogen atmospheres, containment sprays, sump chemicals, radiation, fuel aerosols and possible chemical vapours; tests confirm self-start behavior and demonstrate strong mixing, irrespective of recombiner placement and wet/dry conditions
Battelle Model Containment (Germany/Battelle)	Multiple recombiners (3) in containment (V = 600 m <sup>3</sup> , D= 10 m, H = 10 m); P <sub>max</sub> = 2 bar	Catalytic recombiners with steam exposure, CO, I <sub>2</sub> and other unique environment conditions (e.g., fire) were conducted at 125 °C, 3% H <sub>2</sub>
KALI (CEA)	Single recombiner in containment (V = 15.6 m <sup>3</sup> , D = 2.1 m, H = 4.6 m); P <sub>max</sub> = ~5 bar	Catalytic recombiners with steam, ~10%, cold water spray
H2PAR (CEA)	Single recombiner in containment (V = 7.6 m <sup>3</sup> ; D = 2 m) P <sub>max</sub> = 1 bar	Catalytic recombiners with steam, ~10%, cold water spray; with poisons (aerosols, fission products)

One of the main purposes of these experiments has been for the development of computer code models. Models used up to now within the U.S. EPR project determine the depletion rate of a recombiner with the aid of correlations established from such experiments, where the recombiner was exposed to a homogeneous atmosphere with controlled concentration of steam and hydrogen. Though this procedure is widely considered appropriate, detailed modeling has started recently, partly within EU projects, to better predict the interaction between temperature profile of the plates and convection.

Such development is also motivated by the potential of a recombiner to act as an igniter (see experimental findings mentioned above). Because ignition has been observed in some experiments with hydrogen concentrations above 8%, the fact that recombiners do not completely mitigate that threat is considered a disadvantage of recombiners by

some researchers. The major role of recombiners in the context of the U.S. EPR hydrogen mitigation strategy, however, is to reduce the amount and concentration of hydrogen sufficiently to avoid containment failure as a result of any combustion mode. It is not intended to avoid any ignition within the containment, which is impossible due to the many ignition sources.

#### **5.1.4.3 Conclusion on Recombiners**

Methods for hydrogen control have advanced significantly over the past two decades. Several experiments have been performed to determine the effectiveness of PARs under relevant boundary conditions. In particular, the AREVA NP PAR has demonstrated the capacity for hydrogen control over the full spectrum of possible atmospheric conditions. For the U.S. EPR the primary outstanding uncertainties are with the appropriate arrangement of recombiners within the containment and the consideration of the recombiner as an ignition source. By using information from the experimental programs examining hydrogen distribution, combustion and recombination in plant-specific performance analyses, these uncertainties are reduced. Recombiners are thus a mature component for implementation in nuclear power plants.

#### **5.1.5 Conclusion on Hydrogen Mitigation**

The goal of the hydrogen mitigation system is to avoid fast hydrogen combustion with the potential to fail the containment from the two primary failure contributors: temperature and pressure. An objective for the U.S. EPR is to show that the AICC pressure is below the expected containment failure pressure. Laminar combustion, enveloped by the AICC pressure, therefore, will not fail the containment. Hence, focus is on the effect of flame acceleration, fast combustion and DDT.

In assessing containment integrity with respect to combustion risk for bounding scenarios, the flame acceleration risk is expected to be limited to the steam generator compartments (including pump rooms) for a limited period of time with rupture and convection foils providing venting from these compartments. In combination with hydrogen mixing dampers, this ensures that the containment behaves as a single

convective volume. It can be concluded that this adapted hydrogen mitigation system maintains its capability to safely avoid containment failure due to hydrogen combustion.

The U.S. EPR hydrogen mitigation concept benefits from the broad scope of research on hydrogen risk in the past decades and from the availability of well-qualified components for hydrogen removal, the recombiners. The knowledge gained so far has been incorporated into models and criteria for the prediction of the containment atmosphere dynamics and potential combustion modes. The most recent experimental work has been performed primarily for the purpose of computer model validation for both lumped parameter and finite volume/computational fluid dynamics codes. As a result, less-detailed analysis codes, such as MAAP4 and MELCOR, should be adequate for the overall analysis. Nonetheless, experimental work is ongoing to further refine the knowledge base for hydrogen control.

## **5.2 Core Debris Coolability**

The U.S. EPR design involves provisions for the retention and long-term stabilization of the molten core inside the containment. The corresponding scheme presupposes a depressurization of the primary circuit prior to the formation of a molten pool within the lower plenum of the RPV. After RPV failure the molten corium is intended to first accumulate in the reactor cavity and later relocate, in one event, into a lateral compartment. Spreading of the melt will be followed by flooding, quenching and sustained cooling of the corium.

An assessment on the performance of corresponding components required for core debris coolability begins with a characterization of the main processes involved in this sequence, namely:

- initial release of corium from the RPV
- temporary melt retention in the reactor cavity involving

- 
- accumulation and conditioning of the melt (progression of MCCI, melt properties and layering, chemical reactions and their effect on hydrogen production and fission product release)
  - behavior of the protective shielding during melt attack (thermo-chemical and mechanical integrity)
  - failure of the melt plug (response after contact with oxidic and/or metallic melts)
  - melt stabilization phenomena including
    - spreading of the melt on concrete (dependence on the conditions of melt release after gate failure, homogeneity, MCCI, solidification processes)
    - melt flooding and stabilization (effectiveness of bottom and sidewall cooling, top-side flooding and debris fragmentation)

As an ex-vessel severe accident mitigation strategy, the consequences of MCCI contribute to the transformation of the melt into a stable configuration. In this two-stage stabilization process, retention and spreading, MCCI is not only unavoidable; but, it is actually incorporated into the U.S. EPR solution for severe accident mitigation. Thus, the phenomena associated with MCCI are treated separately in this section to support the degree of topical coverage appropriate for a thorough characterization of the U.S. EPR severe accident mitigation strategy.

Large margins exist with respect to the two phases of melt retention in the reactor cavity and in the spreading compartment, to make the concept robust and to reduce the dependence on research and development results. The retention function has been designed to address a large variety of assumptions regarding the sequences of melt release from the RPV as well as the related melt properties. Conservative design choices have been employed in consideration of scenarios characterized with significant uncertainty. These generally conservative assumptions include decay heat, a multi-step melt release, no late flooding and zero melt dispersal, the highest feasible initial oxide

melt temperature, a non-favorable distribution of heat fluxes inside the molten pool, and a complete separation of molten phases during MCCI.

Supporting the characterization of core debris coolability phenomena are several experimental programs. A considerable fraction of the severe-accident-related activities in nationally and internationally-sponsored programs have been either directly related to the solution of above problems, or can be utilized in that respect. The large contribution of U.S. EPR related programs was achieved by active participation in these projects by AREVA NP. As needed, additional experiment work has been performed internally to supplement the existing knowledge base, including the areas of MCCI and corium cooling in the spreading compartment.

### **5.2.1 Reactor Vessel Failure Modes**

As described in Section 4.2.1, the hypothetical bounding severe accident progresses to a point in which corium relocates into a water filled lower head, resulting in rapid dry out of that region and the formation of a molten pool. The natural convection in a volumetrically heated oxidic pool transfers heat through in the high thermally conductive metallic layer in direct contact with the vessel wall. Sustained local stresses from the layer of molten metal on the vessel wall will eventual lead to vessel failure.

Assuming the necessary conditions for reactor vessel failure are present, the following two vessel failure scenarios are considered most likely: (1) a “localized failure” in which a localized opening occurs near the vessel beltline (releasing molten core debris above the breach), and over time, moves downward, releasing additional debris, or (2) a “hinged failure” in which a localized opening occurs near the vessel beltline immediately followed by tearing of the vessel around nearly its entire circumference, and the lower head hinging/swinging downward and coming to rest on the cavity floor.

The U.S. EPR’s ex-vessel core debris coolability strategy eliminates uncertainties related to reactor vessel failure modes by introducing a temporary core melt retention phase. Nonetheless, the phenomena associated with reactor vessel failure are relevant to the demonstration of the U.S. EPR’s overall core melt stabilization strategy.

### 5.2.1.1 Reactor Vessel Failure Mode Phenomenology

The TMI-2 accident significantly changed the nuclear industry's thoughts about the potential for vessel failure. Investigations after the accident concluded that at least 45% of the core had melted and ~19,000 kg of the core material had relocated to the lower head. Post-accident examinations indicate that about half of that material formed a solid layer near the lower head. Above this solid layer was a layer of fragmented rubble.

Analyses of the TMI-2 accident led to the identification of four potential lower head failure mechanisms: ex-vessel tube rupture, tube weld failure, local vessel failure and global vessel failure. Although all four of these mechanisms are of interest in assessing many current-generation PWR designs, two penetration failure mechanisms were eliminated because the U.S. EPR has no lower head penetrations. Figure 5-1 illustrates the local and global failure mechanisms considered most probable for the U.S. EPR design. In a hypothetical bounding scenario postulated for the U. S. EPR, a localized failure occurs near the interface of the metallic and oxide melts. This localized failure will lead to global failure if the heat loads are axisymmetric or if the vessel starts to thin due to elevated system pressure, in conjunction with sustained heating from relocated debris.

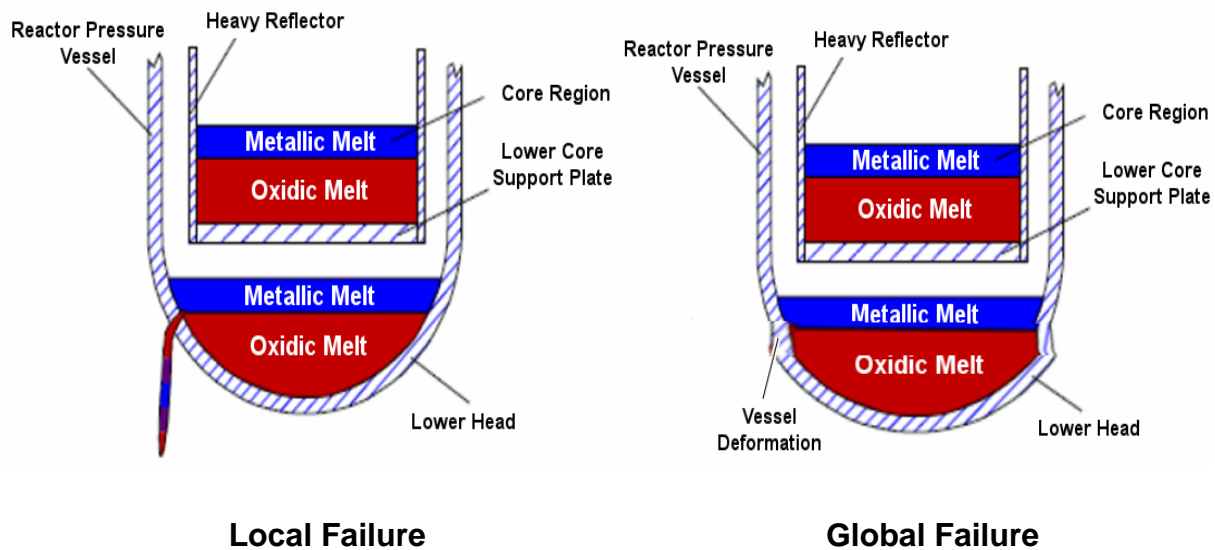


Figure 5-1 Common Reactor Vessel Failure Modes considered for the U.S. EPR

**5.2.1.2 Reactor Vessel Failure Mode Experimental Programs**

Table 5-5 lists several experimental programs that produced two data types of interest in assessing the potential for vessel failure – high temperature material property data that should be incorporated into models and boundary condition data for assessing the potential of vessel failure (References 45 – 48).

**Table 5-5 Experiment Programs Related to Reactor Vessel Failure**

<b>Program (Organization)</b>	<b>Description/Phenomena</b>
Lower Head Failure Program (NRC)	High temperature creep and tensile data for SA533, SA105/106, SS304 and Inconel
Super-Critical Water Reactor Material Property Evaluations (INL)	High temperature thermal diffusivity data for SA533 and SS304
TMI-2 Vessel Investigation Project (OECD)	Data for assessing the potential for melt penetration through a vessel penetration and for assessing the potential for tube rupture, tube ejection, localized and global vessel failure modes
SNL LHF Program (SNL)	One-fifth scale data for predicting vessel failure for a vessel exposed to a well-defined heat load and pressure history

High temperature thermo-mechanical property data, including creep and tensile data for vessel and penetration materials have been compiled from the various NRC programs, including the Lower Head Failure (LHF) Program, up to the 1250 – 1300 K range. Higher temperature data are particularly important for vessel lower head materials, such as the SA508 or SA533B1 steel, because this material undergoes a phase transition, from ferritic to austenitic, at 1000 K. Although it is known that the strength of these materials is inversely proportional to temperature, estimation of their strength at temperatures above the temperature where they undergo this transition was not possible during the LHF Program.

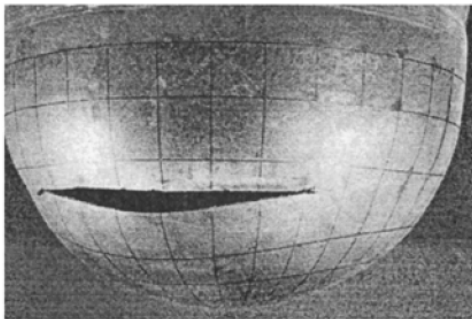
Models developed in the NRC-sponsored LHF Program were applied to determine the failure margin remaining in the vessel during the TMI-2 accident using available plant data and data from nozzles, vessel steel, and debris examined in the OECD-sponsored TMI-2 Vessel Investigation Project. Results provided several key insights about the potential for vessel failure. First, results indicate that there was a large margin-to-failure for tube rupture and tube ejection failure modes. Specifically, the thermal and pressure loads on the lower head were insufficient to fail the weld that joins the tube to the vessel. Second, results indicate that the localized “hot spot” was not due to jet impingement. Third, analyses indicated that global or localized creep rupture was the failure mode with the least margin for TMI-2 scenario. Last, calculations indicate that additional margin, not currently considered in severe accident analyses codes, existed in the vessel lower head during the TMI-2 accident. As discussed in Reference 45, subsequent evaluations suggest that this additional margin was associated with water flowing between cracks within solidified debris and gaps that formed between solidified debris and the vessel.

Reference 48 describes lower head failure tests that were conducted in a one-fifth scale, SA533B1 carbon steel vessel to assess and make recommendations for RPV creep rupture models and identify the effects of heat flux distribution, pressure, penetrations, and weldments on vessel failure. The eight tests performed under the initial NRC-sponsored LHF program considered a range of pressures (5 to 10 MPa), heat flux distributions (uniformed and peaked) and the effects of penetrations. The LHF tests provide unique data and insights about vessel failure.

Several photos from these tests are shown in Figure 5-2 to illustrate some of these insights. For example, photos from the LHF-5 and LHF-3 tests were included because they provide insights about global vessel failure. In reality, “global” vessel failure may be very localized because heat fluxes aren’t perfectly axisymmetric or because of non-uniformities in the vessel thickness during manufacture. Hence, a “global” vessel failure may initiate as a “tear” that may or may not “unzip” prior to depressurization. Obviously, these two types of failures differ significantly in their impact on subsequent accident

progression. Both types of failures were observed in LHF tests with “top-peaked” heat flux distributions (e.g., with heat fluxes that are larger in magnitude near the top of the vessel where the hemisphere is attached to the cylindrical portion of the vessel). The LHF-5 test differed because of an unplanned pressure transient during testing (the pressure went from 10 to 7 MPa), whereas the LHF-3 test remained at 10 MPa.

LHF tests were also conducted to gain insights about the impact of heat flux distribution. However, results illustrated the importance of manufacturing tolerances. Failures were observed to occur at the same location in the LHF-1 and LHF-6 tests, but for different reasons. Post-test exams indicate that the LHF-1 test vessel had a thinner wall at the observed failure location (although the thickness was within the allowed manufacturing tolerances). In the case of the LHF-6 test, an unplanned hot spot occurred.



LHF-3



LHF-5



LHF-1



LHF-6

**Figure 5-2 Reactor Vessel Failure Modes Examined in the LHF Program**

### **5.2.1.3 Reactor Vessel Failure Modes Conclusions**

The research to date supports the premise that reactor vessel failure is most likely to occur from a localized point and eventually expand into a global failure. Heat flux distribution and manufacturing variations were shown to have a strong influence on RV failure. While manufacturing tolerances are generally expected to be tighter for nuclear power plants relative to test programs, heat flux uncertainty is significant. Nonetheless, the U.S. EPR's temporary melt retention feature compensates for this uncertainty as described in Section 5.2.3.

### **5.2.2 Molten Core-Concrete Interactions**

MCCI occurs when molten core debris breaches the reactor vessel and contacts concrete surfaces, whereby the thermal and chemical properties of the melt contribute to the degradation of the concrete. In the U.S. EPR design, MCCI is explicitly considered and even incorporated as an inherent process contributing to the passive response of the U.S. EPR to a severe accident. It is present in both the temporary melt retention and conditioning phase and the melt spreading and stabilization phase.

#### **5.2.2.1 MCCI Phenomenology**

MCCI phenomenology has been presented in several sources (References 49 and 50). The U.S. EPR is unique in that the severe accident response strategy involves deliberate interaction of the core melt with sacrificial concrete (Reference 51). In general, MCCI is the result of different degradation mechanisms of core debris on concrete acting in distinct time scales. The earliest phase of MCCI is characterized by very-high-temperature molten metal and oxide pouring from the RPV and settling as a pool on the concrete surfaces. The pouring can result in spallation or fragmentation of the concrete near where the corium first contacts the concrete. High stored energy and heat transfer from the melt to the concrete drives the ablation process. Certain material constituents of the concrete melt or fragment. This further enhances the heat transfer contact area between the melt and concrete. As the corium settles on the concrete surface, penetrating cracks and fragments produced on the initial contact, the melt

---

begins to react chemically with the concrete, generating various gases including combustible hydrogen and carbon monoxide. Over the long term, the initial stored energy of the melt is exhausted; however, the internal decay heat generation sustains these reactions at much lower rates.

MCCI introduces two major mechanisms contributing to the risk of containment breach: basemat penetration via the ablation process, and containment liner breach via the generation and eventual detonation of combustible gases. To a lesser extent, the gas release process challenges the containment as an over-pressurization mechanism. The risks of MCCI are mitigated by limiting the amount of interacting concrete. The incorporation of concrete material introduces an interesting element of the MCCI process. Normally, the low thermally-conductive corium oxides are heavier than the corium metal. Consequently, a stratification of lighter metal on top of the oxides occurs. As oxides are produced from concrete material, they diffuse easily into the corium oxides; that is, they are highly miscible. Unlike the corium oxides, concrete oxides are lighter than the corium metal. Over time the oxide layer can become lighter than the metal, which can lead to an inversion of the metal and oxide layers as shown in Figure 5-3. Because of the sustained release of gases from the concrete, whether the mixture actually inverts or simply becomes homogenized mixture is an uncertainty in the short term.

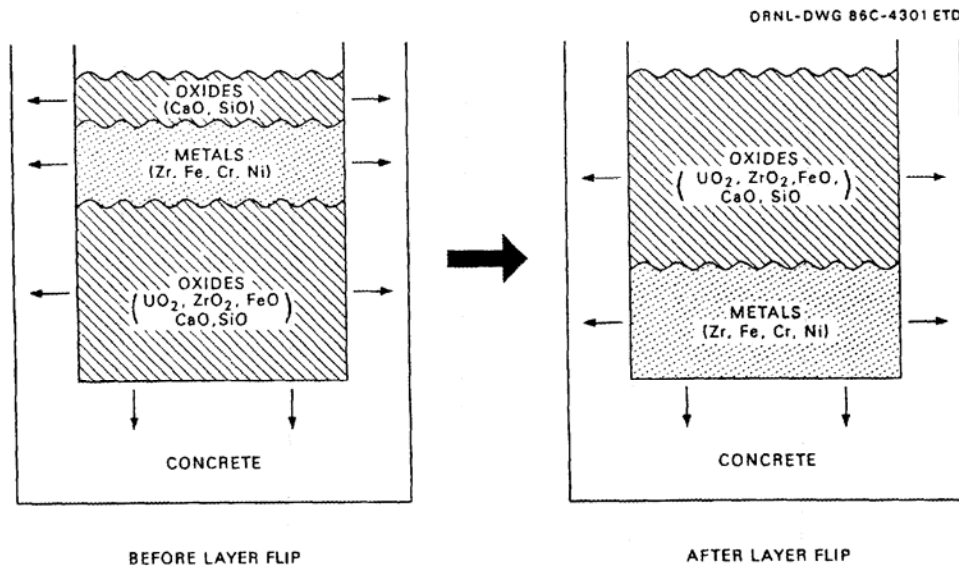


**Figure 5-3 Schematic Presenting Oxide-Metal Layer-Flip Phenomenon.**

The heat transfer to the concrete is highly dependent on the state of the corium/concrete mixture above its surface. While the melting point of a pure substance has a single melting/freezing point, the mixture of different material species, as evolves in the melt pool, results in an amorphous compound with no distinct melting/freezing point. Rather, the mixture exhibits solidus and liquidus temperatures distinct from each other, possibly spanning hundreds of degrees. In addition, certain combinations of material create eutectic compounds with melting temperatures lower than both pure substances. Within this amorphous state, the compound can still be fluid. The presence of internal heat generation from fission product decay heat and the oxidation of zirconium tend to sustain temperatures closer to the liquidus temperature than the solidus temperature. This is important because the viscosity of the melt pool affects the convective currents within the melt pool. A higher viscosity means a lower heat transfer rate. The viscosity of the mixture will increase with decreasing temperature when the temperature of the mixture is between the solidus and liquidus temperatures. Since the rate of ablation depends on the rate of heat transfer to the concrete, the biggest uncertainty associated with the ablation rate relates to understanding how the metals

---

and oxides mix or separate and that influence on heat transfer between the melt and the concrete.

To a lesser extent, heat transfer by thermal radiation and convection from the top surface of the pool competes with the heat transfer driving concrete ablation. These are not considered to be the dominant heat transfer mechanisms; however, they are significant enough that they need to be considered.

### **5.2.2.2 *MCCI Experimentation***

Basic information and insights from past experiments are presented in Table 5-6 (references provided in later subsections). In the experiments involving concrete ablation, molten material has been poured into a concrete crucible, or the material has been melted in the crucible (in situ). Some of the tests are transient tests with no decay heat simulation, while in others the interaction has been prolonged by heating the melt with electricity or chemical reactions. Concrete ablation has been measured by thermocouples embedded in the concrete. When the temperature reading increases above the melting temperature of concrete, it can be concluded that the melt front has reached the thermocouple. In most experiments, only axial (downwards) ablation has been investigated, and the sidewalls have been constructed of a refractory material. Radial erosion of the concrete sidewalls has been investigated in a few of these experiments.

**Table 5-6 MCCI Experimental Programs**

<b>Program (Organization)</b>	<b>Specification</b>	<b>Description/Phenomena</b>
BETA (FZK)	Cylindrical concrete crucible with diameter 38 cm; 300–880 kg of melt at 1800–2300 °C	2D-interaction of various concrete types with heated metallic melts ( $\text{Fe}_2\text{O}_3/\text{Al}$ -thermite) <ul style="list-style-type: none"> <li>- Directional concrete erosion rates and gas generation rates.</li> </ul>
ACE (ANL) MACE (ANL) OECD-MCCI	30x30 cm <sup>2</sup> , 50x50 cm <sup>2</sup> , 120x120 cm crucibles; 300-1790 kg of mostly $\text{UO}_2$ , $\text{ZrO}_2$ , $\text{SiO}_2$ and Cr; heating power of 35 - 150 kW	Heated 1D/2D-MCCI tests with prototypic oxidic melts and various concrete types for wet and dry conditions <ul style="list-style-type: none"> <li>- High initial heat transfer from corium (related to power supplied to the melt).</li> <li>- Significantly lower heat removal after crust forms on upper surface.</li> <li>- Homogenous flux distribution along the pool boundary.</li> <li>- Voiding in corium region beneath crust</li> <li>- Pool swelling followed by eruptions enhances heat removal.</li> <li>- More non-condensable gases (e.g., <math>\text{CO}_2</math>) from limestone-common sand concrete.</li> <li>- Concrete erosion and gas generation rates (multiple types of concrete).</li> <li>- 2D ablation observed</li> </ul>
BALI (CEA Grenoble)	15x300 cm <sup>2</sup> (15cm high); $\text{H}_2\text{O}$ -based liquids as corium simulant	Investigated convection phenomena and heat flux distribution in a volumetrically heated, bubble-agitated fluid with cold sidewalls – showed isotropic melt conditions <ul style="list-style-type: none"> <li>- Heat flux to the top, which envelops that to the side, is about the same as to the bottom over a wide range of gas rates and heat fluxes.</li> </ul>
BALISE (CEA Grenoble)	50x15 cm <sup>2</sup> concrete; $\text{H}_2\text{O}$ and oils as corium simulant	Special effect studies on gas-driven mixing of density stratified non-freezing liquids <ul style="list-style-type: none"> <li>- Correlations for predicting if oxide and metallic melt fractions become mixed</li> </ul>
CORESA (SNT, FANP)	Cylindrical concrete crucible with diameter 50 cm; laboratory (20 kg) and industrial scale (1000 kg)	Investigations on the interaction of metallic/oxidic melts with different types of concrete <ul style="list-style-type: none"> <li>- No melt plugging observed in transfer channel.</li> <li>- Stability of zirconia protective layer.</li> <li>- Emissivity of upper surface of MCCI pool.</li> <li>- Melt spreading distances.</li> <li>- Melt stratification.</li> </ul>
SICOPS-MCCI (AREVA NP)	Laboratory Scale experiments	Sustained-heated small scale tests (melt mass: ~5 kg) investigating the ablation behavior of sacrificial concrete with U.S. EPR-specific oxidic melts

Besides yielding a large amount of data on melt chemistry, gas rate and composition, temperature and erosion rate which serve as the validation basis of existing MCCI models, these experiments also provide insight in the general phenomenology of melt-concrete interaction, in particular regarding the:

- Differences in the behavior between metallic and oxidic melts
- Ratio between radial and axial ablation
- Mixing of metallic and oxidic phases

#### ***5.2.2.2.1 Differences in the Behavior Between Metallic and Oxidic Melts***

The experiments with metallic melts, BETA and CORESA (Reference 52 and 53), showed that progression into the concrete will proceed very quickly, as long as the melt is superheated. At high melt temperatures heat fluxes can be so high that the concrete at the interface is physically disintegrated, so that small pieces are mixed into the melt and are molten not at the interface but either in the bulk or at the upper surface.

This process, involving metallic melts, leads to a fast cool-down and, in later stages, to the formation of metallic crusts at the melt-concrete interface. Further, as the solidification temperature of steel is higher than the decomposition temperature of the concrete, concrete decomposition and melting has been observed to continue even after the metal was completely solidified.

The experiments that employed oxidic corium melts, ACE and MACE (Reference 54 – 56), revealed a different behavior because (1) the thermal conductivity of solid core oxides is very low, and (2) solid oxide melts freeze over a wide temperature range, due to the presence of high-melting refractory (U, Zr)O<sub>2</sub> and low-melting concrete (SiO<sub>2</sub>, CaO) components in the melt. The solidus-liquidus temperature range, within which the melt contains a certain amount of suspended refractory particles, can be more than 1000 K, as seen in Figure 5-4 (reproduced from Reference 58). During contact with a cold medium, such as concrete, the melt becomes surrounded by a crust that is

enriched with refractory material. This crust maintains the molten pool at a high temperature because its low thermal conductivity limits the heat transfer from the pool.

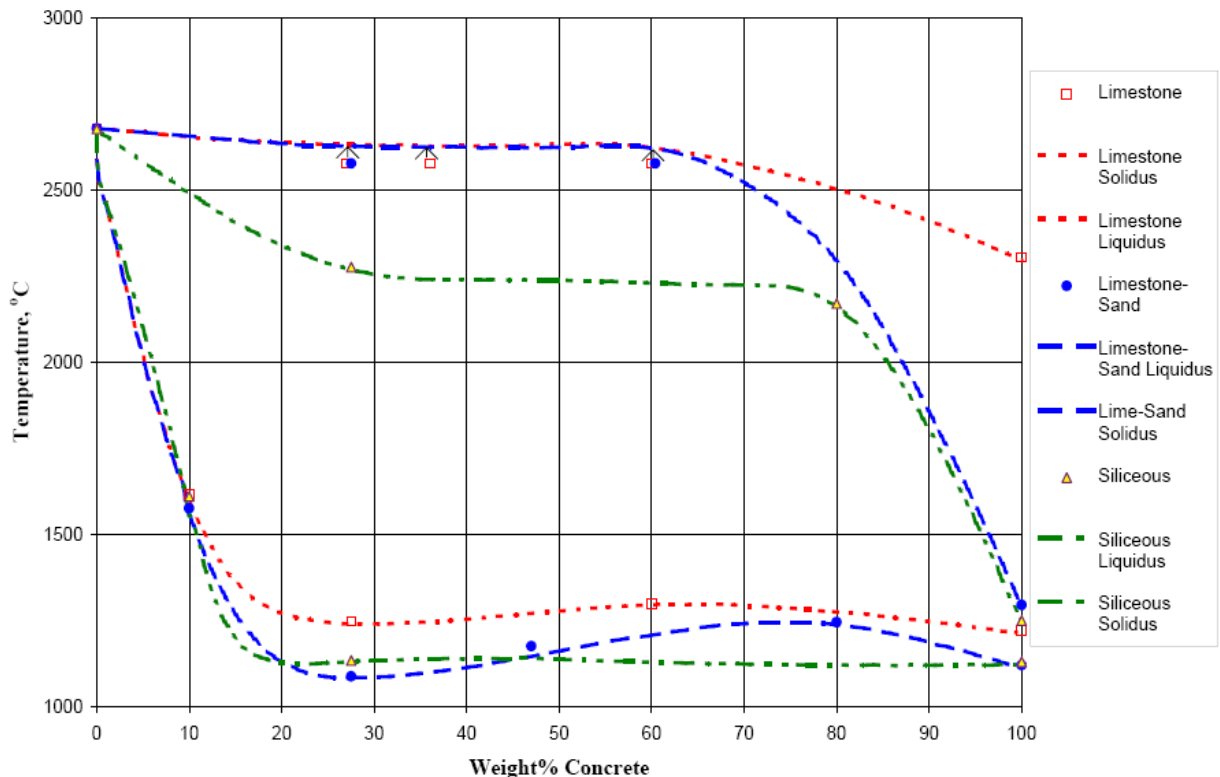


**Figure 5-4 Solidus-Liquidus Temperatures for  $\text{UO}_2\text{-ZrO}_2\text{-Concrete}$  Mixtures**

Due to its low thermal conductivity, measured concrete erosion rates for oxidic core melt were generally much lower than for metallic melts, in the period before reaching equilibrium conditions. For oxidic melts concrete melting is considered to be the dominant ablation mechanism.

The temperature of the oxidic pool practically follows the evolution of the liquidus temperature of the melt, which constantly decreases through the addition of light concrete decomposition products. This steady adaptation ensures that the solid fraction in the bulk of the melt, and with it the viscosity, will remain small at the time of spreading.

**5.2.2.2.2 Ratio of Radial to Axial Ablation**

The intensive mixing provided by gas release from the concrete composition will promote the development of a uniform heat flux distribution within the molten pool, resulting in comparable erosion rates in all directions. For oxidic melts this is confirmed, e.g. by the post-test analysis of MACE-M0 (Reference 57) and by the results of the BALI program (Reference 59). The latter tests demonstrate that the heat flux to the top, which envelops that to the side, is about the same as to the bottom over a wide range of gas release rates and heat fluxes. New experiments on 2D-melt front progression have been performed as part of the OECD-MCCI project (Reference 60 – 62), using large masses of heated prototypic corium. The tests focus primarily on the long-term behavior of the molten pool in existing plants (without spreading compartments), and therefore employ low heat fluxes and melt compositions that have much higher concrete fractions than would be present in the U.S. EPR reactor cavity.

For metallic melts, the transient large-scale tests in the CORESA program also indicate an isotropic behavior with, however, some unexplained deviations. Earlier tests provide little insight in this regard, as well. For the U.S. EPR concept, the related uncertainty has no negative consequences due to the fact that 2D-erosion by a metallic pool can be of relevance only if the melt is stratified with the metallic melt below the oxidic layer. This situation will only occur shortly before gate failure at a time when all corium is already added to the MCCI pool. Also if, at that time, the metal is assumed to be mixed into the oxide (emulsion), the pool behavior will be dominated by the oxidic phase for which the uncertainties, with respect to the spatial distribution of the heat fluxes, are much lower.

As long as the metallic melt is lighter than the uranium-rich oxide, and if the two phases are stratified, the metal can only erode in radial direction. In this situation there can be a kind of focusing of heat fluxes (similar to the in-vessel situation) that will result in a fast progression of the metal layer into the concrete of the sidewall. The metal melt will ultimately be stopped by the protective layer before it can reach the surrounding structural concrete. In the mixed mode the ablation rates are generally lower, so the

protective layer will be reached by the melt much later and at about the same time as the melt reaches the gate.

### **5.2.2.2.3 *Mixing of Metallic and Oxidic Phases***

From the time of the final corium pour from the reactor vessel (mostly oxides) to the moment of gate failure, the melt state is expected to transition from basically the 3-layer system of metal between a lower layer of core-oxide and an upper layer of slag to 2-layer system of molten metal below a core oxide phase. A mixed melt will apply if the MCCI agitates the melt constituents such that stratification between oxides and metals is prevented. Otherwise the metal will settle at the bottom, due to the large density difference (about 1000 kg/m<sup>3</sup>) between the two phases at that time. This inversion phenomenon has been explicitly observed in tests from the ECOSTAR, CORESA, and OECD MCCI programs, among others.

It is generally accepted within the severe accident community that gas release from the concrete composition will promote a uniform heat flux distribution inside the MCCI pool; this view is supported by tests such as MACE, BALI, CORESA, and OECD MCCI. Without gas generation, the heat flux distribution is expected to be the same as for natural convection, with the effect that a significantly higher fraction of decay heat is transported upward than downward. [Note: for the U.S. EPR, this would further increase the time until gate failure; higher heat transfer into the residual RPV (by radiation) improves the chances to collect potentially unreleased parts of the core. The assumption of a uniform heat flux distribution in the molten pool during MCCI is, therefore, conservative.]

The BALI tests (Reference 58) demonstrated that for superficial gas generation rates that are already much lower than the typical rates during MCCI, heat fluxes to the bottom of the pool are practically the same as to the top. The heat transfer to the sides under MCCI conditions was, unfortunately, not investigated in these tests. However, for other geometries, e.g. an RPV-type hemisphere, the values for the heat flux to the sides

were always between those to the top and to the bottom (which are now equal); thus, it can be expected that the heat flux distribution during MCCI will actually be isotropic.

Notwithstanding the experimental restrictions and inconsistent fluid properties, the correlations deduced from the results of the BALISE program (Reference 63) would predict that under the conditions in the reactor cavity of the U.S. EPR, the oxidic and metallic melt components will become mixed by the concrete decomposition gas. Under these mixed conditions, the properties of the created "emulsion" will be dominated by the oxidic melt. Further extension of the BALISE results support the conclusion that the retention function of the reactor cavity is ensured with large margins under either condition (mixed or stratified).

#### ***5.2.2.4 Impact of Submersion on MCCI***

In the case of late reflood or melt spread flooding, a MCCI pool will be covered with water. As theoretically predicted, and experimentally confirmed e.g. in the MACE experiments, the characteristics of the MCCI – in steady-state – do not depend on whether the surface is flooded or not. This is due to the fact that the upward directed heat flux is dominated by the intensity and type of convection within the molten pool, as well as by processes at the melt-concrete interface.

#### ***5.2.2.3 MCCI Conclusions***

As is discussed in the following sections, the phenomena associated with MCCI are incorporated into the U.S. EPR's overall severe accident management strategy. Thus, understanding the uncertainties associated with how the concrete is consumed by corium in different melt states is necessary. The rate of concrete ablation is controlled by the heat transfer from the melt to concrete. Test programs have identified or verified the dominant heat transfer mechanisms. Results from these tests show a strong dependence on melt state, which impacts thermal/chemical reaction rates, driving the ablation process.

Material properties of molten mixtures of corium and concrete, convective currents within a melt pool created by rising gas bubbles and debris streaming, the miscible quality of the melt constituents and the dynamics of crust formation/disintegration on the surface complicate the assessment of heat transfer from the melt to the concrete. These aspects are dependent on the amount and constituency of the original melt, the type of concrete (i.e., its constituent material and corresponding material properties), the melt temperature, and the types of chemical reactions occurring at the melt-concrete interface. Quantitative assessment of these phenomena is difficult because so much can only be inferred from test data.

Beyond the fundamental MCCI phenomena, measurable and certain inferred information, including temperatures (internal energy) and erosion rates, is available to assess uncertainties assuming “average” melt state conditions. Test results provide a good database to characterize ablation rates for different concretes and initial conditions (e.g., corium temperature, energy input). Current understanding of MCCI has been incorporated into computer codes and evaluated for uncertainty.

### **5.2.3 *Temporary Melt Retention in the Reactor Cavity***

For the U.S. EPR, a phase of temporary melt retention in the reactor cavity has been introduced to make the relocation of the melt into the spreading compartment independent of the release sequence from the RPV and of the corresponding state of the melt (characterized by temperature and composition). Reference 64 provides a detailed presentation of this aspect of the U.S. EPR’s severe accident response.

Temporary melt retention is based on the provision of sacrificial and protective layers in the reactor cavity. The sacrificial layer is intended to delay melt progression in the vertical direction and contact with the melt gate until most of the corium inventory has been released from the RPV. During this time the protective layer will restrict the radial penetration into the load-bearing RPV support structure.

### **5.2.3.1 Melt Accumulation and Conditioning Phenomenology**

Melt accumulation and conditioning is a function of the interaction between the corium melt and structural/sacrificial material in the reactor cavity. The choice of the reactor cavity material can have an influence on the melt stabilization process; thus, certain objectives are considered when selecting these materials. These objectives are

- The material must have sufficient stability to provide the time window for melt accumulation.
- The decomposition products of the material must beneficially affect the properties of oxide melt with respect to melt spreading and must result in a unification of the melt states at the onset of spreading.
- Low gas release resulting from material decomposition is preferred.
- The mechanical properties are not to be diminished compared to common construction materials.

Siliceous concrete has been demonstrated to have the optimal physical properties for the melt conditioning/melt retention function of the U.S. EPR. This material serves as the “sacrificial concrete” supported by a protective layer of zirconia. The melt retention function of the reactor cavity is based on the thermal and mechanical stability of the siliceous concrete walls against melt attack. The erosion rate must meet the objective of providing for a sufficient amount of time for core melt to accumulate core melt before melt gate failure. Concurrently, the erosion byproduct must be conducive to spreading when the melt gate does fail. Besides melt accumulation and conditioning, there exists no other requirements to be fulfilled during the retention phase in the reactor cavity. A detailed discussion on the justification of siliceous concrete as a sacrificial material in the reactor cavity is provided in Appendix B.

MCCI has a self-adapting characteristic with respect to the duration of the retention period. The advantage of concrete is that the speed of erosion by the melt is rather well determined. It is essentially a function of the total energy deposited. For an initially low

amount of released melt, the volume-to-surface ratio of the interacting melt and thus the heat flux and ablation rate are also low. This extends the time window for the inclusion of later pours from the RPV. For an initially high amount of released melt, the time window will be shorter – in accordance with the correspondingly reduced requirement.

MCCI has further been shown to favorably affect the constitution of the melt to facilitate spreading. According to Reference 64 the molten oxidic corium, during interaction with the concrete, will approach a state in which its bulk temperature is close to the melt's liquidus temperature, while a refractory solid crust is deposited at the surrounding walls. Therefore, MCCI ensures that, at the time of spreading, the oxidic melt will be highly liquid and will have a correspondingly low viscosity.

### **5.2.3.2 Melt Accumulation and Conditioning Experimental Programs**

Experiments carried out with prototypic oxidic melts, i.e. ACE (Reference 54), MACE 3b (Reference 55), MACE 4 (Reference 56), and most recently OECD-CCI-1 and -2 (Reference 60 – 62) show that both common construction concretes, i.e. limestone common sand (LCS) and siliceous concrete, would be able to meet the objective of sufficient stability and mechanical properties. The erosion behavior of these concretes in response to melt attack is similar and easily described by well-established models, which would ease the verification of the temporary melt retention with analysis codes. On these grounds, these concrete types were chosen as prime candidates for the sacrificial material.

In comparison to siliceous concrete, LCS concrete has the drawback of releasing significantly more non-condensable gas, particularly CO<sub>2</sub>, which would result in an increased pressure in the containment. Therefore, in view of the low gas content objective, LCS concrete was rejected and siliceous concrete selected as the base material.

Following this preselection, the ability of siliceous concrete to condition the oxidic melt for spreading and, at the same time to unify melt properties, is of interest. A precursor for melt conditioning is to oxidize the chemically aggressive constituents U and Zr of the

initially substoichiometric oxidic melt. The concentrations of these components in the oxide vary significantly with the underlying core melt scenario and therefore, the oxidation capacity of the concrete must be sufficient to cover the spectrum of in-vessel Zr oxidation levels.

Iron ore consisting of hematite ( $\text{Fe}_2\text{O}_3$ ) was found to be well-suited for addressing this issue and therefore a part of the siliceous pebble (i.e., primarily the  $\text{SiO}_2$  in the siliceous concrete mixture) was replaced by that material.  $\text{Fe}_2\text{O}_3$  contributes favorably to oxidizing Zr and U. The reaction byproduct Fe does not affect the thermo-chemical characteristics of the metallic melt. In addition, after the dissolved metal inventory in the oxide is depleted, surplus  $\text{Fe}_2\text{O}_3$  accumulates as  $\text{FeO}_x$ ,  $x \geq 1$  in the oxide melt, thus reducing the liquidus temperature and correspondingly, the temperature at which the MCCI takes place. This effect is beneficial for melt relocation into the spreading compartment, as it diminishes radiant heat losses and thus cooling of the melt during spreading.

$\text{SiO}_2$  reduces the fission product release from the MCCI pool because of the formation of silicates when mixed with melt. It further makes the melt less susceptible to energetic reactions with water and maintains the same quality with respect to mechanical strength and decomposition properties as common siliceous concrete.

The primary composition is strictly in accordance with ordinary siliceous concrete, which means that the concentrations of the three basic concrete constituents aggregate, cement and water in both concretes are identical. Specifically, the dry concrete mixture, i.e. the mixture before water addition, contains 15 wt% of Portland cement. The complement is the aggregate concentration, i.e. 85 wt%. The upper bound water content of the dried and hardened concrete is specified to be 5 wt%.

The use of  $\text{Fe}_2\text{O}_3$ , has required replacement of 45 wt% of the siliceous pebble, which in ordinary siliceous concrete constitutes the aggregate, with iron ore. Because naturally occurring modification forms, like iron ore and siliceous pebble, are used to supply

$\text{Fe}_2\text{O}_3$  and  $\text{SiO}_2$ , other constituents of those forms, i.e.,  $\text{MgCO}_3$  (dolomite) and  $\text{CaCO}_3$  (limestone) are also introduced into the concrete system.

The concrete's decomposition enthalpy and temperature are about 1730 kJ/kg and 1100 °C, respectively and thus are in the same range as for ordinary siliceous concrete.

### **5.2.3.3 Melt Accumulation and Conditioning Conclusions**

The introduction of a phase of temporary melt retention in the reactor cavity responds to the expectation that the release of molten material from the RPV will, most likely, not take place in one pour, but over a certain period of time, regardless of melt composition. Without retention, this release would create undefined and potentially unfavorable conditions for melt spreading into the lateral spreading compartment.

Temporary retention, which results in a "spreading in one event," is based on the provision of a layer of sacrificial material that must be penetrated by the melt prior to being allowed to escape from the reactor cavity. The corresponding delay ensures that, even in case of an incomplete first release of melt from the RPV, practically the entire core inventory will be collected in the reactor cavity (if it is not otherwise restabilized, e.g. by late addition of water). The admixture of the sacrificial material equalizes the spectrum of possible melt states at the end of the retention process. This makes the properties of the melt and therefore all subsequent stabilization measures independent of the inherent uncertainties related with the initial release of melt from the RPV.

Concrete has been identified to be a very beneficial kind of sacrificial material. Aside from its easy fabrication and application, it also has the advantage that the accompanying MCCI involves extensively investigated phenomena. Concrete further combines good stability with a high decomposition enthalpy. This is helpful, as a lower final volume of the melt (after incorporation of the concrete decomposition products) results in a smaller thickness of the molten layer after spreading and, as a consequence, in a shorter time for ultimate stabilization. In addition, the use of concrete conditions the melt such that:

- there is significant reduction of the liquidus temperature and, as a consequence, of the actual temperature of the melt
- the viscosity is kept at a low level that ensures easy melt relocation into the spreading compartment after gate failure
- the large volume of gas (hydrogen plus steam) released during thermal decomposition of the concrete ensures intense mixing resulting in homogeneous melt properties, and a nearly isotropic heat flux distribution inside the molten pool.

#### **5.2.3.4 Melt –Protective Layer Interaction Phenomenology**

At the beginning of the phase of temporary retention in the reactor cavity, the lighter metallic corium is located atop the heavier oxide. In this period, the speed of concrete erosion in the region of the metal phase (primarily lateral) will be faster than that in the oxidic phase. This is due to its significant level of superheat, and to the so-called “focusing effect,” in which the metal redirects part of the thermal energy it receives from the oxide into the surrounding wall, thus leading to a fast penetration of the sacrificial concrete layer.

To protect the structural concrete from the metallic melt during this phase, zirconia shielding is installed behind the sacrificial concrete. This protective shield surrounds the entire lower reactor cavity region and thus establishes a defined final limit for melt progression. It essentially predefines the maximum amount of sacrificial concrete that can be added to the melt during its retention in the reactor cavity and makes the retention function independent of the uncertainties regarding two dimensional melt progression, i.e., lateral vs. axial erosion.

Under most conditions, this zirconia layer will only be reached by the oxidic melt at the end of the retention phase. Therefore its main objective is to survive the contact with the metallic melt during the early period, when the metal melt is still atop and heated by the oxide melt.

Ceramic material is in principle highly stable against metallic melts. This is especially true because the superheat of the metal melt during MCCI under stratified conditions is low, and because the metal still has a low oxygen potential during this phase due to the presence of Zr, Si, and/or Cr.

Uncertainty concerning the homogeneity of two-dimensional melt-concrete interaction leaves open the possibility of contact between oxidic melt and zirconia liner at a time when the rest of the liner is still covered with concrete. It is, therefore, important that the protective layer demonstrate stability against both the metallic and oxidic melt fraction under the conditions of an ongoing MCCI in the reactor cavity.

#### **5.2.3.5 Melt –Protective Layer Interaction Experimental Programs**

The high liquidus temperature of zirconia relative to expected melt temperatures leaves infiltration and chemical erosion as the predominant mechanisms for penetrating the protective layer. The appearance and extent of the collective effects of chemical erosion and infiltration of the melt into open pore channels of the  $ZrO_2$  material has been found to depend on the:

- oxygen concentration in the melt
- porosity (size, distribution) of the  $ZrO_2$
- temperature gradient in the  $ZrO_2$
- formation of a sealed sintered layer at the front of infiltration

High temperature increases chemical reactions and diffusion while high oxygen concentration can form liquid Zr-Fe-O, a eutectic combination that can allow erosion at lower temperatures. High porosity provides a larger contact area for penetrating the protective surface. In contrast, sintered zirconia serves to severely retard penetration into zirconia.

Given that the most likely scenario for molten corium-protective layer contact involves metal melts, the primary focus of zirconia stability experiments has employed metal melts. Relative to oxide melts, metals have the capacity to take up oxygen, reducing the creation of Zr-Fe-O liquid. Zirconia-based materials have been tested extensively in the frame of the CORESA project (Reference 53 and Reference 65). For the contact with metallic melts it was found that, under reducing conditions (characterized by the presence of oxygen-getters like Zr, Si, Cr in the metal melt) that apply during the entire retention phase, there is no measurable dissolution, ablation or even infiltration into a sintered ceramic for temperatures of up to 2200 °C over test periods of more than 6 hours. [

]

The most severe situation, and least likely, is pure oxide contact with zirconia. Even under more conservative conditions, the evidence gained in past experimental programs showed that zirconia is dissolved by corium melts only at a slow rate. The medium and large scale CORESA tests demonstrated that zirconia can withstand a variety of oxidic melts containing chemically aggressive oxides for several hours with erosion of only a few cm (see Table 5-7). This is consistent with the findings of the EU-FW5 CIT project (Reference 66), where the measured speed of erosion into a zirconia ceramic by a corium melt with similar chemical composition (high FeO content) was also found to be < 2 cm/h.

The presence of MCCI has been shown to have a mitigative effect on the corrosion of zirconia by the introduction of "cold" concrete decomposition products into the bulk of the melt, which leads to the formation of a subcooled, two-phase mixture, consisting of: (1) a dispersed solid phase that contains mainly refractory material (zirconia, urania), and (2) a liquid phase that contains the concrete decomposition products plus the remaining refractories. As a consequence, the melt is "saturated" in refractory material, further limiting the dissolution of the protective layer.

The MACE/MCCI-OECD tests credited this effect by using a refractory material on the sidewalls. They used urania instead of zirconia because the latter has a high electrical conductivity which would interfere with the facility's electric heating method; however, zirconia is, nevertheless, equally stable under MCCI conditions, as both oxides are chemically very similar. In all tests, despite many hours of MCCI, the protective cover of the sidewalls was never subject to significant erosion.

Several investigations at various scales, with and without MCCI, have demonstrated these results for metal and oxide melts, with and without MCCI. In all cases, penetration of the refractory material is minimal. Table 5-7 summarizes some of these tests and includes the expected U.S. EPR conditions. These tests culminated with the large-scale CORESA 2.1. In this test, a hot steel melt (6 Mg) was kept under atmospheric conditions in an induction furnace lined with a pre-sintered zirconia. A temperature of 2000 °C was again sustained over 15 h. Post test investigation did not show any measurable erosion, despite the fact that mechanical abrasion by the agitated melt was now higher than in a stratified layer. The investigated temperature level of 2000 °C is also higher than expected in the spread melt of the U.S. EPR.

**Table 5-7 Melt Interaction with Refractory Material**

Program	Specification	Description/Result
CIT	< 20 min @ 2000 -2500 °C; 10–20 kg	lab-scale tests; oxide melt (UO <sub>2</sub> -ZrO <sub>2</sub> -FeO <sub>x</sub> ); ablation velocity ~0.5 mm/min
CIRMAT	< 20 min @ 2200 -2800 °C; 10–20 kg	lab-scale tests; oxide melt (UO <sub>2</sub> -ZrO <sub>2</sub> +/-Zr); ablation velocity ~1.5 mm/min without Zr and low superheating
Small-Scale MCCI	10 min @ 2300->2000 °C; 5 kg	lab-scale tests; representative corium melts; silicate concrete and U.S. EPR-concrete; ZrO <sub>2</sub> under MCCI conditions stable; ablation velocity < 2 mm/min
CORESA 1.2a	7 h @ 1700 °C max, 250 kg	Medium-scale; vs. Metallic melt (CrNi-steel), ZrO <sub>2</sub> ramming mass; Contact zone, A ≈ 0.4 m <sup>2</sup> (D = 0.5 m)
CORESA 1.2b	11 h @ 2000 °C max, 280 kg	Medium -scale; vs. Metallic melt (CrNi-steel), ZrO <sub>2</sub> ramming mass, concrete, and bricks; Contact zone: A ≤ 0.4 m <sup>2</sup> (D ≤ 0.5 m)
CORESA 2.1	17 h @ 2050 °C max, 6200 kg	Large-scale; vs. Metallic melt (CrNi-steel), ZrO <sub>2</sub> ramming mass; Contact zone: A = 4.3 m <sup>2</sup> ; no measurable erosion

### 5.2.3.6 Melt –Protective Layer Interaction Conclusions

The breadth of study of melt-zirconia interaction extends well beyond the expectation of events for a severe accident in a U.S. EPR. This body of work supports the application of zirconia as a protective barrier for conditions that exceed the needs of the U.S. EPR. Examination of melt type, with and without MCCI, at various scales has provided results that confirm the stability and the self-sintering behavior of zirconia under U.S. EPR severe accident conditions. Consequently, zirconia is an appropriate protective material that can be used under the physical and chemical conditions in the reactor cavity.

**5.2.3.7 Comment on the Stability of Structure Concrete and the RPV Support**

The top of the protective layer, and with it, the outlets of the ventilation duct have been specified to be safely above the maximum melt level in the reactor cavity. Therefore, the structural concrete around the reactor cavity will not come in direct contact with the melt. The zirconia-based protective layer has a very low thermal conductivity and will therefore delay the heat-up of the concrete in the lower part of the reactor cavity for many hours.

The situation is different above the top of the protective layer. Here the concrete will be subject to thermal radiation from the melt's surface (in the lower part) and to the heating by the hot gas that is released from the melt, which mixes with "cold" steam/air sucked in through the ventilation duct. A corresponding analysis yielded typical temperatures of this gas around the upper part of the RPV that were less than the melting temperature of the concrete. The melting temperature will only be exceeded in the lower part of the reactor cavity, close to the melt's upper surface.

**5.2.3.8 Melt Gate Failure Phenomenology**

The U.S. EPR melt stabilization concept involves two main phases: first a temporary retention and accumulation of the melt in the reactor cavity, and second, the spreading, flooding, and long-term cooling of melt in the spreading compartment. The failure of the melt gate located in the center of the bottom of the reactor cavity initiates the relocation of the melt from the reactor cavity into the spreading compartment.

The melt plug, which isolates the reactor cavity from the spreading compartment,



The retention time in the reactor cavity is determined primarily by the thickness of this concrete cover and not by the delay-to-failure time of the gate after melt contact.

The melt plug is the only location where the sacrificial concrete in the reactor cavity is not backed by a protective layer. Also the lower side of the gate is practically insulated (by the opposing zirconia walls) and will not be cooled otherwise, because the spreading compartment is dry by design. Therefore, the melt plug represents the predefined release location after melt retention in the reactor cavity. The main functional objective for the gate is that it must open with a sufficient cross-section to yield a high mass flow and a resulting quick transfer of the accumulated melt into the spreading area.

The consistency of the melt penetrating the plug will evolve into one of the following conditions:

- a 3-layer system, with heavy oxide at the bottom, metal above and a slag layer on top
- a 2-layer system, with metal at the bottom, and a oxide/slag layer above
- a completely mixed melt with metal dispersed within a lighter oxide

The exact consistency is uncertain. The described cases mainly differ in the efficiency of the heat transfer at the interface between melt and plug during the initial transient phase. This makes the timing of events uncertain; however, the sequence of events is more a function of total energy deposition and considering the high stored energy and decay heat of the melt, the gate failure is evident.

At the end of the retention phase, the erosion front that progresses into the sacrificial concrete will finally approach and uncover the aluminum gate at the bottom of the melt plug. Due to the low-melting point of the aluminum, the mechanism governing failure of the gate, resulting from contact with the melt, is a fast local penetration with subsequent hole enlargement by the flowing melt.

The actual flow area resulting from melt gate failure is also uncertain. As a result of the geometry of the reactor cavity, coupled with the relatively small ratio of the cross section

of the melt plug to the overall reactor cavity surface area (about one-tenth), the melt erosion front is expected to progress uniformly across the scale of the gate. As a result, a large part of the gate will be contacted by the melt within a short period of time (i.e., on the order of minutes). Nonetheless, each of the five cells delineated by the steel support grid under the aluminum gate has area sufficient to quickly relocate the melt from the reactor cavity to the spreading compartment. Hence, the assumption of rapid melt relocation remains valid even if the erosion front is at this smaller scale. If the initial local contact area is postulated to be significantly smaller than the size of one cell of the steel grid, radial erosion would be expected as melt flowed through the smaller hole. Eventually, this would widen the hole to allow all of the melt to relocate.

#### **5.2.3.9 Melt Gate Failure Experimentation**

The actual thermo-mechanical conditions to which the gate is subjected are prescribed by the characteristics of the preceding MCCI. The predicted melt front uniformity causes an uncovering of a significant fraction of the gate's surface within a short period of time, resulting in a uniform heat-up and a failure of the gate over a large cross-section. The uniformity of melt front progression into the concrete can only be judged on the basis of large-scale MCCI experiments, like ACE, MACE (oxidic melts), KAPOOL and CORESA (metallic melts only), see Table 5-6 and Table 5-8 (melt plug/gate).

The evaluation of the corresponding results is hampered by the fact that the technologies applied for the sustained heating of these melts did generally, or under certain conditions during the experiment, involve a positive feedback on local erosion in the sense that inhomogeneities were artificially amplified. Despite this, observed melt progression in these tests, was fairly homogeneous across the entire investigated area.

In addition to heated tests, there also exist several transient large-scale experiments, like KAPOOL (Reference 67) or CORESA (Reference 53). Melt progression in KAPOOL was homogeneous, but the concrete layer was relatively thin (1 cm). CORESA did not provide sufficient bottom area to draw conclusions about the

homogeneity of melt progression, but the results suggest that there exist mechanisms that level out local differences in erosion depth.

Oxidic melts are generally heated either by electrical induction (high frequency AC) or by direct current flow through the melt ("Joule heating" with low-frequency AC). The latter method was applied in all ACE/MACE-tests. It has the disadvantage that the current preferably passes through the hottest regions of the melt (as they represent the lowest electrical resistance). This creates a tendency to make hot regions even hotter. During MCCI, this "positive" feedback is counteracted by the mixing induced by the concrete decomposition gas. Under stagnant conditions (e.g. after the end of the initial melt generation phase in MACE M3b/M4 or during/after bulk cooling) mixing – and therefore heating – may not be sufficiently homogeneous. This can lead to the formation of hot channels between the electrodes and can explain the inhomogeneous erosion of the bottom observed in these tests during the initial phase. After transition into a quasi-steady mode (which, in M3b/M4, occurred after about 20 cm of concrete erosion) these initial inhomogeneities seemed to have disappeared. Further melt progression was practically uniform. In the U.S. EPR, the gate will be reached after 50 cm, or based on applicable experimental program results, about 2 hours of concrete ablation. Therefore, quasi-steady-state conditions are expected.

Based on these complementary results, a quasi-uniform contact is expected independent of whether the gate is initially contacted by an oxidic, mixed or (as predicted by the MCCI analysis) by a metallic melt.

The failure of an aluminum plate exposed to an oxidic melt during MCCI was specifically investigated in the frame of KAPOOL experiments at Forschungszentrum Karlsruhe (FzK) using non-heated (low density) alumina-type melts. In transient experiments with aluminum plates, such as KAPOOL 17, oxidic crusts temporarily delayed the penetration of the gate, but the gate was observed to heat up underneath this crust. The gate failed as soon as the temperature exceeded the thermo-mechanical failure limit of the aluminum. Separately, the MET test demonstrated the vulnerability of an aluminum plate to a high-energy melt progression (Reference 68).

No large-scale gate melt-through experiments with heated oxidic melts have been performed, due to the experimental difficulty in heating the oxidic melt without simultaneously heating the gate, which practically eliminates the use of inductive techniques.

**Table 5-8 Melt Gate Experiment Programs**

<b>Program (Organization)</b>	<b>Specification</b>	<b>Description, Phenomena, Insights</b>
KAPOOL (Fzk)	Ø 20 and Ø 50 cm plate, 92 and 150 kg of oxide melt, thin layer of sacrificial concrete	<p>Transient thermite tests on concrete erosion and gate attack (metal melts); various gate designs simulated including KAPOOL 13-17 with aluminum plates</p> <ul style="list-style-type: none"> <li>- Melt oxide crusts temporarily delayed plate failure, but eventually underlying aluminum plate heated up and failed in 3 of 4 tests.</li> <li>- Concluded that with decay heat, aluminum oxides would remain liquid and plates would fail</li> </ul>
MET-1 (ANL)	Not prototypic	2 cm thick plate of aluminum failed due to oxidic corium attack without any delay.

### **5.2.3.10 Melt Plug Failure Conclusions**

Melt will accumulate at the deepest location in the reactor cavity; that is, atop the melt plug. In this relatively large, flat region, ablation will progress predominantly in a one-dimensional, axial path. Since the melt plug design is not significantly different from surrounding sacrificial concrete, MCCI test programs are applicable. Consequently, the question of melt plug failure is simply a question of how the melt erosion front progresses through the plug. Uncertainties related to melt consistency and thermal characteristics have been examined and the evidence supports the assumption of a relatively homogenous erosion front; which, coupled with the oversized gate geometry, gives assurance of a gate failure sufficient to allow melt to flow into the spreading compartment.

## **5.2.4 Melt Spreading, Flooding and Stabilization**

Long-term cooling of the melt and heat removal in the U.S. EPR is achieved via the melt spreading compartment. This cooling structure has a flat cross-section of 170 m<sup>2</sup> consisting of a sacrificial concrete layer supported by a finned cast iron bottom cooling plate. Cooling channels within the cooling plate permit heat removal from the melt to the plate, in particular when the sacrificial layer is eroded. The crucible supporting the melt spreading compartment is formed by cast iron elements, which are flexibly connected to avoid problems resulting from thermal deformation. Melt arrival triggers the opening of two redundant spring-loaded flooding valves that initiate gravity-driven flow of water from the IRWST. The filling process will be completed within a few minutes (for the specified initial flooding rate of 100 kg/s, the filling process takes less than 5 minutes). The water first fills the central supply duct underneath the spreading compartment. From there, the water enters parallel, slightly tilted channels, formed by the fins at the bottom of the cooling elements. After the vertical space behind the sidewall structure is filled, water will start to pour onto the melt from the circumference of the melt spreading compartment to enhance the stabilization process.

### **5.2.4.1 Melt Spreading Phenomenology**

Once the melt plug and gate are thermally destroyed, the melt is guided through a horizontal transfer channel into the spreading compartment. Due to its large cross-section and its inert, temperature-resistant walls, the transfer channel itself is expected to have no retarding effect on the melt flow. Under the predicted outflow conditions, blockages at the melt front in the transfer channel cannot occur, even for purely oxidic melts. While metallic melts spread "like water" as they generally have a low viscosity and a high heat capacity, an initially liquid oxidic melt can only solidify during contact with the walls of the channel. As these consist of zirconia, which has a low thermal conductivity, the amount of heat that can be absorbed is very low. Superficial crusts are therefore limited to thicknesses less than a few centimeters. Given the propensity for the oxides to contain fission products, internal decay heat generation provides an inherent limitation in the coolability of the melt through the transfer channel. In addition,

debris that might flow with the melt has a limited affinity for attachment to the walls. As there is no other mechanism for heat transfer, any other kind of "volumetric" freezing in the channel is excluded.

As it exits from the transfer channel, the melt will spread under almost dry conditions due to the fact that the spreading compartment is a dead-end room. Only a very small amount of condensate may form inside the room. Though dry conditions are not necessary for a successful spreading, they make the distribution more predictable and eliminate the potential for fuel coolant interactions (FCIs).

Aside from the actual spreading phenomenon, melt spreading also exhibits all the phenomena typical of MCCI as it interacts with the concrete in the compartment. This includes high gas release, substantial melt agitation, and ejection of melt droplets. The phenomena associated with MCCI are discussed in Section 5.2.2.

The key advantage of the spreading compartment is the increase of the surface-area-to-volume ratio, thus, enhancing the overall coolability of the melt. SECY-93-087 recommends a "floor sizing criterion" surface area of  $0.02 \text{ m}^2/\text{MWth}$ . Considering the U.S. EPR's full power of 4590 MWth, the design value of  $170 \text{ m}^2$  greatly exceeds the recommended area of  $92 \text{ m}^2$ .

The U.S. EPR melt spreading concept also precludes ex-vessel steam explosions in the melt spreading area. It is initially dry; the melt has been conditioned with silica-rich sacrificial material by virtue of MCCI before flooding; and the addition of water to the top of the melt after spreading is slow and controlled. It is also anticipated that the proposed design will preclude "stable crust formation" observed in MCCI tests. The addition of silica to "conditioned" corium is expected to yield a lighter oxidic layer on top of the spread melt with an initially superheated metallic melt underneath. This superheated metallic melt will cause high concrete erosion and gas generation rates that will promote crust breakup.

#### **5.2.4.2 Melt Spreading Experimentation**

Table 5-9 summarizes data available for validating various aspects of the proposed U.S. EPR melt stabilization design. As indicated in this table, data have been acquired to determine the heat removal rate from the spreading compartment cooling channels, to ensure that the melt transfer channel does not plug, and to demonstrate MCCI phenomena related to concrete erosion rates, zirconia protective layer stability, ex-vessel steam explosions, melt segregation, and gas generation rate.

The phenomena related to melt spreading have been extensively investigated within the last decade, both theoretically and by dedicated experiments. It was found that the viscosity of the melt is determined mainly by its initial/boundary conditions. Thus, there is consensus that, if a sufficient flow rate and melt superheat are provided, the melt will spread uniformly and cover the entire area provided (Reference 69). This further justifies the chosen strategy of temporary melt retention in the reactor cavity by means of MCCI, as the MCCI ensures the necessary conditions for spreading.

The main objective of the melt-spreading experiments has been to provide data and observations for model development and validation. The CORINE, FARO, COMAS, RIT, VULCANO and KATS experimental programs (Reference 70 – 75) provide valuable insights into the physics of core melt spreading and are to varying degrees directly related to the verification of the U.S. EPR melt retention scheme. The improved understanding has been utilized for the development of various codes and scaling approaches. Their application to the issue of melt spreading for the U.S. EPR has conclusively shown that under the conditions developed by the MCCI in the reactor cavity, the rapid and complete relocation of the melt into the spreading compartment is ensured with large margin.

Experiments with prototypic corium, e.g. in the COMAS project (Reference 72) have yielded spreading lengths that equal the dimensions of the U.S. EPR spreading compartment at relatively low melt discharge rates of 100 kg/sec and below. Such low rates correspond to an opening of less than 0.01 m<sup>2</sup>, or less than one percent of the

---

entire U.S. EPR gate cross-section. The formation and persistence of such small holes is physically excluded as the melt outflow will always result in a minimum open cross-section in the order of about 0.1 m<sup>2</sup>, independent of the postulated initial contact area between melt and gate. The diameter of the created hole will increase steadily during melt outflow, due to the high melt-to-gate heat flux. These phenomena make the discharge process self-adjusting as, for an initially small hole, the duration of the discharge and with it the time for "hole-widening" will be correspondingly extended.

Computer simulations of the U.S. EPR spreading process (Reference 76) which are based on the knowledge gained from the referenced experimental programs, demonstrate that the large mass (hundreds of tons) of the accumulated corium-concrete mixture will ensure that the spreading process is effective and that the spreading compartment is covered uniformly, even for unfavorable initial conditions regarding melt temperature and viscosity. In addition, prior to a severe accident, there is no direct water inflow path into this compartment. As a consequence, except for the possible existence of extremely small amounts of condensate, the compartment will be dry at the time of the melt arrival. While the experimental evidence obtained by the wet spreading tests in the frame of CORINE, FARO, RIT, and KATS test indicates that dry conditions are not required for successful melt spreading, those conditions make the distribution process more predictable, as the potential for local FCI is eliminated.

**Table 5-9 Melt Spreading Experimental Programs**

<b>Program (Organization)</b>	<b>Specification</b>	<b>Description</b>	<b>Results/Insights</b>
CORINE (CEA)	Scaled for non-prototypic simulant melts	Dry and wet 1D-spreading tests with low temperature simulant melts (water/glycerol mixtures), examined freezing/non-freezing, various inflow conditions and geometries	- Demonstrated spreading dependency on initial and boundary conditions
KATS (FzK)	Large spreading distances (~15 m for 1D, ~2m x 3m for 2D); ~180 kg; 2300 K	1D/2D-spreading tests, using high temperature simulant melts (metal/oxide) under dry and wet conditions	- No melt plugging observed in transfer channel. - Spreading not influenced by pre-existing thin water layer.
COMAS (SNU) COMAS-EU (SNU)	30cm x 8 m channel; ~650 kg; 1800 K	1D-spreading test on concrete and metallic surfaces using prototypic corium melts (metal/oxide/mixed) under dry conditions	- No melt plugging observed in transfer channel. - Stability of zirconia protective layer. - Emissivity of upper surface of MCCl pool. - Melt spreading distances. - Melt stratification.
VULCANO (CEA)	0.4x1.2m <sup>2</sup> (19° expansion; 47 kg; ~2200-2400 K	1D-spreading tests, using high temperature simulants as well as prototypic corium melts (oxide) under dry conditions	- Melt spreading distances.
FARO (JRC - Ispra)	0.15x3.2m <sup>2</sup> (17° expansion; ~200 kg; <3000 K)	1D-spreading/pouring tests, using high temperature prototypic melts (core oxide composition) under dry and wet conditions	- No retardation of melt spread in flooded cavity
RIT-Spreading (RIT Stockholm)	Scaled for non-prototypic stimulant melts	1D/2D-spreading, using medium temperature simulant melts (oxide) – dry and wet	- 2D spreading is very efficient, provided the melt flow rate is relatively high and the melt viscosity is relatively low.

### **5.2.4.3 Melt Spreading Conclusion**

The main function of the spreading compartment is to provide an area to spread and cool the molten core material. Spreading increases the surface-area-to-volume ratio of the melt and results in effective and predictable cooling. The U.S. EPR melt spreading concept provides for a much more robust containment when compared to existing reactor containments. In addition to the large spreading area, the design has included several aspects that should further promote debris coolability and melt stabilization (e.g., the inclusion of silica materials, the use of cooling channels beneath the spreading compartment, and melt flooding). Melt travels from the gate through a transfer channel in which blockage is unlikely considering the low conductivity of the channel housing (zirconia) and high stored energy and decay heat.

Based on test results examining the melt retention process, the molten material is expected to spread quickly (i.e., within tens of seconds) and uniformly if:

- The melt temperature and viscosity are low

This condition exists as the result of MCCl in the collection area. It should be noted that in most of the referenced experiments, spreading was effective despite the fact that oxidic melt temperatures were below the liquidus level and, consequently, that the melts were in the slag region. A superheated melt has a significantly lower viscosity and crusts formation will be delayed. In such cases, the melt will spread much better and margins will be larger.

- the mass flow is sufficient

This condition exists if the molten material can be held in the reactor cavity long enough for the most part of the core material to be discharged simultaneously. On the basis of the knowledge gained from these tests, given a large open cross-section and a large melt conditioned through the MCCl process, a uniform spreading will be achieved. This also holds true for a postulated release cross-section of 10% of the U.S. EPR gate area of 2.4 m<sup>2</sup> and for the

most conservative melt release sequences: first oxidic then metallic melt. As a consequence, a layer inversion in the reactor cavity before melt spreading is no longer a necessary condition.

In general, data are available for evaluating most of the relevant phenomena associated with this concept. That fact that there have not been explicit tests to demonstrate MCCI phenomena coupled with melt spreading with heated oxide and metallic melts is of no practical relevance because the decay heat generation during the short period of spreading is negligible. Spreading on concrete was found to not deviate significantly from spreading on inert substrata (without gas generation) so the findings from transient experiments can be transferred. The primary conclusion from melt spreading research is that the ability of the melt to spread has been shown to depend on initial/boundary conditions and flow rate. With the large masses and volumes and low viscosity, spreading is expected to be fast (within minutes) and complete for a broad range of melt conditions. There is a consensus, as formulated in the final documents of the European Group for Analysis of Corium Recovery Concepts (EUROCORE) (Reference 69) that melt spreading is not an issue of further experimentation, since the main problems are now understood.

#### **5.2.4.4 *Melt Flooding and Stabilization Phenomenology***

In a bounding severe accident event, the even spread of molten material is expected to cover the spreading compartment with a thickness of approximately 50 cm. When the melt enters into the spreading area, spring-loaded flooding valves will be opened by a thermal actuator. Through these valves, water from the IRWST passively floods an array of horizontal cooling channels formed by the fins extending from a cast iron liner below a layer of sacrificial concrete that ultimately supports the melt spread. The incoming water first fills the central supply duct underneath the spreading compartment from which it enters the cast iron cooling channels. With the designed initial flooding rate of about 100 kg/s, the filling process will be complete after about 5 min (with two flooding valves open) and water will start to pour onto the melt from the circumference of the spreading room. This overflow will continue until the hydrostatic pressure levels of

the IRWST and spreading room are balanced. The ultimate cooling and solidification of the molten material does not require any special mechanisms, assuming that the heat transfer from the molten material to the water pools is unobstructed. Molten metal material is expected to solidify in a few hours and molten oxide material in a few days.

Decay heat created within the molten spread is extracted first by contact with the sacrificial concrete then through the heat-up and evaporation of water drawn passively from the IRWST. At the time the melt layer comes in contact with the cooling structure at its sides and bottom, its upper surface will be completely flooded. The melt is therefore fully enclosed by water or water-cooled surfaces. The performance objective is that all corresponding heat fluxes to the top, side and bottom must be safely absorbed.

In parallel with the flooding process, the molten spread interacts with the sacrificial concrete layer that covers the horizontal and vertical surfaces of the cooling structure. The presence of this concrete layer ensures that the cast iron cooling structure will be cooled on the outside prior to its first contact with the molten corium.

During MCCI, the temperature and the density of the oxidic melt fraction are steadily reduced by the incorporation of concrete decomposition products. The density difference between the molten metal and oxide will be significant; therefore, the formation of a density-stratified system, with a lighter oxide layer on top of a heavier metal layer is physically unavoidable. This type of stratification has the following consequences:

- The water that pours onto the melt will contact the oxidic melt fraction.

Moderate heat transfer will occur through fractures in this surface which are enhanced by contact with the pool of water.

The formation of an oxidic crust at the top which contributes to the avoidance of

metal and water contact and reduces the likelihood of FCI's (reduced heat transfer from melt to water).

- The sacrificial concrete layer mainly interacts primarily with the metallic melt fraction.

The decomposition and ablation of the concrete layer at the bottom of the melt layer requires a large amount of energy, which is extracted from the metallic melt. Preliminary analysis has shown that this will quickly reduce the temperature of the metal layer below its freezing temperature. The resulting formation of crusts reduces the transient thermal loads during the subsequent contact between the metal layer and the cooling plate.

The described consequences of a separation of layers seem advantageous. They are, however, not necessary for the proper functioning of the spreading compartment. Transient thermal loads on the cooling structure are acceptable, if the metal remains suspended within the oxide during the entire MCCI. In this case the surface of the cooling plate is protected by a solid oxidic crust. In addition, flooding rates into the melt spread compartment are engineered (i.e., low), based on experimental results, to prevent the explosive characteristics of FCI.

The heat carried from the melt into the cooling structure is transferred to the water through both the horizontal and vertical surfaces of the channel fins. As a consequence, even the formation of an insulating steam layer in the upper part of the channel at higher heat fluxes ( $> 80 \text{ kW/m}^2$ ) will not result in critical heat flux (CHF) condition.

#### **5.2.4.5 Melt Flooding and Stabilization Experimentation**

The mechanisms that govern flooding and quenching have been observed in the frame of MACE (ANL), OECD-MCCI, and ECOKATS (FzK) (Reference 77) as identified in

---

Table 5-10. These experiments showed that flooding will lead to bulk cooling and will create an oxidic crust at the top of the melt.

In the U.S. EPR, MCCI will still be occurring within the spreading compartment at the time of flooding. Therefore the melt stratification phenomena observed in the MACE and OECD-MCCI experiments are applicable. Despite the formation of insulating crusts, top flooding is considered to improve the conditions for long-term cooling by crust cracking and fragmentation.

The experiments showed that flooding leads to bulk cooling and creates an oxidic crust at the top of the melt. Depending on whether or not this crust is suspended above the molten phase, different phenomena could be observed. These include initial mixing, crust cracking with water ingress and/or the ejection of material into the fluid pool atop the crust. The last mechanism was identified as being the most promising in achieving long-term cooling of the melt by fragmentation. For this mechanism to be effective, the crust must stay in contact with the melt and not be suspended (i.e., a “floating crust”).

Among the flooding experiments, the MACE tests are the most prototypic for the U.S. EPR case due to the combination of large mass, realistic melt composition and flooding rate. The ECOKATS-2 experiments performed as part of the ECOSTAR project provided an even larger test section but suffered from the use of a simulant oxidic melt (a mixture of alumina, calcia and silica). As a result the quenching behavior after flooding and the morphology of the formed crust may not be fully prototypic. As opposed to MACE, where flooding led to a fast quenching and solidification across the entire surface of the melt, ECOKATS showed only late transition into nucleate boiling and crusts grew slowly from the sides toward the center.

Three MACE melt pool coolability experiments (Reference 78) were performed successfully in which melt pools at various scales were generated on top of LCS concrete basemats and water was added on top. The melt material contained uranium oxide, zirconium oxide, zirconium and some concrete products. The decay heat

generation in the melt was simulated by means of electrical heating. It was found that for these three tests, the effect of the sidewalls dominated the phenomena, since an insulating crust was formed that attached itself to the sidewalls. The crust prevented intimate melt-water contact and the heat transfer rate slowly decreased from approximately 2 to 0.1 MW/m<sup>2</sup>, which is less than the decay heat input to the melt.

Three modes of heat removal from the top of melt pool have been identified. These are the (1) initial melt-water contact; (2) the conduction through the crust; and (3) melt eruptions into water, when the heat generated in the melt is greater than that removed by conduction or water ingress through the crust. In the largest MACE test (incorporating a LCS concrete basemat), analysis of test results concluded that significant water ingress occurred. Continued concrete ablation lowered the level of the melt, leading to the separation of the melt pool from the suspended crust, and the conduction heat transfer decreased substantially. In a smaller integral melt coolability test with siliceous concrete, similar results were observed; however, both gas content and volume reduction due to ablation is less than that of LCS.

Because of the uncertainties associated with crust formation and water ingress on the top and sidewalls of a molten spread, heat transfer through the bottom of the structure becomes important. To quantify the heat removal capability of the horizontal cooling channels, experiments in a fullscale, horizontal 5-m-long channel have been performed (Reference 79). The channel length corresponds to the distance from the central supply channel to the sidewall of the spreading area. The melt was simulated by electrically heating the channel from the top. The channel was integrated into the BENSON test-rig, a separate-effects test apparatus at AREVA NP's facilities in Erlangen, Germany.

As previously described in Section 2.2.3.4, basemat cooling in the spreading compartment is facilitated by a system of nearly-horizontal, parallel channels connected to large reservoirs, i.e., the central supply channel on the inflow and the water pool atop the melt on the outflow side. This characteristic decouples the individual channels from each other. The performed CHF-tests demonstrated that, when a channel is not supplied with water at the "inflow" side, it will "draw" sufficient coolant from the "outflow"

side. Therefore, the individual channels do not "rely" on a certain distribution of the water flow in either the active or passive mode of operation. Consequently, one-channel tests are representative in the sense that, if flow-instabilities do not occur in a single channel over the entire range of relevant heat fluxes (as confirmed in the referenced CHF-tests), they will also not occur in the system of parallel channels under the given decoupled conditions existing in the plant.

The conditions for heat flux prescribed for study in the BENSON tests were based on decay power and expected melt temperatures. As a design objective, the capacity of the cooling structure must always exceed the heat flux provided by the melt. A bounding value for the corresponding downward steady-state heat flux can be obtained, by dividing the decay power in the melt by the total surrounding surface area (top and bottom are 170 m<sup>2</sup> each and the sides are 50 m<sup>2</sup>). Accounting for decay heat levels at the time of melt plug failure and the dispersal of about 25% of the volatile fission products directly into the containment, this yields a value of  $\sim 28 \text{ MW} / 390 \text{ m}^2 = 72 \text{ kW/m}^2$ . In reality, the steady-state heat flux will always be lower than that, because natural convection favors the heat transport to the top. Assuming large uncertainties in decay heat and stored energy, a conservative bound of 100 kW/m<sup>2</sup> can be hypothesized. Transferring the heat to the water pools in the upward or lateral direction is not a problem because the critical heat flux is very high ( $\sim 1000 \text{ kW/m}^2$ , based on test program results). The CHF downward from the molten material is, however, much smaller than in upward or lateral direction. The maximum of the downward heat flux is estimated at approximately 100 kW/m<sup>2</sup>.

In the experiments at higher heat fluxes (minimum of 60 kW/m<sup>2</sup>) a local dryout occurred at the top of the channel. This condition was observed with the cooling element duct experiencing stratification, with steam at the top of the duct and water at the bottom. Nonetheless, structural temperatures remained in a safe range. This desirable performance, which results in high effective CHF margins, is attributed to the fact that heat can enter the water through both the horizontal and vertical surfaces of the cooling

structure. The observed heat removal capacity must be compared with the realistically-expected maximum transient heat flux from the melt.

The results from the AREVA NP full-scale thermal-hydraulic test performed in the BENSON test-rig show that the cooling is effective at heat fluxes up to more than 120 kW/m<sup>2</sup> (limit of the heating system in the test). In accordance with the potential modes of operation, both cocurrent and countercurrent flow of the water/steam mixture have been investigated. Other tests in this program have shown similar performance with the water coolant containing boron and impurities.

The CHF-experiments showed that the heat transfer inside the channels is equally effective under both cocurrent (inflow from IRWST) and countercurrent (inflow from the saturated pool atop the melt) conditions. This robustness eliminates the need to establish and sustain certain flow conditions within the individual cooling channels. Instead it is sufficient to keep the outside of the spreading compartment submerged. In the U.S. EPR design, this is automatically achieved by the connection between IRWST and spreading room. Thus the melt will always be cooled on a fully passive basis; no pumps and no external water supply outside the containment are needed.

**Table 5-10 Melt Flooding and Stabilization Experimental Programs**

<b>Program (Organization)</b>	<b>Specification</b>	<b>Description</b>
MACE (ANL)	2000 kg	1D MCCI experiments using heated prototypic oxidic corium melts with top flooding
MCCI-OECD (ANL)	400 kg	2D MCCI experiments using heated prototypic oxidic corium melts with top flooding
ECOKATS-2 (FzK)	2x2 m <sup>2</sup> ; 3.2 tons; 2100 K	2D spreading test with subsequent transient MCCI, using high temperature simulant melt (thermite)
BENSON CHF-tests (AREVA)	Heat fluxes up to 120 kW/m <sup>2</sup>	Heat transfer and CHF limits within a horizontal, top-heated, rectangular channel under various flow conditions

#### **5.2.4.6 Melt Flooding and Stabilization Conclusions**

The stabilization of the melt in the spreading compartment is based exclusively on cooling and crust formation/break-up. Consequently, there are no limiting thermal-chemical constraints, and there is no need to ensure a certain range of melt compositions, or a certain melt layering or distribution. Due to the high surface-area-to-volume ratio created by the spreading process, and the fact that the melt is completely surrounded by cooled surfaces, a safe enclosure of the corium within crusts will be achieved soon after the end of the MCCI in the spreading area. The denser metallic melt fraction at the bottom is predicted to freeze within the first few hours. Solidification of the decay-heated oxidic melt will take longer but is estimated to be complete also after a few days.

Experimental programs have addressed the impact of melt state and have been valuable in identifying the dominant heat transfer mechanisms. While heat transfer from the top of the molten spread involves a large degree of uncertainty related to the formation and break up of crusts, heat transfer through the bottom and sides has been shown in the BENSON Test Rig tests to be capable of adequately supplementing heat removal at rates approaching 100% of decay heat.

#### **5.2.5 Core Debris Coolability Conclusions**

The previous section has illustrated that the U.S. EPR concept complies with the objectives for melt stabilization. The chosen strategy, to separate the functions of the accumulation of the melt after RPV failure from its long-term stabilization and cooling, avoids uncertain and potentially critical loads on the spreading compartment. The concept involves two main stages, temporary retention and accumulation of the melt in the reactor cavity and its subsequent stabilization and long-term cooling in the spreading area. There is an automatic and fully passive transition between the two states by means of gravity-driven spreading of the accumulated melt after gate failure.

The ex-vessel concept of the U.S. EPR has the advantage that the existing uncertainties regarding:

- possible scenarios
- RPV failure modes
- thermo-chemical phenomena (i.e., MCCI and possible melt stratification)

are eliminated by the introduction of a phase of temporary melt retention in the reactor cavity. This significantly reduces the spectrum of melt states and decouples the spreading process and the final stabilization and cooling from the inherent uncertainties, related to the preceding phases of the accident.

Complex thermo-chemical situations, which are insufficiently understood – such as the role of unoxidized zirconium – are avoided by the admixture of sacrificial concrete, which influences the properties of the melt in a favorable way. The early addition of fission product getters, e.g. SiO<sub>2</sub>, ensures effective retention of low volatile fission products in the melt.

In conjunction with developing the severe accident strategy, as described previously, it was determined that experimental data were needed to support the design and to analyze its operation. Through the many experiment programs sponsored by both U.S. and European research institutions, the U.S. EPR solution has demonstrated that the preceding temporary retention in the reactor cavity does also establish a simple, automatic and passive way to perform this task. In addition, they have provided the phenomenological background and data necessary for understanding and modeling of the key processes involved, addressing uncertainties and extrapolating results to reactor scale by means of validated computer codes.

### **5.3 High Pressure Melt Ejection**

HPME and associated DCH are not considered relevant severe accident phenomena for the U.S. EPR, as defined in Section 3.3. The U.S. EPR design includes features that make the risk from HPME negligible. The key feature is the primary depressurization system; however, low core power density, a RPV lower head without

penetrations and a torturous pathway from the reactor cavity to the upper containment all contribute to preventing or mitigating the potential consequences of high pressure melt ejection. In coming to the conclusion that the HPME event is remote, the existing literature on this subject was evaluated and summarized in this section to provide a technical basis for this position.

### **5.3.1 High Pressure Melt Ejection Phenomenology**

HPME is a postulated mechanism for the release of finely dispersed core debris into the containment atmosphere, corresponding to a rapid blowdown of the RCS, and, thus facilitating rapid heat transfer between core debris and the containment atmosphere, potential hydrogen combustion, oxidation of metallic aerosols and overpressurization of the containment. The resulting DCH has been assessed as a means of early containment failure because the stored energy of the debris, including potential energy release through debris oxidation and hydrogen burning, is enough to cause containment overpressurization if a large quantity of the core inventory participates. The extent of pressurization thus depends upon:

- the amount of debris which would be discharged at vessel failure
- the containment geometry which could be conducive to or an impediment to dispersal beyond the reactor cavity
- the fraction of the debris that could be finely fragmented and dispersed into the containment atmosphere

The fundamental issue for DCH is whether a massive dispersion of core debris, in the form of fine particulates, into the containment atmosphere is credible. Six precursors can be identified which would be necessary for such an outcome:

- *Large Core Melt* – core coolability must be completely lost with no opportunity for recovery

- *High Pressure* – the reactor vessel must fail at high pressure, providing a significant force to push out a large volume of core debris
- *Entrainment Potential* – core debris must remain either in the blowdown streamlines or close enough to be entrained from the reactor vessel
- *Affinity to form Particulates* – the debris must break up into fine particles that enhance the surface-area- to-volume ratio, facilitating rapid heat transfer from the particles
- *In-containment Aerosol Dispersal* – the plant geometry must be such that debris dispersal can occur from the reactor cavity to the remainder of the containment
- *Long Residence in Containment Atmosphere* – the particles must remain airborne long enough to transfer energy and react chemically if in contact with steam or oxygen.

Of these precursors, high pressure and in-containment aerosol dispersal were identified as being the primary sources of uncertainty in NUREG/CR-5809 (Reference 15). These factors have been explicitly addressed through design of the U.S. EPR.

Assuming the failure of several highly reliable design-basis protection systems, core damage is a possible outcome. The extent of core damage depends on the accident scenario and any operator activities associated with further accident progression and accident mitigation. The design of the U.S. EPR severe accident response features considers a hypothetical complete degradation and melting of core inventory and support structure, including the heavy reflector. As a result, the large core melt precursor is a bounding initial condition for further consideration of the HPME event.

In considering the HPME event for the U.S. EPR, actuation of the highly reliable primary depressurization system is expected. Nonetheless, previous investigation into HPME has concluded that the nature of RCS breach is different at high pressure, compared to low pressure. Natural circulation flows transport high-temperature steam throughout the

RCS, driving potential creep rupture of components other than the RPV lower head, such as the hot leg or the pressurizer surge line. In this scenario, the likelihood of RPV failure in the lower head is considered low in relation to these possible competing RCS failure locations. This has been demonstrated by several analyses provided in open literature (Reference 80) for current-generation nuclear power plants and is even more likely for the U.S. EPR design, because of the absence of lower head penetrations. At a failure location far removed from the RPV lower head, passive RCS depressurization would occur without significantly entraining molten debris residing in the RPV lower head. For the bounding situation of a total loss of core integrity, the melting of the heavy reflector would create a bypass for flow between the reactor vessel inlets and outlets. For lesser melts, based on the experience of TMI-2 coupled with the low core power density of the U.S. EPR, a stable crust formation could be expected on the top of the debris pool by the time of RPV creep rupture failure. The presence of the solid crust layer would be sufficient to prevent the direct contact between the gaseous phase and the liquid phase of the core debris during blowdown, thereby preventing any entrainment of molten core debris from inside the vessel during RCS depressurization.

To maximize the entrainment potential in an HPME, the lower head must fail. For the two most common lower head failure modes, local sidewall penetration and global circumferential failure, entrainment potential and the affinity to form particulates are compensating factors. The smaller local sidewall penetration is postulated to be near the interface of the heavy oxide and lighter metallic melts. As a result, entrainment via this sidewall penetration would remove the metallic melt, which, at the high velocities associated with a small hole should form particulates efficiently. Despite the expected expansion of the local penetration, the heavier oxide would be more susceptible to impaction around the hole, thus leaving a significant quantity of melt within the reactor vessel lower head. Conversely, a global failure of the lower head would efficiently remove the contents of this region; however, the lower gas velocities associated with this failure mode would be less likely to cause the melt to form particulates. Although, not considered as likely, a smaller penetration at the very bottom of the lower head

would comprise the most severe reactor vessel failure mode, optimizing both entrainment and debris particulation.

Debris particles under high pressure would be driven from the reactor cavity region toward the remainder of the containment. Challenging this dispersal phenomenon are any flow resistive obstacles along the various pathways. The U.S. EPR has several such obstacles beginning with the narrow gap between the reactor vessel and reactor cavity. Beyond that, the U.S. EPR's compartmentalized containment design requires that debris travel toward the steam generator equipment room where vents, in the form of mixing dampers and rupture foils, will open to promote atmospheric mixing. Heavy particulates will tend to impact on surfaces at every turn or orifice and to accumulate at those locations. Consequently, the flow stream will have had the majority of the debris removed prior to reaching the outer containment region, where heat transfer to the atmosphere could lead to overpressurization. Instead, impacting debris will impart much of its energy to the various compartment walls at a much slower rate than if it could maintain a fine aerosol form and reach the outer containment region.

For those smallest particles that could conceivably arrive in the containment, the residence time necessary for heat transfer from the remaining aerosols is probably sufficient to remove sensible heat from these particles prior to any settling of the remaining core debris particles. Nonetheless, the promotion of atmospheric mixing resulting from the blowdown of the reactor vessel or from hydrogen recombiners and natural circulation driven by cold containment surfaces, should provide sufficient opportunities for interaction of debris with obstacles to allow core debris to settle in short order.

### **5.3.2 High Pressure Melt Ejection Experimental Programs**

Several experiments and analyses have been performed to study HPME inspired by the 1981 Zion Study (Reference 81). In addition, the evaluation of the various reactor cavity configurations in current-generation nuclear power plants under a variety of scenarios was presented in a DCH closure report for Westinghouse large dry containment plants

(Reference 82). In terms of size and environmental conditions, the U.S. EPR is very similar to the Westinghouse containment. This work on DCH closure demonstrated a conditional containment failure probability of less than 0.1, which was considered a sufficient threshold for declaring closure. Many of referenced activities in the closure report were NRC-sponsored and administered by SNL beginning in the early 1980s. Table 5-11 presents a summary of major test programs that examined HPME and associated DCH (compiled from Reference 83). These programs have focused on Westinghouse large dry containment designs at very large scales from 1:40 to 1:6. During this same period of time, the NRC also sponsored a scaling study specifically in support of the resolution of the DCH issue (Reference 15). A key result from that study was that pressure and cavity geometry were the dominant DCH contributors.

From 1983 - 1991 SNL conducted experiments on 1:10 linearly-scaled cavity geometry of the Zion nuclear power plant containment. These were the High Pressure Melt Streaming (HIPS) and Surtsey experiments (Reference 84 - 87). While the HIPS test employed an open cavity configuration, for the Surtsey experiments, the cavity was completely enclosed in a large vessel. No attempt was made for either test series to maintain the geometric similarity of containment internals. Both these tests examined the dispersal of debris from a simulated cavity geometry and assessed the phenomena of jet geometry, gas solubility, and aerosol generation. In most of these tests, dense aerosol clouds surrounded the debris jet, and sweepout from the cavities was nearly complete in all cases. These test series validated the major hypotheses of HPME and demonstrated the substantial influence of structures in capturing the debris outside of the reactor cavity (in HIPS) and the influence of cavity geometry (in Surtsey).

The influence of the containment configuration outside the reactor cavity and instrument tunnel has been demonstrated by several programs including the Electric Power Research Institute (EPRI)-sponsored experiments at Argonne National Laboratory (ANL) known as the CWTI tests (Corium-Water Thermal Interaction) (Reference 88). The experimental configuration represented selected major features of the Zion reactor lower containment compartment cavity and the upper compartment at a 1:30 linear

scale. Reactor materials (principally UO<sub>2</sub> and stainless steel) were used and were created by an exothermic thermite reaction. Molten debris was injected downward into a simulated cavity which was connected to an expansion volume that was partitioned similar to the lower and upper compartments of a containment. The objectives of the tests were to examine sweepout and heat transfer between core debris and water; steam generation; hydrogen generation; and to characterize the spatial distribution of dispersed debris. The results demonstrate that the structure in the lower compartment is very effective in separating the debris from the high velocity gas stream and depositing the debris on the containment floor in close proximity to the instrument tunnel. The substantial effect of the seal table structure (representing the floor separating the Zion containment compartments) was that a major fraction of the entrained debris was deposited on the lower containment floor.

A similar set of experiments was performed in 1/10th and 1/6th scale mockups of the Surry containment in facilities at SNL (Reference 89). Containment compartmentalization had a substantial influence on the pressurization that could occur within the containment as a result of HPME. One significant outcome of these experiments was that despite an increased in containment pressure to conditions at which hydrogen combustion could occur, the hydrogen burned was essentially just that created during the event. Hydrogen that was previously in the containment atmosphere did not appear to be consumed on a timescale that significantly influenced containment pressurization.

**Table 5-11 Survey of DCH-Relevant Experiments**

<b>Experiment</b>	<b>Number of Tests</b>	<b>Scale</b>	<b>Cavity Type</b>	<b>Water</b>
SNL/DCH	4	1:10	Zion	None
SNL/TDS	7	1:10	Surry	None
SNL/LFP	6	1:10	Surry	None
SNL/WC	3	1:10	Zion	None; Cavity
SNL/IET-Zion	9	1:10	Zion	Cavity; Cavity-Basemat
SNL/IET-Surry	3	1:5.75	Surry	None; Cavity-Basemat
ANL/CWTI	2	1:30	Zion-like	Cavity-Basemat
ANL/IET	6	1:40	Zion	None; Cavity
ANL/U	3	1:40	Zion	None
FAI/DCH	4	1:20	Zion	Basemat; Cavity-Basemat

### **5.3.3 High Pressure Melt Ejection Conclusions**

For a DCH event to occur the precursors (large core melt, high pressure, entrainment potential, affinity to form particulates, aerosol dispersal, long residence in containment atmosphere) must all be present; however, based on scaling analysis and experiments, pressure and in-containment aerosol dispersal were the dominant contributors influencing containment overpressurization from DCH. While the approach to severe accident mitigation in the U.S. EPR does not attempt to minimize core melt potential following the onset of core damage, the other factors are difficult and unlikely conditions to obtain. In fact, the U.S. EPR containment is expected to respond in a manner similar to Westinghouse large dry containments; thus, experiments related to those

containment designs are applicable to the U.S. EPR. In addition, the U.S. EPR's primary depressurization system is a manually actuated system, with redundancy, capable of reducing pressure to below HPME concern for all relevant accident scenarios. Without lower head penetrations, a failure of the lower head resulting from high pressure creep rupture is unlikely, thus shifting the melt pool to the periphery of the blowdown streamline. If the lower head is assumed to fail, the expected failure mode would be a local side wall failure, as has been discussed in Section 5.2.1. As a result, the majority of the entrained heavy metallic melt would immediately deentrain on the reactor cavity walls. The torturous pathway to the containment atmosphere would prevent the necessary in-containment aerosol dispersal and long residence time required. Hydrogen combustion could accompany the HPME; however, based on the SNL results from Surry mockup studies, the extent of the hydrogen combustion is not expected to exacerbate the effects described in Section 5.1.3.

The issue of HPME-driven DCH is considered resolved for current-generation PWRs. The U.S. EPR design, incorporating several design features that are capable of either similar or enhanced preventive response to an HPME, precludes the potential mechanisms for HPME initiation and subsequent DCH. Consequently, this issue should also be considered resolved for the U.S. EPR design.

## **5.4      *Containment Performance***

### **5.4.1    *General Overpressurization***

The containment provides the ultimate protective barrier with regard to release of radioactivity to the environment in the event of a severe accident. Related to containment overpressurization, the relevant severe accident design objectives for the U.S. EPR containment are:

- to maintain a leak-tight barrier for 24 hours following core damage
- beyond the initial 24 hours, the containment will continue to act as a barrier against uncontrolled fission product release

- to assure that elevated pressures and temperatures that may result from a severe accident do not cause its uncontrollable failure

#### **5.4.1.1 *General Overpressurization Phenomenology***

The addition of mass and energy into a contained volume will typically result in increased pressure and temperature within that contained volume. During a severe accident, the primary sources of mass and energy that could cause containment overpressurization can occur as the result of RCS depressurization (either by LOCA or actuation of the primary depressurization valves) coupled with the generation of non-condensable gases from MCCI and steam addition resulting from quenching and stabilization of molten core debris in the spreading compartment.

Following the initial pressure rise from RCS depressurization, the containment pressure will be moderated passively by the heat capacity of the containment walls and internal structures. Further pressure reduction is made possible first by the CGCS, which through the use of PARs, in the presence of oxygen, recombines hydrogen and oxygen into water vapor. The recombination of hydrogen alone does not impact containment pressure; however, the conversion of hydrogen into a condensable form enhances the performance of the SAHRS containment spray by maximizing the water vapor concentration.

The SAHRS containment sprays are started manually following the initial 12 hours of a severe accident. This feature both decreases containment pressure by condensing the steam generated in the containment and reduces the potential for further pressure increase by removing decay heat from within the containment airspace and from the molten core material in the spreading compartment.

Details on the CGCS and SAHRS systems appear in Sections 2.2.2 and 2.2.4, respectively.

#### **5.4.1.2 General Overpressurization Experimentation and Discussion**

As previously described, the U.S. EPR-specific response to containment overpressurization is ultimately provided by an active spray system. This system is functionally equivalent to those present in current-generation PWRs for the mitigation of design basis LOCAs. The basis for these installed units draws on test program experience including Carolinas-Virginia Tube Reactor Containment (Reference 90) and Brookhaven National Laboratory's Containment Spray Experiments (Reference 91). The 12-hour delay allows the CGCS to perform with a high degree of reliability to fulfill its design goal of reducing hydrogen concentration to 4% in within that time.

Both the CGCS and SAHRS are highly reliable systems. The 47 independent PARs and the second full line of SAHRS heat removal capacity provide for a degree of redundancy beyond that of current-generation LWRs. In traditional severe accident space, single failure is not a consideration in system design; however, the U.S. EPR severe accident systems can accommodate such a failure and still perform their function, thereby underlining the reliability of these systems.

#### **5.4.2 Fuel-Coolant Interactions**

FCI is a process by which molten fuel transfers its thermal energy to the surrounding coolant, leading to break-up of corium with possible formation of a coolable debris bed or potential evolution to an energetic steam explosion. Two modes of contact between the molten corium and coolant are considered:

- A pouring contact mode, where corium is poured into a pool of water. This mode could conceivably occur within the RPV when corium relocates into the water-filled lower head of the vessel.
- An injection or stratified contact mode, where a pool of corium is flooded by water. This mode can occur within the RPV as a consequence of reflood of the RPV, or later, during either molten pool formation inside the lower head or the designed flooding of the melt in the spreading area.

Considerable research has been conducted to assess the potential for and effects of steam explosions resulting from the rapid energy transfer between relocating core materials and water. This section identifies the phenomena of interest and previous efforts to assess the potential for in-vessel or ex-vessel steam explosions.

#### **5.4.2.1 *Fuel-Coolant Interactions Phenomenology***

Steam explosions occur when heat is transferred from the melt to water over a very short time scale (~ 1 msec.). The major stages of a steam explosion (as depicted in Figure 5-5) are:

- Initial coarse mixing of melt and water during which heat transfer is generally characterized by stable film boiling;
- Triggering that causes local destabilization of film boiling and local fragmentation of melt into small drops, on the order of 0.01 to 0.1 mm in diameter;
- Explosive propagation of the region of rapid heat transfer through the coarse mixture, and expansion driven by steam at high pressure.

Coarse mixing results in some melt quenching with associated steam and hydrogen production. During mixing, some of the molten drops may spontaneously fragment into much smaller drops, on the order of 0.01 to 0.1 mm in diameter. This localized fragmentation or triggering event may be produced by natural oscillations in the vapor film about the drop leading to fuel-coolant contact, or it may be induced by shock waves from falling objects, contact of the fuel with the bottom surface, entrance of the fuel into a region of colder water, or by turbulence generated in part of the mixing region. If the fragmentation is rapid enough, local shock waves can be produced, which can cause neighboring drops to fragment. If such a chain reaction escalates, a steam explosion can result.

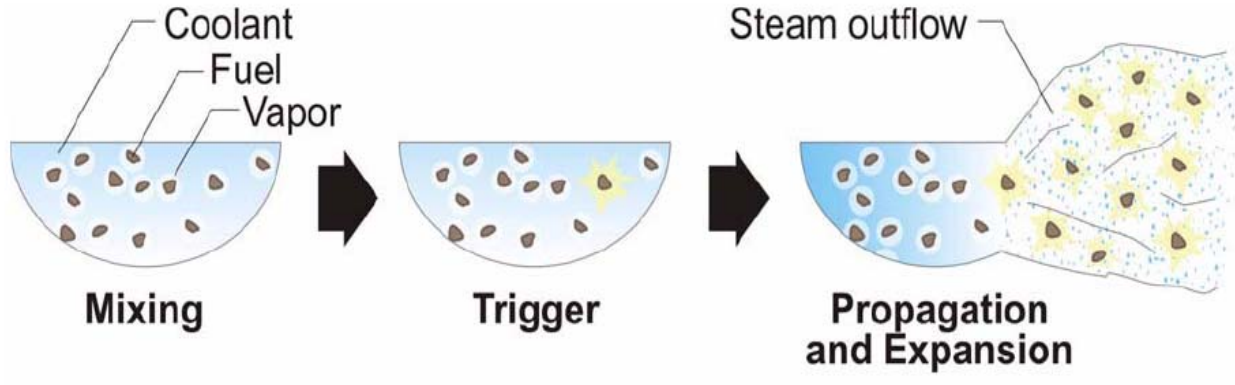


**Figure 5-5 Steam Explosion Stages**

Research indicates that the likelihood and magnitude of steam explosions depend on various initial and boundary conditions, including:

- mass, compositions, and temperature of the molten material
- water mass, depth, and temperature
- vessel geometry, degree of confinement, and the presence and nature of flow restrictions and other structures
- fuel-coolant contact mode (e.g., pouring, melt entry velocity, pour diameter, extent of mixing)
- ambient pressure
- timing and strength of any external triggers that might be present.

Steam explosions can involve a variety of high-temperature molten materials including uranium and its oxides. Spontaneous (no external trigger) steam explosions have been observed for aluminum, iron, tin, and associated oxides in all possible contact models including melt pours, stratified water over melt, and reflooding. High ambient pressure

and low water subcooling have been shown to reduce the probability of spontaneous steam explosions at experimental scales; however, explosions can still occur if the necessary triggers are available.

Experimentally measured conversion ratios (the work done divided by the thermal energy available) range from zero to values approaching the thermodynamic limit. Explosion pressures up to nearly 200 MPa have been measured. If unoxidized zirconium is present, mixing of this metal at high temperatures with water in the lower plenum would promote rapid oxidation (and increase the amount of energy released during FCIs); hence, the FCI process possesses a feedback response that can make it self-sustaining. Consequently, if the proper configuration of fuel and coolant can exist, the possibility of a steam explosion leading to the failure the vessel lower head cannot be disregarded.

In assessing the impact of an in-vessel FCI, three alternative scenarios can be postulated:

- No steam explosion, but violent boiling;
- One or more relative low-yield steam explosions and nonexplosive quenching;
- A large steam explosion involving a significant fraction of the melt, triggered spontaneously or by a low-yield steam explosion.

Because of the resulting disruption (and possible dispersal) of internal structures and residual core materials, the occurrence of even a relatively low-yield steam explosion could significantly alter subsequent damage progression in a severe accident.

#### **5.4.2.2 Fuel-Coolant Interactions Experimental Programs – In-vessel**

It is possible that a large in-vessel steam explosion could be sufficiently energetic to cause a breach of the reactor vessel, including a breach of the reactor vessel that generates containment-failing missiles e.g., the alpha mode of containment failure that was initially identified in the Reactor Safety Study (RSS), also known as WASH-1400

(Reference 20). Either event would completely alter the course of the accident by causing the immediate ejection of fuel and fission products from the reactor vessel. The second possibility would essentially lead to simultaneous uncontrolled venting of the containment to the environment.

There have been several efforts utilizing expert elicitation to quantify the likelihood of an energetic steam explosion that fails the vessel and leads to an alpha mode containment failure. In the first effort, the RSS, experts estimated the alpha failure probability to be 0.01 (given that a core melt accident occurs), although experts also acknowledged that the uncertainty in this failure probability was large by assigning a pessimistic, upper bound estimate of 0.1. Since the RSS, several small and intermediate scale tests have been completed (see reviews of these tests in References 92 through 94). Several analytical models developed using data from these tests predicted conversion ratios less than 5.3% and masses of actively participating molten corium less than 5000 kg. Such small masses yielded alpha mode failure probabilities of 0.0001 or less. However, in the first NRC-sponsored Steam Explosion Review Group (SERG-1, Reference 95) the experts provided an upper bound failure probability estimate of 0.1 (for high pressure events) and an upper bound failure probability of 1.0 (for low pressure events). Mean value estimates for alpha mode failure probabilities (given that a core melt accident occurs) range from 0.001 (for high pressure events) to 0.01 (for low pressure events).

Since the SERG-1 evaluation, additional FCI research has been conducted to further reduce uncertainties and improve the technical basis for alpha mode failure estimates given by the experts (Reference 96). One major insight gained from these experiments was that steam voiding around hot debris particles causes the mixing region to be depleted of water, in part due to vaporization associated with rapid melt-to-coolant heat transfer and, in part due to displacement of remaining water mass away from the interfacial region.

In June 1995, the NRC convened the SERG-2 workshop (Reference 97) to reassess the alpha mode failure issue and to evaluate the current understanding of other FCI

issues of potential risk significance. At this workshop, 9 of the 11 SERG-2 experts concluded that the probability of an alpha mode failure was very low (e.g.,  $10^{-3}$  or smaller). These experts based their judgments primarily on data indicating that there are limits to the mixing that may occur during FCIs. Experts agreed that there was still much uncertainty in the triggering process; thus, the experts invoked conservative estimates with respect to triggering processes. For cases where data were obtained using prototypic reactor melts interacting with saturated or subcooled water at ambient pressure (0.1 MPa), only one or two cases exhibited weak steam explosions and then, only when an external trigger was used. At higher pressures, data indicated that an explosion is difficult to trigger.

Similarly, in 1999, the ROAAM methodology (see Section 3.1) was applied to address in-vessel steam explosion and subsequent alpha mode containment failure for the AP600 reactor vessel (Reference 18). Both the AP600 reactor vessel and U.S. EPR reactor vessel have no lower head penetrations. The conclusion was that “steam-explosion-induced lower head failure in an AP600-like reactor is ‘physically unreasonable.’”

Table 5-12 summarizes parameters of several facilities and experiments using prototypic materials to investigate steam explosions. Those identified are the FARO, KROTOS, and TROI programs (References 98 – 103). Although the geometry and size of these test facilities differ (see Figure 5-6), each contains the same functional components:

- A melt generator or furnace
- A release vessel
- An interaction chamber or sections, and
- A plate or “melt catcher”

The TROI, KRYTOS, and FARO facilities are generally of similar size, pressure, capacity, and capability with respect to prototypic materials testing.

**Table 5-12 Fuel-Coolant Interactions Experiment Programs**

Facility	Phenomena / Insights	Geometry/Test Parameters				
		Section Diameter, mm	Melt Jet Diameter, mm	Water Depth, m	System Pressure, MPa	Melt Composition and Mass, kg
Fuel Melt And Release Oven (FARO, JRC – Ispra)	Integral test investigating premixing, quenching, propagation, and FCI energetics.	47-700	100	0.1 - 5.0	0.1 - 5.0	UO <sub>2</sub> -ZrO <sub>2</sub> (w/ and w/o Zr and SS); 18-250 kg
KROTOS (JRC – Ispra)	Smaller scale tests investigating premixing, quenching, propagation, and FCI energetics	95-200	30-50	1.0	0.1 - 1.0	UO <sub>2</sub> -ZrO <sub>2</sub> ; 1.4 - 10.0 kg
Test for Real cOrium Interaction (TROI, KAERI)	Integral tests investigating premixing, quenching, propagation, and FCI energetics	600	~38-50	0.67	0.1 - 2.0	ZrO <sub>2</sub> and UO <sub>2</sub> -ZrO <sub>2</sub> ; 5 to 13.7 kg

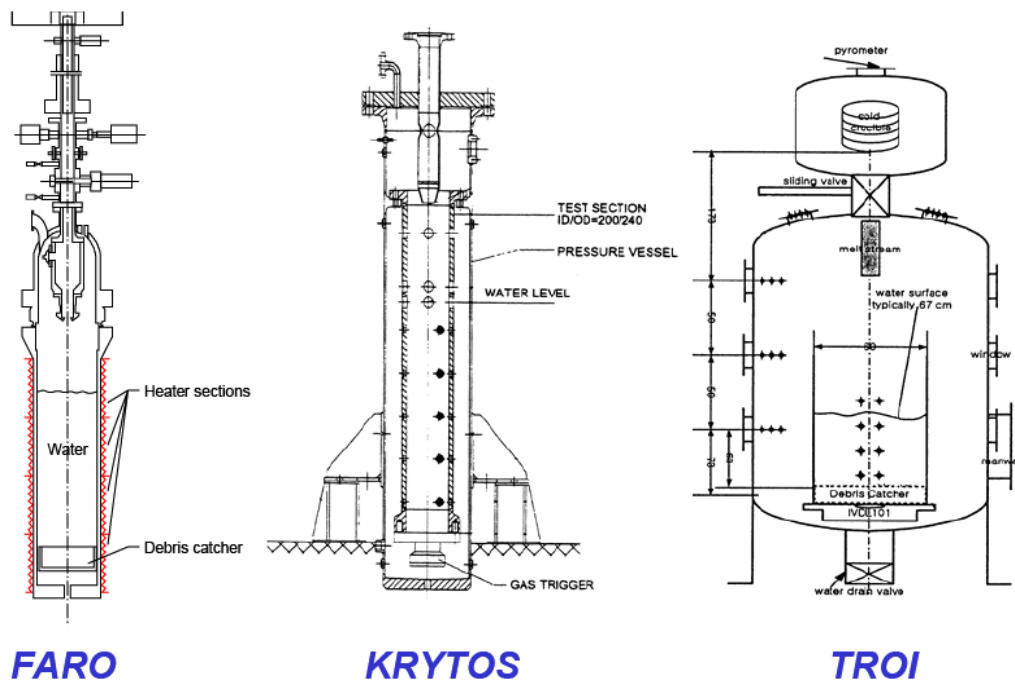


**Figure 5-6 Geometry of Steam Explosion Facilities Testing with Prototypic Materials (not to scale)**

#### 5.4.2.3 Fuel-Coolant Interactions Experimental Programs – Ex-vessel

As discussed in Section 5.2.4, the U.S. EPR includes several design measures that preclude ex-vessel steam explosions, such as an initially dry reactor cavity and dry spreading area, the addition of silica-rich sacrificial material to the melt before ex-vessel flooding, and the controlled addition of water to the top of the melt after spreading. Following a LOCA or RCS depressurization, condensation may form in the spreading compartment. However, several tests, including KATS, which have shown that for water layers of height 1 - 10 mm, the presence of water did not have any adverse effects on the global spreading. Moreover, while local steam explosions occurred for both the metallic and oxidic melt, they were never very energetic and they blew away the water in front of the melt thus avoiding further reactions along the flow path. Discussion of the principal tests related to flooding of the spreading compartment appears in Section 5.2.4.5.

#### **5.4.2.4 Fuel-Coolant Interactions Conclusions**

Based on the unique design of the U.S. EPR, the large body of research conducted by several institutions, and the opinions of experts worldwide, the likelihood of FCI resulting in containment failure from either in-vessel or ex-vessel mechanisms is considered remote. Related to the U.S. EPR-specific design, two design characteristics inherently impede potential containment failure:

- the additional structure surrounding the U.S. EPR reactor vessel further mitigates adverse consequences of an in-vessel FCI-induced steam explosion by eliminating a clear path to the containment shell
- the design of the spreading compartment preserves a dry environment eliminating the “fuel” required to create an ex-vessel steam explosion

It follows that explicit treatment of U.S. EPR fuel/coolant interactions is unwarranted. The existing data are deemed sufficient to demonstrate that the potential for an energetic in-vessel steam explosion is negligible.

### **5.5 Equipment Survivability**

Equipment, including instrumentation, important to severe accident response is identified in Section 2.0. In most scenarios, a severe accident evolves from a preceding design basis event. Therefore, all severe accident response equipment is required to fulfill at least the design basis qualification requirements. Similar assessment of such equipment is not required for beyond design basis severe accidents; however, containment conditions (i.e., temperature, pressure, humidity, and radiation) predicted by a suite of relevant analyses will be used to assess the equipment relative to applicable testing data.

As to the environmental conditions to which the instrumentation is exposed during a severe accident, four location categories can be defined:

- In-Core/In-RCS

- Inside containment
- SAHRS-compartment
- Annulus

With exception of the SAHRS compartments, the safeguard buildings are not subject to harsh environmental conditions during a severe accident.

### **5.5.1 *In-core / In-RCS***

The instrumentation in this category includes:

- Wide-range core outlet temperature thermocouples
- RCS pressure sensors
- PDS valves

The exposure of the instrumentation will be dependent on in-vessel phenomena prior to RPV failure (for example, see Table 4-2). Analytical methods used to evaluate severe accidents incorporate models and correlations to explicitly address the applicable in-core phenomena. Requirements for design basis events set qualification for pressure, water chemistry, and radiation dose. Temperature sensors having performance objectives unique to severe accidents will be assessed based on analysis.

### **5.5.2 *Inside Containment***

The instrumentation in this category includes:

- Containment isolation valves and position sensors
- Containment pressure sensors
- H<sub>2</sub> monitors

- 
- IRWST water level and temperature
  - Dose rate measurement, i.e. gamma-sensitive detector
  - Post accident sampling system
  - Thermocouples inside insulation liner to measure temperature of RPV lower head
  - Flooding valves and flooding valve position sensors
  - Thermocouples in spreading compartment main cooling channel

Environmental conditions inside the containment which may be more severe during a severe accident than during design basis events are:

- Static pressure
- Potential short term pressure spikes due to H<sub>2</sub> combustion
- Temperature
- Presence of gases such as steam (i.e. humidity), hydrogen, carbon monoxide.
- Radiation and deposition of radioactive aerosols

#### **5.5.2.1 *Pressure, Temperature, and Humidity***

The development of pressure, temperature, and humidity as a function of time during a severe accident takes into account the effects of:

- Steam release from the RCS inventory.
- Fission product release from the fuel and associated decay heat production.
- Hydrogen release resulting from zirconium oxidation and MCCI, and its recombination and combustion.

- 
- Energy release from the melt during MCCI.
  - CO release from the melt due to MCCI, its recombination and combustion.
  - Steam release resulting from quenching of the melt and the evaporation of water due by decay heat in the spreading area.

Analytical methods used to evaluate severe accidents incorporate models and correlations to explicitly address these processes and phenomena.

#### **5.5.2.2 *Temperature Spikes Due to H<sub>2</sub> Combustion***

The only severe accident instrumentation directly exposed to hydrogen combustion, should it occur, are the hydrogen sensors themselves. With the exception of at least two sensors in the dome for long-term hydrogen monitoring, as mentioned previously, these instruments do not need to survive initial combustion of the hydrogen produced during core oxidation, as a second large combustion event is not expected. The hydrogen produced at a later point during MCCI in the reactor cavity and spreading compartment will burn immediately, making further H<sub>2</sub> measurement irrelevant.

All other severe accident instrumentation still needed after combustion of H<sub>2</sub> produced during core oxidation can be placed safely away from any potential hydrogen combustion locations, e.g. the lower annular compartments. If combustion at their respective locations cannot be precluded from analysis of relevant scenarios, the impact on the equipment will be assessed.

The instrumentation and/or parameters that are needed to monitor H<sub>2</sub> combustion include:

- Containment pressure
- IRWST water level and temperature (depending on their location)
- Gamma-sensitive detector

Other instrumentation that must continue to function after the combustion of H<sub>2</sub> produced during core oxidation will not be affected by the combustion event. This includes:

- Thermocouples inside insulation liner to measure temperature of RPV lower head
  - No H<sub>2</sub> combustion is expected in the reactor cavity before RPV failure.
- Ex-core neutron flux measurement
  - No H<sub>2</sub> combustion is expected in the reactor cavity before RPV failure
- Flooding valves and flooding valve position sensors.
  - Located in isolated compartments.
- Thermocouples in spreading compartment main cooling channel
  - No H<sub>2</sub> effect considered.
- Containment isolation valves and their position sensors
  - located in lower annular compartments

### 5.5.3 **SAHRS-Compartment**

The severe accident measurements and control functions belonging to this category are:

- Actuation of SAHRS and its associated systems (ESW, CCW, containment isolation valves)
- SAHRS inlet and outlet temperatures
- SAHRS pump pressure

- SAHRS volumetric flow rate

Because the SAHRS is located in safeguard buildings 1 and 4, the SAHRS is not exposed to any severe-accident-related conditions until its operation is initiated.

After actuation of the SAHRS, the limiting conditions (e.g., temperature, boron concentration, fission product concentration, etc.) of contaminated IRWST water flowing through the system are considered for assessing the performance of SAHRS components.

#### **5.5.4 *Annulus***

The measurements belonging to this category are:

- Annulus pressure (subatmospheric)
- Dose rate downstream filters
- Volume flow rate downstream filters

The annulus environment is not expected to be seriously challenged during a relevant severe accident scenario as defined in Section 3.3.

## **6.0 ANALYSIS METHODS**

Analysis methods document the analytical basis established to justify resolution of severe accident safety issues associated with the severe accident performance of the U.S. EPR. An overview of the analytical methodology is presented with a description of how the various computer codes are used together to provide comprehensive coverage of relevant severe accident phenomena associated with the U.S. EPR. A description is provided of each code's applicability to severe accident phenomena and a summary of code capabilities. In addition, this section provides a summary of the validation and verification basis for each code and the scope of deterministic severe accident analyses for the U.S. EPR.

### **6.1 *Overview of U.S. EPR Analytical Methodology***

The U.S. EPR analytical methodology is based on the use of MAAP4.07 (Reference 2) as the primary integral analysis tool and the use of MELTSPREAD-1.4 (Reference 104) and WALTER (Reference 105) to supplement the integrated results. A significant code development effort was undertaken by AREVA NP through a contract with Fauske and Associates Inc. (FAI). The purpose was to expand the capabilities of MAAP4 to allow the analytical treatment of severe accident phenomena in the U.S. EPR. The end result of these efforts was a revision to MAAP4 (i.e., version 4.07), which now allows for the vast majority of U.S. EPR severe accident phenomena to be analyzed in an integrated method. The use of other separate-effects codes and the need for manual coupling of inputs and outputs has been effectively minimized resulting in a robust analytical methodology.

The separate-effects codes MELTSPREAD-1.4 and WALTER were used to confirm some of the MAAP4.07 calculations and, in some cases, to provide a more detailed treatment of one or more phases of a severe accident. The flow of data to and from the various codes is depicted in Figure 6-1. The relationship between the three codes is not one of mutual exclusion. All phases of the severe accident are treated by MAAP4.07 and there is considerable overlap in the scope of phenomena addressed by each code.

MAAP4.07 is used to develop the boundary and initial conditions for defining the problems analyzed with MELTSPREAD-1.4 and WALTER. The separate-effects codes are then used to verify selected parameters used to characterize the various system performance parameters in MAAP4.07. These codes and the relationship between them in the U.S. EPR analytical methodology will be described in the following subsections.

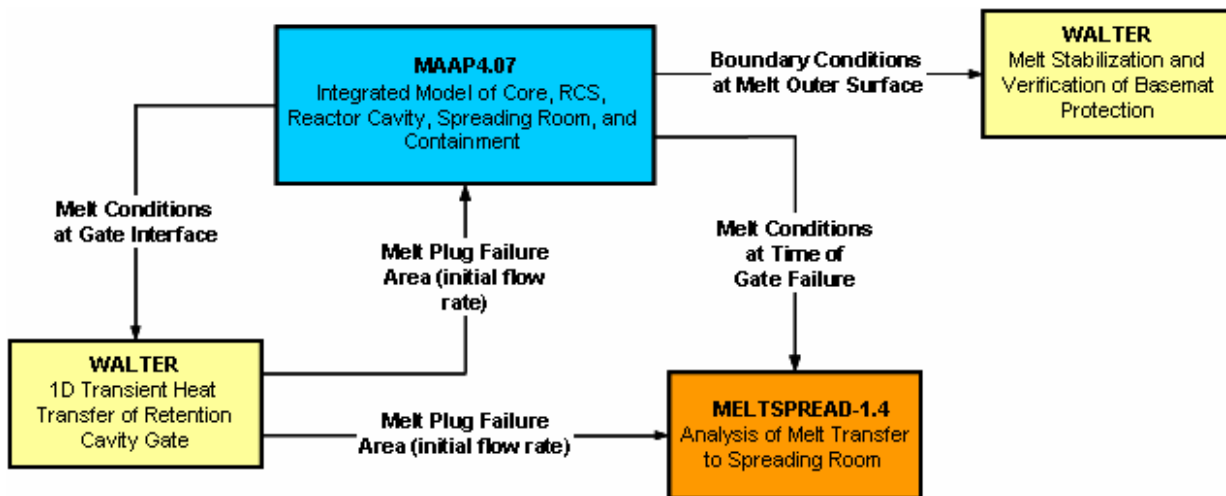


**Figure 6-1 Overview of U. S. EPR Severe Accident Analytical Methodology**

### 6.1.1 MAAP4.07

MAAP4 is an integral systems analysis computer code for assessing severe accidents and is developed and maintained by FAI for the EPRI. MAAP4 includes models required for analysis of a wide spectrum of severe accident phenomena that might occur within the primary system and containment. MAAP4 has the capability to simulate the progression of a severe accident sequence, including the release of fission products, from a set of initiating events to either a safe, stable state or to an impaired containment condition. MAAP4.07 is the first version of MAAP4 specifically addressing the severe accident phenomena unique to the U.S. EPR.

The basic MAAP4 code architecture consists of a main program that directs the execution through several high level subroutines. These subroutines call a sequence of

system and region subroutines at each time step, which in turn call phenomenological subprograms as required. The integration technique used in MAAP4 is an explicit, first order, Euler method. The user also has the option of selecting an alternate second order; Runge-Kutta integration method. The MAAP4 time steps vary through program execution based on user specified maximum and minimum limits. Separate time step ranges can be specified for the core and containment regions.

This section describes MAAP4.07 and the features that have been included to enable analytical modeling of the U.S. EPR (Reference 106). The major areas of MAAP4 that underwent modification are summarized in this section, with the application (Section 6.2.1), validation (Section 6.3.1), and use (Section 6.4.1) of these new models described later in this report.

#### **6.1.1.1 *Compartment-Specific Concrete and Corium Heat Transfer***

The MAAP4 Generalized Containment Model (GCM) was modified for MAAP4.07 to permit various concrete properties to be specified for various containment nodes. Of particular interest in the U.S. EPR design is the need to differentiate between the concrete used for structures in most of the nodes and the sacrificial concretes that are used in the reactor cavity region and the spreading room. Additionally, the model was also modified to provide routines that could calculate the convective heat transfer from the melt to the concrete or enable a user to input an average heat transfer coefficient between the melt and the sacrificial concrete wall.

Prior to MAAP4.07 only one type of ablative concrete could be specified. In MAAP4.07, the material property parameters for the ablative concrete are generalized to allow specification of multiple types of ablative concrete. The specification of heat transfer coefficients at the melt-concrete interface has also been generalized. The heat transfer related parameters can now be uniquely specified for each corium pool in the MAAP4.07 model. In addition, instead of specifying a constant heat transfer coefficient, the user can allow the code to calculate the heat transfer based on the Rayleigh

number. This allows the specific convection characteristics for each corium pool geometry to be considered in the heat transfer modeling.

#### **6.1.1.2 Containment Heat Sinks**

A new heat sink subroutine was developed for calculating the heat transfer associated with containment structures. This subroutine includes variable-size nodes and the ability to represent a liner of any material type. Two-sided heat sinks can have one liner per surface and can represent the energy transfer being initiated through either surface. In addition, the ability to control the CHF correlation along each heat sink surface has been implemented in the form of a Kutateladze number which can be specified by the user. This allows the user to have more control over the heat transfer characteristics at the heat sink surface, which can be important given the fact that MAAP4.07 is only capable of modeling rectangular heat slabs which must have the same area on both sides.

#### **6.1.1.3 RPV Lower Head Extensive Failure**

In MAAP4.07, the RPV failure is a two-step process with an initial local failure of the lower head by creep rupture, followed by an extensive lower head failure. The model for predicting the initial local failure is unchanged in MAAP4.07. The extensive RPV lower head failure is determined by the failure location, the mass of molten debris in the lower head, and the temperature distribution in the RPV wall. A new model was implemented to include the potential for accelerated failure of the lower head as a result of corium discharge through an initial local failure site. As molten debris is discharged through the initial failure site, the surrounding wall will be ablated by the high temperature flow and the extent of this ablation will determine the number of azimuthal regions destroyed by the molten debris flow.

In previous versions, the MAAP4 models did not consider the potential damage to adjacent nodes in the RPV wall caused by direct contact of the high temperature corium as it drains. The new criterion for lower head extensive failure is based on the experimental observation that melting of the steel on direct contact with corium

dramatically increases the ablation rate (Reference 105) causing the wall to fail to such an extent that it cannot hold the remaining corium inside. An interface temperature between the drainage flow and the wall is evaluated by function which calculates the instantaneous contact temperature between the high temperature molten debris and the steel wall. If the contact temperature in any node below the initial failure site is greater than the melting point of steel, an extensive failure is assumed to occur by downward ablation. (Since there are several radial nodes through the RPV wall, the average wall temperature node at each azimuthal location is the temperature used to determine the potential for extensive failure.)

#### **6.1.1.4 *Ex-Vessel Thermal Radiation to RPV***

MAAP4.07 includes the ability to model thermal radiation from a corium pool surface to the RPV. A thermal radiation model for the reactor cavity was developed to approximate the energy transfer from the accumulated core debris to the reactor vessel outer wall, as well as to the vertical cylindrical segment of the reactor cavity. Prior to RPV failure, the vessel is covered with reflective insulation. When vessel failure occurs, it is assumed that the dynamics of the failure destroy the insulation. Therefore, when the core materials accumulate in the reactor cavity, the debris is assumed to radiate upward to the outer surfaces of the RPV lower plenum nodes and the the cylindrical section of the reactor cavity. The RPV lower plenum wall outer surface, which is nodalized into 5 azimuthal sections, exchanges radiation with the other reactor cavity surfaces, including the top surface of the corium pool. The cylindrical segment of sacrificial concrete is represented as a single node that transmits or receives thermal radiation from the corium pool of the RPV lower plenum wall. Collectively, this energy transfer influences the transient response of the RPV lower head nodes while the melt resides in the reactor cavity.

The energy transfer from the accumulated core debris in the reactor cavity is due to radiation from the debris upper surface. The heat flux leaving the debris is determined by establishing an average temperature to which the corium radiates in the complicated enclosure geometry. This average temperature is determined by an area-weighted

average of the temperature for the surfaces comprising the outer wall of the RPV lower plenum and the vertical cylindrical segment of the reactor cavity.

Once the energy flux from the debris is evaluated, it is distributed to the RPV and sacrificial concrete heat sink surfaces as an energy flux that is consistent with the user-specified view factors given from the debris to the RPV lower plenum outer wall surfaces and the vertical segment of the reactor cavity. A stand-alone approach has been recommended by FAI to calculate the view factors based upon radiation enclosure theory to ensure a complete energy balance. In this stand-alone assessment, the lower head wall is represented as a cone with bottom disk. The bottom disk of the cone is the outer surface of the bottom node of the RPV lower plenum; the strips on the surface of the cone represent outer surfaces of the four other RPV nodes. The view factors between the various surfaces involved are then determined, i.e., the upper surface of the core debris, the area of the vertical reactor cavity wall, the outer surface of the bottom node of the RPV lower plenum, the outer surface of second RPV node, the outer surface of the third RPV node, the outer surface of fourth RPV node, and the outer surface of fifth RPV node. The sum of all view factors for each surface is 1. In addition, the view factors also satisfy the condition that

$$A_i \times F_{ij} = A_j \times F_{ji}$$

where  $A_i$  is the surface area of node  $i$  and  $F_{ij}$  is the view factor from surface  $i$  to surface  $j$ . The calculated view factors are input to the analysis as user-defined view factors within the reactor cavity enclosure configuration. It is assumed that the RPV surfaces can not “see” each other, i.e. the view factors are zero. Of particular note here is that this energy transfer from the surface of the core debris and its distribution to the RPV outer wall surfaces is a heat flux boundary condition, but one that is consistent with radiation within an enclosure.

The RPV may experience a failure causing part of, or the entire lower head, to become detached. In this case, the corium pool in the reactor cavity can radiate into the vessel through the opening and heat the remaining core and other inner structures. The

MAAP4 code was modified to address this concern. In the MAAP4.07 code, the vessel may first fail locally at any point on the RPV wall. A second failure, if it occurs, is assumed to be a global failure condition. If a global failure occurs, the portion of the lower head between the row of failed nodes and the RPV bottom is assumed lost and its mass is added to the inventory of the corium pool in the reactor cavity. The energy transport into the lower internals of the RPV is calculated using the radiation model in the reactor cavity enclosure as described above. The incident radiation from the cavity is then imposed on the outer surfaces of the remaining structures in the vessel, which may include lower plenum equipment, the core support plate, the core barrel, and the upper plenum (if the core is gone).

#### **6.1.1.5 *Increase the Containment Nodes, Junctions, and Heat Sinks***

MAAP4.07 includes an increase in the number of containment nodes, to enable more detailed modeling of the containment building. The number of nodes has been increased from 40 to 120 and the number of junctions has been increased from 120 to 200. The maximum number of distributed structural heat sinks remains at 200 and the maximum number of lumped structural heat sinks also remains at 200. With this expanded size of the generalized containment model, the user has the flexibility to represent additional details of the containment. These maximum values greatly exceed those needed to represent the U.S. EPR containment building.

#### **6.1.1.6 *Containment Local and Global AICC Calculation***

Prior to MAAP4.07 AICC pressure and temperature for complete combustion of hydrogen and carbon monoxide was evaluated only locally, i.e., within a specific compartment. To perform a global AICC calculation, MAAP4.07 takes the summation of all gas masses within the containment the containment average temperature prior to the burn, the total energy of all the gases and the total volume of the reactor building and evaluates the adiabatic isochoric temperature and pressure caused by complete combustion. Basically, the same routine is used for evaluation of the parameters with the only difference between the local and global evaluations being that the local values

are those typical of a specific node whereas the global values are summed over the entire containment volume.

#### **6.1.1.7 Core Heavy Reflector**

The U.S. EPR core design differs from the current-generation PWR core designs modeled by the MAAP4 code. Specifically, the current designs have a core region surrounded by a water baffle region, which is typically considered the core bypass, with the core barrel region surrounding this bypass. With the use of a heavy reflector/core barrel in the U.S. EPR, and the resulting elimination of the bypass region, the accumulation of molten material within the core under severe accident conditions would result in direct attack by the molten core material on the core barrel. The relatively large thickness of this steel component will subsequently delay the relocation of the melt into the lower plenum. In the MAAP4.07 model, severe core degradation would result in melting of the core material, accumulation of this material within the core region, and eventual melting through the core former plates that form the inner region of the bypass zone (water baffle).

The MAAP4 model was modified to represent this more substantial heat structure and the radial attack associated with lateral relocation of the molten core material. Typically, five radial nodes are used to represent the thickness of the core barrel and the number of vertical nodes in this component is the same as in the core region. The intimate contact between the outermost core nodes and the innermost core barrel nodes is assumed to start when debris begins to form in the core nodes. In the first several minutes, heat flux from the core to core barrel is dominated by the formation of a thermal boundary layer in both the high temperature core node and low temperature core barrel node. The thermal boundary layers will expand through the entire thickness of the core and core barrel nodes. During the boundary layer expansion, the heat flux calculated by MAAP4.07 is dependent on the thermal conductivities of the core and core barrel nodes, the temperature of the core node, the temperature at the interface, and the thickness of the thermal boundary layers. Quasi-static conduction will dominate the rest of the time. Crust can form between the molten core and the core barrel at the

interface, and a layer of molten steel will exist between the crust and the solid part of the core barrel. The crust acts as a thermal resistance between the molten core and the molten steel of the core barrel. Steady-state temperature profiles are used in the two intermediate layers (crust and molten steel) to assess the heat flux through them. Heat is transferred by conduction through the crust and by both conduction and convection through the molten steel layer. As the thermal attack of the core barrel progresses, the core barrel is assumed to remain intact until the molten steel layer penetrates through the entire thickness at a given elevation. When penetration occurs, the molten core debris at that elevation and all elevations above the failure location is influenced by drainage of the molten core material through the failure site in the core barrel and, thus, into the downcomer region. This enables molten core material to flow into the lower plenum.

Following the initial failure, core material drains over the outer surface of the core barrel and energy is transported from the molten core debris to the core barrel outer surface. If this energy transport is sufficient to cause the wall to approach the melting temperature, the failure location can propagate downward and enable an increased amount of molten material to drain into the lower plenum. To assess this behavior, MAAP4 was modified so that the energy transfer to the outer surface uses the average velocity of the melt flowing through the initial failure site. The velocity was approximated by calculating the velocity that would occur due to gravitational acceleration over half of the reactor core (the core barrel is expected to fail somewhere close to the axial midpoint). Using this velocity, the average heat transfer coefficient was assessed using the Reynolds analogy.

The temperature difference for energy transfer is the difference between the melt temperature and the melt solidus temperature rather than the surface temperature of the structure. This is due to the limitation that freezing of the molten material provides on the overall energy transfer, i.e. the energy transfer rate is limited by the temperature difference between the melt and the crust that it forms on the boundary.

Once the heat flux has been determined, the total energy transfer to the wall is assessed based on the drainage time. This heat flux is converted into a temperature increase that is then added to the nodal average temperature in the vessel wall to determine if the failure could propagate downward to a specific node. This downward propagation of the failure location is consistent with the observations from the TMI-2 post-accident inspection.

#### **6.1.1.8 Hybrid (Ag-In-Cd and B<sub>4</sub>C) Control Rods with SS Clad**

The use of hybrid control rods necessitated creation of a second group of control rods within the MAAP4 core model. The current model is limited to one group of control rods that can be Ag-In-Cd or B<sub>4</sub>C but not both types simultaneously. Therefore, a second group was added so that Group 1 could model one type, and Group 2 could simultaneously model the second type.

The MAAP4 core model tracks the mass and energy of the individual components within a core node. This includes the existing independent components of fuel, fuel cladding, and Group 1 control rod material with its cladding. Thus, the new component of Group 2 control rod material with its cladding was required. The addition of a new independent component required significant changes to numerous core-related subroutines so that heat-up, oxidation, and material relocation phenomenology properly account for the influence of the new component within the existing model architecture. Due to the constraints of the MAAP4 core model, axial segregation of Ag-In-Cd and B<sub>4</sub>C rod groups was not possible. The only alternative was to have the Groups 1 and 2 uniformly distributed axially and radially. This simplification is acceptable since the major focus of the B<sub>4</sub>C modeling enhancement is to account for the combustible gases generated in the oxidation of the control rod material. In addition, the amount of combustible gas generated from the oxidation of B<sub>4</sub>C is small compared to the total quantity of combustible gas generated in the oxidation of the other materials in the core. The U.S. EPR design does not currently include hybrid control rods and therefore, there is currently only a single group of control rods defined in the MAAP4.07 model.

### **6.1.1.9 *Passive Autocatalytic Recombiners***

Based on previous testing of AREVA NP's PAR design, a performance correlation, specific to these units, was derived. MAAP4.07 now includes both the original PAR correlation and the new correlation developed by AREVA NP. Designation of which correlation to apply is specified through user input.

The AREVA NP PAR rate equation, as incorporated into MAAP4.07 (Reference 106), is shown below:



### **6.1.1.10 *Generic Break Location in the Pressurizer***

MAAP4.07 calculates the thermal-hydraulic response of the pressurizer, including the discharge from relief valves and safety valves. The standard representation of a pressurizer break includes four junctions: one vertical junction at the bottom head of the pressurizer that is connected to Receiver Volume 1, one horizontal junction at the side of the pressurizer connected to Receiver Volume 2, one horizontal junction at the top head of the pressurizer connected to Receiver Volume 3, and one vertical junction at the top head of the pressurizer connected to Receiver Volume 4. Using this model, a

rupture in the side of the pressurizer can be represented using the opening that is connected to Receiver Volume 2. To provide the capability to generalize the break location, variables have been added such that a break can be established anywhere along the height of the pressurizer.

With these defined, the pressurizer can experience a break at any location and the fission products that would be released due to the discharge of either gas or water will also be discharged to the containment through this break. Since the pressurizer model does not provide direct representation of the water-borne fission products, the fission product inventories discharged through this break are represented as the volumetric flow from the break multiplied by the concentration of fission products in the primary system. In this way, the pressurizer is modeled as having the same fission product concentration as the RCS. Fission products discharged from the pressurizer are also included in the fission product balance.

#### **6.1.1.11 *Two Simultaneous Breaks from the PRT to Containment***

Modeling of two simultaneous breaks from the PRT has been accomplished by considering that the PRT has a single rupture disk with discharge piping to two containment nodes downstream of the rupture disk. While testing of the containment model shows that there is essentially no difference between pressures in the various containment nodes within the range of uncertainties associated with the breakage of the rupture disk, to provide a consistent basis, the failure of the rupture disk is based on the difference between the PRT pressure and the algebraic average of the pressures in the two containment nodes. The model assumes that the discharge areas from the rupture disk to the different containment nodes may not be equal. Therefore, the model partitions the discharge from the PRT in terms of the available area for discharge. As illustrated in Figure 6-2, the flow area into node "A" is larger than the flow area into node "B." Hence, the fraction of the flow into node "A" is determined by the ratio of the node "A" area to the sum of the two areas. This model is activated if the node "B" flow area is non-negligible.

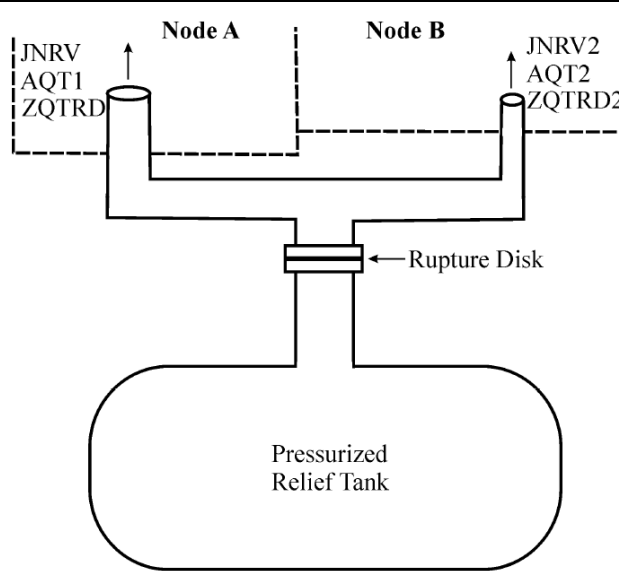


**Figure 6-2 Pressurized Relief Tank Model**

The above model describes the flow rate out of the PRT. For some sequences, the discharge locations could be submerged under water. Under these conditions, the logic in the code determines if one or both of the junctions are submerged based on water levels and elevations of the junction openings in the compartment. If only one junction is submerged, this junction is opened to enable water to drain back into the PRT as long as the water level in the node is above the discharge location. If both of the discharge locations are submerged, the flow rate draining back into the PRT is again area averaged to determine how much of the water is drained from node “A” and how much is drained from node “B.” In this manner, the PRT model provides for stable operation of sequences with a single discharge location as well as for a dual discharge into containment nodes.

#### **6.1.2 MELTSPREAD-1.4**

The MELTSPREAD computer code was developed by ANL and is a transient, one-dimensional, implicit finite difference computer code used to predict the spreading behavior of high temperature melts flowing under the influence of gravity across horizontal surfaces submerged in a depth of water, or without the effects of water if the

surface is initially dry. MELTSPREAD-1.4 is the most recent versions and will be used in conjunction with the integral severe accident code MAAP4.07 to evaluate the U.S. EPR's severe accident performance. MELTSPREAD-1.4 contains several evolutionary code changes from MELTSPREAD-1.0 described in Reference 104. For current applications in nuclear reactor safety, the substrates specifically treated include steel and concrete, and the high temperature melts encompass a wide range of compositions of reactor core materials (corium) including a distinct oxide phase (predominantly  $\text{UO}_2$ ,  $\text{ZrO}_2$ , steel oxides) plus a metallic phase (predominantly Zr, steel).

The code requires inputs pertaining to the containment geometry and the melt "pour" conditions onto the containment floor and calculates the spreading and freezing behavior of the melt within the confines of the containment, including the following physical processes:

- heat transfer to overlying water and to the substrate
- heat-up/ablation of the substrate
- concrete decomposition
- heat transfer enhancement from gas sparging
- internal heat generation from both decay heat and chemical reactions between concrete decomposition products and melt constituents
- leading edge immobilization resulting from crust growth or bulk (slurry) freezing
- spreading of melt over previously spread/solidified material
- impingement heat flux where containment structures are contacted by the flowing melt

The code is used to predict conditions at the end of the transient spreading stage, including melt relocation distance, depth profile, substrate ablation profile, and transient

wall heat-up. The code output provides input to other codes, such as MAAP4 for MCCI or structure response codes, to evaluate long-term behavior following the transient spreading stage. Alternatively, MELTSPREAD-1.4 contains simplified modules for quasi-steady MCCI and melt coolability calculations that may be used for long-term, quasi-steady solutions.

### **6.1.3 WALTER**

The code WALTER is an engineering tool for the assessment of one-dimensional heat conduction problems. WALTER is used to calculate transient temperature-profiles in the sacrificial and protective layers within the reactor cavity as well as simulate the effect of basemat cooling in the spreading area.

Besides pure conduction, WALTER also considers melting/freezing processes. While for single-component systems such phase changes are assumed to occur at a certain melting temperature, multi-component systems are treated in a different way. Here a freezing range is considered spanning between input defined solidus and liquidus temperatures. To characterize the completeness of melting for each node, the liquid fraction is introduced as the ratio between liquid and total mass. The determination of the actual liquid fraction of a node is not part of the solution of the heat conduction equation but results from a post processing of the resulting temperature distribution.

Through the numerical scheme of the code, WALTER is adapted to the solution of heat conduction problems in solids. However, it can also account for natural convection in stratified, horizontal and volumetrically heated liquid layers. This ability allows its application to the EPR melt retention concept.

#### **6.1.3.1 Geometrical Representation**

For the modeling of one-dimensional heat conduction problems, the calculational domain can be separated into a number of "layers." Each layer can be associated with individual material properties and can consist of any number of calculation nodes. The number of nodes determines the achievable numerical accuracy.

Layers can either be in direct contact or separated by “gaps.” Gaps represent discontinuities, across which heat transport can be proportional to a time- and/or temperature-dependent heat transfer coefficient.

#### **6.1.3.2 Conduction Model**

WALTER solves the transient one-dimensional heat conduction equation. At phase change boundaries the consumption/release of latent heat is considered. Either a discrete melting point or, for multi-component materials, a solidus-liquidus range is modeled. Within this range material properties depend on the actual liquid fraction. Volumetric heating rates can be individually specified for each material layer, with either constant or time-dependent values.

#### **6.1.3.3 Initial and Boundary Equations**

Initial temperatures are defined via input in a way that individual values can be assigned to each material layer. Pre-existing temperature profiles can be approximated by multiple layers of the same material of different initial temperatures.

Second- and third-order boundary conditions can be considered for each defined surface, including internal gaps. A wide spectrum of situations can thus be covered, including the simple cases of adiabatic or ideal contact conditions.

#### **6.1.3.4 Heat Transfer Models for the Boundaries**

Heat transfer models are implemented by calling a corresponding subroutine characterized by a specific reference number. Currently models exist for thermal radiation, for boiling heat transfer, and convective heat transport in molten regions. The thermal radiation conforms to a standard Stephan-Boltzmann formulation. Concurrent convective heat transfer can be simply superimposed with a total heat transfer coefficient.

To cover situations in which the surface is flooded with water, a full set of correlation for the different boiling regimes is included in the code. These correlations cover the entire

range from one-phase convection to film-boiling. Transition points are detected and boiling regimes are automatically switched.

The different regimes considered in dependence on the actual surface temperature are: convective heat transport in the water phase, nucleate-boiling, transition-boiling and film-boiling. Correlations for these different regimes, as well as for the transition points between them are implemented. In all of these correlations, the properties of water and steam are calculated as temperature dependent.

The numerical scheme used in the WALTER code is adapted to the solution of heat conduction problems in solid bodies and has been extended to describe the freezing and melting processes, along with natural convection, in the liquid layers. Convection can be either driven by volumetric heat sources or by external temperature differences. This model is based upon the scheme described in Reference 107, and is applicable throughout a wide range of Rayleigh numbers up to  $10^{14}$ .

## **6.2 Code Applicability**

In this section, the particular application of each code identified in Figure 6-1 is associated with a set of relevant phenomena it was designed to address. There is some overlap in the scope of phenomena covered in the various codes, which is addressed in this section. To allow comparison and consistency in the discussion, a generic table of relevant severe accident phenomena, as originally presented in Table 5.2, is used to evaluate each code's capabilities.

### **6.2.1 MAAP4.07**

As the primary integral tool for analyzing severe accidents in the U.S. EPR, the bulk of the phenomena are included within the capabilities of MAAP4.07. However, certain capabilities of MAAP4.07 have recently been developed in order to more fully address some of these phenomena. The new capabilities of MAAP4.07 are identified in Table 6-1 along with the code applicability.

**Table 6-1 MAAP4.07 Severe Accident Phenomena Modeling Capability**

Phenomena	MAAP4.07
1. Fuel rod degradation	Yes
2. Melt progression/ablation through surrounding core structure	Yes*
3. Core melt relocation to lower head	Yes
4. In-vessel fuel-coolant interaction	No
5. In-Vessel Oxide/Metal separation	Yes
6. Crust formation and failure	Yes
7. In-vessel debris formation	Yes
8. RCS/RPV failure modes	Yes*
9. Melt conditioning in reactor cavity/MCCI	Yes*
10. Melt spreading in spreading compartment	No
11. MCCI in spreading compartment (w/oxide-metal stratification)	Yes* (No)
12. Spreading compartment flooding and basemat cooling	Yes*
13. Steam/hydrogen transport	Yes
14. Hydrogen recombination	Yes*
15. In-containment hydrogen combustion	Yes
16. Long-term heat removal from the containment.	Yes*
17. Fission product transport in containment.	Yes

\* New and/or modified capability with MAAP4.07

### 6.2.1.1 Fuel Rod Degradation

The overheating and possible melting of the fuel, clad and control components in the core are simulated in MAAP4.07. All important heat transfer processes between the fuel, cladding, control rods, and coolant components are modeled in each core node. Clad ballooning is evaluated based on the pressure differential between the fuel-cladding gap and the primary system. As fuel degradation continues throughout an accident, MAAP4.07 tracks the progression of mass between adjacent core cell nodes. Criteria are used to establish that each core cell node is in one of five distinct damage states ranging from fully intact fuel assemblies to fully molten. For each different damage state, MAAP4.07 has appropriate models for calculating the heat transfer within

the core cell and between adjacent cells. The damage state also determines the ability of the material to relocate either radially or axially.

#### **6.2.1.2 *Melt Progression/Ablation through Surrounding Core Structures***

Molten material has the ability to flow either axially or radially in MAAP4.07. The calculated porosity of each core cell determines the mobility of the material within the cell and the material surrounding it. When the core bounding cells reach a specified damage state, they are capable of thermally attacking the core bounding heat structures (heavy reflector/core barrel and lower core support plate). The detailed modeling of the heavy reflector failure was described in Section 6.1.1.7.

#### **6.2.1.3 *Core Melt Relocation to Lower Head***

After failure of either the heavy reflector/core barrel or the lower core support plate, MAAP4.07 models the relocation of molten material to the lower head. This model is detailed enough to simulate the rate of relocation, in addition to its timing. After calculating a rupture in the core barrel, for example, MAAP4.07 would relocate only the core material that lies above the rupture location and is able to flow out the hole. In addition, MAAP4.07 calculates the resulting flow rate of debris through the opening and from this flow rate, simulates the gradual widening of the hole due to the flow of debris through it. The details of the newly incorporated models for heavy reflector failure and extensive core barrel failure were described in Section 6.1.1.7.

#### **6.2.1.4 *In-vessel Fuel-Coolant Interaction***

High energy in-vessel FCI is not treated by MAAP4.07. Only ex-vessel FCI is treated, as discussed in a later section.

#### **6.2.1.5 *In-Vessel Oxide Metal Separation***

In MAAP4.07, the debris bed is segregated into a particulate bed, a continuum oxidic crust surrounding a central oxidic debris pool, and an overlying metallic layer. The oxidic debris pool is homogeneously mixed and has uniform thermophysical properties,

while the metal layer rises to the top of the debris pool. The determination of whether a region is in a solid or liquid state, and of the liquid superheat are based on the average debris temperature.

#### **6.2.1.6 Crust Formation and Failure**

In MAAP4.07, crusts can be formed at three surfaces in the continuum debris pool: the top, the RPV wall, and the internal structures. The crust temperature profile is assumed to be one-dimensional and parabolic to account for the internal decay heat generation. The debris crust has the same material composition as the debris pool and assumed temperature profiles are used to describe the heat transfer rates. In MAAP4.07, specific models for the crust buildup at the leading edge of the melt front during heavy reflector failure were described in Section 6.1.1.7.

#### **6.2.1.7 In-Vessel Debris Formation**

In MAAP4.07, debris is formed when a core cell reaches a specific damage state based on the material properties and the amount of material left in the core cell. Debris is relocated from the core to the lower head of the RPV and it accumulates over time as more and more of the support structures in the core undergo failure. The state of the debris in the lower head is simulated throughout the in-vessel phase of the accident and changes due to conditions in the lower head as well as the availability of water in the RPV.

#### **6.2.1.8 RCS/RPV Failure Modes**

RCS and RPV failure occur primarily by creep rupture in MAAP4.07. The RPV lower head, hot leg, and steam generator tube material properties, including Larson-Miller creep rupture parameters, are entered by the user. Using the high temperature and stress within these primary system components, a failure by creep rupture is calculated.

The newly incorporated reactor cavity thermal radiation model for MAAP4.07 was described in Section 6.1.1.4. The reactor cavity thermal radiation model becomes

active when the RPV ruptures and a corium pool begins to form in the reactor cavity. Thermal radiation is transferred from the top surface of the corium pool to the RPV lower head based on the calculated temperatures of each surface and the view factor between them. After RPV lower head failure, the reactor cavity radiation model continues to calculate the exchange of energy between the material in the cavity and the remaining components in the RPV.

#### **6.2.1.9 MCCI/Melt Conditioning in the Reactor Cavity**

In MAAP4.07, several subroutines are combined to model the MCCI process in the reactor pit and the spreading room. Molten core debris is considered to be in direct contact with the containment heat structures, allowing the heat transfer within these heat structures to be calculated by the original heat structure subroutine. MAAP4.07 has been enhanced with the new capability to calculate the heat transfer coefficients within the melt based on a Rayleigh number correlation, rather than by user input. Therefore, as the convection characteristics change during the course of MCCI, the heat transfer characteristics also change based on phenomenological evaluation. The debris within the reactor cavity is homogeneously mixed and debris crusts have the same composition as the molten debris. Steady-state relationships are used for heat transfer and level swell, and chemical reactions are treated by an equilibrium model.

#### **6.2.1.10 Melt Spreading in the Spreading Compartment**

The dynamics of melt spreading are not modeled in MAAP4.07. Rather, the assumption is made that the debris relocates from the reactor cavity to the spreading room and is spread instantly over the available area. The timing of melt relocation from the reactor cavity to the spreading room can be controlled by user-specified control functions. These control functions will be designed to reflect the most bounding gate failure and melt spreading times resulting from the WALTER and MELTSPREAD analyses, respectively.

### **6.2.1.11 MCCI in the Spreading Compartment**

MCCI in the spreading compartment is treated in the same way by MAAP4.07 as MCCI in the reactor cavity. MAAP4.07 treats the corium pools outside of the RPV as homogeneously mixed. The distribution of mass and energy between chemical species is tracked; however, there is no segregation of layers based on density.

### **6.2.1.12 Melt Flooding and Basemat Cooling**

The MAAP4.07 GCM has all the capabilities necessary to model melt flooding and quenching. Compartments containing water pools can be modeled (i.e., IRWST) and connected to the rest of the containment through various methods. Each flow path in MAAP4.07 can represent a simple opening which is always open throughout a transient, or the flow path can be initially closed and fail open based on several different criteria: overpressure, heat sink ablation thickness, or at a user-specified time. The containment thermal-hydraulic routines assure the conservation of energy and momentum during transient flooding and quenching processes.

MAAP4.07 has several new capabilities for modeling basemat cooling. Containment heat sinks may be described with heat slabs containing up to 40 variable-sized nodes for detailed modeling of the thermal profile. This new feature also allows modeling of a liner on each side of the containment heat slabs. These capabilities allow for modeling of composite walls that contain heat slabs of multiple material types and that are exposed to a high thermal gradient, as in the case of basemat cooling. The MAAP4.07 GCM is capable of modeling nodes with water throughput and heat transfer. Thus, cooling of molten corium from below can be appropriately modeled along with heat transfer and evaluation of potential for CHF. The MAAP4.07 heat sinks have also been made more flexible for modeling complicated heat transfer problems by making available a user-specified Kutateladze number for each side of containment heat sinks. This allows the user to have some control over the heat transfer correlation used to determine CHF during basemat cooling.

### **6.2.1.13 *Steam/Hydrogen Transport***

MAAP4.07 uses a general control volume and flow path approach to modeling gas and liquid transport, similar to other lumped parameter codes. The user has the flexibility of modeling a general arrangement within the containment of up to 120 control volumes and 200 junctions. Restrictions are imposed on how many different compartments may be used to model containment compartments that house the primary system main components. Steam and hydrogen are released into the containment from the primary system and during MCCI. The mixture of water and non-condensable gases travels throughout the containment based on the flows needed to balance the basic conservation equations. There is only one velocity for the gaseous components and one velocity for the liquid components, and gas flow is shut off for junctions that become covered in water.

### **6.2.1.14 *Hydrogen Recombination***

MAAP4.07 allows for the use of two different hydrogen recombination models. In addition to the original NIS correlation (Reference 2), MAAP4.07 includes the AREVA NP model based on experiments with AREVA NP PARs. The expanded MAAP4 PAR model also includes the new capability of defining multiple PARs of different sizes within each compartment.

### **6.2.1.15 *In-Containment Hydrogen Combustion***

MAAP4.07 calculates hydrogen and carbon monoxide combustion within the containment. Four basic phenomenological aspects are addressed by the mechanistic model for combustion used in MAAP4.07. First, the intrinsic flammability of a gaseous mixture at a specified temperature and pressure are calculated. Second, the extent of combustion and the duration of combustion are determined to calculate the pressure and temperature in a region. Third, an ignition criterion is used when no obvious ignition source is present. Finally, MAAP4 accounts for the variation of flammability limits with temperature and the potential for autoignition.

The energy production rates are calculated and the reaction rates, based on the availability of CO and H<sub>2</sub>, are adjusted in the containment compartments. Combustion in an open volume originating at an ignition source is idealized as the growth and upward translation of a spherical fireball. The goal of this simplified model is to predict the pressure and temperature in the containment during the reaction and the combustion completeness, which is directly related to the pressure and temperature. MAAP4.07 modeling of combustion also includes the calculation of laminar flame speed based on the temperature, pressure and mole fractions of fuel and inertant. The modeling of detonations is not considered by MAAP4.07.

#### **6.2.1.16 Long-Term Heat Removal from the Containment**

The MAAP4.07 Generalized Engineered Safeguards Features (GESF) model has all the capabilities to model long-term heat removal from the containment. The GESF model contains pumps, heat exchangers, a water source, a containment discharge location, and various user specified controls. There can be up to three separate containment spray trains modeled in MAAP4.07. The first two spray trains are dedicated to the upper and lower compartment sprays, respectively. However, the third train is more general and can be used to model a variety of different containment cooling systems.

#### **6.2.1.17 Fission Product Transport in Containment**

The fission product model is initialized with core activities and fractional decay heat as provided by a fission product inventory code. The elements whose fission masses are required by MAAP4.07 are Xe, Kr, I, Rb, Cs, Sr, Ba, Y, La, Zr, Nb, Mo, Tc, Ru, Ss, Te, Ce, Pr, Nd, Sm, Np and Pu. MAAP4.07 also requires the masses of Cd, In, Ag, Sn, and Mn which are structural materials that may become part of the melt and could be released as aerosols. The MAAP4.07 fission product model considers 12 fission product groups:

#	Fission Product Group
1	Noble Gases and Radioactivity Inert Aerosols
2	CsI + RbI
3	TeO <sub>2</sub>
4	SrO
5	MoO <sub>2</sub>
6	CsOH + RbOH
7	BaO
8	La <sub>2</sub> O <sub>3</sub> + Pr <sub>2</sub> O <sub>3</sub> + Nd <sub>2</sub> O <sub>3</sub> + Sm <sub>2</sub> O <sub>3</sub> + Y <sub>2</sub> O <sub>3</sub>
9	CeO <sub>2</sub>
10	Sb
11	Te <sub>2</sub>
12	UO <sub>2</sub> + NpO <sub>2</sub> + PuO <sub>2</sub>

MAAP4.07 addresses many issues related to fission product and aerosol modeling, which allows for some modeling flexibility relative to the way certain fission product and aerosol phenomena are analyzed by the code, such as the choice of the fission product release correlation, multipliers to change the rates of condensation of aerosols, and multipliers to affect the decontamination factor.

Fission product vapors and aerosols are transported throughout the primary system and containment along with steam, hydrogen and other gases. A fractional volume exchange rate is calculated and used to predict the flow of fission products from one containment compartment to another.

Deposited fission products can move between containment compartments if water pools are present. In the containment, fission products that are deposited are assumed to be dissolved in any available water pools. In the primary system, this transport is not credited since there are usually no water pools in the primary system associated with fission products. Also no convective transport by water of deposited fission products is accounted for in the steam generators.

Portions of the initial fission product and structural material inventories can be transported out of the core as the fuel and cladding melt. When the core material exits

the vessel it moves into the various containment compartments either by entrainment in a high-velocity gas stream or by simply overflowing into another compartment. Any fission products that are mixed with the core material will be transported on a fractional volume basis. When the core material falls into the reactor cavity, fission products residing in molten core debris are released as a result of the interaction with concrete.

### 6.2.2 MELTSPREAD-1.4

MELTSPREAD-1.4 is a separate-effects code that is used to provide a more detailed model of melt spreading. Using the code applicability table previously defined, the applicability of MELTSPREAD-1.4's phenomenological models is summarized in Table 6-2.

**Table 6-2 Severe Accident Phenomena Modeling Capability**

Phenomena	MELTSPREAD-1.4
1. Fuel rod degradation	No
2. Melt progression/ablation through surrounding core structure	No
3. Core melt relocation to lower head	No
4. In-vessel fuel-coolant interaction	No
5. In-Vessel oxide/metal separation	No
6. Crust formation and failure	No
7. In-vessel debris formation	No
8. RCS/RPV failure modes	No
9. Melt conditioning in reactor cavity/MCCI	No
10. Melt spreading in spreading compartment	Yes
11. MCCI in spreading compartment (w/oxide-metal stratification)	Yes
12. Spreading compartment flooding and basemat cooling	No
13. Steam/hydrogen transport	No
14. Hydrogen recombination	No
15. In-containment hydrogen combustion	No
16. Long-term heat removal from the containment	No
17. Fission product transport in containment	No

The detailed description of analytical models and associated numerical methodologies employed within MELTSPREAD-1.4 to predict melt spreading phenomena are described in Reference 104.

#### **6.2.2.1 *Melt Spreading in Spreading Compartment***

The ability to model spreading of molten core debris is the principal application of MELTSPREAD-1.4. MELTSPREAD-1.4 tracks the transient evolution of the distribution of molten materials (both metallic and oxidic) in the form of spreading distance, velocity and depth as a function of time. MELSPREAD-1.4 can also track the thermo-mechanical properties of the evolving melt as well as its immobilization.

#### **6.2.2.2 *MCCI in Spreading Compartment***

For the purposes of the U.S. EPR analytical approach, MCCI in the spreading area using MELTSPREAD-1.4 is not of critical importance because MCCI is analyzed in more detail using MAAP4.07. It is more important to adequately model the initial conditions of the melt prior to spreading, and use the MCCI models to confirm that the sequence of events within the spreading compartment is appropriate (i.e., adequate melt spreading prior to appreciable ablation of the basemat concrete).

MELTSPREAD-1.4 tracks the time-dependent depth of both oxidic and metallic layers within the spreading compartment. These results are output as the total depth of metallic and oxidic layers of debris in the spreading compartment, but detailed information is not provided concerning the relative position of each constituent within the pool.

#### **6.2.3 *WALTER***

WALTER is a separate-effects code that is used to calculate transient temperature profiles in the sacrificial and protective layers within the reactor cavity and to simulate the effect of basemat cooling in the spreading compartment. Using the code

applicability table previously defined, the applicability of WALTER's phenomenological models is summarized in Table 6-3.

**Table 6-3 Severe Accident Phenomena Modeling Capability**

Phenomena	WALTER
1. Fuel rod degradation	No
2. Melt progression/ablation through surrounding core structure	Yes
3. Core melt relocation to lower head	No
4. In-vessel fuel-coolant interaction	No
5. In-vessel oxide/metal separation	No
6. Crust formation and failure	No
7. In-vessel debris formation	No
8. RCS/RPV failure modes	No
9. Melt conditioning in reactor cavity/MCCI	Yes
10. Melt spreading in spreading compartment	Yes
11. MCCI in spreading compartment (w/oxide-metal stratification)	No
12. Spreading compartment flooding and basemat cooling	Yes
13. Steam/hydrogen transport	No
14. Hydrogen recombination	No
15. In-containment hydrogen combustion	No
16. Long-term heat removal from the containment.	No
17. Fission product transport in containment.	No

WALTER is a supplemental code that is used to support the conclusions developed from other codes. In all scenarios, WALTER calculates the transient thermal conditions within structures, allowing conclusions to be drawn regarding their overall stability when subject to a specific heat flux. The applicability of this code to support the analysis of gate failure and cooling structure performance is based upon the fact that the heat transfer problem to be solved is explicitly calculated by WALTER. While WALTER is not used to predict melt spreading, WALTER is used to evaluate the performance of the reactor cavity gate, the failure of which defines the start of spreading processes.

### **6.3      *Validation of Analytical Tools***

All three codes used for severe accident analysis in the U.S. EPR were qualified for use and application to the analysis of plant-specific severe accident phenomena.

Considerable work was performed in validating the main integral code MAAP4.07 since it is used as the primary analysis tool. Most of the validation work to date has been performed by FAI, although AREVA NP has supplemented benchmarking studies related to MCCI. In addition, AREVA NP plans to continue validation work with MAAP4.07 by doing code comparison studies with other codes, such as MELCOR 1.8.6. This validation work is expected to be complete in early 2007. The validation and/or verification strategy and results for all three codes used in the U.S. EPR severe accident analytical methodology are described in this section. Details relating AREVA NP's activities using MELCOR 1.8.6 are presented in Appendix C.

#### **6.3.1      *MAAP4.07***

The MAAP4.07 code comes with an established validation basis from its widespread use in the nuclear industry on many different plant designs. However, modifications have been made to MAAP4 in order to create version 4.07 and these modifications have been the target of additional validation studies. The main area of focus of these validation studies was in the area of MCCI since this represents the primary area of source code modifications in MAAP4.07.

FAI has performed a large number of benchmarks using MAAP4.07 to simulate various MCCI experiments. The results of these studies are summarized in this section. More important, MAAP4.07 now provides a user the ability to perform dynamic benchmarks of MCCI experiments. AREVA NP has used this new capability to perform dynamic benchmarks of two additional MCCI experiments: the CCI-2 (Reference 61) and CCI-3 (Reference 62) tests. The results of the CCI-2 and CCI-3 validation studies are also discussed in this section.

### **6.3.1.1 MCCI Dynamic Benchmarks**

The MAAP4.07 GCM was compared to the ACE, BETA, CCI-2 and CCI-3 molten debris coolability experiments as part of the MAAP4 dynamic benchmark feature. While this benchmark focuses on MCCI, its scope is not limited to the primary issue of ablation. Rather, this is an integral benchmark that can contribute to the validation of multiple models, including ablation, debris temperature, heat transfer to the overlying gas space and heat transfer to surrounding structural heat sinks in both the gas space and the debris space.

#### **6.3.1.1.1 ACE: Advanced Containment Experiments**

##### **Background**

Large scale MCCI tests have been performed at ANL as part of the internationally supported Advanced Containment Experiments (ACE) program (see Reference 108 - 110). The objectives of the ACE tests were to investigate the thermal-hydraulics and chemical processes of MCCI and to expand the database for further development and validation of MCCI/fission product release codes.

The test apparatus consisted of eight water panels assembled in pairs to form four walls. The concrete basemat, concrete/metal inserts, and corium inventory were contained within these walls. The inner surface of the north and south walls contained picture-frame assemblies with 25 tungsten rod electrodes, which were connected near the top of the corium by four tungsten coils that heated the corium locally until it became electrically conducting. Dimensions within the assembled apparatus were 53.0 cm x 50.2 cm.

A rectangular two-piece lid covered the test apparatus and connected it to the main gas line. The entire lid was water-cooled. There were four ports in the lid: one for aerosol collection and gas sampling/exhaust and three for viewing the corium by an optical pyrometer and two video cameras.

All corium constituents, including the  $UO_2$ , were present in powder form and blended uniformly.

Two types of concrete were used for the experiments: siliceous (Si) and LCS. The composition of the concrete for ACE tests L2, L6, and L7 (described in the following section) is listed in Table 7-4. Table 7-5 lists the composition of corium for these ACE tests. During the experiments, corium inventory was heated up by the tungsten electrodes to form a molten debris pool. Concrete erosion was monitored by the thermocouple arrays located inside the basemat.

**Table 6-4 Concrete Compositions for the ACE Experiments**

<b>Concrete Type</b>	<b>L2</b>	<b>L6</b>	<b>L7</b>
	Si	Si	LCS
<b>Constituent</b>	<b>L2</b>	<b>L6</b>	<b>L7</b>
SiO <sub>2</sub>	69	69	28.3
CaO	13.5	13.5	26.0
Al <sub>2</sub> O <sub>3</sub>	4	4	3.5
K <sub>2</sub> O	1.4	1.4	0.6
Fe <sub>2</sub> O <sub>3</sub>	1.0	1.0	1.6
TiO <sub>2</sub>	0.8	0.8	0.14
MgO	0.7	0.7	9.6
Na <sub>2</sub> O	0.7	0.7	1.1
MnO	0.03	0.03	0.05
BaO	0.02	0.02	0.03
SrO	0.02	0.02	0.03
Cr <sub>2</sub> O <sub>3</sub>	0.01	0.01	0.009
H <sub>2</sub> O+CO <sub>2</sub>	7.9	7.9	27.5

**Table 6-5 Corium Compositions for the ACE Experiments**

<b>Constituent</b>	<b>L2</b>	<b>L6</b>	<b>L7</b>
UO <sub>2</sub>	216	219	188.5
ZrO <sub>2</sub>	42.5	18.5	59.4
Zr	13.4	21.1	17.7
Zirc-4	-	-	1.1
Fe <sub>2</sub> O <sub>3</sub>	-	-	-
NiO	-	-	-
Cr <sub>2</sub> O <sub>3</sub>	-	-	-
SS-304	-	9.1	0.6
CaO	3	7.3	11.5
MgO	-	-	-
SiO <sub>2</sub>	20.9	16.9	12.5
BaO	0.8	0.79	1.4
La <sub>2</sub> O <sub>3</sub>	0.6	0.6	1.14
SrO	0.5	0.5	0.96
CeO <sub>2</sub>	1.3	1.3	2.32
MoO <sub>2</sub>	0.9	0.94	1.7
SnTe	0.2	-	-
ZrTe <sub>2</sub>	-	0.2	0.18
Ru	-	0.38	-
B <sub>4</sub> C	-	-	1.0
Ag	-	1.19	-
In	-	0.22	-

## Results

The ACE L2 test (Reference 108) investigated the interaction of a partially oxidized PWR corium melt with siliceous concrete. The average electrical heating power over the duration of the test was about 220 kW. The average heat loss to the water-cooled panels was about 120 kW. The electrical heating power and heat loss to the sidewall were prescribed as boundary conditions. The molten pool temperature was measured to be about 2400 K at the start of ablation, and remained around 2400 K. The average downward concrete ablation rate was 7.8 mm/min. Charts comparing MAAP4.07 and test results for corium temperature and ablation depth are illustrated in Figure 6-3 and Figure 6-4.

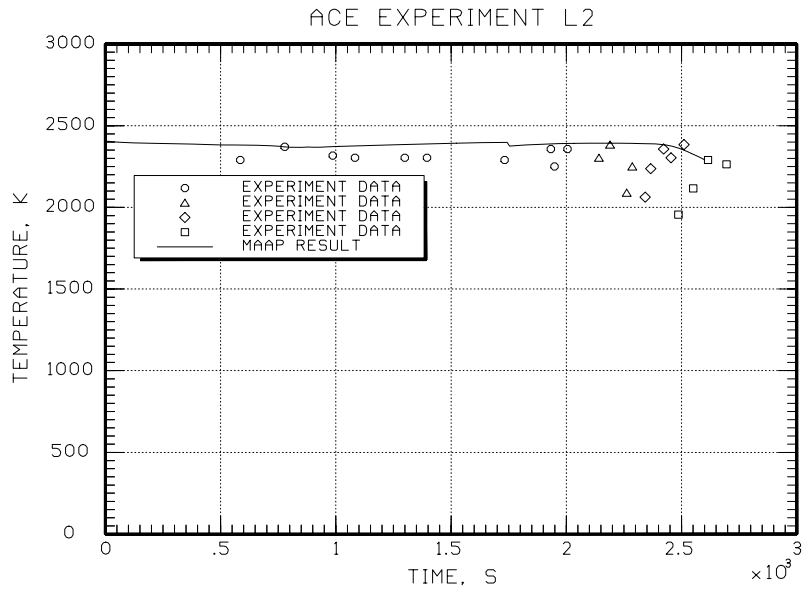


Figure 6-3 ACE L2 Melt Temperature Predictions

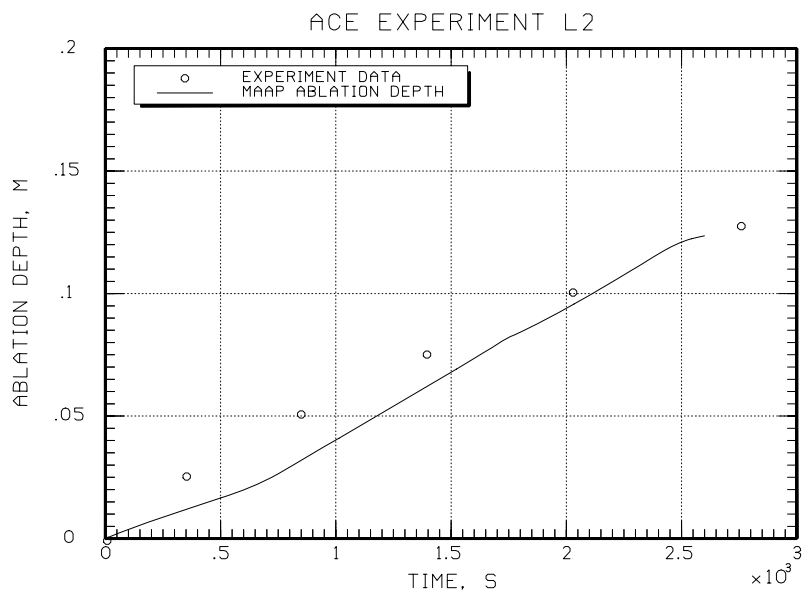
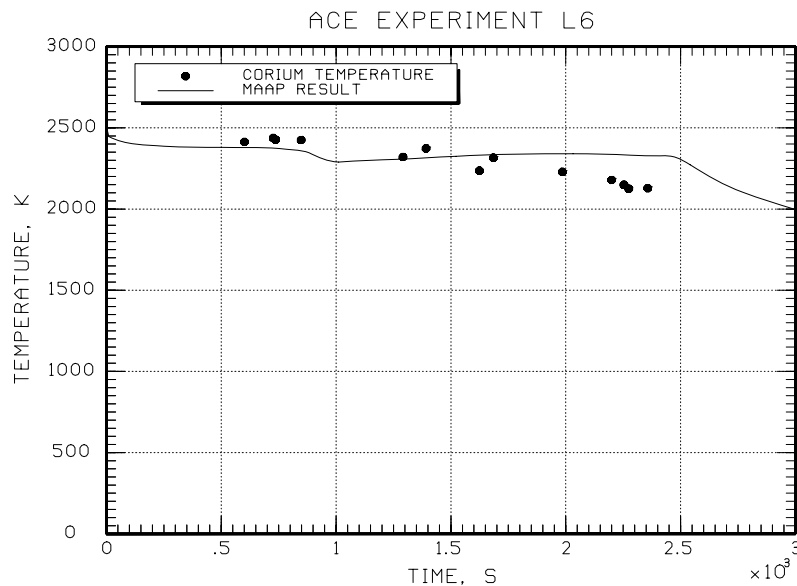
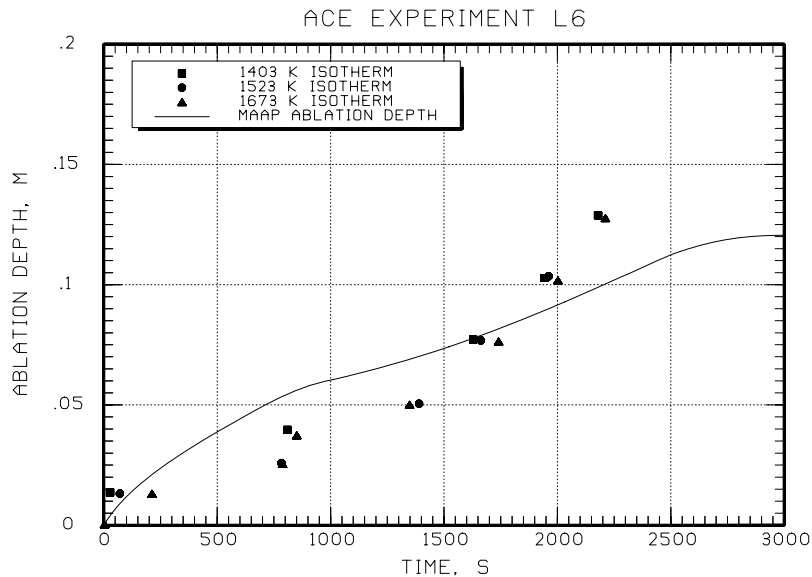


Figure 6-4 ACE L2 Ablation Depth Predictions

The ACE L6 test (Reference 109) studied the interaction of a partially oxidized PWR corium melt with siliceous concrete. Four 7 cm thick concrete/melt inserts were supported on a lip around the upper surface of the basemat to provide a source of zirconium and steel. The inserts were simply lumped into the constituents of the corium at the start of ablation. The electrical heating power was about 200 kW. Heat loss to the sidewall was high, about 125 kW. Ablation rate was low at the start of the test and high at the end. Total ablation depth was about 13 cm during 40 min. The melt temperature, as measured by an optical pyrometer, was high ( $> 2000$  K). Electrical heating power and heat loss to the sidewall were prescribed as boundary conditions. Charts comparing MAAP4.07 and test results for corium temperature and ablation depth are illustrated in Figure 6-5 and Figure 6-6.



**Figure 6-5 ACE L6 Melt Temperature Predictions**



**Figure 6-6 ACE L6 Ablation Depth Predictions**

Partially oxidized BWR corium (70% Zr oxidized), LCS concrete, and a total electrical heating power of 130 kW were used for the ACE L7 test (Reference 110). Similar to the ACE L6 test, a 5.7 cm concrete/metal insert was installed above the basemat to provide a source of zirconium. It was lumped into the corium at the start of ablation. About 3 cm of downward erosion of concrete was observed in 30 min. The low power density of BWR corium and higher decomposition enthalpy of the LCS concrete resulted in the low concrete ablation depth. MAAP4.07 validation predictions and observed erosion depth and corium pool temperature are shown in Figure 6-7 and Figure 6-8.

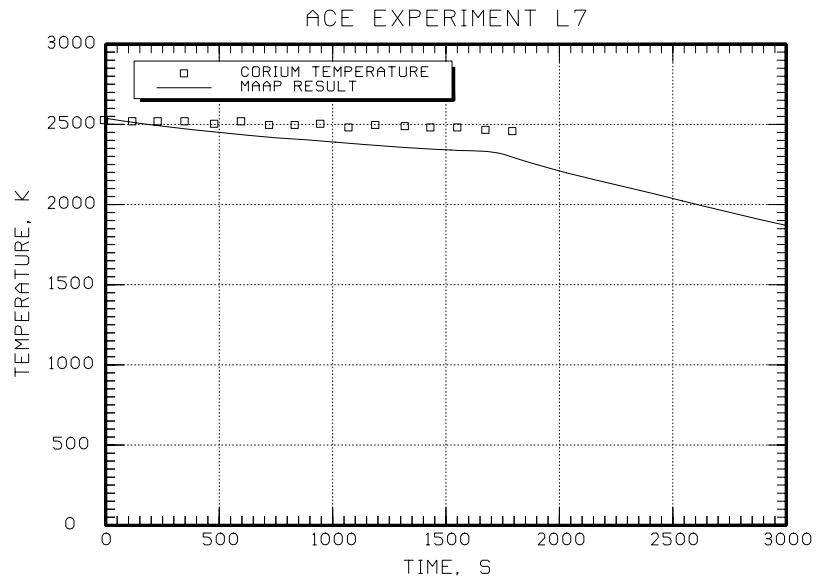


Figure 6-7 ACE L7 Melt Temperature Predictions

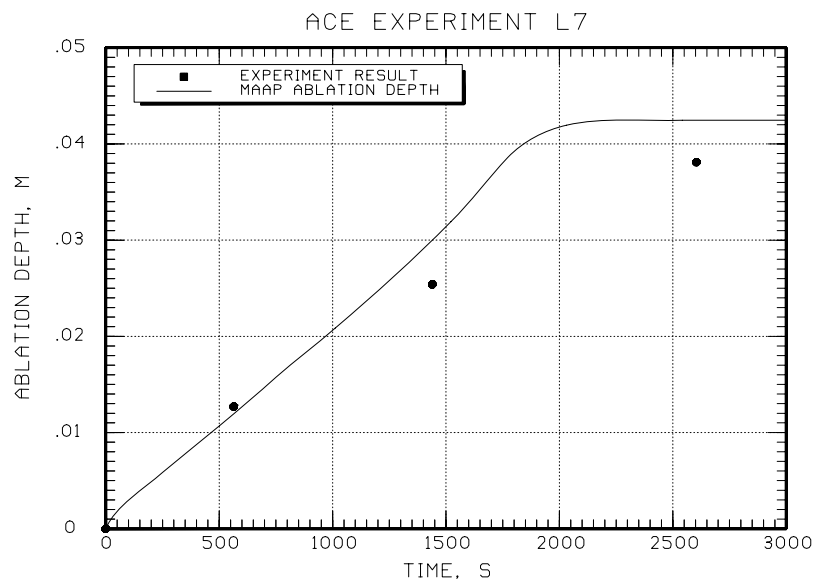


Figure 6-8 ACE L7 Ablation Depth Predictions

Collectively, agreement between MAAP4.07 and the data from ACE tests L2, L6, and L7 for corium temperature and erosion depth is good and absent of any obvious calculated bias.

### ***6.3.1.1.2 BETA: Large Scale Metal/Oxide Interaction Experiments***

#### **Background**

The BETA tests (References 111 and 112) comprise a series of large scale metallic melt experiments conducted at Forschungszentrum Karlsruhe (FzK) in Germany. This series of experiments was originally designed to provide a database for validation of severe accident codes. The crucible of the test section is made of siliceous concrete. Similar to the other experiments (ACE and CCI), arrays of thermocouples were fabricated in the concrete.

The BETA V5.1 experiment (Reference 111) investigates the influence of high zirconium content in the metal phase and its consequences on aerosol release. In the experiment, an 80 kg mass of solid zirconium metal was deposited at the bottom of the crucible. About 350 kg of high temperature melt was heated by chemical reaction in the thermite reaction tank above the concrete crucible. The composition of the melt was 300 kg of steel (90% Fe, 5% Cr, and 5% Ni) and 50 kg of oxides (65% Al<sub>2</sub>O<sub>3</sub>, 20% SiO<sub>2</sub> and 15% CaO). The metallic phase and then the oxidic phase of the melt were poured on the top of the zirconium metal. The time required to dissolve the zirconium was less than one minute. The metallic phase of the melt was continuously heated by an induction coil on the outside of the crucible. The average heating power was about 330 kW.

The BETA V5.2 experiment studied the effects of high zirconium content, the presence of B<sub>4</sub>C and lower decay power on the corium-concrete interaction. The corium used in this test was exactly the same as that used for V5.1, with the exception of an additional 6 kg of B<sub>4</sub>C encapsulated in a steel container that was added to the melt. The heating power, about 200 kW, was lower than that of V5.1. Nonetheless, the time required to dissolve the zirconium was short, similar to V5.1.

---

## Results

In the BETA V5.1 experiment, the observed downward ablation rate was approximately 17 mm/min, resulting in a total concrete erosion depth of 50 cm in 29 minutes. The observed lateral erosion terminated in about 250 seconds with a total lateral erosion depth of 5 cm. This could be due to the combined effects of high heating power (compared to V5.2), which was concentrated in the metal phase, and the shallow pool. Because downward ablation was so rapid, the pool actually moved away from the eroding sidewall.

The electrical power was prescribed as a boundary condition. The upward heat loss was also prescribed, but its assumed value was zero due to the mass of oxide material covering the metallic mass. This corresponds to an adiabatic boundary condition at the upper surface of the melt. The phenomenon of separation of the melt from the sidewall described previously cannot be properly modeled by MAAP4.07. Radial erosion must be terminated after 250 seconds by prescribing a similar adiabatic sidewall boundary condition.

A comparison of the predicted axial erosion distance and the debris temperature with experimental data is shown in Figure 6-9 and Figure 6-10. The experimental results show that the oxidation of zirconium dominates the interaction for the first 2 to 3 minutes. This resulted in an initially high hydrogen release, high concrete erosion rate, and high void level in the melt pool. The early chemical energy release, mainly from the reaction of zirconium with the silicon of the melting concrete, is considerably higher than the heating power used to simulate the decay heat in the debris. Due to the very effective downward and lateral heat transfer to the melting concrete, the melt temperature showed a sharp decrease to the solidus temperature within 200 seconds. Figure 6-9 shows good agreement of the MAAP4.07 melt temperature predictions with the experimental data with MAAP4.07 predicting a slightly higher melt temperature over most of the experiment. Figure 6-10 shows excellent agreement of the MAAP4.07 ablation depth predictions in both the axial and lateral directions.

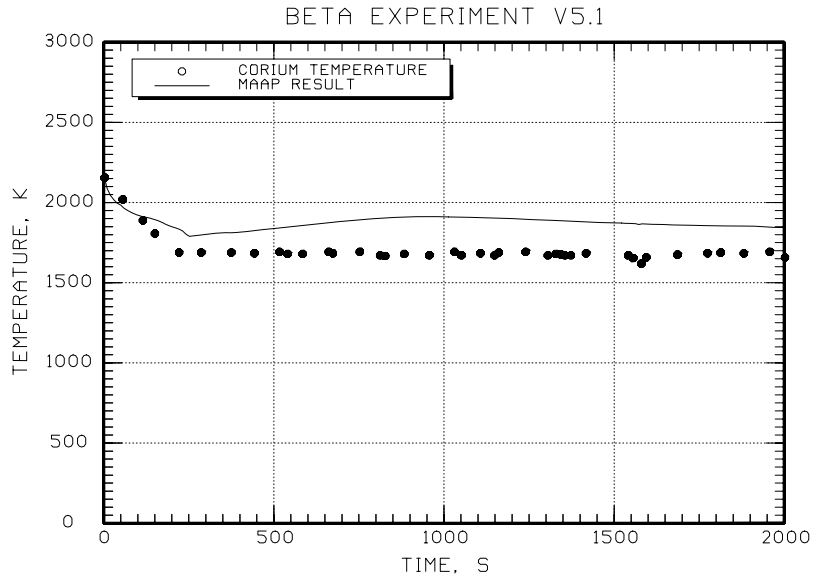


Figure 6-9 BETA V5.1 Melt Temperature Predictions

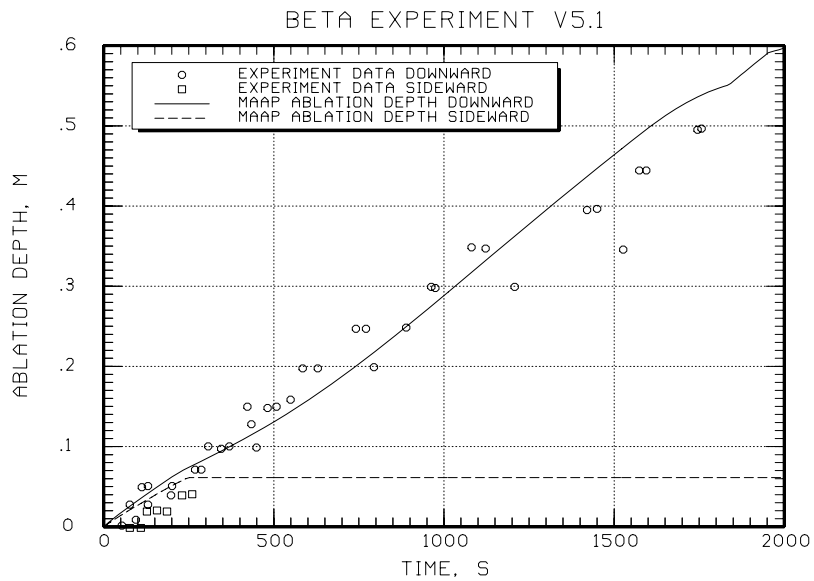
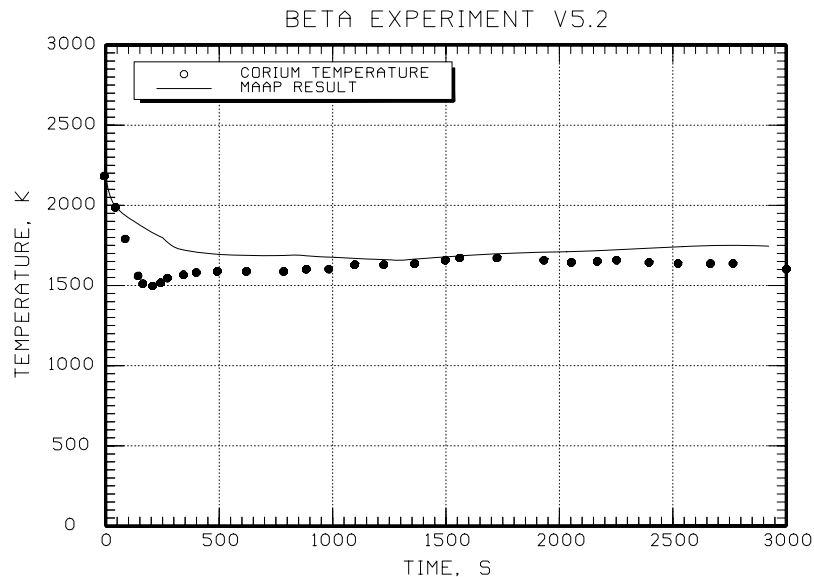
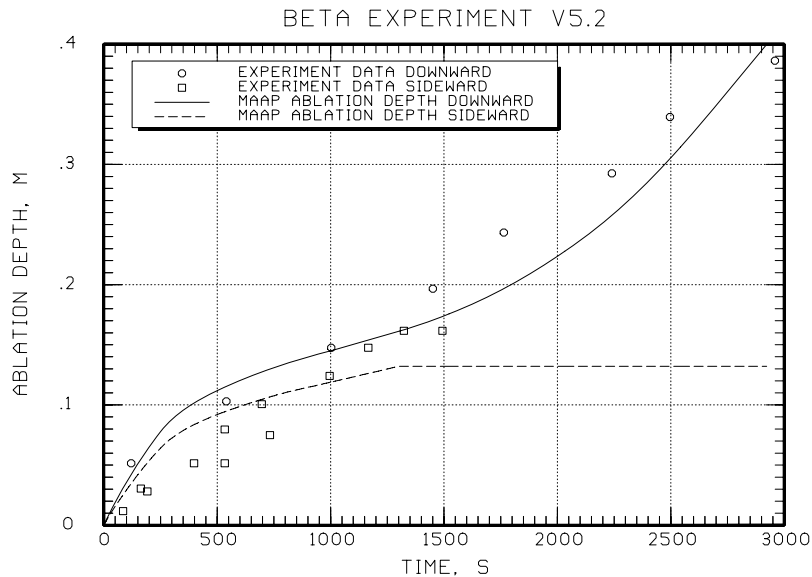


Figure 6-10 BETA V5.1 Ablation Depth Predictions

The BETA V5.2 experiment (Reference 112) tested the effects of fission products and B<sub>4</sub>C during the melt/concrete interaction. For this test, the experiments applied the same boundary conditions as those of BETA V5.1. The axial erosion rate was approximately 8 mm per minute with a total erosion depth of 40 cm in 50 minutes; within the sidewall, the erosion rate was about 7 mm per minute, i.e. a total erosion depth of about 16 cm in 21.7 minutes. The sidewall heat loss was turned off at time 21.7 minutes similar to the V5.1 experiment to prevent continued sidewall erosion. The agreement between MAAP4.07 results and experimental data for corium temperature and ablation rates, as shown in Figure 6-11 and Figure 6-12 was generally good.



**Figure 6-11 BETA V5.2 Melt Temperature Predictions**



**Figure 6-12 BETA V5.2 Ablation Depth Predictions**

### 6.3.1.1.3 Core Concrete Interaction Experiment 2 (CCI-2)

#### Background

CCI-2 was a two-dimensional experiment investigating MCCI for a 400-kg, fully oxidized PWR core melt initially containing 8.0 wt% LCS concrete. The details of the experimental apparatus, as well as the test procedure and results, are fully documented in Reference 61. The CCI-2 experiment was designed to provide information in three main areas:

- lateral vs. axial power split during dry core-concrete interaction
- integral debris coolability data following late phase flooding
- data on the nature and extent of the cooling transient following breach of the crust formed at the melt-water interface

The test facility contained the test apparatus itself, along with a power supply for direct electrical heating (DEH) of the corium, a water supply system, two steam condensation (quench) tanks, an off-gas system, and the data acquisition system. The entire test apparatus was housed in an explosion-rated containment cell with remote controls for water and gas flows.

## **Apparatus**

The CCI-2 test section was approximately 3.4 m tall with an internal cross section that measured 0.5 m by 0.5 m. The concrete basemat depth was initially 0.55 m.

The lower test section, where the MCCI occurred, contained two opposing walls made of LCS concrete. The other two opposing walls contained tungsten electrodes to heat the melt throughout the ablation process. The tungsten electrodes not only provided initial heating of the melt, but they were also embedded within the concrete to a depth of approximately 0.35 m to maintain a uniform heated surface. The tungsten electrodes were backed by a MgO refractory sublayer. In addition, the walls above the melt were also composed of refractory MgO. The middle section, just above the lower test section, was made of MgO refractory material. The walls in the upper section along with the lid were composed of locally obtainable LCS concrete.

## **Melt Formation**

The melt pool was formed through an exothermic thermite chemical reaction that produced the target initial melt mass over a time period of approximately 30 seconds. Two iron/alumina sparklers, wrapped with nichrome starter wire, are used to ignite the initial corium charge (powder). This initiated the thermite reaction that formed the initial melt mass.

The tungsten electrodes then took over in order to simulate decay heat in the formed melt mass. The electrodes completely covered the portion of the MgO side walls that were exposed to the corium. The electrodes also penetrated into the concrete walls, but were not powered until the concrete began to ablate and additional banks of

tungsten rods became exposed to corium. In this fashion a uniform heating of the melt was maintained throughout the experiment.

The flooding of the melt was accomplished through weirs installed in the upper test section. Water was supplied from a storage tank at the flow rate needed to keep the water level constant at 0.5 m. Melt flooding was initiated 300 minutes into the experiment. The experiment was terminated at approximately 423 minutes based on the fact that concrete temperatures were stabilized and input power was reduced to 15% of the initial power (power supply in constant voltage mode).

## Results

The CCI-2 benchmark simulation was executed for 300 minutes (18000 s). Pertinent results from the CCI-2 simulation are shown in Figure 6-13 and Figure 6-14, along with the corresponding experimental data from Reference 61. The results show good agreement with the experimental data.

In Figure 6-13 the MAAP4.07 erosion rates for the basemat and sidewall are plotted. Since the MAAP4.07 heat transfer characteristics for each of the concrete walls are identical, the erosion rate predictions by MAAP4.07 are similar for the radial and axial directions. These predictions agree well with the CCI-2 results out to an experiment time of approximately 250 minutes. After this time MAAP4.07 overpredicts the erosion distance.

In Figure 6-14 the MAAP4.07 average corium temperature is plotted. The melt temperature is slightly overpredicted in the initial stages of the experiment but shows the correct trend of decreasing melt temperature with increasing concrete fraction. The temperatures are also in good agreement with the experimental data for the duration of the experiment.

The two main uses of MAAP4.07 MCCI calculations are to give accurate predictions of concrete ablation and melt temperatures. The concrete ablation levels are important for performing accurate plant calculations involving thermal attack of the basemat and other

reactor cavity structures. The melt temperature predictions are important for calculation of accurate melt properties as they change with increasing MCCI, and ultimately for predicting the spreading and stabilization behavior of the melt. The agreement of the MAAP4.07 predictions of these two important parameters is sufficient validation for using MAAP4.07 in severe accident calculations involving similar types of concrete.

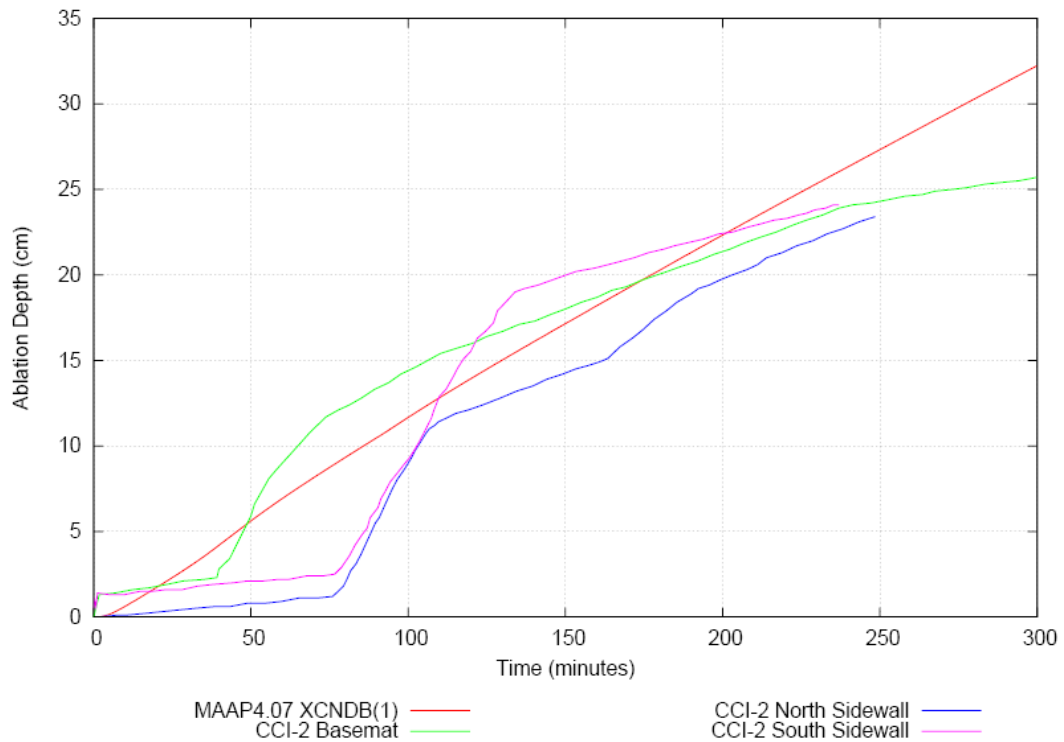


**Figure 6-13 MAAP4.07 Predicted Erosion Rates vs. CCI-2 Data**

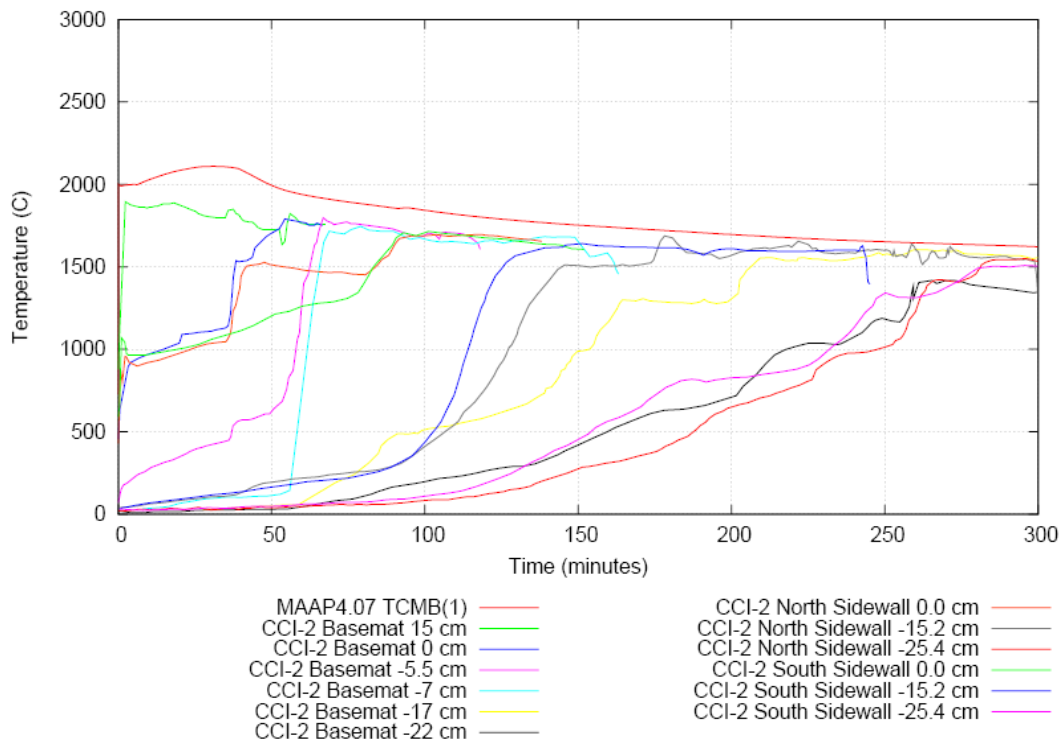


**Figure 6-14 MAAP4.07 Predicted Average Melt Temperatures vs. CCI-2 Data**

#### **6.3.1.1.4 Core Concrete Interaction Experiment 3 (CCI-3)**

##### **Background**

CCI-3 was a two-dimensional MCCI experiment that used much of the same test apparatus and assembly as the CCI-2 experiment. The experiment investigated MCCI for a 375-kg fully oxidized PWR core melt initially containing 15.0 wt% siliceous concrete. The details of the experimental apparatus, the test procedure, and the results are fully documented in Reference 62.

Many of the same methods that were used in the CCI-2 experiment were also employed in the CCI-3 experiment. The major differences between CCI-3 and CCI-2 were:

- Use of siliceous concrete rather than LCS concrete
- Slightly different initial debris constituent

- Slightly different initial conditions of the melt at the time of onset of ablation

## Results

The CCI-3 benchmark simulation was executed for 100 minutes (6000 s). Pertinent results from the CCI-3 simulation are shown in Figure 6-15 and Figure 6-16, along with the corresponding experimental data from Reference 62. The results show fair agreement with the experimental data.

In Figure 6-15 the MAAP4.07 erosion rates for the basemat and sidewall are plotted. The CCI-3 data display some non-uniformity between the axial and radial erosion depths and the MAAP4.07 predictions lie between the two extremes. This occurs because the MAAP4.07 representation of the concrete erosion is equivalent to the average of the lateral and downward components of the real physical ablation profile.

In Figure 6-16 the MAAP4.07 average corium temperature is plotted. There is good agreement between the MAAP4.07 predicted average melt temperature and the peaks of the sidewall thermocouple responses. The basemat thermocouples register an abnormally low temperature due to the significant delay in ablation at the basemat centerline. It is unclear from the description of the CCI-3 experiment what caused the unexpected ablation delay at the basemat centerline. However, the agreement between MAAP4.07 and the melt temperatures at the sidewalls indicates accurate modeling of the melt heat transfer in the radial direction. These results demonstrate that MAAP4.07 has been validated for the calculation of MCCI involving molten pools in which the heat flux is expected to be isotropic.

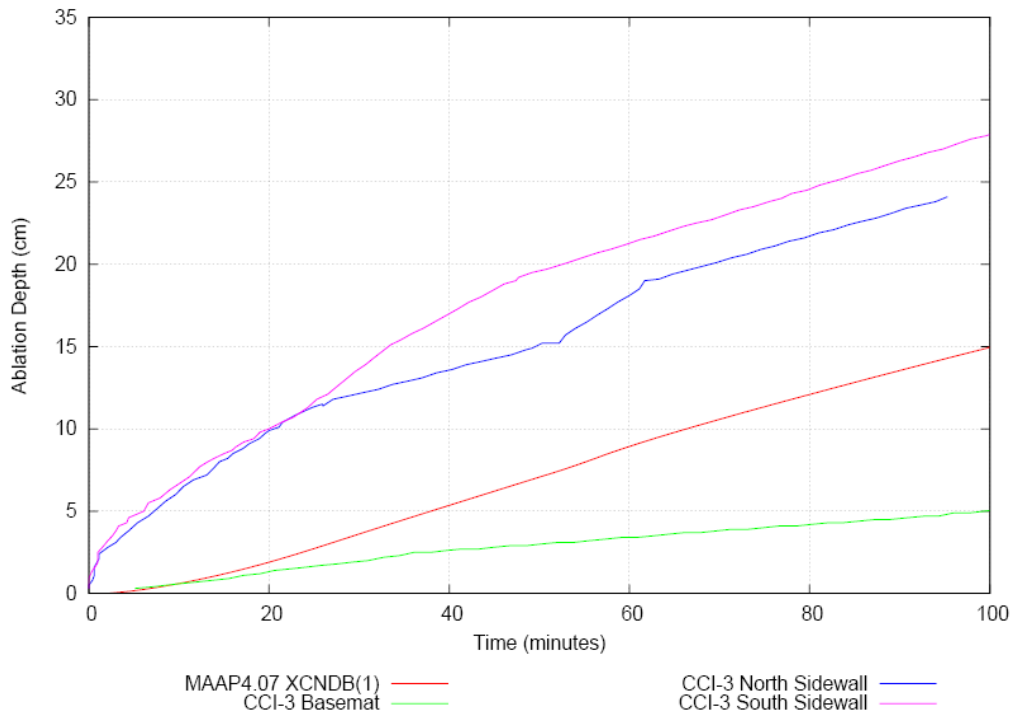


**Figure 6-15 MAAP4.07 Predicted Erosion Rates vs. CCI-3 Data**

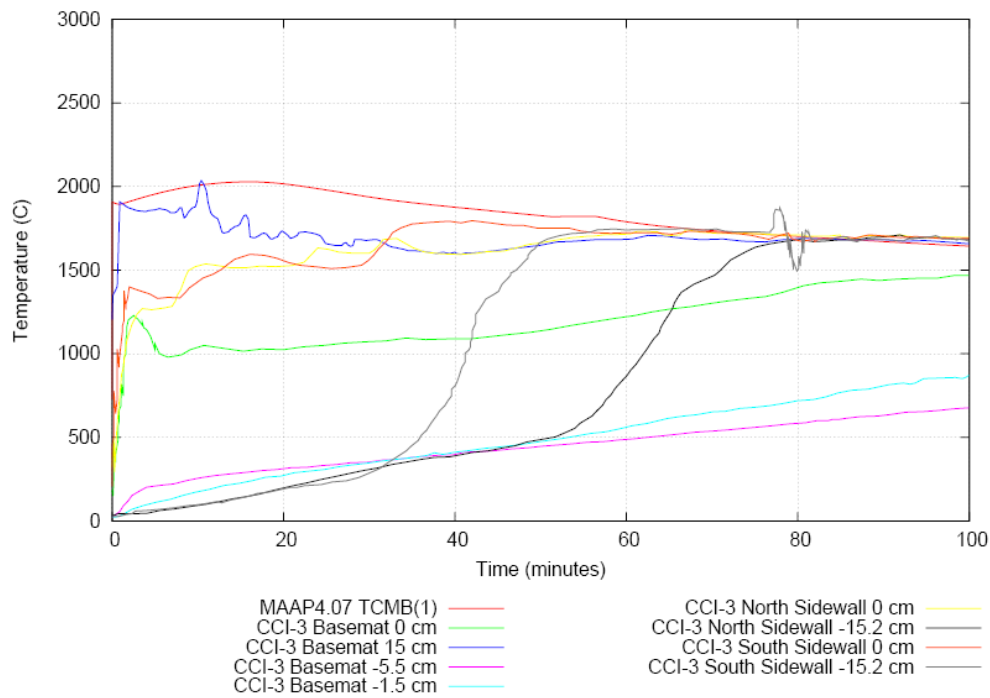


**Figure 6-16 MAAP4.07 Predicted Average Melt Temperatures vs. CCI-3 Data**

### **6.3.1.1.5 Conclusions**

Corium temperature and concrete ablation rates are well predicted for ACE L2, L6, L7, BETA V5.1, V5.2, CCI-2, and CCI-3. The results of the validation studies indicate a proper distribution of the input power to the upward (thermal radiation plus convection to gas) and lateral/axial (convection to concrete) power losses. Thus, the selection of model parameters for corium convection is appropriate for these tests. The good agreement of the MAAP4.07 predictions for the ablation rate demonstrates that the MAAP4.07 MCCI model contains an adequate treatment of concrete thermo-physical data and chemistry. The good agreement of the MAAP4.07 predictions for the corium temperature shows that the MAAP4.07 MCCI subroutines correctly treat the heat transfer performance at the crust/concrete interface as well as the natural circulation conditions within the corium pool.

### **6.3.2 MELTSPREAD-1.4**

To validate MELTSPREAD-1.4 for analysis of the U.S. EPR, AREVA NP relies upon the studies described in Section 7.0 of Reference 104. An important part of the MELTSPREAD-1.4 development has been the comparison of model predictions with relevant analytical solutions and experiment data. These studies have been performed by both ANL and AREVA NP. Some of the validation studies completed to date that support the use of MELTSPREAD-1.4 as an analytical tool include comparisons of:

- Fluid mechanics algorithm with the analytical solution for a one-dimensional dam break problem
- Fluid mechanics algorithm with water simulant spreading test data in a 1/10 linear scale model of the Mark I containment
- Integrated code predictions with the molten steel spreading test data in an approximate mockup of a Mark I containment

There is currently a lack of spreading data for prototypic oxide materials (i.e.,  $UO_2/ZrO_2$ /concrete oxides). A summary of the validation database for MELTSPREAD-

1.4 is provided below. Detailed discussion concerning these calculations is provided in Section 7 of Reference 104.

### **6.3.2.1 Comparison with Dam Break Analytical Solution**

To validate the hydrodynamics modeling of the code, the fluid mechanics algorithm was compared with the analytical solution for a one-dimensional dam break problem. The details associated with this analytical comparison are provided in Section 7 of Reference 104. Of principal interest in this case was whether correct spreading depths and velocities were calculated. The sample calculation modeled a 20-m-long flow channel with a barrier at the midpoint. Half of the channel was initially filled with water to a uniform depth of 10 cm. At time zero, the barrier representing the dam was removed and the water was allowed to relocate under the influence of gravity.

Using MELTSPREAD-1.4, the height distribution of the water at selected times was calculated as well as the leading edge velocity. These results were compared to the analytical results obtained by manual computation. The hydrodynamics model in MELTSPREAD-1.4 slightly underpredicted the theoretical advancing front depths through the calculated time domain (maximum deviation of ~5% at 20 seconds). After transient effects had diminished, the calculated leading edge velocity showed reasonable agreement with the theoretical values (maximum deviation of ~10%). These results indicate that the correct fully-developed flow behavior is calculated to within a reasonable tolerance.

### **6.3.2.2 Comparison with Water Simulant Spreading Data**

The fluid mechanics algorithms reasonably predicted spreading depths and velocities from a theoretical dam break scenario. The analytical results of MELTSPREAD-1.4 were also compared to water relocation data in a more complex, scaled Mark I containment geometry discussed in References 113 and 114. The relevant data used for comparison is based on a 1/10 linear scale model of the Peach Bottom pedestal and drywell. MELTSPREAD-1.4 was used to calculate various parameters associated with melt spreading, including transient depth profiles and arrival times for 4 measured

locations. Detailed discussion concerning this comparison is provided in Section 7 of Reference 104.

The results of the comparison of the predictions of the hydrodynamics model in MELTSPREAD-1.4 with the water simulant data demonstrate reasonable consistency between predicted and actual arrival times and transient depth profiles within the pedestal and drywell regions of a Mark I containment. Nonetheless, it is important to note that in these scenarios the heat transfer and freezing effects of the melt have been neglected.

### **6.3.2.3 Comparison with Molten Steel Spreading Data**

Additional validation work is presented in Reference 104 to demonstrate the ability of the code to predict spreading behavior, including heat transfer and freezing effects. To support the validation of the code, analytical results were compared with steel spreading test data from the Japanese SPREAD experiments. In these experiments, molten steel was poured into a cylindrical concrete cavity and was free to spread over an open floor through an open junction. The details associated with the test apparatus are discussed in detail in Section 7 of Reference 104; however, it is important to note that the scaled configuration of the test apparatus is similar to the actual configuration of the U.S. EPR CMSS spreading area.

Two scenarios were used to support the validation of the code. The first of these scenarios involved the spreading of molten steel into a dry cavity (Test 15) while the second tested the effect of spreading in a flooded cavity (Test 22). For the subject scenarios, the experimentally-determined final debris distributions were compared with the results predicted using MELTSPREAD-1.4. For Test 15, the calculated melt penetration distance outside of the failure junction agreed to within 11% of the experimentally measured distance. For Test 22, the calculated melt penetration distance outside of the failure junction agreed to within 13% of the experimentally measured distance.

After the MELTSPREAD-1.4 validation analyses discussed in Section 7 of Reference 104 were performed, minor evolutionary code changes were made. For example, the densities of solid and liquid  $ZrO_2$  were switched in the property subroutines to correct a previous code error. Further revision resulted from the identification of certain corium enthalpy/temperature routines that required modification but did not tangibly change the analytical results of the code.

To ensure that the validation database of MELTSPREAD-1.4 was not compromised, AREVA NP reevaluated the consistency of its predictions using the experimental results of the SPREAD experiments. To do this, AREVA NP developed comparable analytical models to those used in the original validation studies. For Test 15, the calculated melt penetration distance outside of the failure junction agreed to within 6% of the experimentally measured distance. For Test 22, the calculated melt penetration distance outside of the failure junction agreed to within 10% of the experimentally measured distance. These results indicate that MELTSPREAD-1.4 can not only rely upon the validation database discussed in Reference 104 but that it also models melt spreading phenomena with reasonable accuracy. Nonetheless, it is important to note that while MELTSPREAD-1.4 reasonably predicts spreading phenomena, detailed comparison of analytical predictions to experimental spreading data for materials for which the code was principally developed ( $UO_2/ZrO_2$ /concrete oxides) has not been performed.

### 6.3.3 **WALTER**

To validate WALTER for analysis of the U.S. EPR, AREVA NP has analyzed a number of physical scenarios and compared the code predictions with known analytical solutions. The description of these validation studies are provided in Reference 105 and are also summarized below. The representative problems considered for validation of WALTER are categorized according to the following physical characteristics:

- Stationary temperature profiles in solid layers

- 
- Transient temperature profiles in infinite solid layers
  - Modeling of liquid layers and phase-change

A number of scenarios were investigated using WALTER and comparing the predicted numerical result with the known analytical solutions. The conclusions drawn relative to WALTER for each of these validation case categories are provided below.

- *Stationary temperature profiles in solid layers.* Cases investigating steady-state heat transport through a composite wall and heat generation and transport within a volumetrically heated layer were performed. WALTER was able to accurately predict the steady-state temperature profiles within solid layers.
- *Transient temperature profiles in infinite solid layers.* A case investigating the transient temperature profile within an infinite solid layer was performed. Temperature profiles predicted by WALTER exactly matched the theoretical results.
- *Modeling of liquid layers and phase-change.* Cases investigating the freezing front into a liquid layer, ice formation on a top-cooled water pool heated from the bottom, convective heat transfer through a horizontal liquid layer, and volumetrically heat pools with both cooled and adiabatic upper and lower surfaces were performed. The phase change models were found to be fully symmetric in their calculation of freezing or melting front. Calculation of the progression of the freezing front position and timing matches the analytical solution well. Calculation of convective heat transport through a horizontal liquid layer is well in range of the uncertainties given by the correlations used for a wide range of Rayleigh and Prandtl numbers. The predicted heat flux out of a volumetrically heated pool with cool upper and/or lower surface and the calculated up/down split match well with the predicted dependence upon Rayleigh number. The calculated pool temperatures, for both the heated and cooled cases, match the steady-state temperatures well.

---

These results support the conclusion that WALTER is a stable numerical solver that can be used to solve transient one-dimensional heat transfer problems.

## **6.4 Description of U.S. EPR Analytical Models**

This section describes the development of the MAAP4.07 integral model, the MELTSPREAD-1.4 spreading model, and the WALTER models for the melt plug and stabilization process for the U.S. EPR. The focus of this section is on the general modeling approach taken in using each of these codes. This is intended to provide an overall summary of the scope of these models and their limitations.

### **6.4.1 MAAP4.07**

The development of the MAAP4.07 model for the U.S. EPR involved the development of a completely new plant-specific parameter file. The approach taken in developing the main sections of the parameter file is discussed here.

#### **6.4.1.1 Reactor Coolant System**

The reactor coolant system was modeled in MAAP4.07 using the geometry for the main coolant lines, RPV, reactor core, safety injection systems, pressurizer, RCS depressurization system, and steam generators (SGs).

##### **6.4.1.1.1 Main Coolant Lines**

In MAAP4.07, the nodalization for the main coolant lines is fixed in the code rather than being specified by the user. Therefore, the built-in nodalization of the main coolant lines was used to model the U.S. EPR. The arrangement consists of a broken loop (for cases with a break) representing a single loop of the RCS and an unbroken loop representing the remaining three loops of the RCS.

The nodalization of the main coolant lines is separated into gas nodes and water nodes. The gas nodes of the broken and unbroken loops are identical and consist of a hot leg, cold leg, hot leg SG tubes, cold leg SG tubes, and an intermediate leg. The broken loop

contains the pressurizer attached to the hot leg. The water nodes of the broken and unbroken loops are likewise identical and consist of the unbroken loop intermediate leg, unbroken loop SG tubes, broken loop intermediate leg and the broken loop SG tubes (Note: regions of the hot and cold legs are lumped together with RPV, core and downcomer).

#### **6.4.1.1.2 Reactor Pressure Vessel**

Like the main coolant lines, the nodalization of the RPV is fixed within the code. The RPV contains gas nodes to represent the core, downcomer, lower plenum, and upper plenum. There are two water nodes: one for the core and one for the downcomer.

The MAAP4.07 RPV also contains several heat sinks to represent heat transfer between the RPV and the containment. There are heat sinks to represent the core, downcomer, upper plenum and dome. Heat transfer from the bottom head of the RPV explicitly accounts for its hemispherical geometry in the calculation of creep rupture.

#### **6.4.1.1.3 Reactor Core**

The reactor core nodalization is also a fixed part of MAAP4.07. The core is nodalized into 5 radial rings and 14 axial levels. There are two non-fuel levels below the active core and two non-fuel levels above the active core. The heavy reflector and core barrel are represented as an additional set of 5 outer rings that form the core radial bounding heat structure. The heavy reflector and core barrel have the same axial nodalization as the rest of the core.

#### **6.4.1.1.4 Safety Injection Systems**

In MAAP4.07 safety injection systems are not modeled explicitly but are treated as sources of mass and energy for the primary system. The MAAP4.07 GESF model was used to represent the safety injection systems of the U.S. EPR. The MAAP4.07 High Pressure Injection system was used to model the U.S. EPR MHSI system and the MAAP4.07 Low Pressure Injection System was used to model the U.S. EPR LHSI.

Each train of safety injection is tied to one of the MAAP4.07 independent pump models. The U.S. EPR MHSI and LHSI pump head–capacity curve and net positive suction head (NPSH) requirements were entered into the parameter file. In addition, the LHSI and MHSI heat exchangers were modeled in each train of MAAP4.07 safety injection. Each train was aligned to take suction from the IRWST and discharge into the hot and/or cold legs, as appropriate.

#### **6.4.1.1.5 Pressurizer**

The MAAP4.07 pressurizer is not subject to user-specified nodalization. Plant-specific design data used to model the pressurizer and surge line consist of geometric data, elevations, and masses needed to characterize the component. The U.S EPR MAAP4.07 model used in severe accident analyses does not model pressurizer heaters or sprays, as they are unnecessary for severe accident analyses of the U.S. EPR.

#### **6.4.1.1.6 Reactor Coolant System Depressurization**

At top of the pressurizer there are 3 PSVs and 2 severe accident depressurization valves, which are modeled separately in the U.S EPR model. The PSVs open and close consistent with their setpoints while the severe accident depressurization valves open and stay open when they are activated manually at a core outlet temperature of 1200 °F (650 °C).

#### **6.4.1.1.7 Steam Generators**

The MAAP4.07 code allows for selection of a one-region or a two-region SG model, but does not allow for user-specified nodalization. The two-region model was chosen for the U.S. EPR to represent separately the tube region and the dryer region. Each U.S. EPR SG was characterized in the MAAP4.07 parameter file by entering basic design data for the SG such as structural masses, internal volumes and areas, elevations of key pieces of equipment, and material identification of structural components.

In addition to the main components of the SG, additional data were developed in the parameter file to characterize the main steam isolation valve (MSIV) and main steam relief valves (MSRVs). The setpoints for these valves were entered along with their flow areas and the area of the steam line. Finally, feedwater control logic and setpoints were entered to characterize the MFW control system, and the EFW initiation setpoint, flow rate and delay times were entered.

#### **6.4.1.2 Core Melt Stabilization System**

The core melt stabilization system (CMSS) was modeled in MAAP4.07 using inputs for the reactor cavity and spreading room concrete, debris, containment nodes, containment junctions, and containment heat sinks.

##### **6.4.1.2.1 Reactor Cavity**

The reactor cavity was represented as a single containment node with a volume-to-height profile that represents the real cavity geometry and the presence of the RPV. The reactor cavity was connected to the spreading room by way of a corium failure junction that represents the area of the opening created by the failure of the melt plug. This failure path is opened automatically when all the concrete has been eroded and the temperature of the melt is greater than the melting temperature of aluminum.

The reactor cavity floor (including the melt plug), side walls (region in contact with corium), and upper wall (not in contact with corium) were modeled as individual heat sinks. The reactor cavity floor heat sink was modeled as a one-sided heat sink with a thickness of 50 cm (thickness of concrete) and no liner. The reactor cavity walls were modeled as one-sided heat sinks with a concrete thickness of 50 cm and a zirconium liner thickness of 20 cm.

In addition to the geometrical details of the reactor cavity, the material properties for the sacrificial concrete and zirconium were modeled. The FeSi/PZ15/8 concrete is characterized by its constituents and the corium-concrete pseudo-binary phase

diagram. Appropriate models, based on the Rayleigh number, are applied to simulate the heat transfer from the corium pool.

#### **6.4.1.2.2 Spreading Room**

The spreading room and steam chimney were lumped together as a single containment node. In addition to the melt plug failure connection described above, there are additional junctions between the spreading room/chimney and the SG compartment and the cooling channels.



In addition to the geometrical details of the spreading room, the material properties for the siliceous sacrificial concrete and cast iron were modeled. Like the sacrificial concrete in the reactor cavity, the siliceous concrete is characterized by its composition and the corium-concrete pseudo-binary phase diagram. Appropriate models, based on the Rayleigh number, are applied to simulate the heat transfer from the corium pool.

#### **6.4.1.3 Severe Accident Heat Removal System**

The SAHRS was modeled in the MAAP4.07 parameter file including all three modes of operation: passive flooding, containment spray, and active recirculation. The details of these models are described below.

##### **6.4.1.3.1 Passive Flooding**

Passive flooding is modeled by providing control logic to MAAP4.07 to activate the gravity-driven flow of water from the IRWST when the melt plug fails plus some user-

specified delay. To achieve good code performance, the condition of having two water-solid containment nodes adjacent to each other was avoided by adding some artificial gas volume above the spreading room, cooling channels, and IRWST. The junction elevations and total volume of the containment were preserved in making this modeling simplification.

#### **6.4.1.3.2 Containment Spray**

The containment spray system was modeled using a single train of the MAAP4.07 GESF model. The SAHRS pump characteristics for head capacity and NPSH were entered into the MAAP4.07 general pump parameters. The containment spray system was configured as taking suction from the IRWST and discharging to the containment dome control volume. The SAHRS heat exchanger performance characteristics were also modeled in MAAP4.07 to cool the spray flow being discharging it into the containment.

For the initial studies with the U.S. EPR parameter file, the spray actuation pressure was chosen as 5 bar. When the containment dome pressure reaches this value, the sprays are actuated with one-pump operation. There is the option of making a local parameter change, via restart, in order to actuate the second pump, to model various SAHRS modes of operation.

#### **6.4.1.3.3 Active Recirculation**

Active recirculation is modeled in MAAP4.07 using a train of the GESF model. The same SAHRS pump train that was used to model the containment spray system is also used for the active recirculation flow. The GESF model contains three separate trains that are capable of modeling sprays. The first train was used for the containment upper head sprays as described above. The second train is intended for lower compartment sprays which do not exist in the U.S. EPR. The third train is intended as a general spray system, which offers more flexibility in specifying user parameters. This third train was configured to represent the active recirculation mode of the SAHRS.

---

The active recirculation mode was configured to draw water from the IRWST and discharge to the cooling channels beneath the spreading room. The flow is pumped by the SAHRS pump and cooled by the SAHRS heat exchanger, which were already modeled for the containment spray system. This system is put into operation after the containment sprays have been operating for a time sufficient to reduce the containment pressure to a reasonably low value.

#### **6.4.1.4 Containment**

##### **6.4.1.4.1 General Arrangement**

The U.S. EPR containment is composed of approximately 140 compartment rooms. These rooms were then lumped together into 27 larger volumes (nodes) that make up the containment model. Except for the cases of the spreading area, cooling channels, reactor cavity and IRWST, the nodes are simply modeled as rectangular boxes. This means that the lowest compartment room floor elevation and the highest compartment room ceiling elevation bound the height of the node. The volume for each node is simply the sum of all of the volumes of the individual compartment rooms in that node. A general arrangement for the U.S. EPR containment model is shown in Figure 6-17 with the containment compartments identified in Table 6-6.

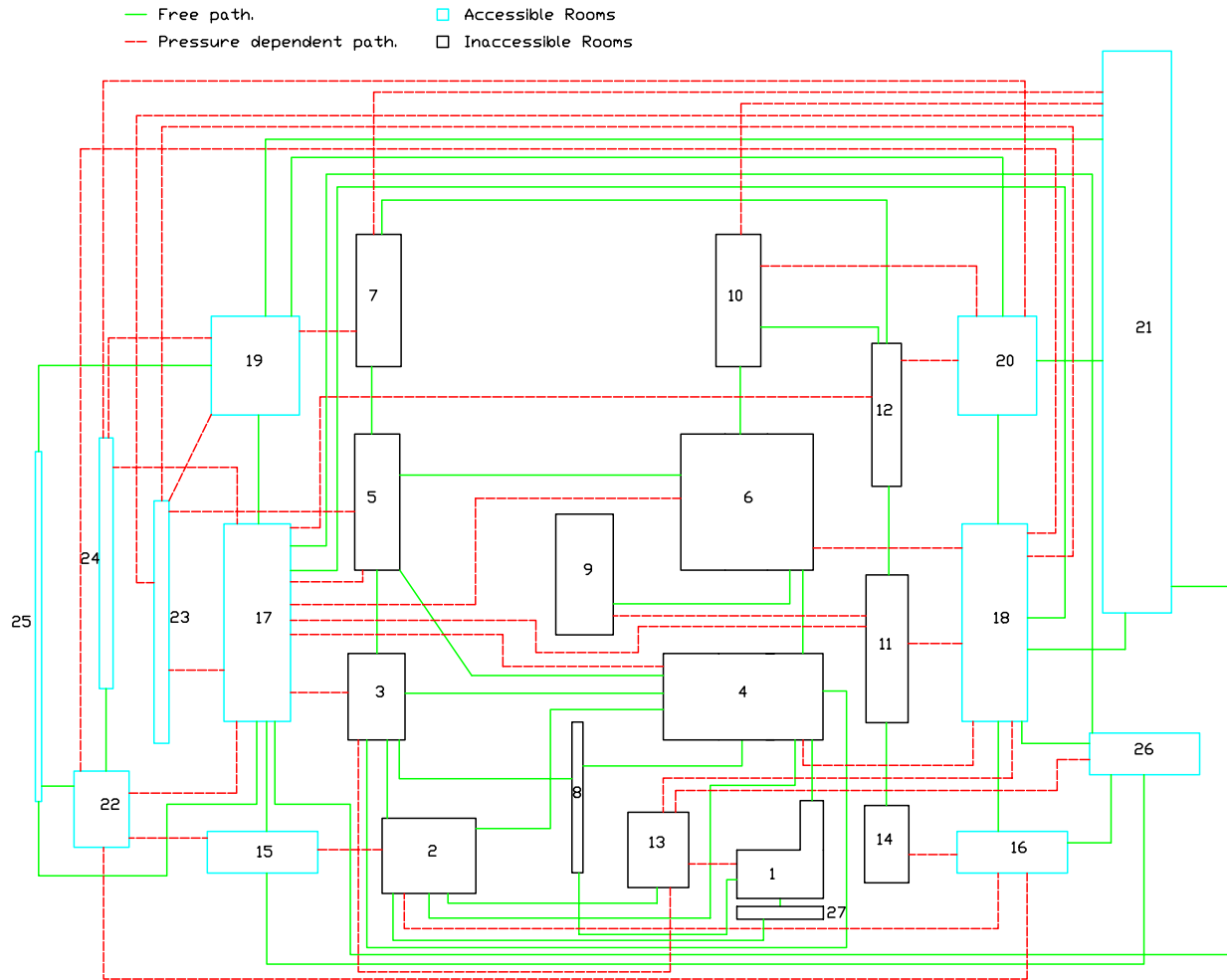


**Figure 6-17 U.S. EPR MAAP4 Containment Model**

**Table 6-6 U.S. EPR MAAP4.07 Containment Nodes**

<b>Node</b>	<b>Description</b>
1	Spreading Room and Steam Chimney
2	IRWST
3	Lower Equipment Rooms L1
4	Lower Equipment Rooms L2, L3 and L4
5	Middle Equipment Rooms L1
6	Middle Equipment Rooms L2, L3 and L4
7	Upper Equipment Rooms L1
8	Reactor Pit
9	Reactor Cavity
10	Upper Equipment Rooms L2, L3 and L4
11	Surge Line, below
12	Pressurizer
13	Components
14	LCQ Heat Exchanger, etc
15	Lower Annular Rooms L1 and L2
16	Lower Annular Rooms L3 and L4
17	Middle Annular Rooms L1 and L2
18	Middle Annular Rooms L3 and L4
19	Upper Annular Rooms L1 and L2
20	Upper Annular Rooms L3 and L4
21	Lower and Upper Dome L1, L2, L3 and L4
22	Access
23	Staircase South
24	Staircase North
25	Elevator
26	Hot Piping
27	Cooling Channel

A series of junctions was installed between compartments. These junctions represent open flow paths and pressure-dependent flow paths between compartments. Also, one junction is used to represent the gate, the failure of which is required to move the corium from the reactor cavity to the spreading area. The junctions are defined by their source and destination node, predominant orientation (horizontal or vertical), elevation, flow area, and, in the case of pressure-dependent flow paths, burst pressure differentials.

#### **6.4.1.4.2 Heat Sources/Sinks**

Two types of heat sinks are modeled in MAAP4.07. The first type, distributed heat sinks, comprises one-dimensional heat structures located between the compartment nodes. These heat sinks can be a wall or a floor located between two compartments, or a wall located within a compartment. The second type of heat sink is the lumped heat sink, which represents significant masses of equipment, piping, piping supports, grates, stairwells, platforms, and other structures located within a compartment. The U.S. EPR is composed of more than 800 heat structures. These heat structures were then subdivided into the two types of heat sink. Due to MAAP4.07 limitations on the number of heat sinks allowed for each type, the number of total heat sinks was collapsed by grouping heat sinks together by material similarity and location. This resulted in a total of 159 distributed heat sinks and 72 lumped heat sinks in the model.

#### **6.4.1.4.3 Combustible Gas Control**

Combustible gas control is achieved in the U.S. EPR model through the use of PAR units. Within the U.S. EPR containment, the 47 AREVA NP PARs, comprising 6 small units and 41 large units, were distributed throughout the compartments. The locations and types of PARs, with respect to their node locations (see Figure 6-17), are presented in Table 6-7. Parameters such as characteristic burn radii, characteristic compartment heights, and limiting H<sub>2</sub> volume fraction, are entered into the MAAP4.07 model to allow for the correct activation of the PAR units.

**Table 6-7 Number and Location of AREVA NP PAR Units**



**6.4.2 MELTSPREAD-1.4**

The U.S. EPR model of molten reactor core materials (corium) spreading in the CMSS spreading area was modeled with the MELTSPREAD-1.4 code. MELTSPREAD-1.4 is a transient, one-dimensional, computer code that has been developed to predict the gravity-driven spreading of corium. The corium can have a wide range of compositions of reactor core materials and concrete. The code requires input that describes the containment geometry and the melt pour conditions.

The U.S. EPR MELTSPREAD-1.4 input was developed from geometric, material and performance information available from the documents available describing the U.S. EPR. Physical properties not specific to the U.S. EPR were taken from open source documentation.



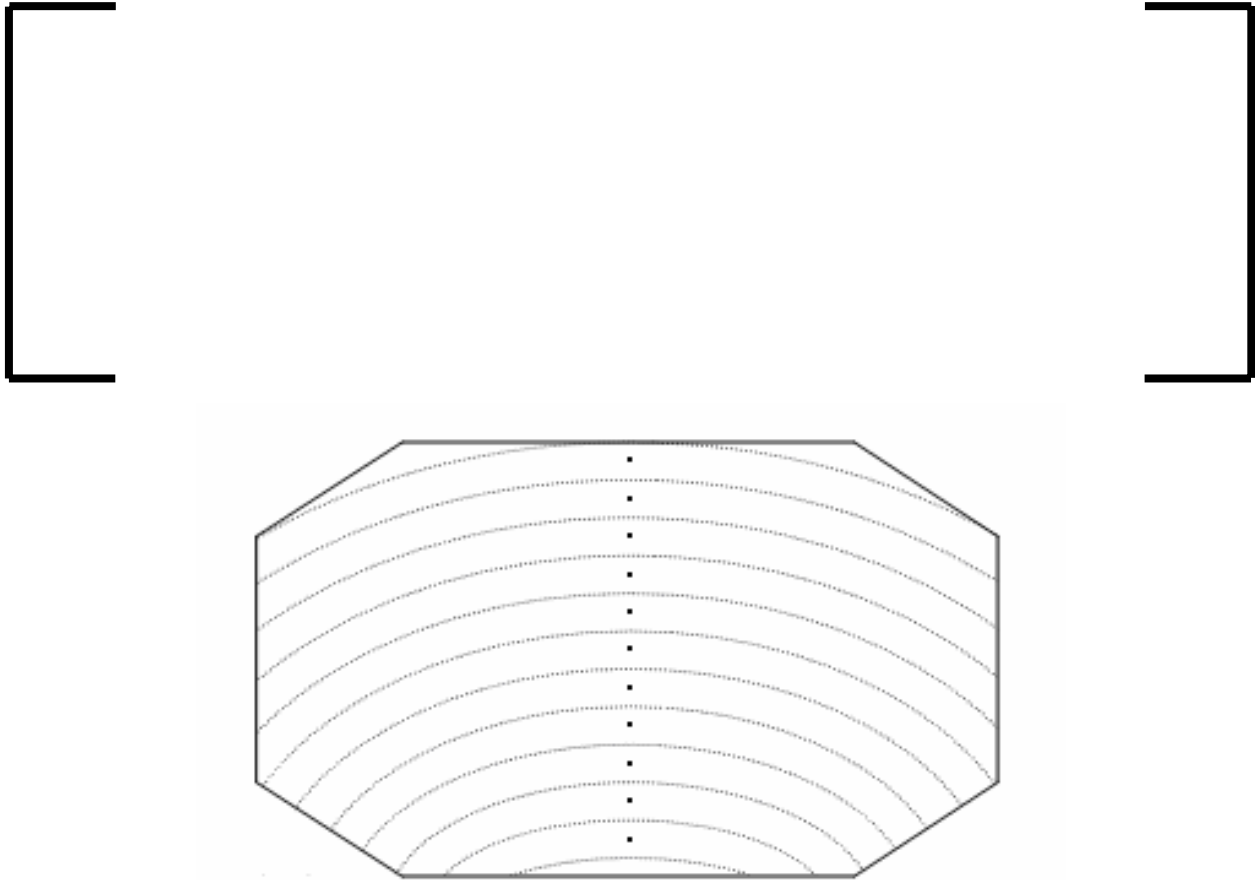


**Figure 6-18 Representative User-defined Nodalization Scheme used in MELTSPREAD-1.4**

Using these inputs, the code then calculates transient hydrodynamic and heat transfer behavior and determines the spreading and freezing behavior of the melt. The code predicts conditions at the end of the spreading stage, including melt relocation distance, depth profile, substrate ablation profile, and wall heatup.

### **6.4.3 WALTER**

WALTER is an engineering tool used for the assessment of the one-dimensional heat conduction problem. In the frame of the verification of the U.S. EPR melt retention concept, the WALTER code is used to model the thermal response of the aluminum plate in the melt plug and of the cast iron cooling structure in the CMSS spreading area.

In addition, the code is applied to predict the thermal impact of the melt and the response of the protective layers and concrete walls in the cavity, melt discharge channel and spreading compartment. The code requires input that describes the geometry, the material properties and the boundary conditions of the region to be analyzed.

Physical properties not specific to the U.S. EPR were taken from open source documentation. The boundary conditions, consisting mainly of interface temperatures, were consistent with those used in the MELTSPREAD-1.4 and MAAP4.07 analyses.

There were two phenomena that were analyzed using WALTER. The first was the ablation of the aluminum plate beneath the sacrificial layer of concrete that together forms the melt plug. This analysis was performed to find out whether or not the 4 cm thick aluminum plate is ablated rapidly. The second was the response of the cast iron cooling structure on top of the cooling channels in the spreading area. This analysis was performed to make sure that if the corium was able to ablate the sacrificial layer of concrete, that the layer of cast iron would not be ablated.

For the melt plug case, two runs were performed. One was performed where the oxidic layer was resting on the aluminum plate. The other was performed with the metallic layer resting on the aluminum plate. After the thicknesses of these layers were calculated, the appropriate values were entered into the input deck. Since this is a one-dimensional code, the nodalization scheme simply divides each layer into  $n$  equal thicknesses. In this case, the layers were, from top to bottom: corium, aluminum plate, semi-infinite ceramic. Between the melt plug and the semi-infinite ceramic layer, an air-gap was modeled.

For the cast iron case, one run was performed. Assuming that in order for corium to reach the cast iron, the entire thickness of sacrificial concrete needed to be ablated. This ablated concrete then became part of the oxide layer of the corium. It was also assumed that the metallic layer, which is more dense, would settle to the bottom of the melt and be in contact with the cast iron layer. The nodalization scheme was similar to

the one developed for the melt plug case. However, in this case, the layers were, from top to bottom: oxidic melt, metallic melt, cast iron, semi-infinite ceramic. An air-gap was assumed to be below the cast iron and will be filled with water when the spreading area cooling system is activated.

In both cases it was assumed that the oxidic portion of the melt would have a decay heat value of  $0.333 \cdot 10^6 \text{ W/m}^3$  calculated by knowing the initial core full power, the total mass of  $\text{UO}_2$  in the corium and the decay heat fraction based upon the time at which the corium is released from the reactor cavity (supplied by MAAP4.07).

Using these inputs, the code then calculates the transient temperature profiles in the aluminum melt plug and the cast iron layer as a function of time.

## **6.5 Calculation Matrix for Safety Issue Resolution**

Considering the high degree of uncertainty often associated with severe accident progression, the assignment of event studies can be speculative. Accordingly, a 3-fold strategy for the development of a sufficient calculation matrix is employed incorporating:

- Best-estimate calculations of relevant events (per discussion in Section 3.3)
- Uncertainty analysis calculations to explicitly address CGCS issues (per 10 CFR 50.44)
- Supplemental Sensitivity calculations.

### **6.5.1 Best-Estimate Analysis**

Best-estimate calculations are included to define the performance targets appropriate for a relevant discussion. Such calculations will be best-estimate considering both risk factors leading to a particular event and the subsequent phenomenological progression. SECY-93-087 provides guidance to applicants for performing a systematic assessment of the risks associated with full-power operation, low power operation, shutdown and external events. As discussed in Section 3.3, relevant severe accident events will be

screened based on Level 1 PRA results, supplemented with qualitative assessment of Level 2 PRA candidate scenarios relative to containment release mechanisms. For the purpose of addressing severe accident safety issues, the inherent remote nature of severe accidents is considered a sufficient basis for eliminating single failures related to the U.S. EPR severe accident response features for these analyses. Table 6-8 identifies a list of initiating events being considered for the U.S. EPR Level 1 PRA. Nonetheless, prudent engineering practice, based on regulatory precedent, requires that the acceptable design of a plant's severe accident response features include sufficient supporting justification to show that the design choices and analytical treatments realistically describe the engineered behavior of the system during a severe accident.

**Table 6-8 Postulated Initiating Events**

<b>Initiating Event (IE) Description</b>
ATWS
Fire
Flood
Interfacing System LOCA
Loss of BOP
LOCA (Small, Medium, or Large)
Loss of Condenser Heat Sink
Loss of Component Cooling Water
Loss of Feedwater Flow
Loss of Instrument or Control Air
LOOP
Inadvertent Opening of a MSSV
Loss of One Emergency Bus
Steam Generator Tube Rupture
Steam Line Break (Inside and Outside Containment)
Turbine Trip

From a completed Level 1 PRA, relevant scenarios are defined as those having CDFs greater than  $10^{-8}$ /yr. In addition, certain scenarios with lower CDF values will be

considered relevant if the processes and phenomena characterizing the event can serve as a bounding scenario; thus, eliminating the need to look at a family of relevant scenarios. As a result, scenarios are classified in three types according to the objective of their application:

- relevant scenarios are defined as those having CDFs greater than  $10^{-8}/\text{yr}$ . These cases form the basis for the design and verification of the severe accident design measures. They are equally applied to all severe accident measures. The verification goal for this scenario class is to show that the severe accident measures function as designed and the leaktightness and operability of the containment system is maintained,
- bounding scenarios are exclusively employed to demonstrate the robustness of both individual and integral measures. These cases may have a CDF less than  $10^{-8}/\text{yr}$ ; however, they are selected based on processes and phenomena that also characterize one or more relevant scenarios.

For the justification of the mitigation features, these two kinds of scenarios are further defined as:

- The relevant scenarios are core melt scenarios with successful RCS depressurization before ultimate severe accident criteria (e.g., core outlet temperature  $650\text{ }^{\circ}\text{C}$ ) which are bounding with respect to the severity, for the challenge under consideration, and which have a non-negligible frequency. They are used as a basis for the design measures,
- The bounding scenarios are chosen from among the different core melt scenarios with passive reflooding via the accumulators, due to delayed RCS depressurization or active in-vessel reflooding and which involve worsening situations due to reflooding: they are considered "bounding" when the worst time of the reflooding is considered to determine the most

---

severe boundary conditions. These scenarios are used to demonstrate the robustness of the mitigation of features, and to justify that the containment leaktightness and integrity are maintained.

The results of the U.S. EPR Level 1 PRA are expected to reflect robustness of the design to severe accidents with the number of relevant scenarios limited to a minority subset, such as the LBLOCA, small-break LOCA (SBLOCA), and SBO scenarios that will be illustrated in Section 8.

Within the subset of scenarios meeting the CDF threshold ( $CDF < 10^{-8}/yr$ ), both “representative” and “bounding” events will be categorized based on dominant phenomena as evaluated from test programs, scaling analyses, and engineering judgment. Events presenting similar severe accident performance will be grouped into an “Accident Progression Bin” and documented by a single “representative” or “bounding” calculation. AREVA NP will identify scenarios by the associated design features that have been incorporated into the U.S. EPR to prevent the initiation of the particular scenario and/or to mitigate the subsequent severe accident (specifically identifying diverse and/or redundant systems). In addition, a basis for acceptability will be specified.

Table 6-9 lists several severe accident scenarios that are considered probable candidates for the final calculation matrix based on previous and ongoing scoping analysis.

**Table 6-9 Possible Representative and Bounding Scenarios Identified to Address Key Severe Accident Issues**

Issue	Relevant Scenarios	Bounding Scenario
<p><b>RCS Depressurization</b></p> <ul style="list-style-type: none"> <li>- PDS Discharge Capacity</li> <li>- Justification of human error tolerant design of PDS</li> <li>- Loads for which PDS has to cope</li> <li>- Load bearing capacity of vessel support</li> </ul>	<ul style="list-style-type: none"> <li>- LOOP (SIS delayed or unavailable)</li> <li>- LB LOCA (SIS unavailable)</li> <li>- SB LOCA cold leg fast secondary cooldown</li> </ul>	<ul style="list-style-type: none"> <li>- SBO, PDS actuated at 650 °C, late SIS recovery</li> <li>- SBO with delayed PDS actuation (range 1 hour beyond 650 °C)</li> <li>- SBO with delayed PDS actuation with primary pump leakage</li> <li>- Instantaneous circumferential vessel failure at 20 bar (uplift forces)</li> </ul>
<p><b>Hydrogen Risk</b></p> <ul style="list-style-type: none"> <li>- Global loads of hydrogen deflagration and prevention of detonation</li> <li>- Local dynamic loads</li> <li>- Thermal loads</li> <li>- Spray actuation (SAHRS)</li> </ul>	<ul style="list-style-type: none"> <li>- Candidate for “best-estimate plus uncertainty” examining breaksize, reflooding potential, and vessel failure scenarios</li> </ul>	
<p><b>Corium stabilization</b></p> <ul style="list-style-type: none"> <li>- Range of corium release conditions from the vessel</li> </ul>	<ul style="list-style-type: none"> <li>- LB LOCA with unavailability of SIS (high decay heat) fast corium release from the vessel</li> <li>- SB LOCA cold leg fast secondary cooldown (low decay heat, slow corium release from the vessel)</li> </ul>	<ul style="list-style-type: none"> <li>- LOOP with late SIS recovery. Corium and water release. Range of vessel failure pressure (1-20 bar)</li> </ul>
<p><b>Prevention of containment over-pressurization</b></p> <ul style="list-style-type: none"> <li>- Rapid increase of pressure</li> <li>- Worst conditions to start the SAHRS</li> </ul>	<ul style="list-style-type: none"> <li>- LB LOCA with unavailability of SIS</li> <li>- Start of SAHRS actuation at 160°C water temperature.</li> </ul>	
<p><b>Limitation of radiological releases</b></p> <ul style="list-style-type: none"> <li>- Highest containment radiological source term</li> </ul>	<ul style="list-style-type: none"> <li>- LB LOCA with unavailability of SIS</li> <li>- LOOP (SIS delayed or unavailable) without filtered annulus ventilation 24 hours</li> <li>- SGTR</li> </ul>	

### **6.5.2     *Uncertainty Analysis***

The nature of severe accident phenomena is such that large uncertainties exist for certain design conditions. Consequently, a degree of conservatism, and in some cases, bounding conservatism, is often employed in the evaluation of design elements to demonstrate sufficient margins to safety. Such conservatism in deterministic analyses is not always a practical solution and an alternative approach must be employed.

The performance of the U.S. EPR CGCS is a candidate for uncertainty analysis. 10 CFR 50.44 requires that the containment design accommodate hydrogen generation equivalent to a 100% metal-water reaction of the fuel cladding and that containment hydrogen concentration stay below 10%. Scoping analyses suggest that simply assuming the transport of all the hydrogen generated from this process instantaneously into the containment is not possible; therefore, an explicit consideration of the time dependent nature of hydrogen production, release, and recombination is appropriate.

Hydrogen production during a severe accident develops over time with peaks in particular phases of an accident. Best-estimate analyses show that production occurs both in-vessel from steam-clad reactions and ex-vessel from MCCI. Because of recombiners and the potential for auto-ignition, the amount of hydrogen in the containment is always less than the amount of produced hydrogen. As an alternative to identifying specific bounding cases leading to large hydrogen releases, Reference 19 provides a statistical approach to the problem. This approach provides a quantitative method that allows for a broader consideration of accident progression. It can also provide insights to other design areas of interest.

### **6.5.3     *Supplemental Deterministic Studies***

The calculation matrix will address several important issues related to demonstrating the U.S. EPR's severe accident response features. Of particular interest are the following:

---

Severe accident primary circuit depressurization

- PDS line discharge capacity
- justification that PDS is a human error tolerant design
- loads with which PDS has to cope with
- the load bearing capacity of the vessel support

Mitigation of hydrogen risk

- limitation of the hydrogen deflagration pressure characterized by AICC pressure and prevention of hydrogen detonation
- conditions of hydrogen flame acceleration which could induce dynamic pressure loads
- maximum thermal loads on the containment shell and in containment for design of severe accident materials and the qualification of severe accident instrumentation
- influence of activation of the spray system

Justification of ex-vessel melt stabilization concept

- the range of corium release conditions from the vessel

Prevention of containment overpressurization

- most rapid pressure increase in the containment
- loads with which the SAHRS have to cope with

Limitation of radiological releases

- highest containment radiological source term

Deterministic sensitivity studies will be provided in addition to the best-estimate and uncertainty analyses to supplement the discussions related to these issues, as necessary.

## 7.0 SAMPLE PROBLEM ANALYSES

The purpose of this section is to demonstrate both the implementation of the AREVA NP analytical methodology as well as the integral severe accident response of the U.S. EPR.

### 7.1 *Introduction*

As has been previously discussed, the U.S. EPR includes a number of features to mitigate the effects of a severe reactor accident. In order to demonstrate expected severe accident performance of the U.S. EPR, a diverse spectrum of accident scenarios was selected. These scenarios include an LBLOCA, LOOP, and SBLOCA. Each of these scenarios represents a specific family of severe accident classes for which the phenomenologically bounding plant response can be investigated.

- **LBLOCA** – Due to maximized decay heat, the LBLOCA represents the limiting case with respect to melt stabilization and early containment pressurization.
- **LOOP** – A loss of all AC power results in a peak pressure transient within the primary system. Peak primary system pressure represents the limiting conditions for depressurization and well as the likely initiator of a SGTR. LOOP also represents the category of scenarios in which a minimum set of equipment is available and establishes the time window within which AC power must be restored to control containment pressure. The SBO represents a bounding LOOP in which all backup power supplies are also unavailable.
- **SBLOCA** – Due to the high steam levels within the primary system combined with the slow nature of the accident evolution, the SBLOCA is the limiting case in terms of hydrogen production because the conditions for oxidation are maximized.

A description of the accident scenario as well as the results of subsequent analyses and associated conclusions is provided in the following sections.

## **7.2 Scenario Description**

The scenarios considered for the demonstration of the U.S. EPR's severe accident response are the LBLOCA, SBO (a bounding LOOP), and SBLOCA. Representative analyses were performed using both integral studies as well as more detailed, separate effect studies of certain phenomena.

### **7.2.1 Integral Analysis Scenarios**

Integral analyses were performed using MAAP4 to predict the plant response to the LBLOCA, SBO, and SBLOCA scenarios. The event scenarios analyzed were run using the MAAP4 model discussed in Section 7.4 configured to run the scenarios described below.

#### **7.2.1.1 LBLOCA**

The initiator for the LBLOCA is a complete severance of the pressurizer surge line followed by trip of the reactor and RCPs, isolation of main feedwater (MFW), start of the emergency feedwater (EFW) and a coincident failure of all four active trains of SI. Following injection of the accumulators, the water level in the core will reach a level below the top of the active fuel. Because the active SI is unavailable, the core will start to heat up and ultimately reach the severe accident pressurization valve setpoint, signaling the start of the severe accident. The progression of this accident scenario and its associated severe accident phenomena are quantitatively described in Section 7.3. An additional LBLOCA crossover case was included to show the effects of SAHRS operation including the crossover from containment spray mode to active flooding mode.

#### **7.2.1.2 SBO**

The initiator for the SBO is a complete loss of all off-site sources of AC power (i.e., a LOOP), all four EDGs, and both SBO diesels. While this is an extremely remote event due to the number of AC power sources available for the U.S. EPR, it provides a bounding representation of the plant response. Given that all AC power sources are

unavailable only those features that can be powered off of DC power would be available (i.e., the dedicated severe accident valves would be operable but the SI systems and active SAHRS modes would not be). Following the initiator the reactor will trip and MFW and EFW would not be available. Following boil-off of the secondary inventory of the steam generators, the RCS temperature and pressure will start to increase until the point where the SRVs on the pressurizer will start to cycle. RCS fluid will drain into the PRT until the point that the rupture disks fail on over pressure and release inventory into the containment. The continued loss of inventory into the containment will result in core uncover and heat up until the severe accident depressurization valve set-point is reached signaling the start of a severe accident. The progression of this accident scenario and its associated severe accident phenomena are quantitatively described in Section 7.3.

#### **7.2.1.3 SBLOCA**

The initiator for the SBLOCA is a small break in the cold leg mid-loop followed by trip of the reactor and RCPs, isolation of MFW, start of EFW and a coincident failure of all four active trains of SI. Following the break will slowly start to depressurize and empty the pressurizer. On the low pressurizer level signal, a partial cooldown via the MSRT will occur. The accumulator will inject providing inventory to cover the core and the heat from the primary system will be removed via the EFW system. Once the Condensate Storage Tanks (CST) inventory is depleted, core cooling is lost causing an increase in core temperature. Ultimately core uncover is expected to occur resulting in a heat up until the severe accident depressurization valve setpoint is reached signaling the start of a severe accident. The progression of this accident scenario and its associated severe accident phenomena are quantitatively described in Section 7.3.

#### **7.2.1.4 LBLOCA Crossover**

The initiator for the LBLOCA Crossover is a LBLOCA described above in Section 7.2.1.1. Both trains of SAHRS spray are initiated at 12 hours from the time the core temperature reaches 650 °C. At 18 hours from the start of the sprays, one of the

spraying SAHRS trains switches from sprays to active flooding. The initiation of sprays is accompanied by an immediate decrease in containment pressure and a gradual decrease in available NPSH. When active flooding begins, the IRWST level drops and there is a greater rate of power removal from the heat exchanger. Because the active flooding recirculates water from the spreading area to the IRWST, the IRWST water temperature increases as the IRWST water absorbs the decay heat from the core melt. The progression of this accident scenario and its associated severe accident phenomena are quantitatively described in Section 7.3.

## **7.2.2 Separate Effect Analyses**

As discussed in Section 7.1, the separate effect codes MELTSPREAD and WALTER were used to model certain severe accident phenomena important to the U.S. EPR design. These phenomena were modeled using separate effect codes to allow for a more detailed analysis of the phenomena than was offered by MAAP4. These phenomena include spreading of molten core debris, failure of the reactor cavity gate, and melt stabilization of the spreading compartment cooling structure.

### **7.2.2.1 Reactor Cavity Gate Failure**

Failure of the gate in the reactor cavity was modeled using the separate effects code WALTER. WALTER was used to predict the failure of the gate by determining if the 4 cm-thick aluminum gate is ablated rapidly when contacted by molten core debris. This analysis was performed in a limiting manner as opposed to modeling scenario specific timing. Therefore, the conclusions of WALTER hold for any scenario not just for the LBLOCA. Two limiting cases were run; one where the oxidic layer was resting on the aluminum plate and the other was performed with the metallic layer resting on the aluminum plate. In the case where the oxidic layer was atop the plate, the aluminum melt plug completely melts within 25 to 30 seconds after first contact with the melt (as shown in Figure 7-1 where the entire temperatures of the gate plug is above the melting temperature of aluminum). In the case where the metallic layer was atop the plate, the

plug completely melts within 20 to 25 seconds after first contact with the melt (as shown in Figure 7-2).

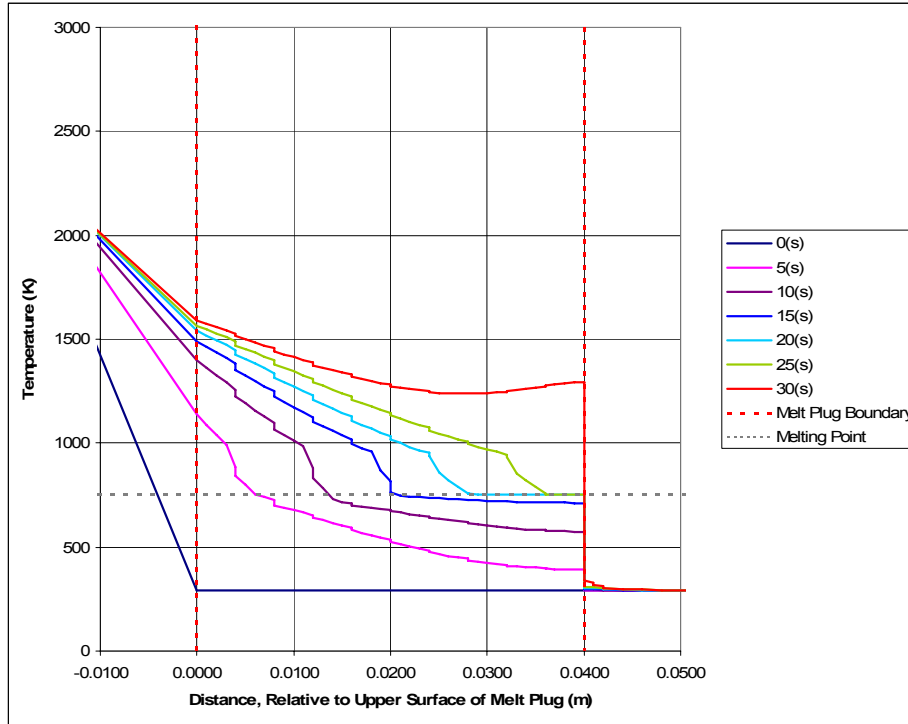
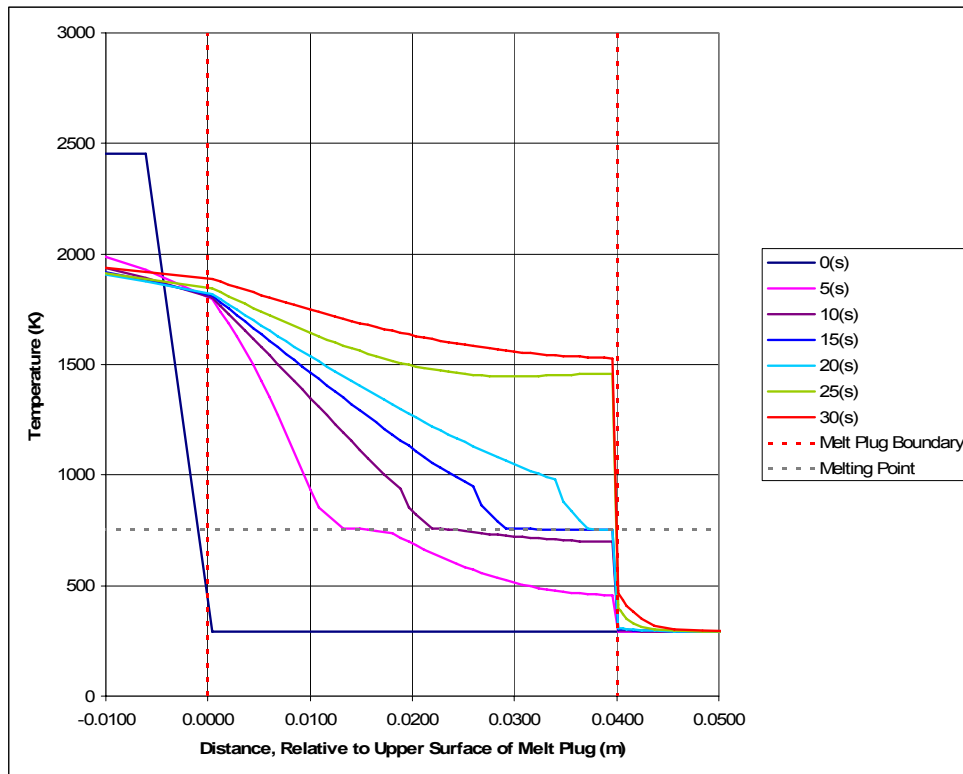


Figure 7-1 Aluminum Gate Temperature Profile with Oxidic Melt



**Figure 7-2 Aluminum Gate Temperature Profile with Metallic Melt**

**7.2.2.2 Molten Debris Spreading**

Based on the mass and physical conditions of the molten core debris within the reactor pit at the time of gate failure, MELTSPREAD analysis show that completes spreading is expected. Using the boundary conditions predicted by MAAP4.07 relative to corium inventory, temperature, and decay heat level during a LBLOCA, SBO, and SBLOCA the key results are shown below in Table 7-1.

**Table 7-1 Events of Concern for the Representative Model**

--	--

These results are based on a limiting assumption that 1/8 of the gate area is opened. With this minimum opening area, the duration of the pour into the spreading compartment is expected to be sustained for around 1 minute for all three scenarios. In all cases it was shown that only a minimal amount of concrete ablation in the spreading area is predicted at the time of complete spreading.

### **7.2.2.3 Melt Stabilization**

The conclusions of MAAP4 relative to melt stabilization can be augmented by those predicted by WALTER. Like the WALTER analysis performed for gate performance, this analysis was also done in a bounding manner as opposed to on a scenario specific basis. Therefore, the conclusions of WALTER hold for any scenario not just for the LBLOCA. In this scenario, WALTER was used to predict the response of the surface of the cooling structure when contacted by molten core debris with passive flooding active. As shown in Figure 7-3, this limiting analysis predicted none of the cast iron cooling structure was ablated. After 12 hours of contact between the corium and the cast iron cooling structure, the interface temperature begins to decrease. Therefore, in this scenario, with the maximum temperature of the cast iron structure being 1256 K at 12 hours, there is nearly 200 K difference between the temperature and the melting point of the structure. Figure 7-4 shows the temperature profile at various points in the melt and structure versus time.

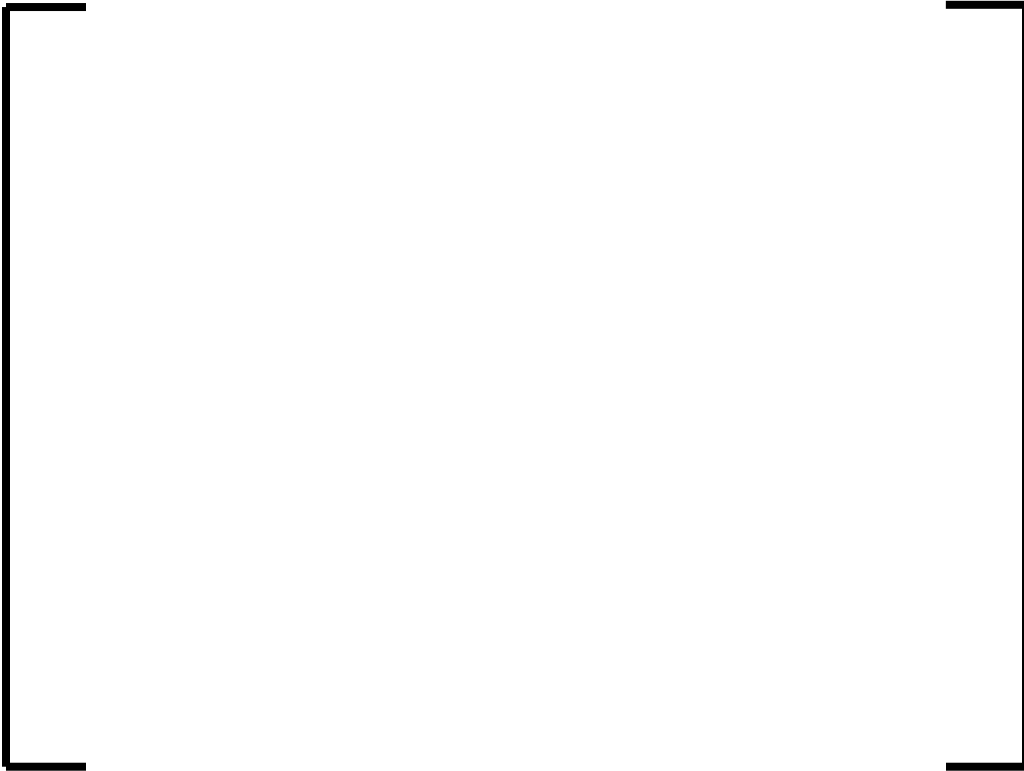


**Figure 7-3 Cooling Structure Temperature Profile**



**Figure 7-4 Melt and Structure Temperature Profile**

### **7.3 Results of Integral Analyses**

This section documents the integral plant response to the three bounding event scenarios described in Section 7.2.

#### **7.3.1 Large Break Loss of Coolant Accident (LBLOCA)**

The predicted U.S. EPR response during an LBLOCA event described in Section 7.2 is provided in Figures 7-5 to 7-27. The sequence of events and important results are provided in Table 7-2 and Table 7-3, respectively.

**Table 7-2 Event Progression of a LBLOCA**



**Table 7-3 Key Results from a LBLOCA**

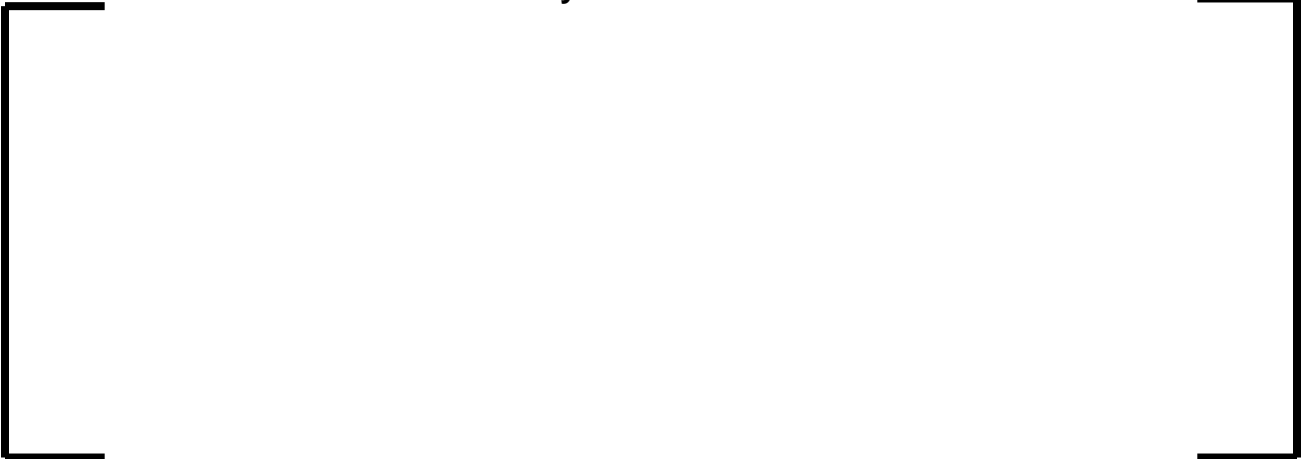




**Figure 7-5 Core Outlet Temperature (LBLOCA)**



**Figure 7-6 Two-Phase Water Level in Core (LBLOCA)**



**Figure 7-7 RCS Pressure (LBLOCA)**



**Figure 7-8 RCS Water Inventory (LBLOCA)**

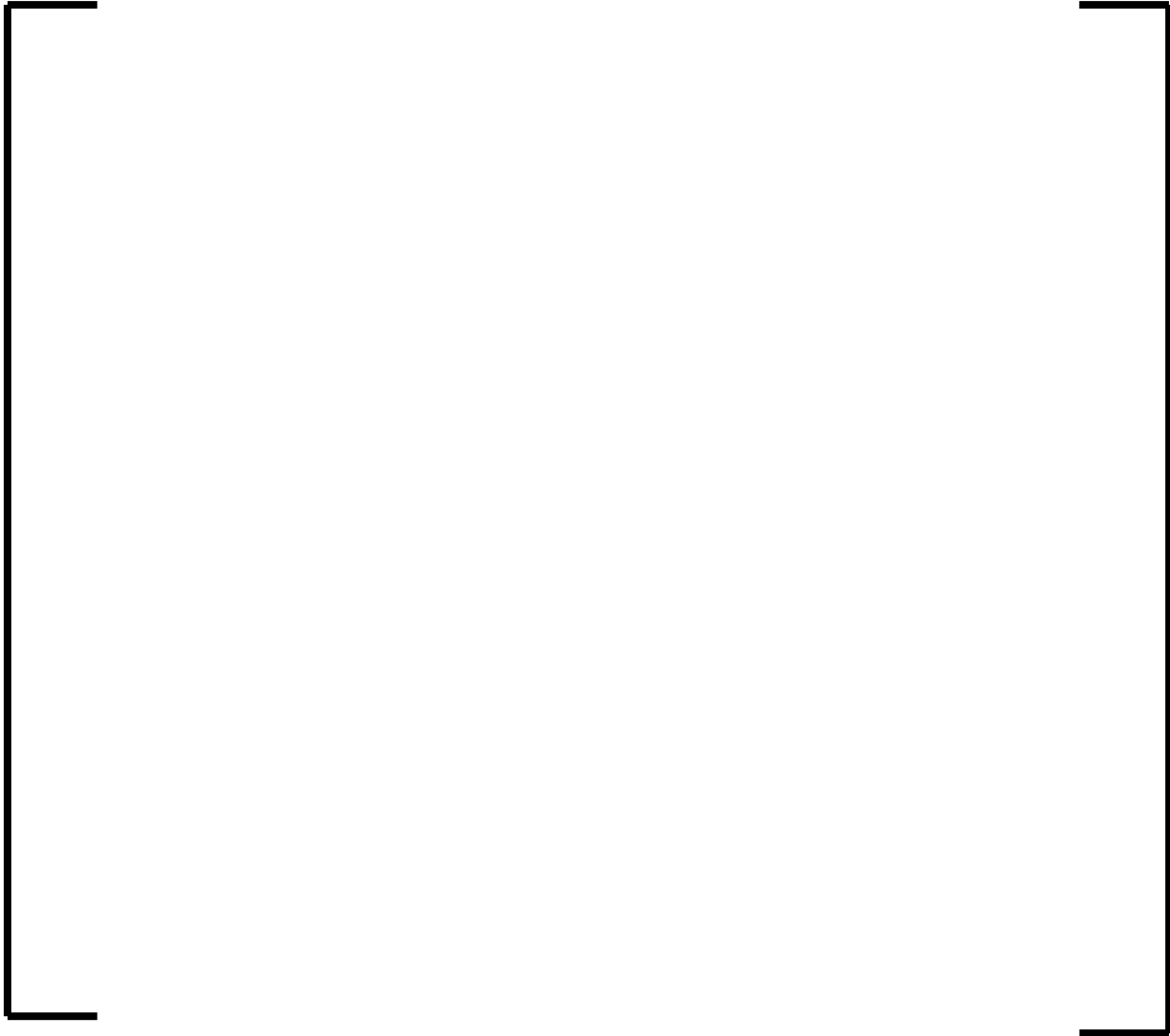


**Figure 7-9 In-Vessel Hydrogen Production (LBLOCA)**

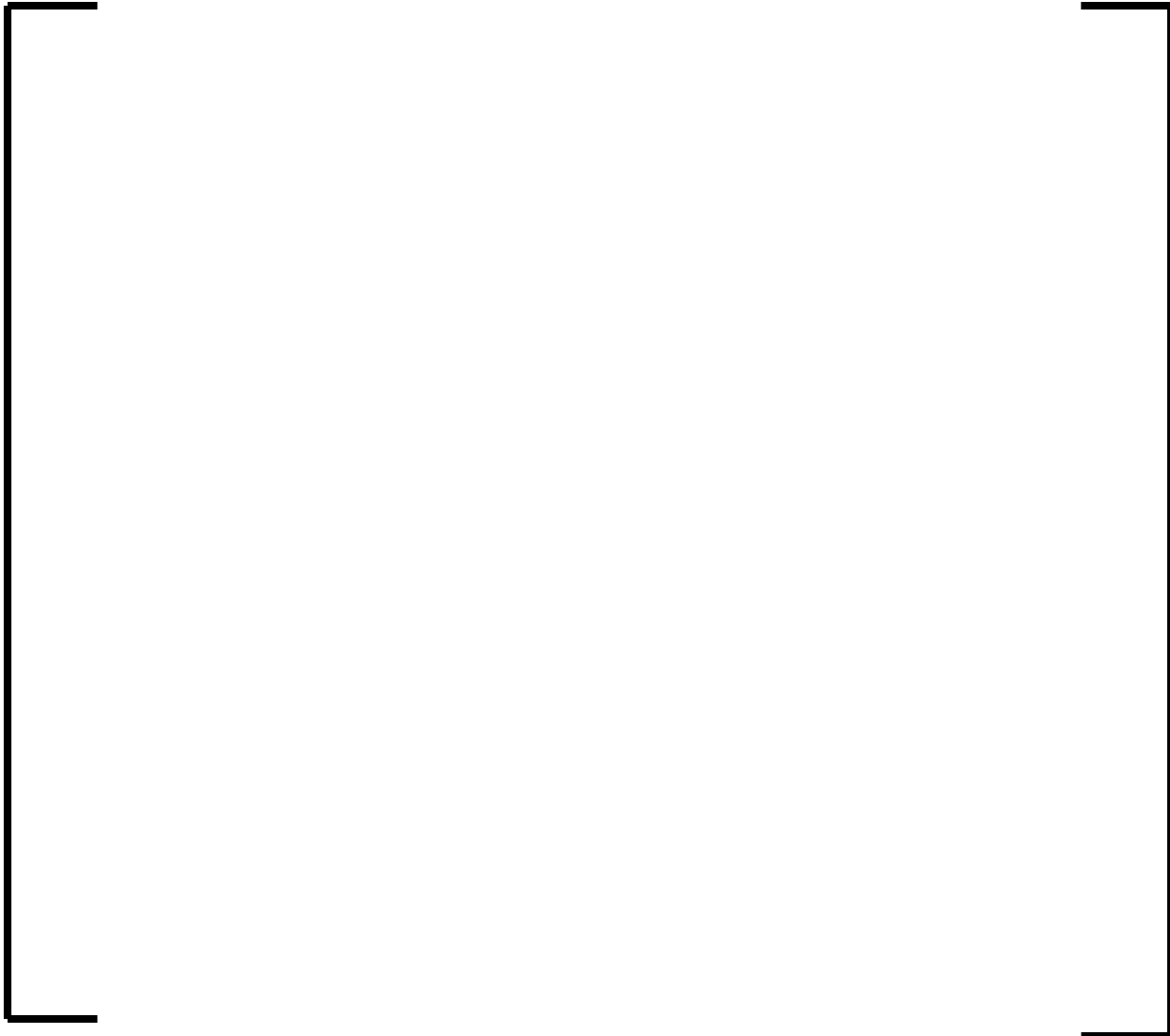


**Figure 7-10 Hydrogen Release Rate (LBLOCA)**



**Figure 7-11 Mass of Corium in Lower Head (LBLOCA)**



**Figure 7-12 Mass of Material in Core (LBLOCA)**

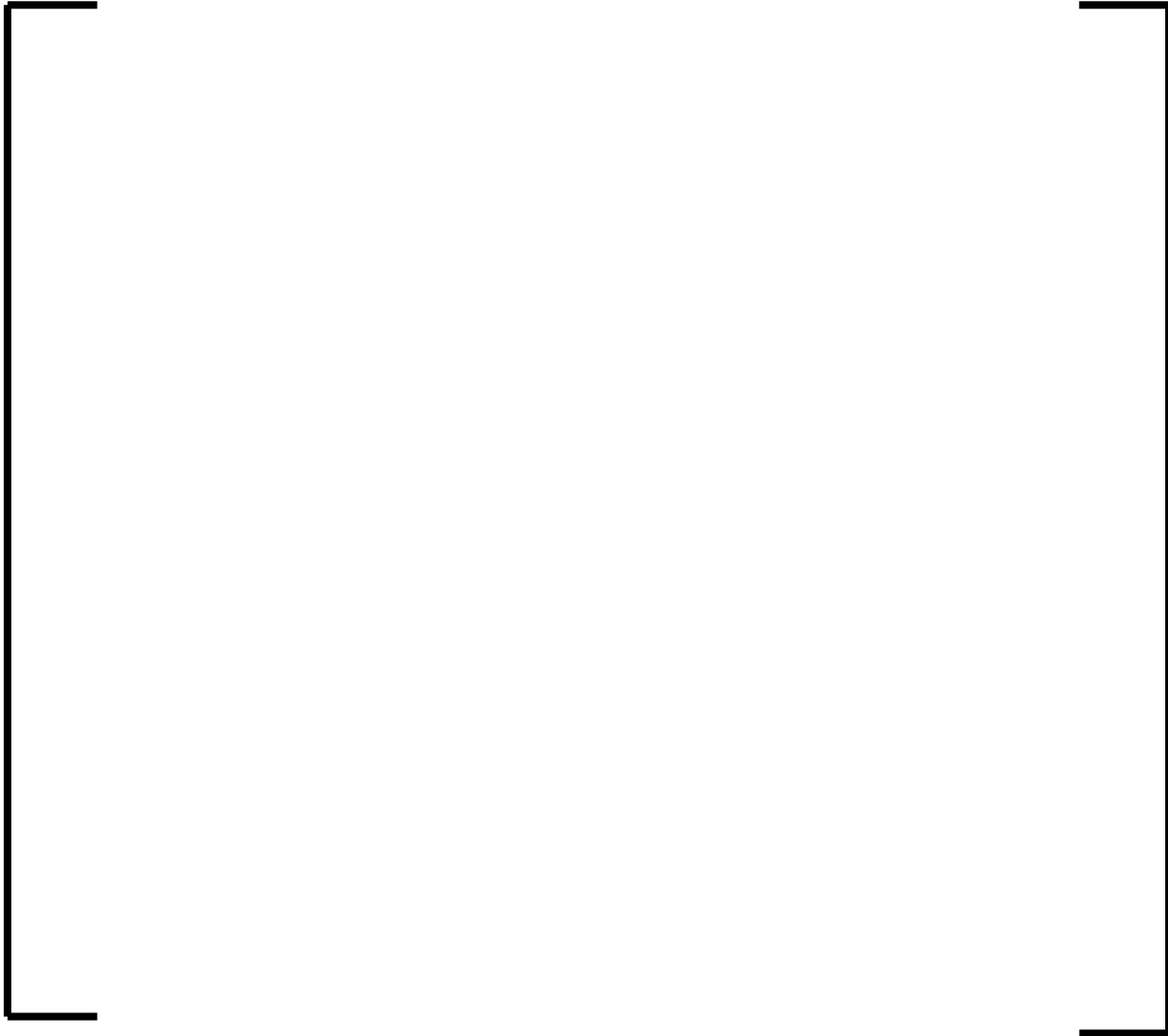


**Figure 7-13 Mass of Material in Lower Head and Core (LBLOCA)**

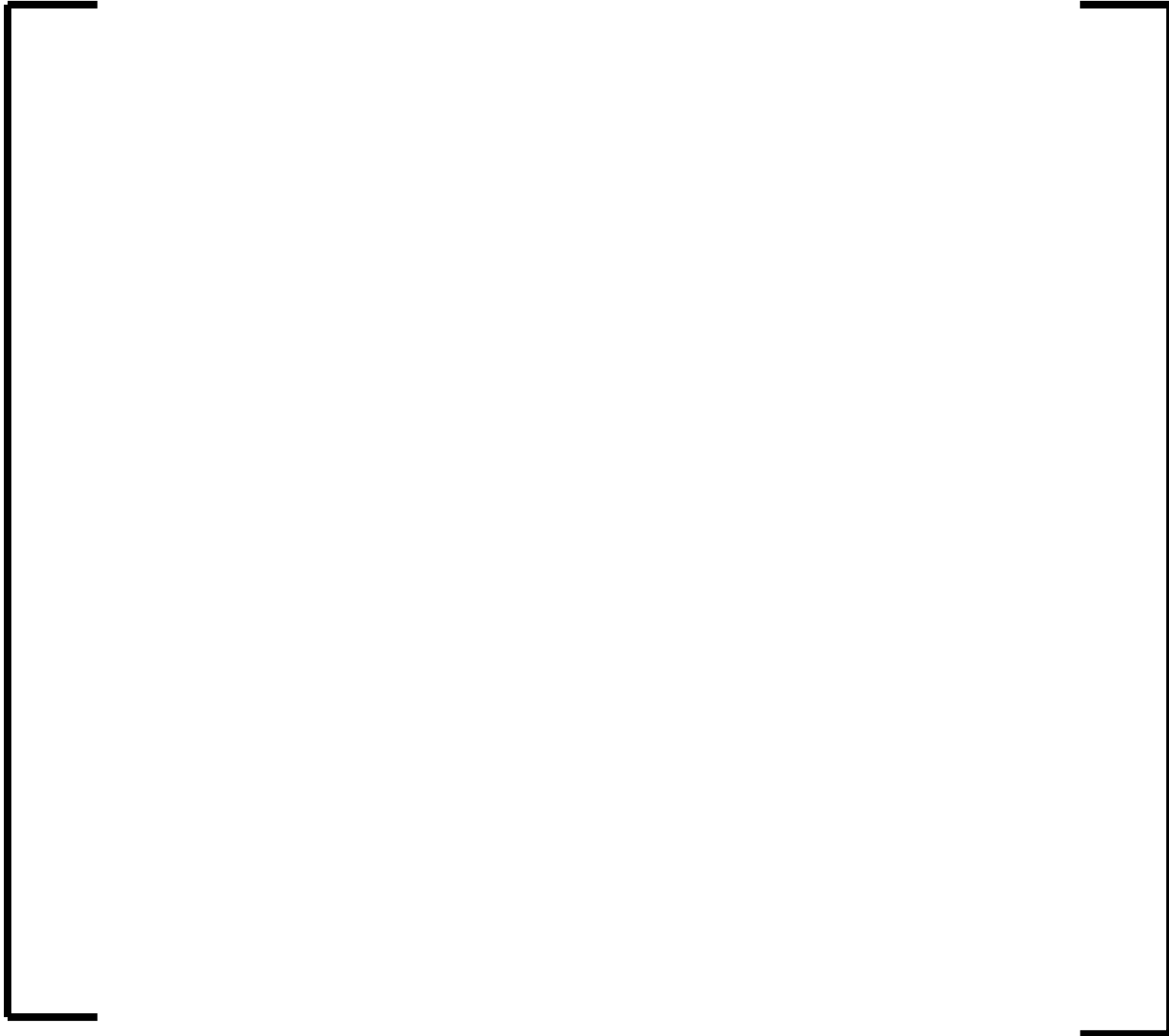


**Figure 7-14 Containment Pressure (LBLOCA)**



**Figure 7-15 Average Hydrogen Mole Fraction in Containment (LBLOCA)**

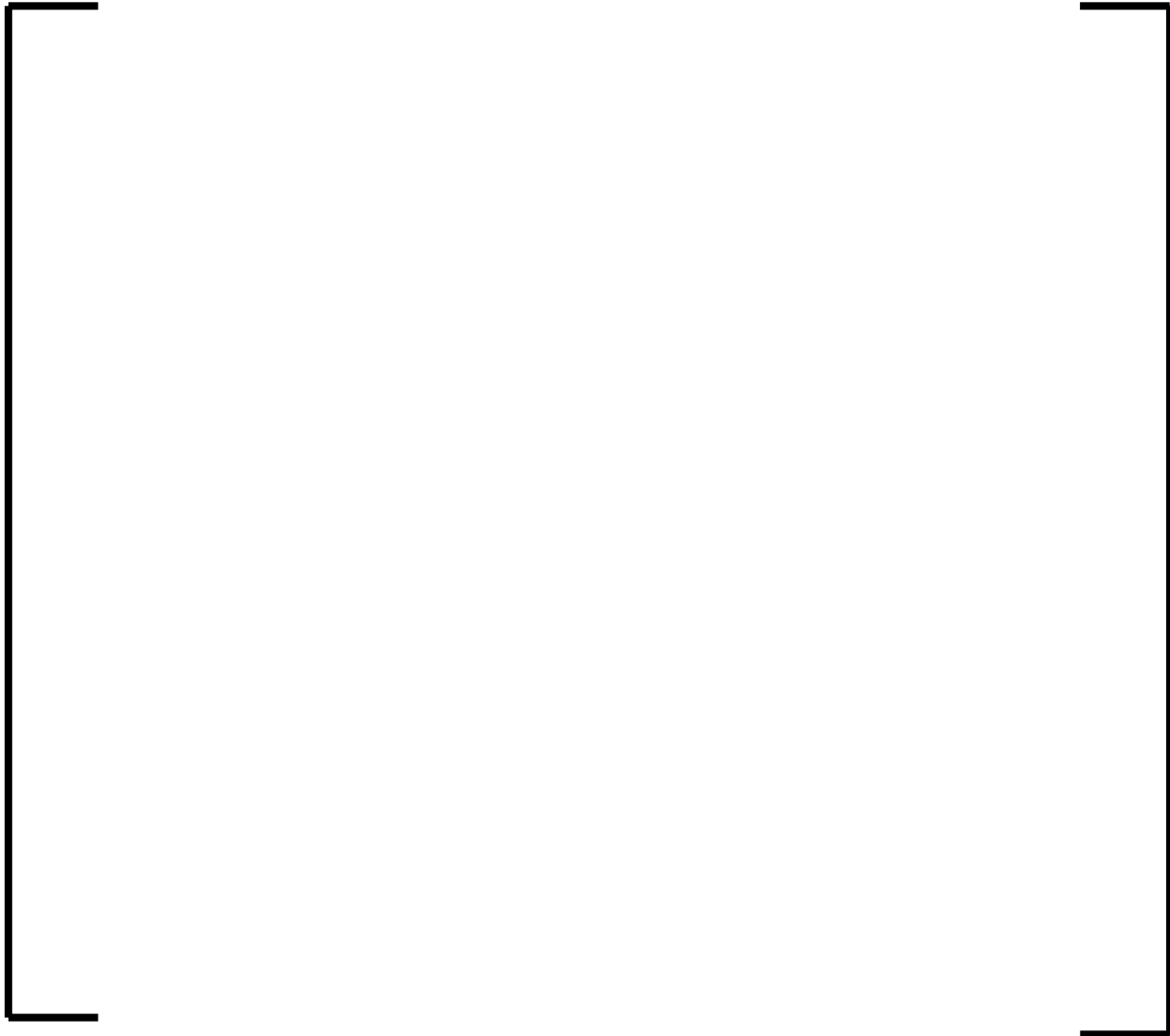


**Figure 7-16 Average Mole Fraction of Air in Containment (LBLOCA)**

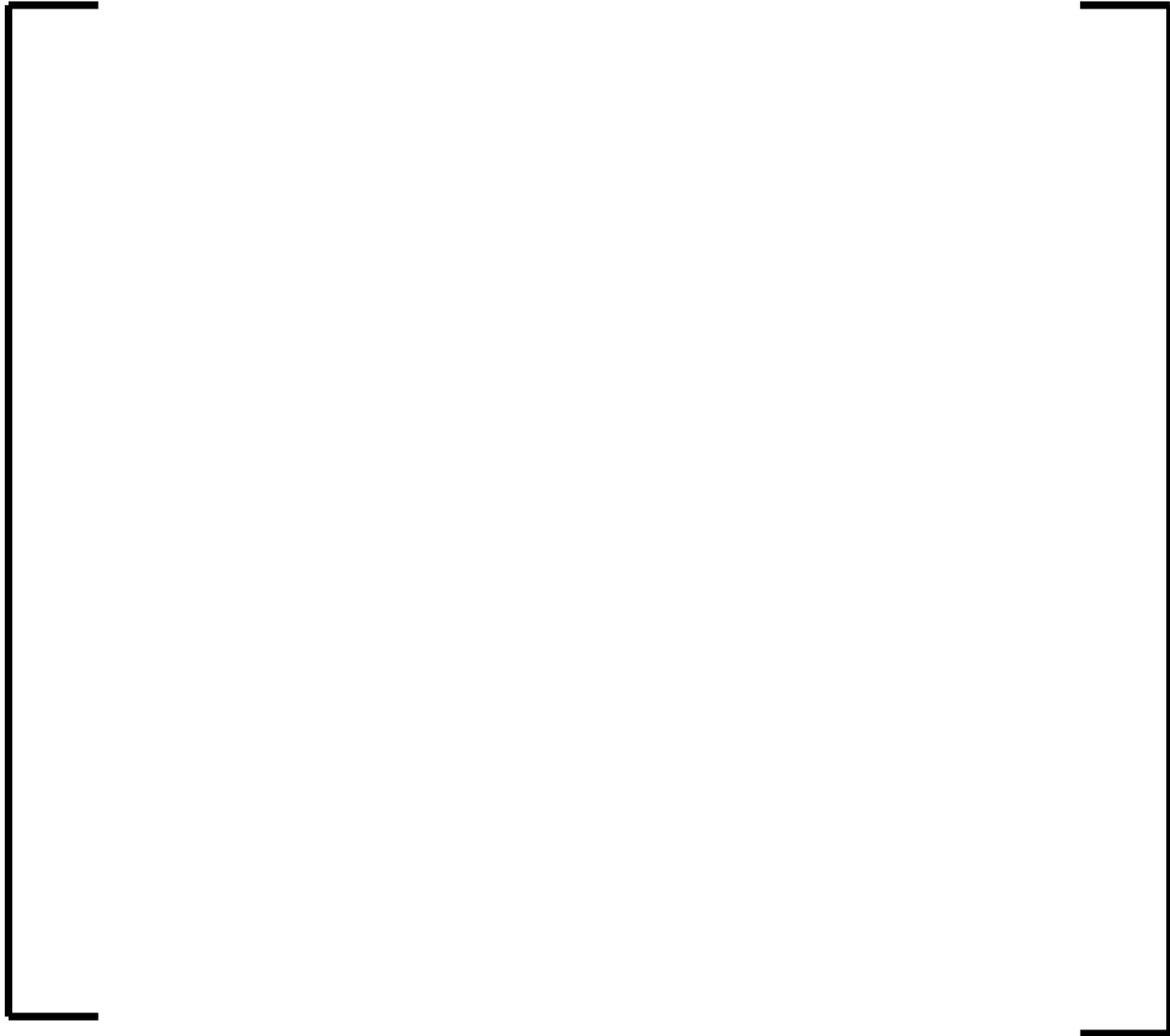


**Figure 7-17 Average Mole Fraction of Steam in Containment (LBLOCA)**

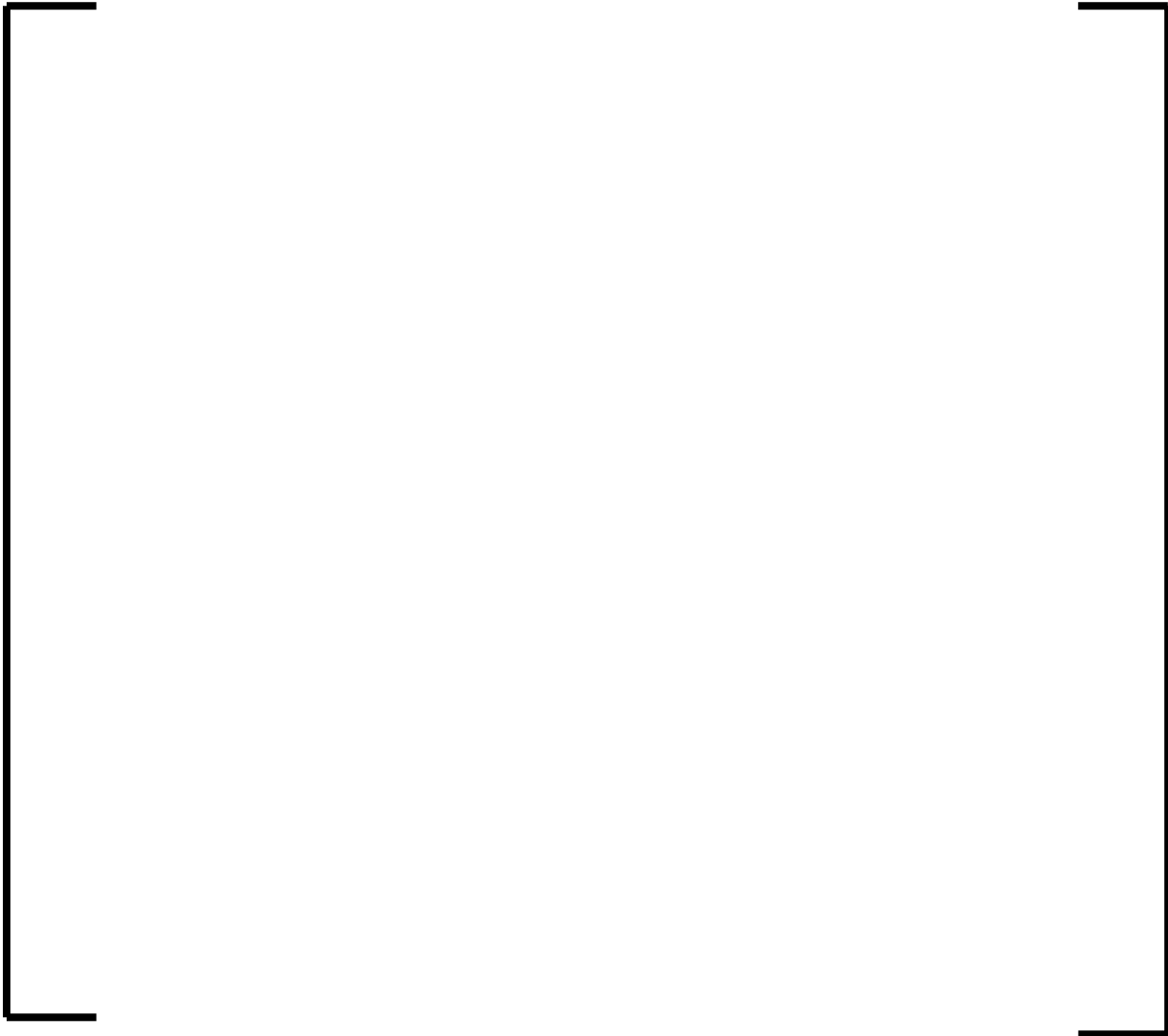


**Figure 7-18 Hydrogen Mass in Containment (LBLOCA)**

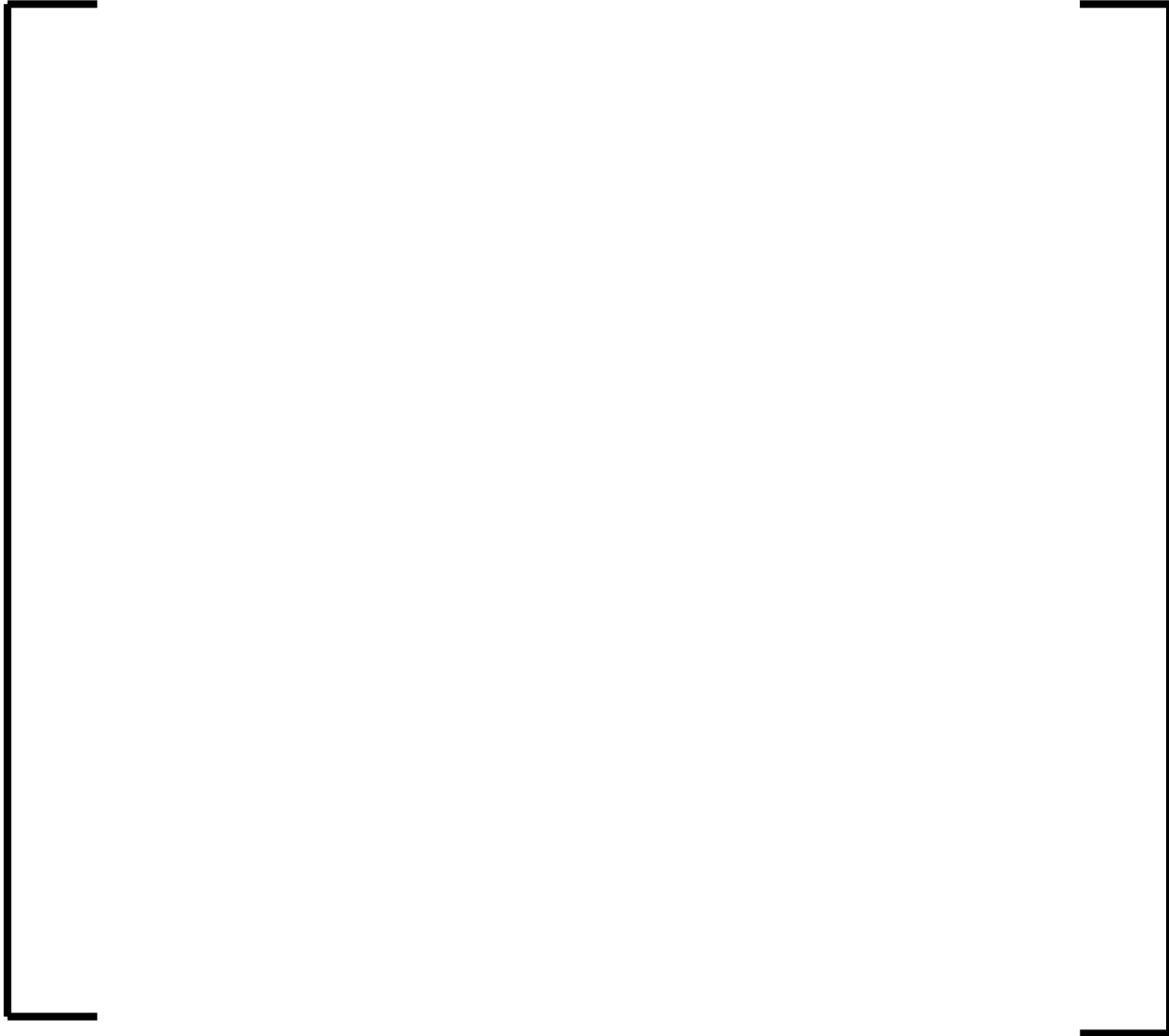


**Figure 7-19 Mass of Corium in Reactor Pit (LBLOCA)**

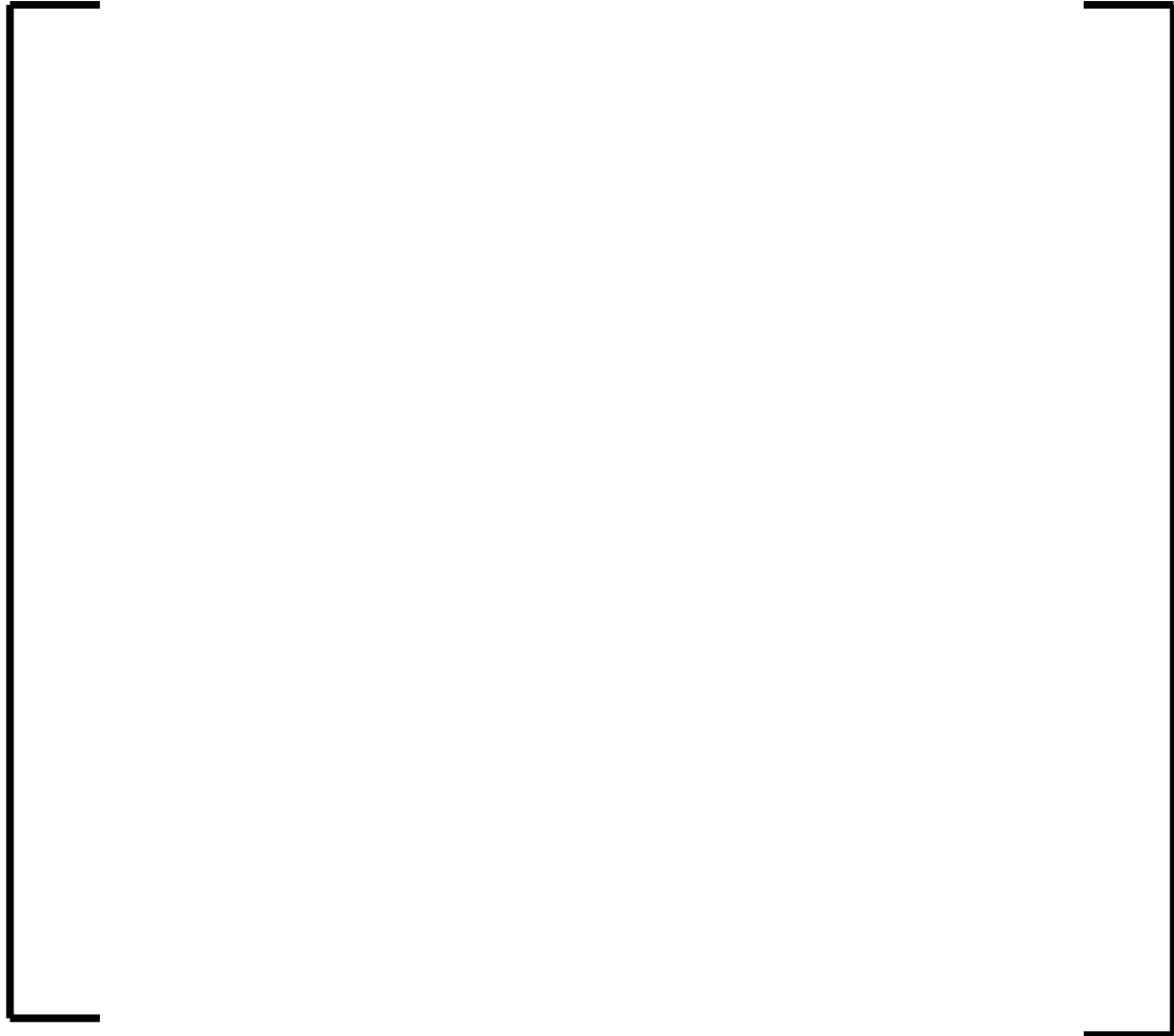


**Figure 7-20 Mass of Corium in Spreading Compartment (LBLOCA)**

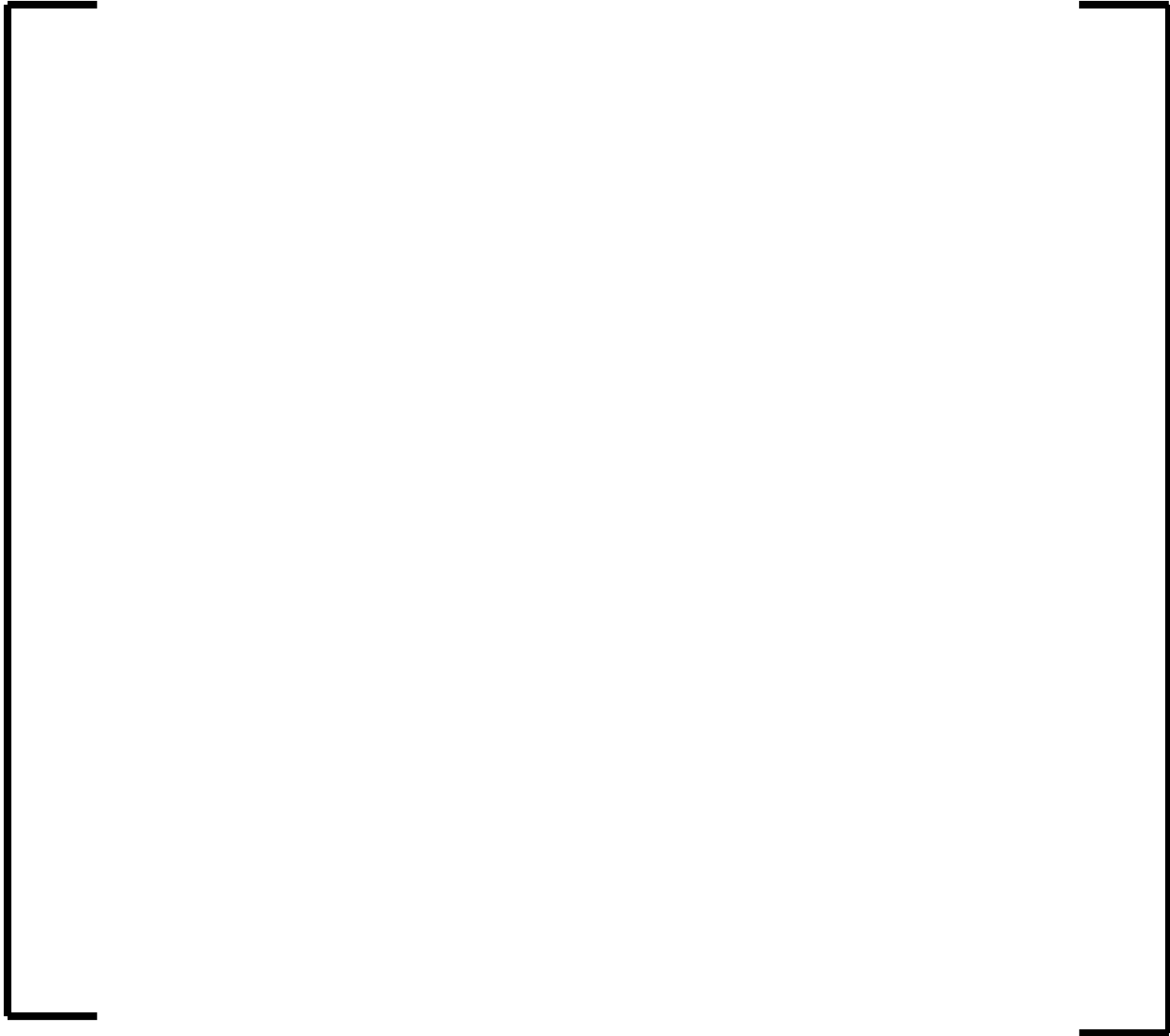


**Figure 7-21 Spreading Room Ablation (LBLOCA)**



**Figure 7-22 Reactor Cavity Ablation (LBLOCA)**

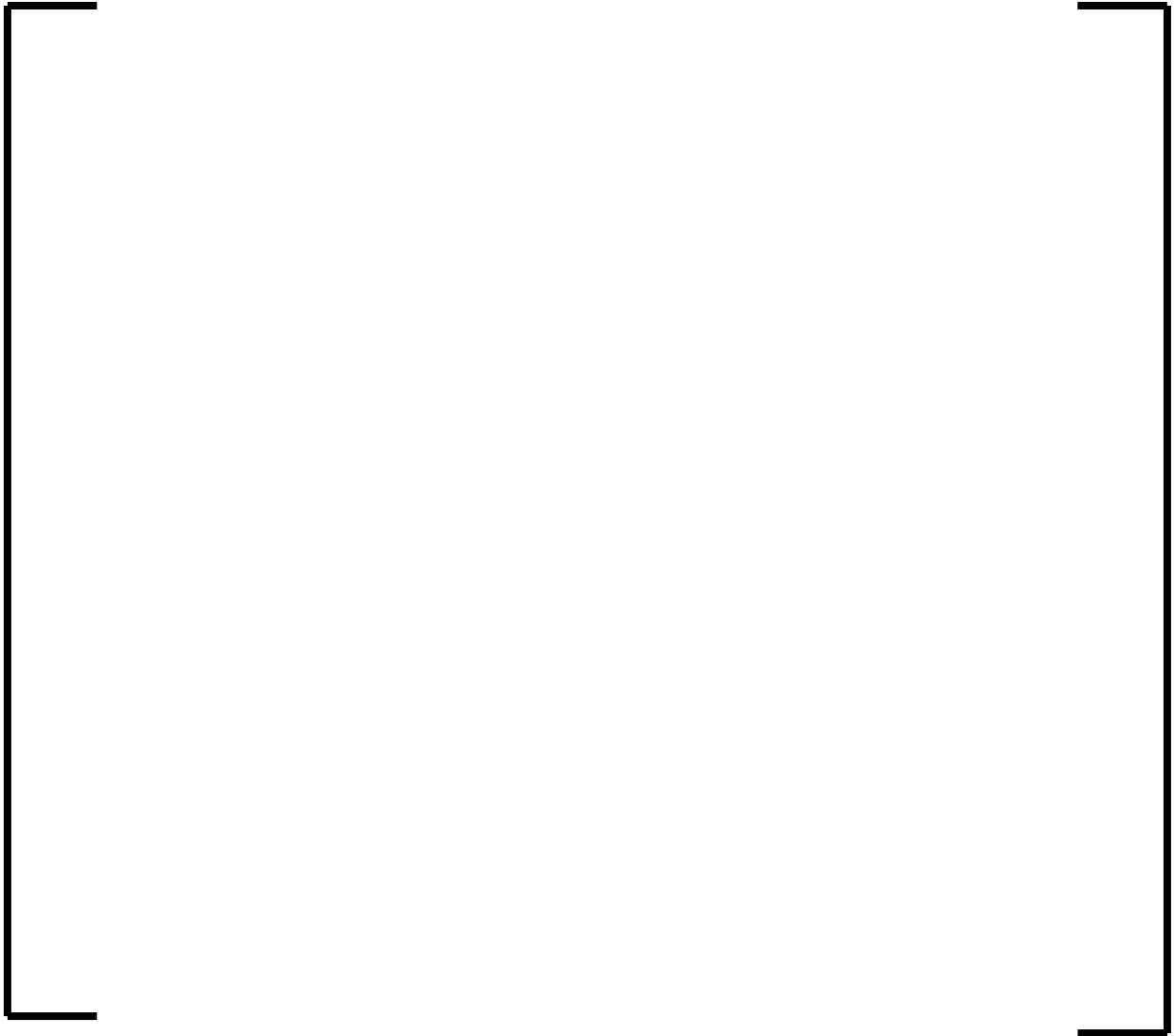


**Figure 7-23 Spreading Room Water Level (LBLOCA)**

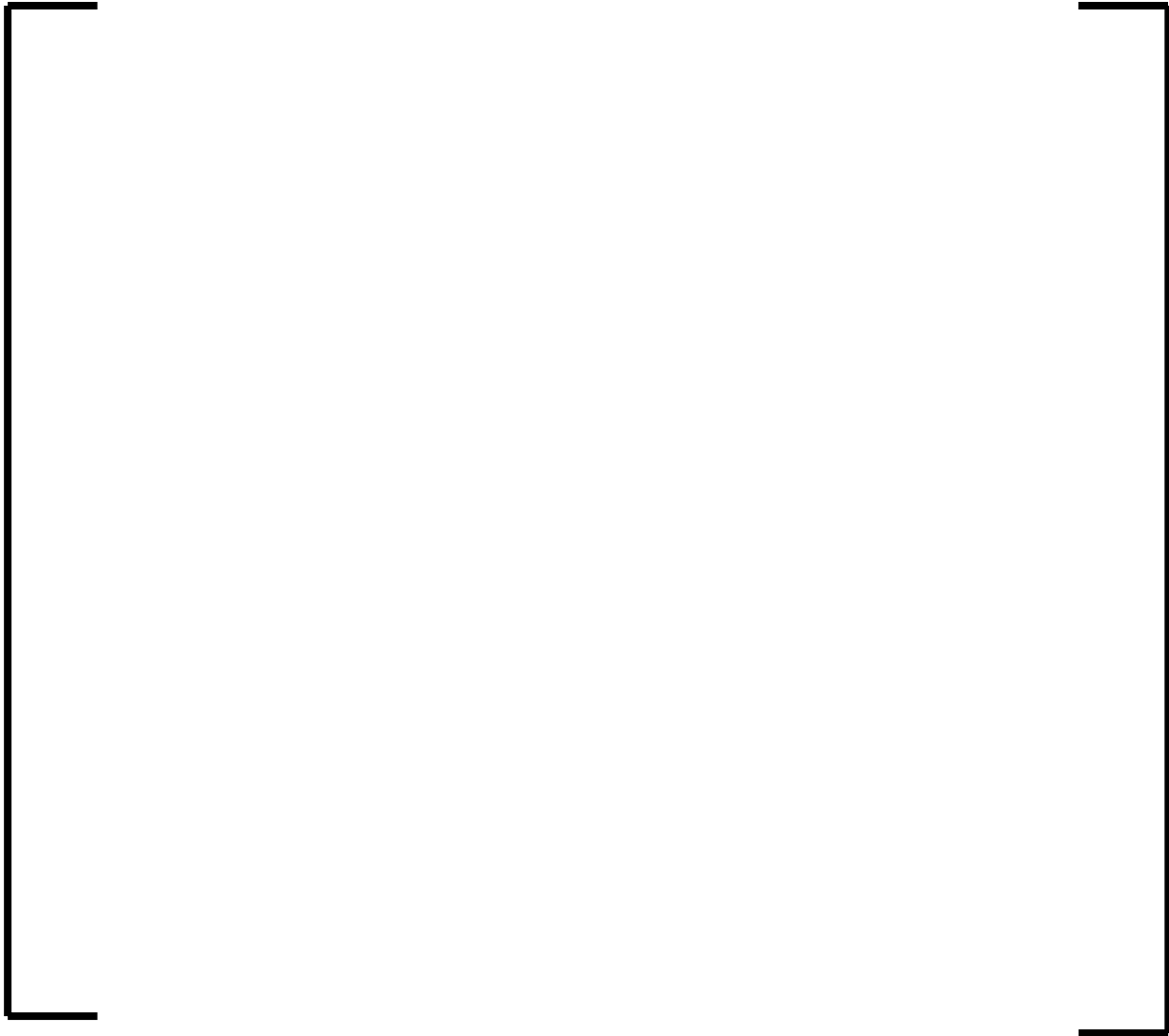


**Figure 7-24 IRWST Water Level (LBLOCA)**

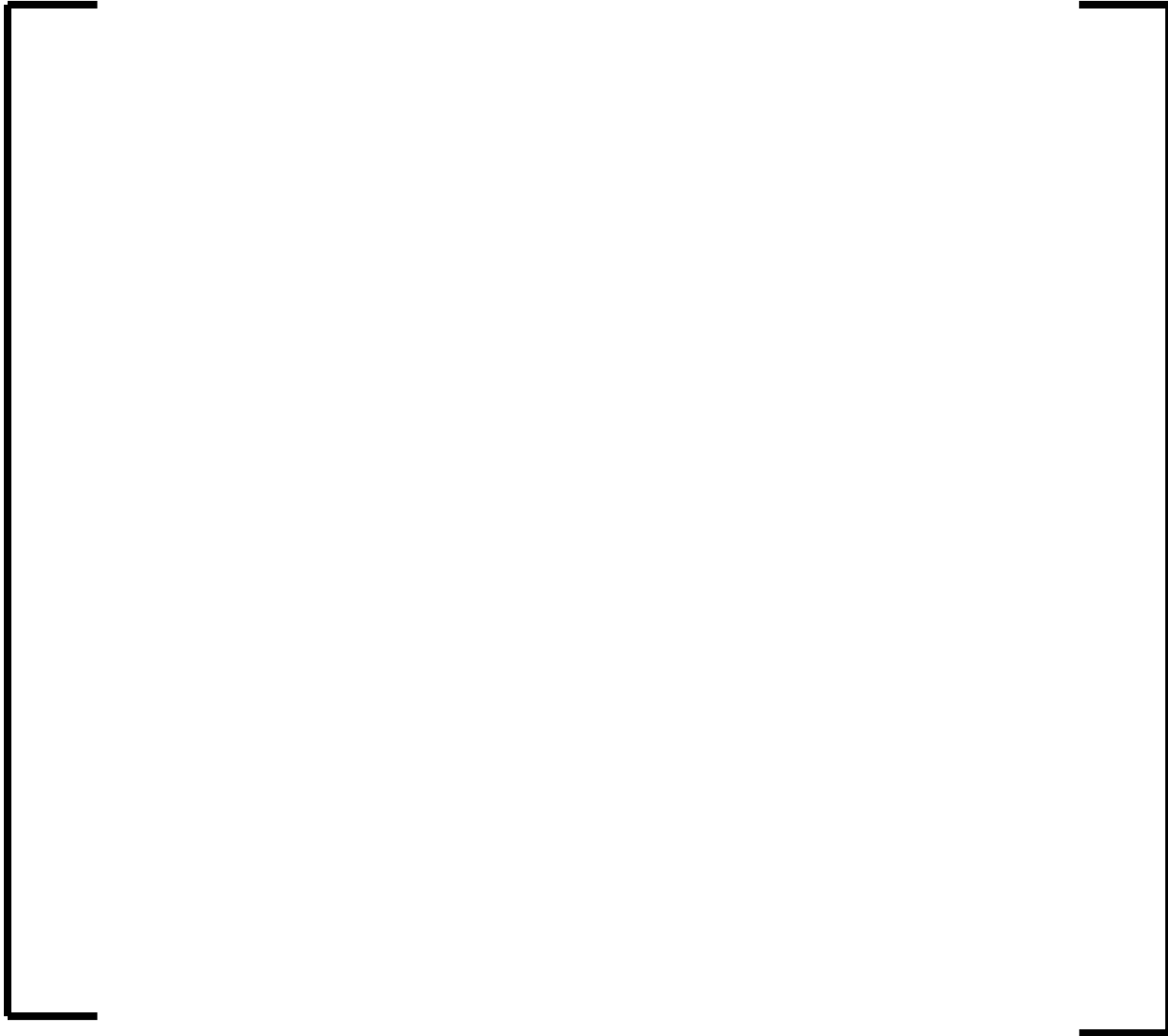


**Figure 7-25 Corium Temperature in Reactor Pit (LBLOCA)**

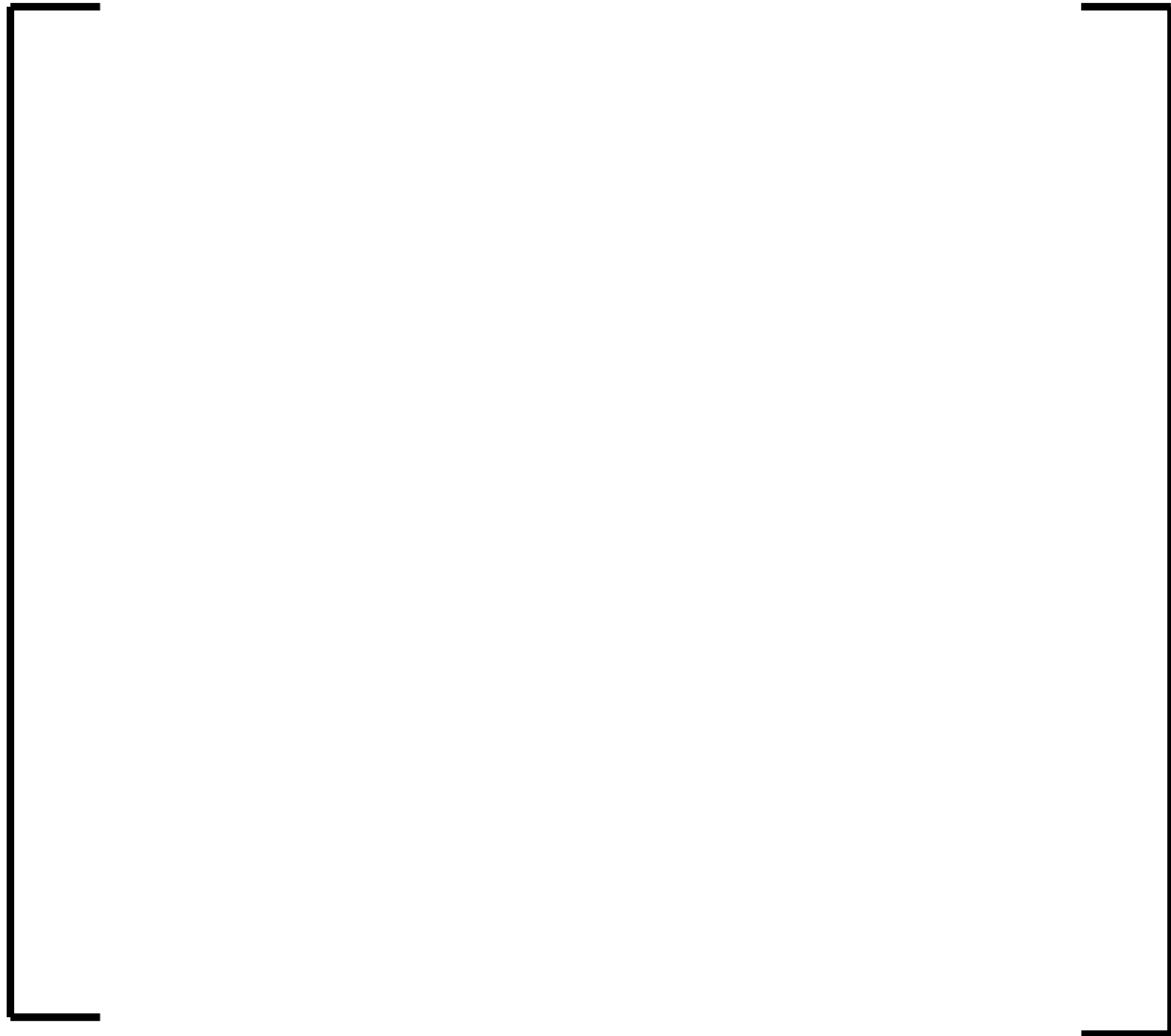


**Figure 7-26 Containment Spray Flow (LBLOCA)**

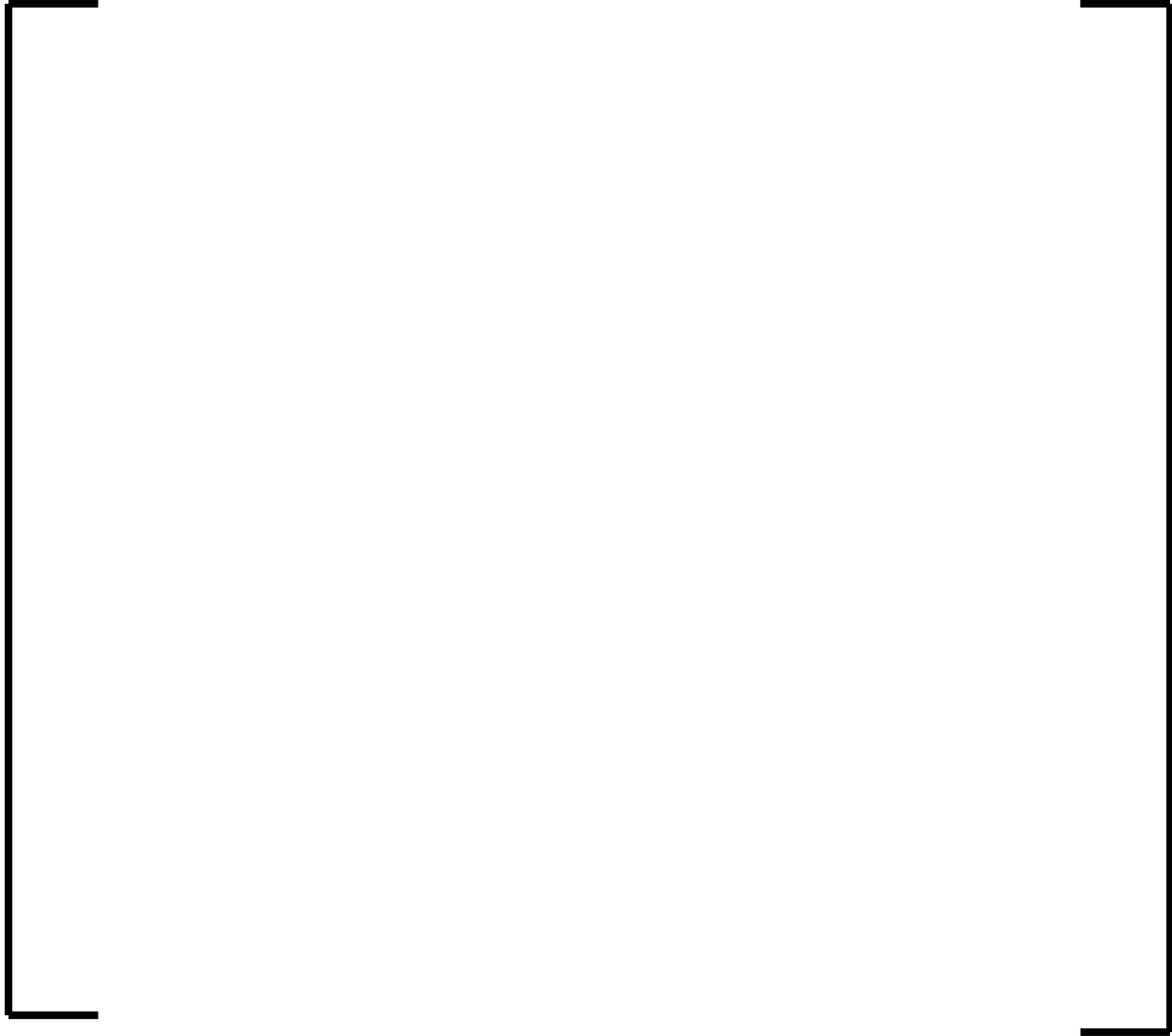


**Figure 7-27 SAHRS Suction Temperature (LBLOCA)**

**7.3.2 Loss of Off-site Power**

The predicted U.S. EPR response during a SBO event described in Section 7.2 is provided in Figures 7-28 to 7-50. The sequence of events and important results are provided in Table 7-4 and 7-5, respectively.

**Table 7-4 Event Progression of a SBO**

--

**Table 7-5 Key Results from a SBO**

--



**Figure 7-28 Core Outlet Temperature (SBO)**



**Figure 7-29 RCS Pressure SBO**



**Figure 7-30 RCS Water Inventory (SBO)**



**Figure 7-31 Two-Phase Water Level in Core (SBO)**



**Figure 7-32 In-Vessel Hydrogen Production (SBO)**



**Figure 7-33 Hydrogen Release Rate (SBO)**



**Figure 7-34 Mass of Corium in Lower Head (SBO)**



**Figure 7-35 Mass of Material in Core (SBO)**



**Figure 7-36 Mass of Material in Lower Head and Core (SBO)**



**Figure 7-37 Containment Pressure (SBO)**



**Figure 7-38 Average Hydrogen Mole Fraction in Containment (SBO)**



**Figure 7-39 Average Mole Fraction of Air in Containment (SBO)**



**Figure 7-40 Average Mole Fraction of Steam in Containment (SBO)**



**Figure 7-41 Hydrogen Mass in Containment (SBO)**



**Figure 7-42 Mass of Corium in Reactor Pit (SBO)**



**Figure 7-43 Mass of Corium in Spreading Compartment (SBO)**



**Figure 7-44 Spreading Room Ablation (SBO)**



**Figure 7-45 Reactor Pit Ablation (SBO)**



**Figure 7-46 Spreading Room Water Level (SBO)**



**Figure 7-47 IRWST Water Level (SBO)**



**Figure 7-48 Corium Temperature in Reactor Pit (SBO)**

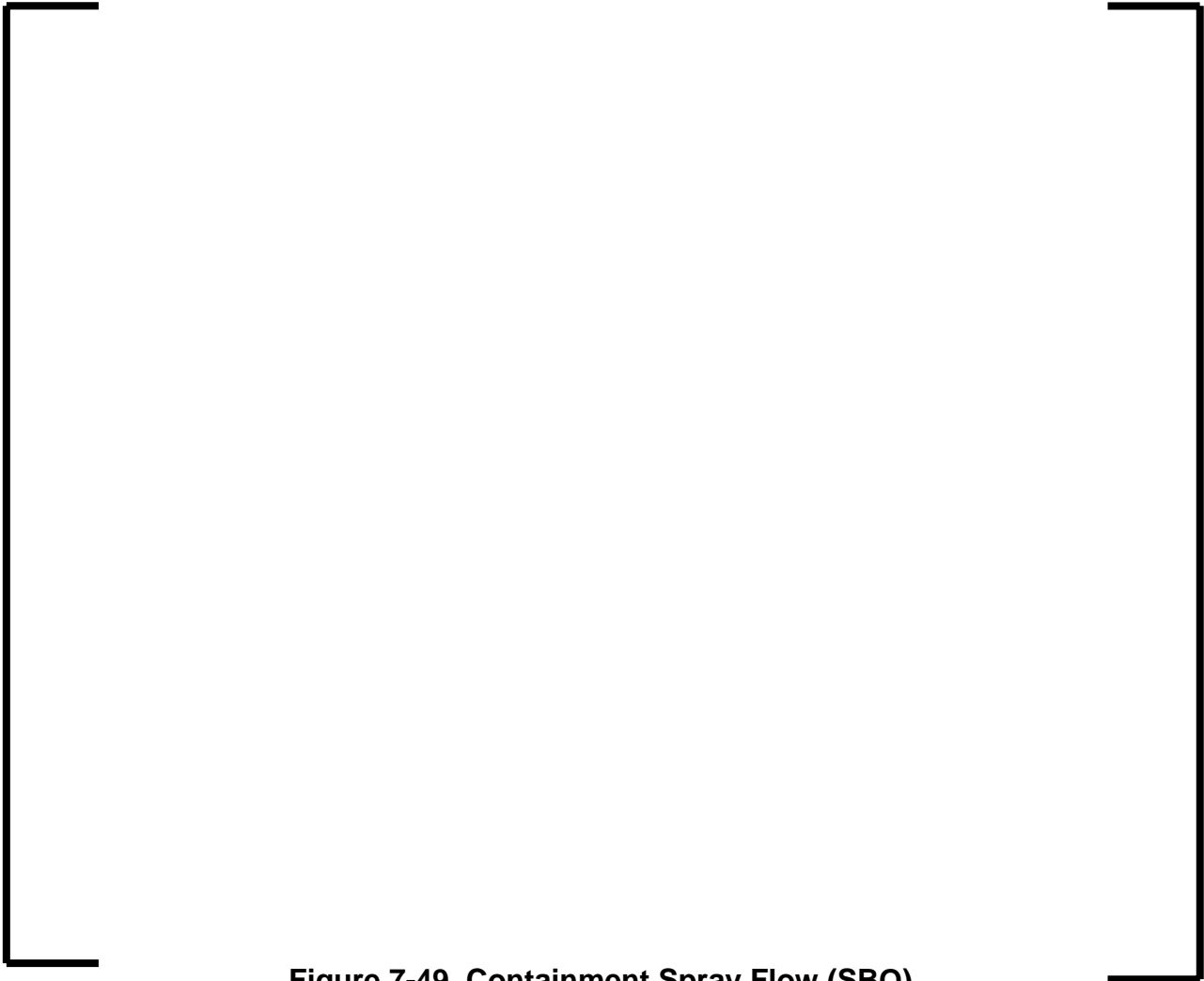


**Figure 7-49 Containment Spray Flow (SBO)**



**Figure 7-50 SAHRS Suction Temperature (SBO)**

**7.3.3 Small Break Loss of Coolant Accident (SBLOCA)**

The predicted U.S. EPR response during an SBLOCA event described in Section 7.2 is provided in Figures 7-51 to 7-73. The sequence of events and important results are provided in Table 7-6 and Table 7-7, respectively.

**Table 7-6 Event Progression of a SBLOCA**

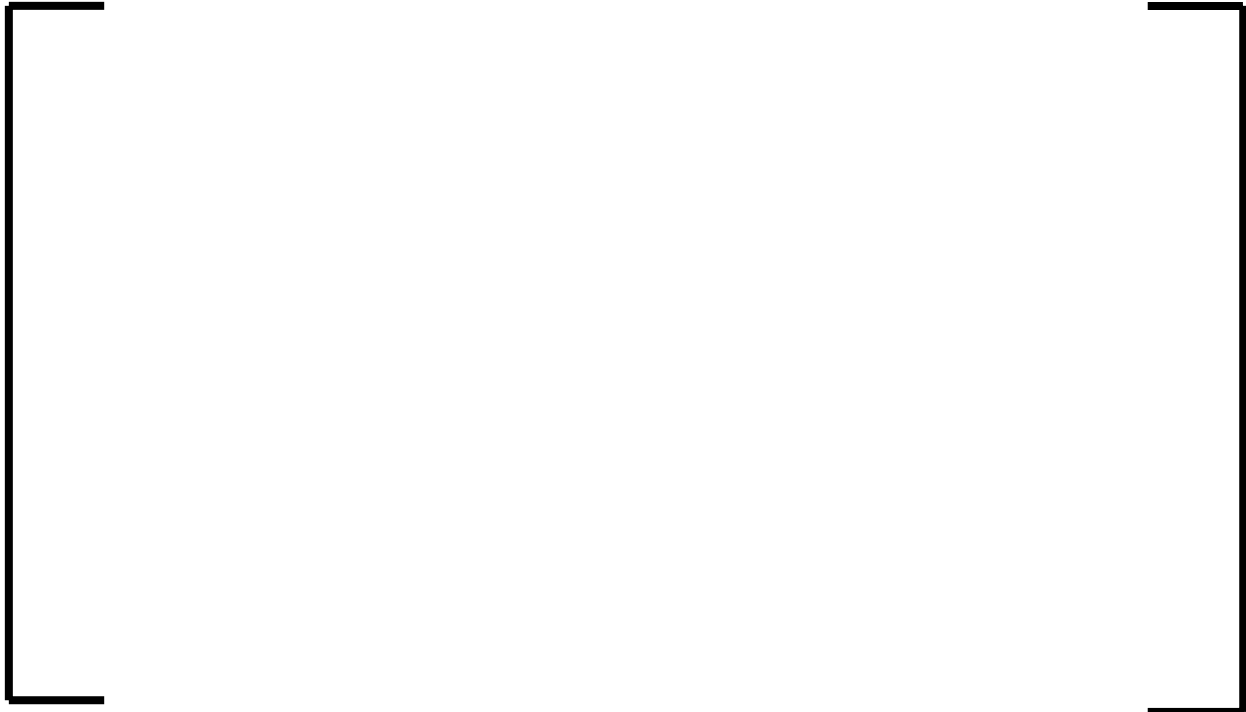


**Table 7-7 Key Results from a SBLOCA**





**Figure 7-51 Core Outlet Temperature (SBLOCA)**

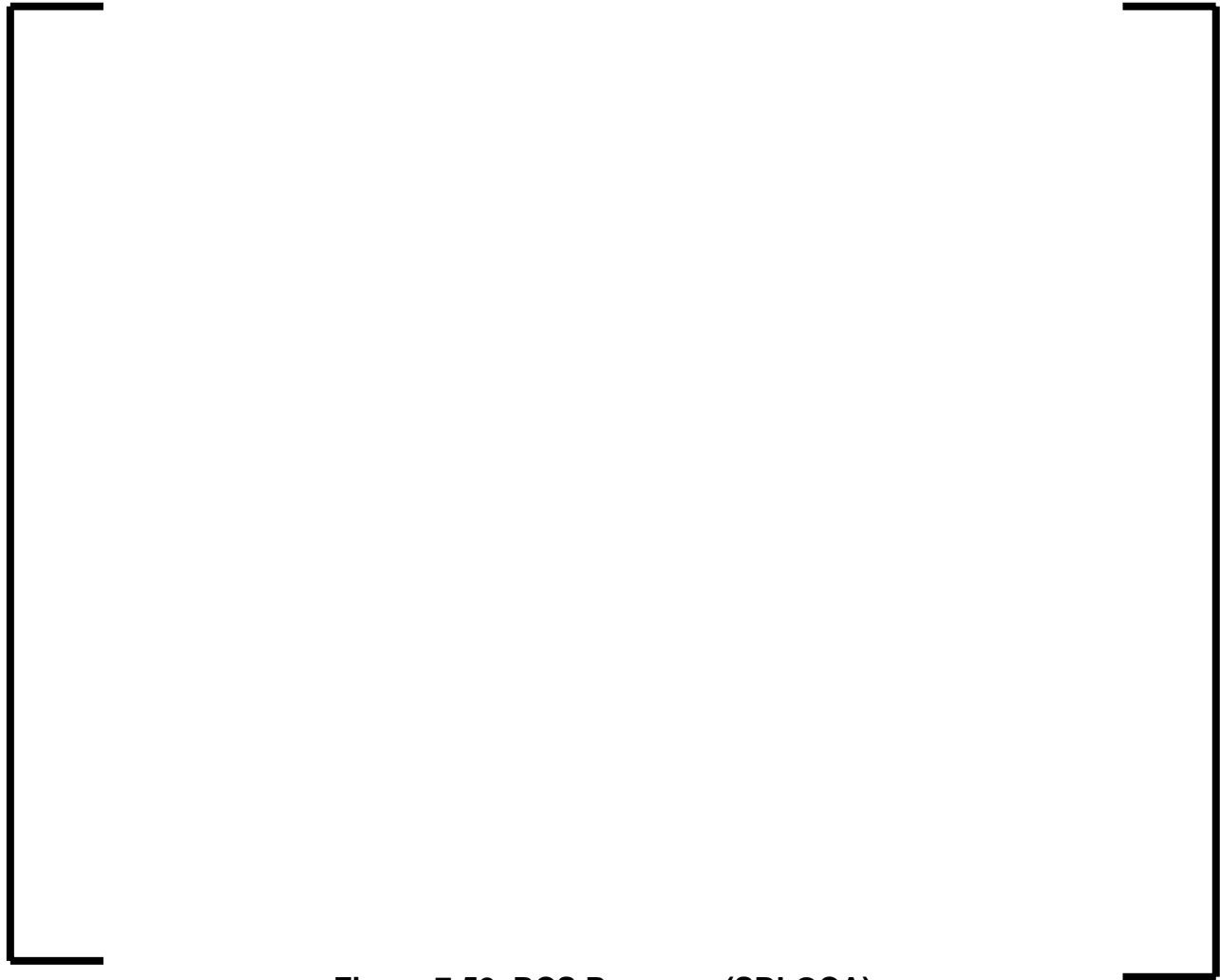


**Figure 7-52 RCS Pressure (SBLOCA)**



**Figure 7-53 RCS Water Inventory (SBLOCA)**



**Figure 7-54 Two-Phase Water Level in Core (SBLOCA)**



**Figure 7-55 In-Vessel Hydrogen Production (SBLOCA)**

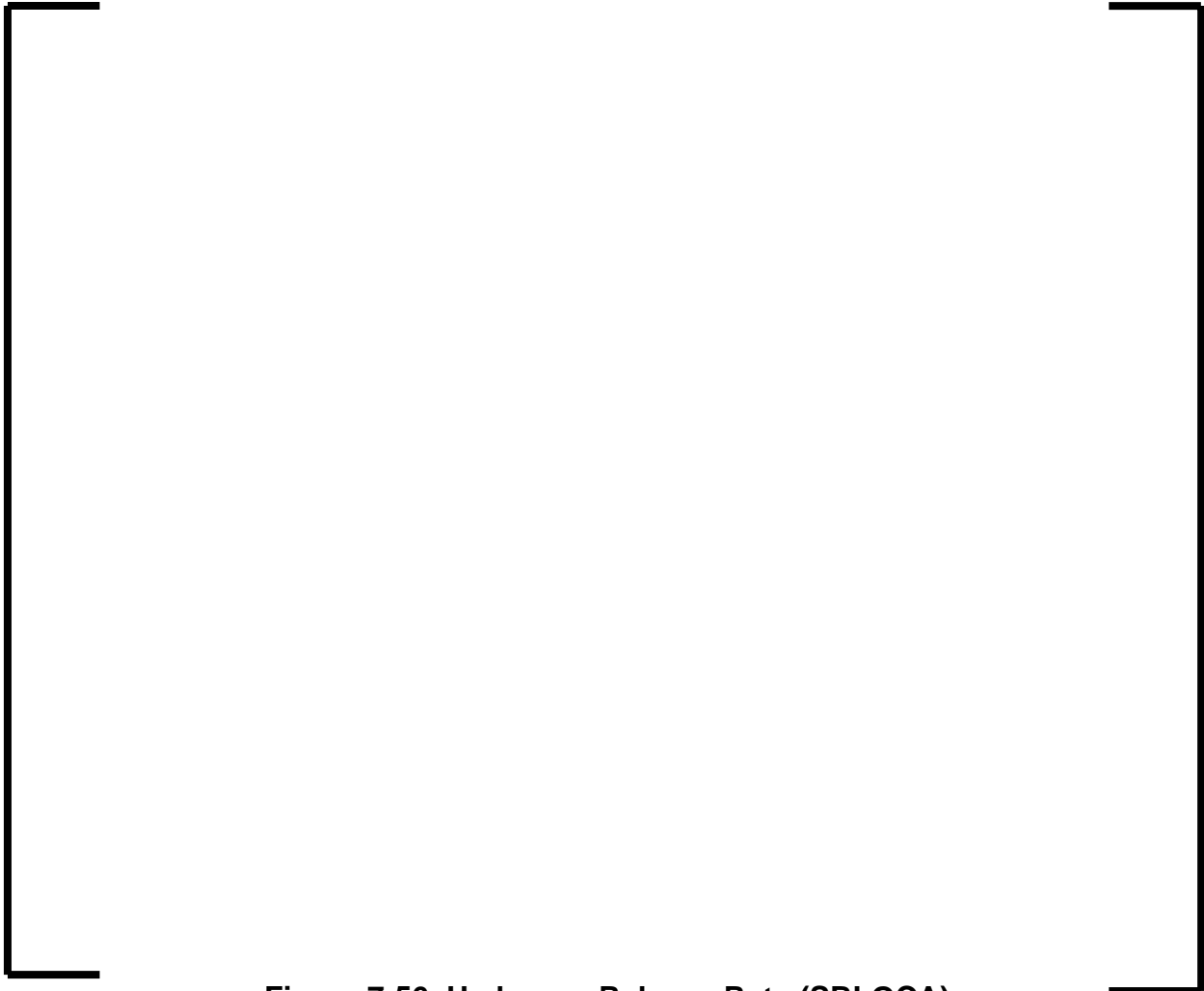


**Figure 7-56 Hydrogen Release Rate (SBLOCA)**



**Figure 7-57 Mass of Corium in Lower Head (SBLOCA)**



**Figure 7-58 Mass of Material in Core (SBLOCA)**



**Figure 7-59 Mass of Material in Lower Head and Core (SBLOCA)**

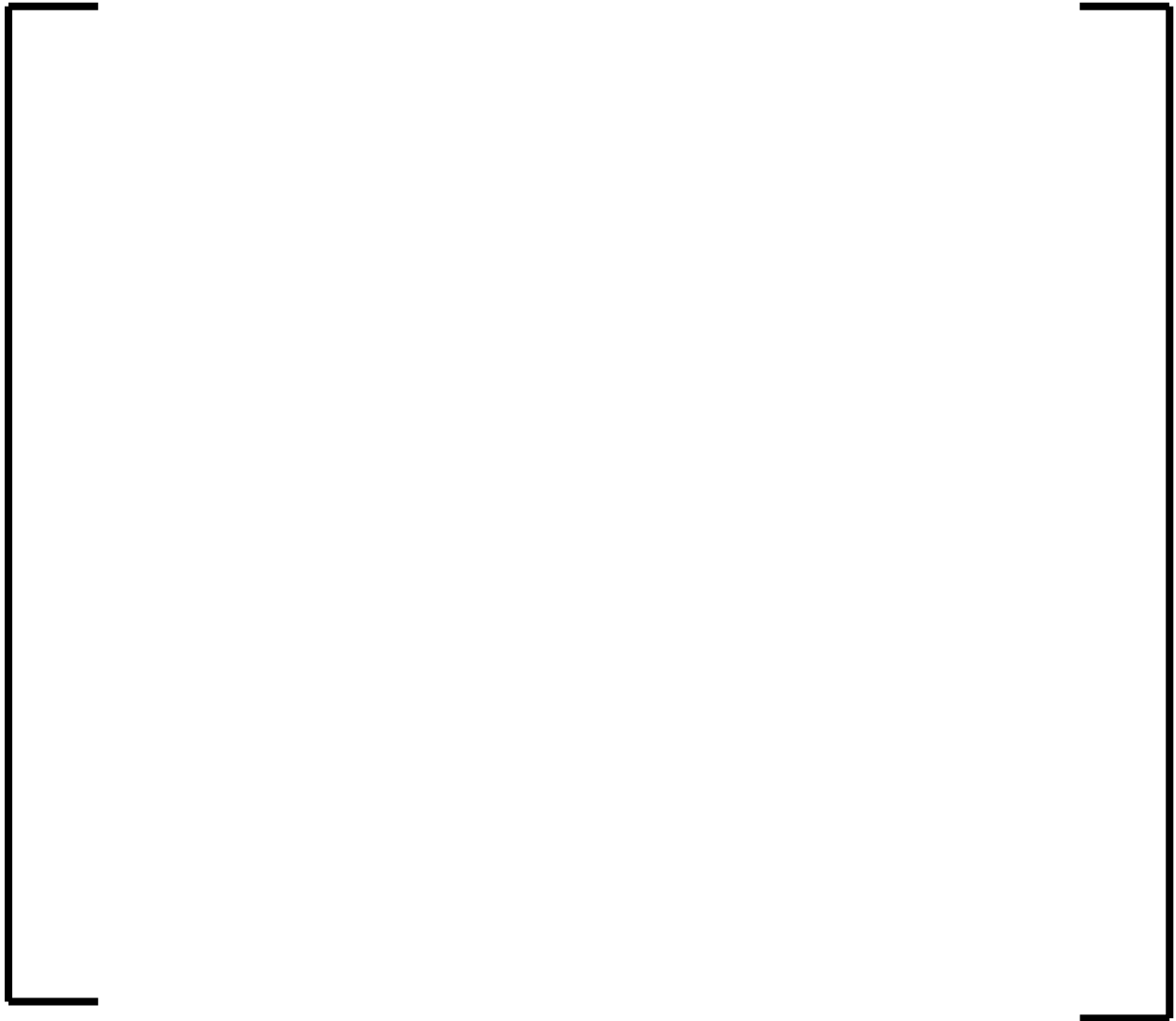


**Figure 7-60 Containment Pressure (SBLOCA)**



**Figure 7-61 Average Hydrogen Mole Fraction in Containment (SBLOCA)**



**Figure 7-62 Average Mole Fraction of Air in Containment (SBLOCA)**



**Figure 7-63 Average Mole Fraction of Steam in Containment (SBLOCA)**



**Figure 7-64 Hydrogen Mass in Containment (SBLOCA)**

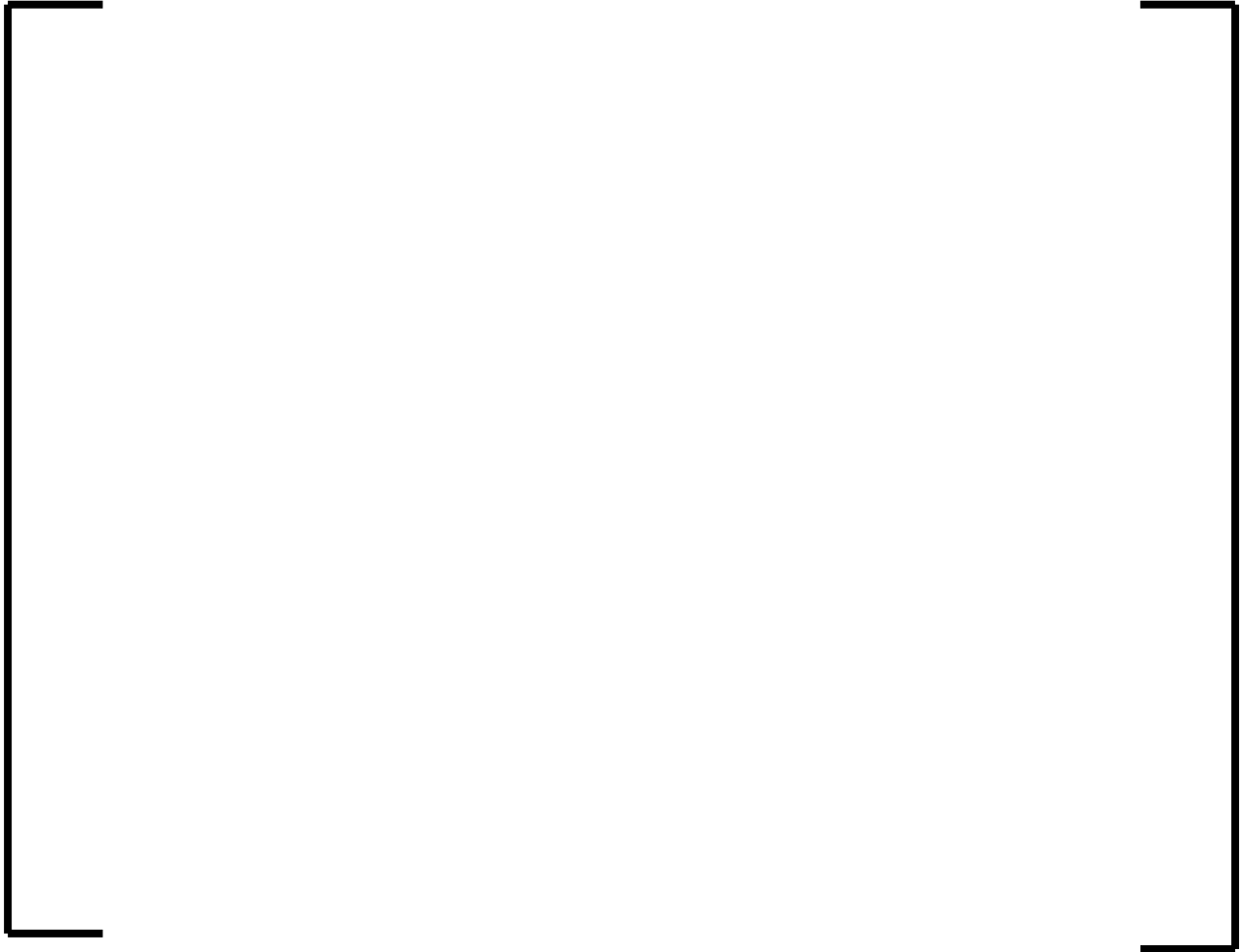


**Figure 7-65 Mass of Corium in Reactor Pit (SBLOCA)**



**Figure 7-66 Mass of Corium in Spreading Compartment (SBLOCA)**



**Figure 7-67 Spreading Room Ablation (SBLOCA)**



**Figure 7-68 Reactor Pit Ablation (SBLOCA)**



**Figure 7-69 Spreading Compartment Water Level (SBLOCA)**



**Figure 7-70 IRWST Water Level (SBLOCA)**



**Figure 7-71 Corium Temperature in Reactor Pit (SBLOCA)**



**Figure 7-72 Containment Spray Flow (SBLOCA)**



**Figure 7-73 SAHRS Suction Temperature (SBLOCA)**

**7.3.4 Large Break Loss of Coolant Accident Crossover (LBLOCA Crossover)**

The predicted U.S. EPR response during an LBLOCA crossover event described in Section 7.2 is provided in Figures 7-74 to 7-96. The sequence of events and important results are provided in Table 7-8 and 7-9, respectively.

**Table 7-8 Event Progression of a LBLOCA Crossover**



**Table 7-9 Key Results from a LBLOCA Crossover**

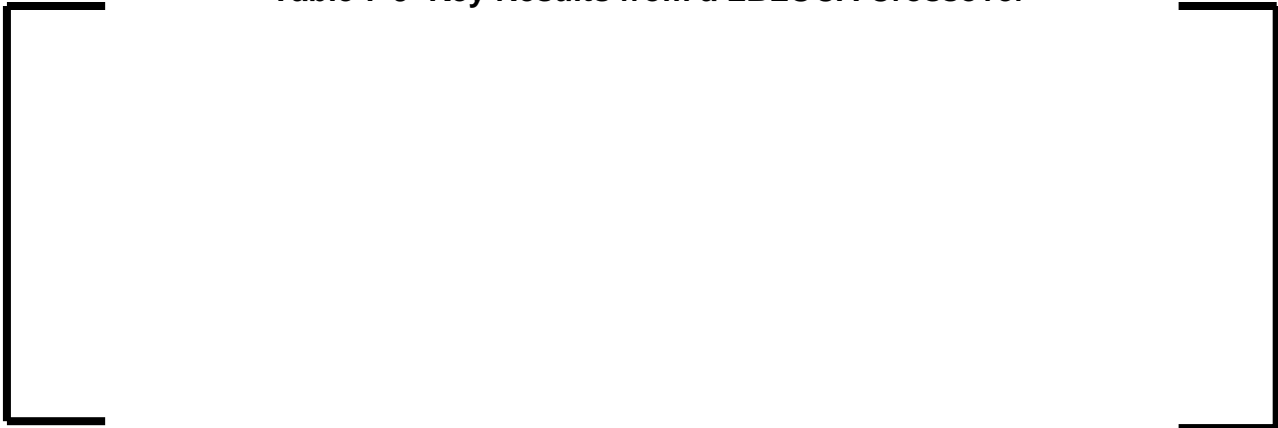




**Figure 7-74 Core Outlet Temperature (LBLOCA Crossover)**



**Figure 7-75 RCS Pressure (LBLOCA) Crossover)**



**Figure 7-76 RCS Water Inventory (LBLOCA Crossover)**



**Figure 7-77 Two-Phase Water Level in Core (LBLOCA Crossover)**



**Figure 7-78 In-Vessel Hydrogen Production (LBLOCA Crossover)**



**Figure 7-79 Hydrogen Release Rate (LBLOCA Crossover)**



**Figure 7-80 Mass of Corium in Lower Head (LBLOCA Crossover)**



**Figure 7-81 Mass of Material in Core (LBLOCA Crossover)**



**Figure 7-82 Mass of Material in Lower Head and Core (LBLOCA Crossover)**



**Figure 7-83 Containment Pressure (LBLOCA Crossover)**

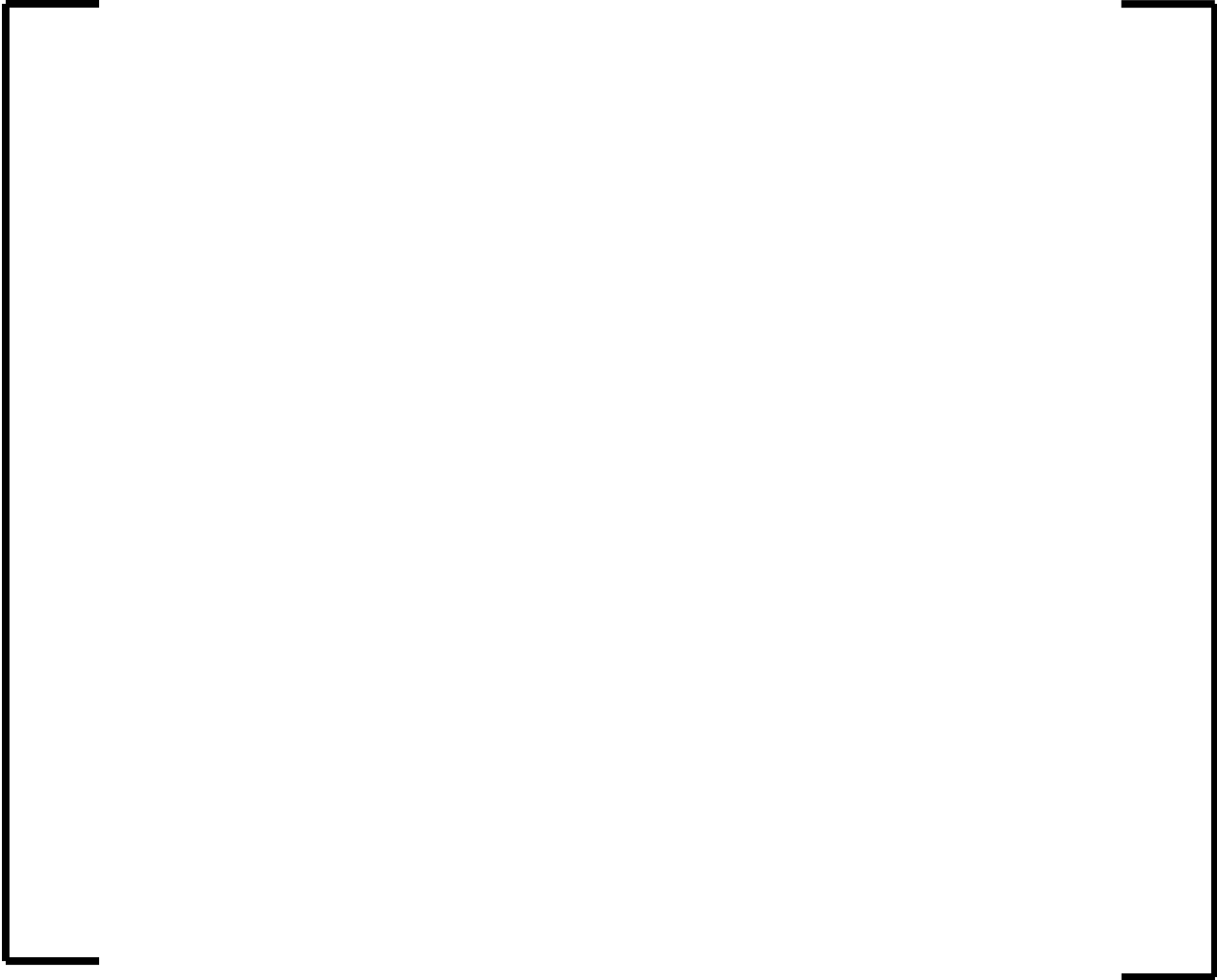


**Figure 7-84 Average Hydrogen Mole Fraction in Containment (LBLOCA Crossover)**



**Figure 7-85 Average Mole Fraction of Air in Containment (LBLOCA Crossover)**



**Figure 7-86 Average Mole Fraction of Steam in Containment (LBLOCA Crossover)**



**Figure 7-87 Hydrogen Mass in Containment (LBLOCA Crossover)**

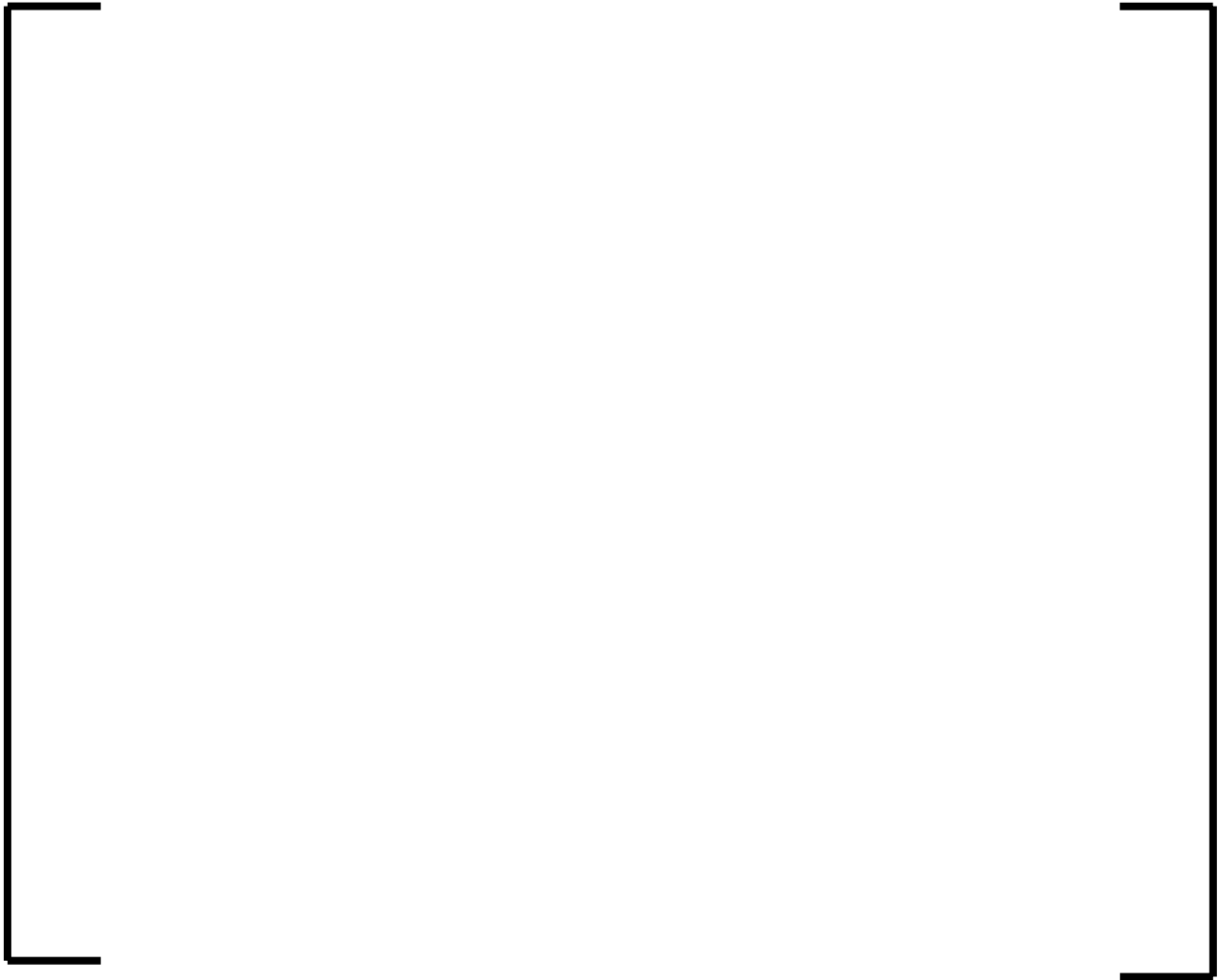


**Figure 7-88 Mass of Corium in Reactor Pit (LBLOCA Crossover)**



**Figure 7-89 Mass of Corium in Spreading Compartment (LBLOCA Crossover)**



**Figure 7-90 Spreading Room Ablation (LBLOCA Crossover)**

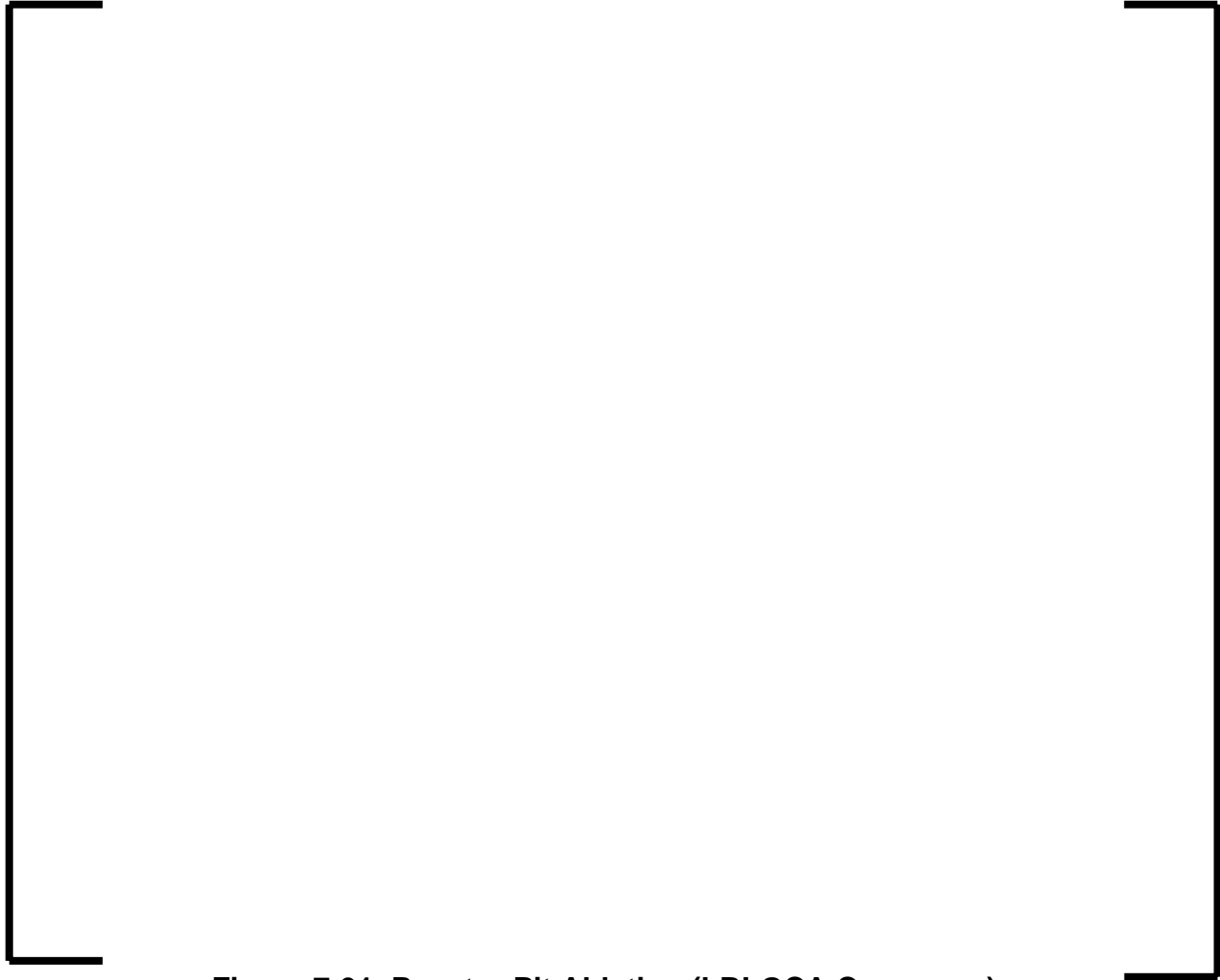


**Figure 7-91 Reactor Pit Ablation (LBLOCA Crossover)**



**Figure 7-92 Spreading Compartment Water Level (LBLOCA Crossover)**



**Figure 7-93 IRWST Water Level (LBLOCA Crossover)**



**Figure 7-94 Corium Temperature in Reactor Pit (LBLOCA Crossover)**



**Figure 7-95 Containment Spray Flow (LBLOCA Crossover)**



**Figure 7-96 SAHRS Suction Temperature (LBLOCA Crossover)**

## **8.0 CONCLUSION**

This topical report has been prepared with specific attention to SECY-93-087 guidance on severe accident safety issue resolution and phenomenological analyses supporting PRA success criteria. This report describes the technical bases for the U.S. EPR approach and methods applied to resolve these safety issues as will be documented in the U.S. EPR DCD. The primary topics include the U.S. EPR severe accident design philosophy, key processes and phenomena, the experimental bases for the severe accident design features and analytical techniques and tools used to assess hypothetical severe accident sequences, the major computer code models, and examples of severe accident analyses.

Application of AREVA NP's safety issue resolution evaluation methodology will provide insight into plant-specific severe accident processes and phenomena and form the basis for a calculation matrix of deterministic studies addressing severe accident safety issues based on existing regulatory guidance. An analytical methodology featuring the MAAP4.07 code as the principal analysis tool has been developed with updates specifically addressing phenomena in postulated severe accidents for a U.S. EPR.

The conclusion is that the approach for demonstrating the performance of the U.S. EPR during a severe accident is systematic, complete, and comprehensive and will provide sufficient insight for resolution of severe accident safety issues for the U.S. EPR. Results of the of this approach will appear in the U.S. EPR DCD, including quantification of the performance ranges and limits of U.S. EPR severe accident response features.

## 9.0 REFERENCES

1. U. S. NRC Standard Review Plan, NUREG-0800, most recent revision.
2. Fauske and Associates, Inc., 1994a. MAAP4—Modular Accident Analysis Program for LWR Power Plants, vol. 2, Part 1: Code Structure and Theory, prepared for Electric Power Research Institute, May 1994.
3. Sandia National Laboratories, NUREG/CR-6119, Rev. 2, MELCOR Computer Code Manuals, vol. 1: Primer and User's Guide, Version 1.8.5, Prepared by Sandia National Laboratories for the U.S. Nuclear Regulatory Commission, Office of Nuclear Regulatory Research, 2000.
4. U. S. Code of Federal Regulations, most recent revision.
5. US NRC, Policy Statement on Severe Reactor Accidents Regarding Future Designs and Existing Plants, Volume 50, page 32138, of the Federal Register dated August 8, 1985.
6. US NRC, Policy Statement on Safety Goals for the Operations of Nuclear Power Plants, Volume 51, page 28044, of the Federal Register, dated August 4, 1986.
7. US NRC, Policy Statement on Nuclear Power Plant Standardization, Volume 52, page 34844, of the Federal Register dated September 15, 1987.
8. US NRC, Policy Statement on The Use of Probabilistic Risk Assessment Methods in Nuclear Regulatory Activities, Volume 60, page 42622, of the Federal Register, dated August 16, 1995.
9. US NRC, SECY-90-016, "Policy, Technical, and Licensing Issues Pertaining to Evolutionary and Advanced Light-Water (ALWR) Designs," issued January 12, 1990, and the corresponding staff requirements memorandum (SRM), issued June 26, 1990.
10. US NRC, SECY-93-087, "Evolutionary Light Water (LWR) Certification Issues and Their Relationship to Current Regulatory Requirements," issued April 2, 1993, and the corresponding SRM, issued July 21, 1993.
11. Sauvage, E.C., et al., "OSSA – An Optimized Approach to Severe Accident Management: EPR Application," Proceedings of ICAPP '06, Reno, NV, June 2006.
12. Pilch, M. M., Yan, H., Theofanous, T. G., "The Probability of Containment Failure by Direct Containment Heating in Zion," NUREG/CR-6075, SAND93-1535, December 1994.

13. Theofanous, T. G., "On the proper formulation of safety goals and assessment of safety margins for rare and high-consequence hazards," Reliability Engineering and System Safety, Vol. 54, pp. 243-257, 1996.
14. Scobel, J. H., Theofanous, T. G., Sorrell, S. W., "Application of the risk oriented accident analysis methodology (ROAAM) to severe accidents management in the AP600 advanced light water reactor," Reliability Engineering and System Safety, Vol. 62, pp. 51-58, 1998.
15. Technical Program Group, "An Integrated Structure and Scaling Methodology for Severe Accident Technical Issue Resolution," NUREG/CR-5809, EGG-2659, November 1991.
16. Zuber, N., Wilson, G. E., et al., "An integrated structure and scaling methodology for severe accident technical issue resolution: Development of methodology," Nuclear Engineering and Design, Vol. 186, pp. 1-21, 1998.
17. Technical Program Group, "Quantifying Reactor Safety Margins, Application of Code Scaling, Applicability, and Uncertainty Evaluation Methodology to a Large Break, Loss-of-Coolant Accident," NUREG/CR-5249, December 1989.
18. Theofanous, T. G., et. al., "Lower head integrity under steam explosion loads," Nuclear Engineering and Design, Vol. 189, pp. 7-57, 1999.
19. Gauntt, R. O., "An Uncertainty Analysis for Hydrogen Generation in Station Blackout Accidents Using MELCOR 1.8.5," The 11th Topical Meeting on Nuclear Reactor Thermal-Hydraulics (NURETH-11), Pope's Palace Conference Center, Avignon, France, October 2-6, 2005.
20. US NRC, "Reactor Safety Study-An Assessment of Accident Risks in U.S. Commercial Nuclear Power Plants," WASH-1400 (NUREG-75/014), October 1975.
21. Kottke, P., et al., "Scale Analysis of Combined Thermal Radiation and Convection Heat Transfer," Journal of Heat Transfer, Transactions of the American Society of Mechanical Engineers, Vol. 126, Issue 2, pp. 250 – 258, April 2004.
22. Deutsch, J. M. and Narayan, O., "Correlations and scaling in one-dimensional heat conduction," Physical Review E, The American Physical Society, Vol. 68, 041203, 2003.
23. Fischer, K., et al., "Scaling of Containment Experiments (SCACEX)," The 10th International Topical Meeting on Nuclear Reactor Thermal Hydraulics (NURETH-10), Seoul, Korea, October, 2003.

24. Konovalikhin, M. J., "Investigations on Melt Spreading and Coolability in a LWR Severe Accident," Dissertation, Royal Institute of Technology, Stockholm, Sweden, November 2001.
25. NEA Group of Experts, "In-Vessel and Ex-Vessel Hydrogen Sources," NEA/CSNI/R(2001)15, October 2001.
26. Firnhaber, M., Trambauer, K., Hagen, S., Hofmann, P., "CORA-13 Experiment on Severe Fuel Damage," NEA/CSNI-(93) 17, GRS-106, KfK 5287, July 1993.
27. Martinson, Z. R., et al., "PBF Severe Accident Fuel Damage Test 1-3 Test Results Report," NUREG/CR-5354, October 1989.
28. Coryell, E. W., "Summary of Important Results and SCDAP/RELAP5 Analysis for OECD LOFT Experiment LP-FP-2," NUREG/CR-6160, NEA/CSNI-(94) 3, April 1994.
29. Firnhaber, M., "ISP 28: Phebus-SFD B9+ Experiment on the Degradation of a PWR Type Core," NEA/CSNI/R(92)17, Volumes 1 and 2, 1992.
30. Clément, B., Hanniet-Girault, N., et al., "The First International PHEBUS Fission Product Program for Investigation of Phenomena of Severe Water Reactor Accidents," Nucl. Eng. Des., 226, pp. 5-82, 2003.
31. Hering, W., et al., OECD Document, "Comparison Report on the Blind Phase of the OECD International Standard Problem N°45, Exercise (QUENCH-06)," ISP45-OECD, Report FZKA-6677, 2002.
32. Hering, W., et al., "Comparison and Interpretation Report of OECD International Standard Problem N°45 Exercise (QUENCH-06)," ISP45-OECD, Report FZKA-6722, 2002.
33. Karwat, H., "SOAR on Containment Thermalhydraulics and Hydrogen Distribution," NEA/CSNI-(99) 16, June 1999.
34. Royen, J., "Final Comparison Report on ISP-35: NUPEC Hydrogen Mixing and Distribution Test (Test M-7-1)," NEA/CSNI-(94) 29, December 1994.
35. Firnhaber, M., et al., "ISP37: VANAM M3 - A Multi Compartment Aerosol Depletion Test with Hygroscopic Aerosol Material," NEA/CSNI-(96) 26, December 1996.
36. Breitung, W., et al., "Flame Acceleration and Deflagration-to-Detonation Transition in Nuclear Safety," NEA/CSNI-(2000) 7, October 2000.
37. Nakakura, H., et al., "Hydrogen Combustion Analysis of Dry Type PWR in Japan," Proceedings of the ICONE 8 conference, Baltimore, MD, April 2-6, 2000.

38. C. K. Chan et al., "The structure of horizontal hydrogen-steam diffusion flames," OECD workshop on the implementation of hydrogen mitigation techniques, NEA/CSNI-(96) 8, Winnipeg, Manitoba, Canada, May 1996.
39. Fineschi, F., et al., "Mitigation of hydrogen hazards in water cooled power reactors," IAEA-TECDOC-1196, Vienna, Austria, February 2001.
40. Hosler, J. and Sliter, G., "PARs for Combustible Gas Control in Advanced Light Water Reactors," OECD/NEA/CSNI Workshop on the Implementation of Hydrogen Mitigation Techniques, Winnipeg, AECL-11762, NEA/CSNI/R(96)8, 1996.
41. Fischer, K., "Qualification of a Passive Catalytic Module for Hydrogen Mitigation," Nuclear Technology, Vol. 112, pp. 58-62, 1995.
42. Koroll, G. W., et al, Hydrogen Recombiner Development at AECL, OECD/NEA/CSNI Workshop on the Implementation of Hydrogen Mitigation Techniques, Winnipeg, AECL-11762, NEA/CSNI/R(96)8, 1996.
43. Rongier, P. and Studer, E., "H2PAR Facility," OECD/NEA/CSNI Workshop on the Implementation of Hydrogen Mitigation Techniques, Winnipeg, AECL-11762, NEA/CSNI/R(96)8, 1996.
44. Eckardt, B., et al., "Containment Hydrogen Control and Filtered Venting Design and Implementation," Proceedings of the OECD Workshop on the Implementation of Severe accident Management Measures, NEA/CSNI/R(2001)20, Paul Scherer Institute, Villingen, Switzerland, September 2001.
45. Rempe, J. L., et al., "Light Water Reactor Lower Head Failure Analysis," NUREG/CR-5642, EGG-2618, October 1993.
46. Rempe, J. L., Condie, K. G., and Knudson, D. L., "Thermal Properties for Candidate SCWR Materials," INL/EXT-05-01030, December 2005.
47. Stickler, L. A., Rempe, J. L., et al., "Calculations to Estimate the Margin-to-Failure in the TMI-2 Vessel," NUREG/CR-6196, EGG-2733, February 1994.
48. Chu, T. Y., et al., "Lower Head Failure Experiments and Analyses," NUREG/CR-5582 (SAND98-2047), February 1999.
49. Alsmeyer, H., Second OECD (NEA) CSNI Specialist Meeting on Molten Core Debris-Concrete Interactions, NEA/CSNI(92)10, KfK 5108, 1992.
50. Sevón, T., "Molten Core – Concrete Interactions in Nuclear Accidents: Theory and Design of an Experimental Facility," Master's thesis, Helsinki University of Technology, October 2005.

51. Nie, M. and Fischer, M., "Use of Molten Core Concrete Interactions in the Melt Stabilization Strategy of the EPR," Proceedings of the 2006 International Congress on Advances in Nuclear Power Plants (ICAPP '06), Reno, NV, June 4-8, 2006
52. Firnhaber, M., "ISP 30: BETA V5.1 Experiment on Melt-Concrete Interaction," NEA/CSNI/R(92)9
53. Nie, M., Fischer, M., and Koller, W., "Status of Interpretation of selected transient MCCI experiments conducted in the frame of the CORESA R&D project," Proceedings of Jahrestagung Kerntechnik. Stuttgart, Germany, 14-16, May 2002.
54. Thompson, D.G., et al, "Compilation, Analysis and Interpretation of ACE Phase C and MACE experimental data – MCCI Thermohydraulic results," ACEX TR-C-14, Vol. 1; Argonne Nat. Lab. Nov. 1997.
55. Farmer, M.T. et al., "Mace Test M3b Data Report Volume 1," MACE-TR-D13, EPRI TR-108806, November 1997.
56. Farmer, M.T. et al., "Mace Test M4 Data Report," MACE-TR-D16, August 1999.
57. Spencer, B.W., et al., "MACE Scoping Test," MACE-TR-D03, Argonne Nat. Lab., June 1991.
58. Roche, M. F., Solidus and Liquidus Temperatures of Core-Concrete Mixtures, NUREG/CR-6032, ANL-93/9, June 1993.
59. Bonnet, J.-M., "Thermal Hydraulic Phenomena in Corium Pools for Ex-Vessel Situations: The BALI Experiment," Proceedings of the ICONE 8 conference, Baltimore, USA, April 2000.
60. Farmer, M. T., Lomperski, S., Kilsdonk, D. J., Aeschlimann, R. W., "OECD MCCI Project 2-D Core Concrete Interaction (CCI) Tests: CCI-1 Test Data Report- Thermalhydraulic Results," OECD/MCCI-2004-TR01, January 2004.
61. Farmer, M. T., Lomperski, S., Kilsdonk, D. J., Aeschlimann, R. W., "OECD MCCI Project 2-D Core Concrete Interaction (CCI) Tests: CCI-2 Test Data Report- Thermalhydraulic Results," OECD/MCCI-2004-TR05, October 2004.
62. Farmer, M. T., Lomperski, S., Kilsdonk, D. J., Aeschlimann, R. W., "OECD MCCI Project 2-D Core Concrete Interaction (CCI) Tests: CCI-3 Test Data Report- Thermalhydraulic Results," OECD/MCCI-2005-TR04, October 2005.
63. Tourniaire, B., Bonnet, J.-M., "Study of the Mixing of Immiscible Liquids by Sparging Gas Results of the BALISE Experiments," The 10th International Topical Meeting on Nuclear Reactor Thermal Hydraulics (NURETH-10), Seoul, Korea, October 2003.

64. Nie, M., "Temporary Melt Retention in the Reactor Pit of the European Pressurized Water Reactor (EPR)," Dissertation, Universität Stuttgart, Institut für Kernenergetik und Energiesysteme, February 2005.
65. Hellmann, S., et al. "Physico-Chemical and Material Aspects of the Core Melt Retention Concept of the EPR," OECD Workshop on Ex-Vessel Debris Coolability, Karlsruhe, Germany, November 1999.
66. Adroguer, B., et al., "Corium Interactions and Thermochemistry (CIT project)," European Commission, INV-CIT (99)-P040, December 1999.
67. Eppinger, B., et al., "KAPOOL Experiments on Melt-through of a Metal Plate by an Overlying Melt Pool," FZKA 7024, Forschungszentrum Karlsruhe, August 2004.
68. Farmer, M., "Melt Eruption Test (MET-1) Results," presentation at the 6th Program Review Meeting of the MCCI-OECD Project, Madrid, Spain, April 2005.
69. Seiler, J.-M., et al., "European Group for analysis of Corium Recovery Concepts – EUROCORE: Synthesis report," February 2002.
70. Veteau, J. M., Wittmaack, R., "CORINE Experiments and Theoretical Modelling," FISA-95-EU Research on Severe Accidents, EUR 16896 EN, 1996.
71. Silverii, R., Magallon, D., "FARO LWR Programme, Test L26-S Data Report, Technical Note," EU 4th FWP, EXV-CSC(98)-D007, 1998.
72. Steinwarz, W., et al, "COMAS Spreading Experiments with Prototypic Oxidic Corium Melts for Optimization of Spreading compartment Designs," ICONE7, Tokyo, Japan, April 19-23, 1999.
73. Konovalikhin, et al, "Experimental Simulation of Core Melt Spreading in Two Dimensions" The 9th International Topical Meeting on Nuclear Reactor Thermal Hydraulics (NURETH-9), San Francisco, October 1999.
74. Cognet, G. et al, The VULCANO Spreading Programme Article, EU 4th FWP, EXV-CSC(98)-D018, SARJ-98.
75. Eppinger, B., et al, Simulationsexperimente zum Ausbreitungsverhalten von Kernschmelze: KATS 8-17, Forschungszentrum, Karlsruhe, FZKA 6589, March 2001.
76. Wittmaack, "Simulation of free surface flows with heat transfer and phase transition and application to corium spreading in the EPR," Nuclear Technology, Vol. 137, March 2002.

77. Alsmeyer, H., et al, Experiment ECOKATS-2 On Melt Spreading and Subsequent Top Flooding Test and Data Report, Forschungszentrum, Karlsruhe, FZKA 7084, January 2005.
78. Sehgal, B.R., and Spencer, B. W., Ace Program Phase D: Melt Attack and Coolability Experiments (MACE) Program, Second OECD (NEA) CSNI Specialist Meeting on Molten Core Debris-Concrete Interactions, NEA/CSNI-(92) 10, KfK 5108, Karlsruhe, Germany, 1-3 April 1992.
79. Fischer, M., Herbst, O., and Schmidt, H., "Demonstration of the heat removing capabilities of the EPR spreading compartment," presented at the 3rd International symposium on two-phase flow modelling and experimentation, Pisa, Italy, September 22-24, 2004.
80. P. D. Bayless et al., "Severe Accident Natural Circulation Studies at the INEL," NUREG/CR-6285, INEL-94/0016, February 1995.
81. Commonwealth Edison Company of Chicago, "Zion Probabilistic Safety Study," Vols. 1-10, USNRC Accession Number 8109280420, September 1981. Portions summarized in NUREG-1150, "Severe Accident Risks: An Assessment for Five U.S. Nuclear Power Plants," December 1990.
82. Pilch, M. M., et al., "Resolution of the Direct Containment Heating Issue for All Westinghouse Plants With Large Dry Containments or Subatmospheric Containments," NUREG/CR-6338, SAND95-2381, 1996.
83. Pilch, M. M., et al., "The Probability of Containment Failure by Direct Containment Heating in Surry," NUREG/CR-6109, SAND93-2078, 1995.
84. Tarbell, W. W., et al., "High-Pressure Melt Streaming (HIPS) Program Plan," SAND82-2477, NUREG/CR-3025, Sandia National Laboratories, 1984.
85. Tarbell, W. W., et al., "Results from the DCH-1 Experiment," SAND86-2483, NUREG/CR-4871, Sandia National Laboratory, 1987.
86. Tarbell, W. W., et al., "DCH-2: Results from the Second Experiment Performed in the Surtsey Direct Heating Test Facility," SAND87-0976, NUREG/CR-4917, Sandia National Laboratory, 1988.
87. Allen, M. D., et al., "Experiments to Investigate to Direct Containment Heating Phenomena With Scaled Models of the Zion Nuclear Power Plant in the Surtsey Test Facility," NUREG/CR-6044, 1994.
88. Spencer, B. W., et. al., "Hydrodynamics and Heat Transfer Aspects of Corium-water Interactions," EPRI NP-5127, Argonne National Laboratory, 1987.

89. Blanchat, T. K., et al., "Experiments to Investigate Direct Containment Heating Phenomena With Scaled Models of a Surry Nuclear Power Plant," NUREG/CR-6152, 1994.
90. Schmitt, R. C. et al., "Simulated Design Basis Accident Tests of the Carolinas Virginia Tube Reactor Containment – Final Report. Idaho Nuclear Corporation Report IN-1403, 1970.
91. Hilliard, R. K., et al., "Removal of Iodine and Particles by Sprays in the Containment Systems Experiment," Nuc. Tech. 10, pp. 499-519, April 1971.
92. Corradini, M. L., "Vapor Explosions: A Review of Experiments for Accident Analysis," Nuclear Safety, 32, No. 3, July - September 1991.
93. Fletcher, D. F., "Steam Explosion Triggering: A Review of Theoretical and Experimental Investigations," Nuclear Engineering and Design, 155, 1995.
94. Corradini, M. L., Kim, B. J. and Oh, M. D., "Vapor Explosions in Light Water Reactors: A Review of Theory and Modeling," Progress in Nuclear Energy, 22, No.1, pp.1-117, 1988.
95. Steam Explosion Review Group (SERG), A Review of Current Understanding of the Potential for Containment Failure Arising from In-Vessel Steam Explosions, Nuclear Regulatory Commission Report, NUREG-1116, February 1985.
96. Basu, S. and Speis, T. P., "An Overview of Fuel-Coolant Interactions (FCI) Research at NRC," presented at the 23rd Water Reactor Safety Information Meeting, NUREG/CP-0149, Vol. 2, Bethesda, Maryland, October 23-25, 1995.
97. Basu, S., and Ginsberg, T. "A Reassessment of the Potential for an Alpha-Model Containment Failure and a Review of the Current Understanding of Broader Fuel-Coolant Interaction Issues," Report of the Second Steam Explosion Review Group (SERG-2), NUREG-1524, 1996.
98. Magallon, D., Huhtiniemi, I., and Hohmann, H., "Lessons Learnt from FARO/TERMOS Corium Melt Quenching Experiments," Nuclear Engineering and Design, 189, pp.223-238, 1999.
99. Magallon, D. and Huhtiniemi, I., "Corium Melt Quenching Tests at Low Pressure and Subcooled Water in FARO, Nuclear Engineering and Design," 204, pp.369-376, 2001.
100. Huhtiniemi, I., Magallon, D., and Hohmann, H., Results of Recent KROTOS FCI Tests: Alumina versus Corium Melts, Nuclear Engineering and Design, 189, pp.379-389, 1999.

101. Huhtiniemi, I. and Magallon, D., Insight into Steam Explosions with Corium Melts in KROTOS, Nuclear Engineering and Design, 204, pp.391-400, 2001.
102. Kim, J. H., et al., "A Study on Intermediate Scale Steam Explosion Experiments with Zirconia and Corium Melts," Transactions of the International Congress on Advanced Nuclear Power Plants (ICAPP), Hollywood, FL, June 9-13, 2002.
103. Song, J. H., Kim, J. H., Min, B. T., and Hong, S. W., "The Effect of Composition on the Mechanism of Prototypic Steam Explosion," The 11th Topical Meeting on Nuclear Reactor Thermal-Hydraulics (NURETH-11), Pope's Palace Conference Center, Avignon, France, October 2-6, 2005.
104. EPRI TR-103413, "The MELTSPREAD-1 Computer Code for the Analysis of Transient Spreading and Cooling of High-Temperature Melts – Code Manual," December 1993.
105. AREVA NP Inc. Technical Document, 38-9008026-000, "Description, Verification and Application of the Computer Code WALTER," December 2005.
106. AREVA NP Inc. Technical Document, 38-9026695-000, "Development of MAAP4 Models for EPR-Specific Plant Design Features."
107. Baker, L., Faw, R. E., and Kulacki, F. A., "Post-accident Heat Removal – Part I: Heat Transfer Within an Internally Heated, Non-boiling Liquid Layer," Nuclear Science and Engineering, 61, pp. 222-230, 1976.
108. Thompson, D. H. and Fink, J. K., "ACE MCCI Test L2: Test Data Report Volume I - Thermal Hydraulics," Argonne National Laboratory, November 1988.
109. Thompson, D. H. and Fink, J. K., "ACE MCCI Test L6: Test Data Report Volume I - Thermal Hydraulics," Argonne National Laboratory, August 1991.
110. Thompson, D. H. and Fink, J. K., "ACE MCCI Test L7: Test Data Report Volume I - Thermal Hydraulics," Argonne National Laboratory, November 1991.
111. Alsmeyer, H. and Firnhaber, M., "Specification of the International Standard Problem ISP-30: BETA V5.1 Experiment on Melt\_Concrete Interaction," KfK and GRS, September 1990.
112. Alsmeyer, H., "Report on Recent BETA Experiments V5.1, V5.2 & V6.1," CSARP Meeting, Bethesda, MD, May 6-10, 1991.
113. Theofanous, T. G., Amarasooriya, W. H., Yan, H., and Ratnam, U., "The Probability of Liner Failure in a Mark I Containment," NUREG/CR-5423, 1990.

114. Sienicki, J. J., Chu, C. C. and Spencer, B. W., "Comparison of MELTSPREAD-1 Calculations of Corium Depth Next to the Mark I Liner with NUREG/CR-5423," NUREG/CR-6025, Section 4, 1993.

## **APPENDICES**

**Appendix A Basic Data and Calculations**

Preliminary values for certain key design parameters. Values have been abbreviated to two significant digits.

**Table A-1 Reactor Vessel Parameters**

--	--

**Table A-2 Reactor Cavity Parameters**

--	--

**Table A-3 Spreading Compartment Parameters**

--	--

**Table A-4 Containment Parameters**

--	--

## Appendix B Supporting Information on Sacrificial Concrete

### B.1 Introduction

The U.S. EPR is equipped with a spreading compartment to prevent basemat attack and basemat melt-through from molten corium in a severe accident. Component arrangement is shown in Figure B-1.

The principal idea behind the U.S. EPR spreading compartment is to spread the molten core on a large area lateral to the RPV. This measure transfers the core melt in a coolable configuration by significantly increasing the surface/volume ratio of the melt. The decay heat is removed from the melt's upper surface by flooding and quenching the melt from the top and at the melt's underside and lateral boundaries by the cooling structures of the spreading compartment.

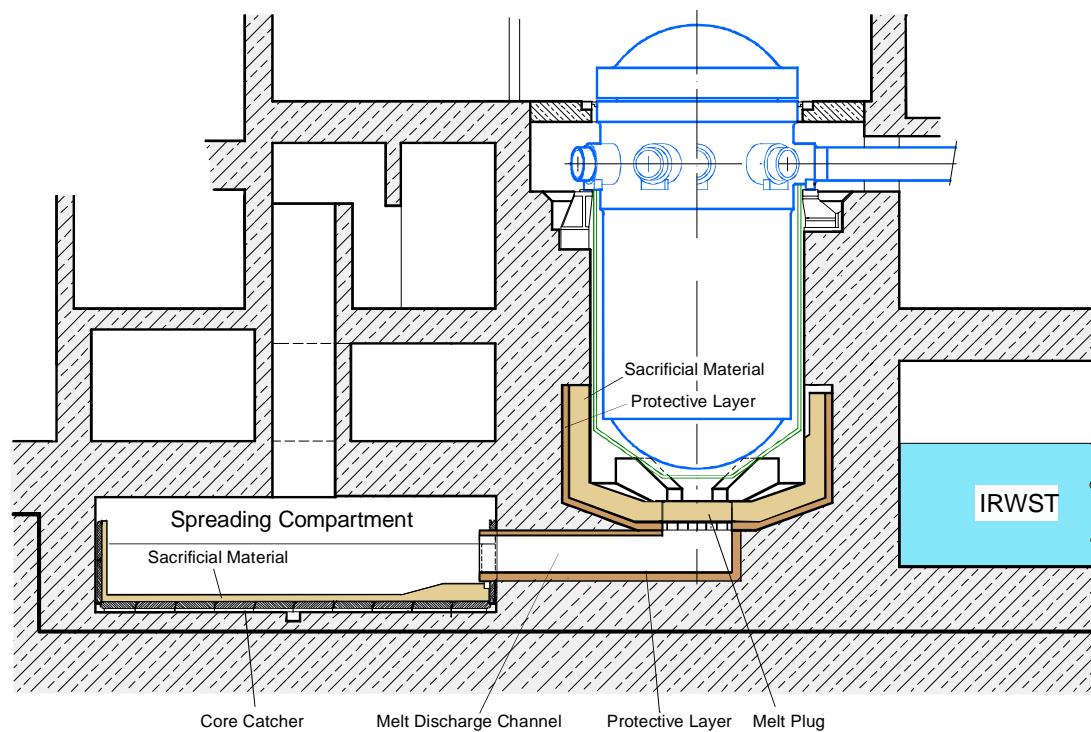


**Figure B-1 Cross-Section through the Core Melt Stabilization System of the EPR**

In response to a potential stepwise melt release from the RPV, the overall approach includes temporary melt retention in the reactor cavity. The objectives of the retention are:

- (i) to accumulate the melt inventory before discharging it into the spreading compartment in one event
- (ii) to condition the melt in terms of achieving favorable melt properties for melt spreading in parallel to restricting the spectrum of melt compositions at the time of spreading.

Melt accumulation is achieved by a layer of sacrificial concrete through which the melt must erode before it contacts and destroys the melt gate and spreads into the spreading compartment.

The interaction between melt and concrete, denoted MCCI, yields melt properties which are favorable for melt spreading. As the amount of the ablatable concrete is limited, the MCCI in the reactor cavity further restricts the spectrum of melt compositions at the time of spreading.

This Appendix provides a rationale why concrete has been selected as sacrificial material and for the choice of the aggregate composition. It further gives an overview of the mechanical and erosion properties of that concrete.

### ***B.2. Rationale for Selecting Concrete as Sacrificial Material***

Concrete was chosen as sacrificial material because of the following reasons:

1. MCCI is a relatively well-investigated severe accident phenomenon, for which a large experimental data base is available.
2. Representative experiments employing prototypic melts and different types of concrete, e.g. the ACE (Reference B-1) and MACE (Reference B-2 and B-3) tests showed that the concrete ablation rate approximately follows the power supply to the melt related to the boundary area of the pool. Further, they indicated that, due to the convective mixing by the generated gas, the MCCI favors a homogeneous heat flux distribution along the boundaries of the pool.

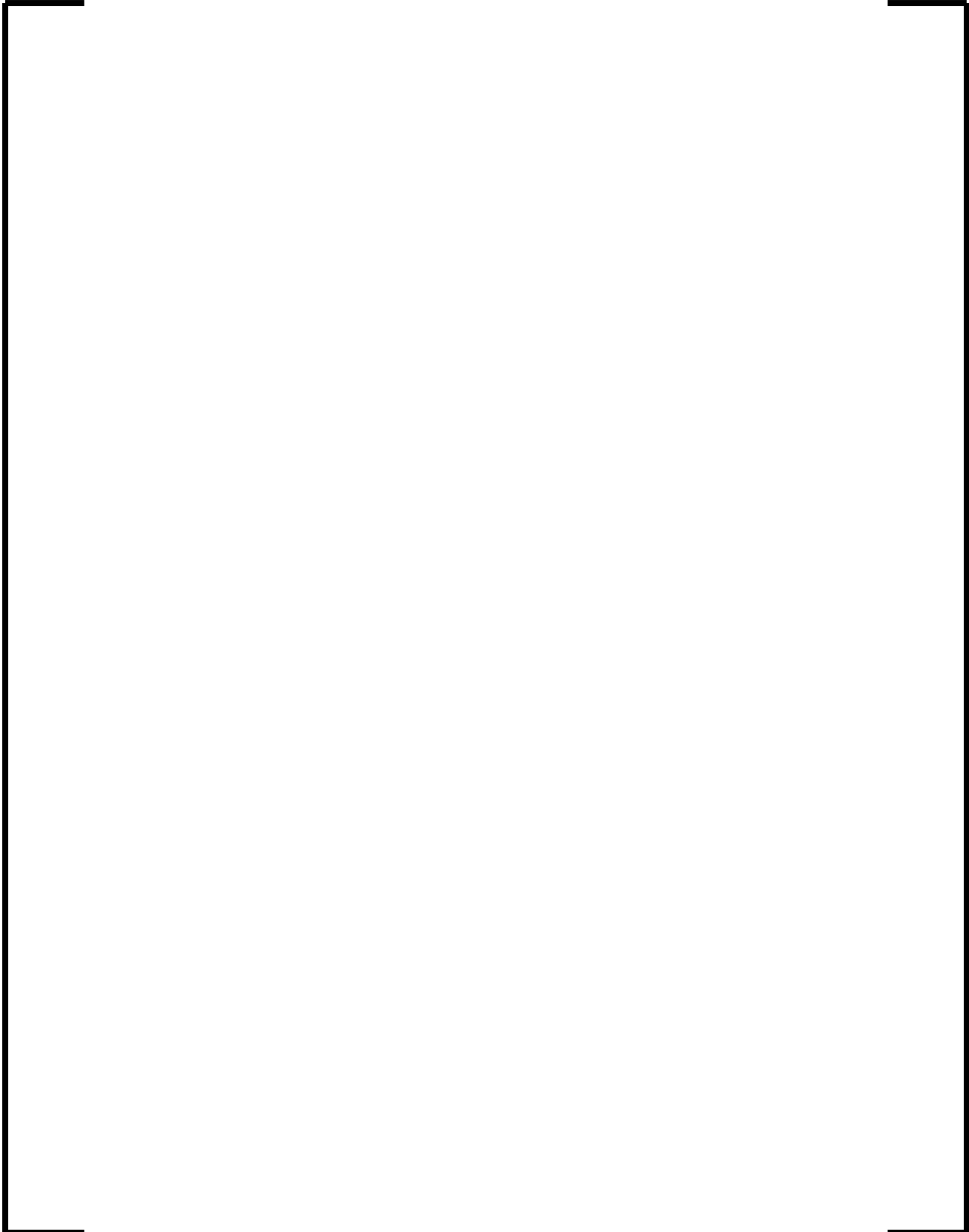
Combination of both effects yields self-adjusting characteristics of the MCCI which means that the velocity of the melt front progression into the concrete adjusts to the decay heat level and to the volume/surface ratio of the melt. Applied to the melt retention in the reactor cavity, the idea is that for an initially low amount of released melt, the decay heat, the volume/surface ratio of the interacting melt and thus the heat flux and ablation rate are also low. This extends the time that melt pours from the reactor pressure vessel can occur. For an initially high amount of released melt, this time window decreases in accordance with a reduced requirement for accumulating the melt.

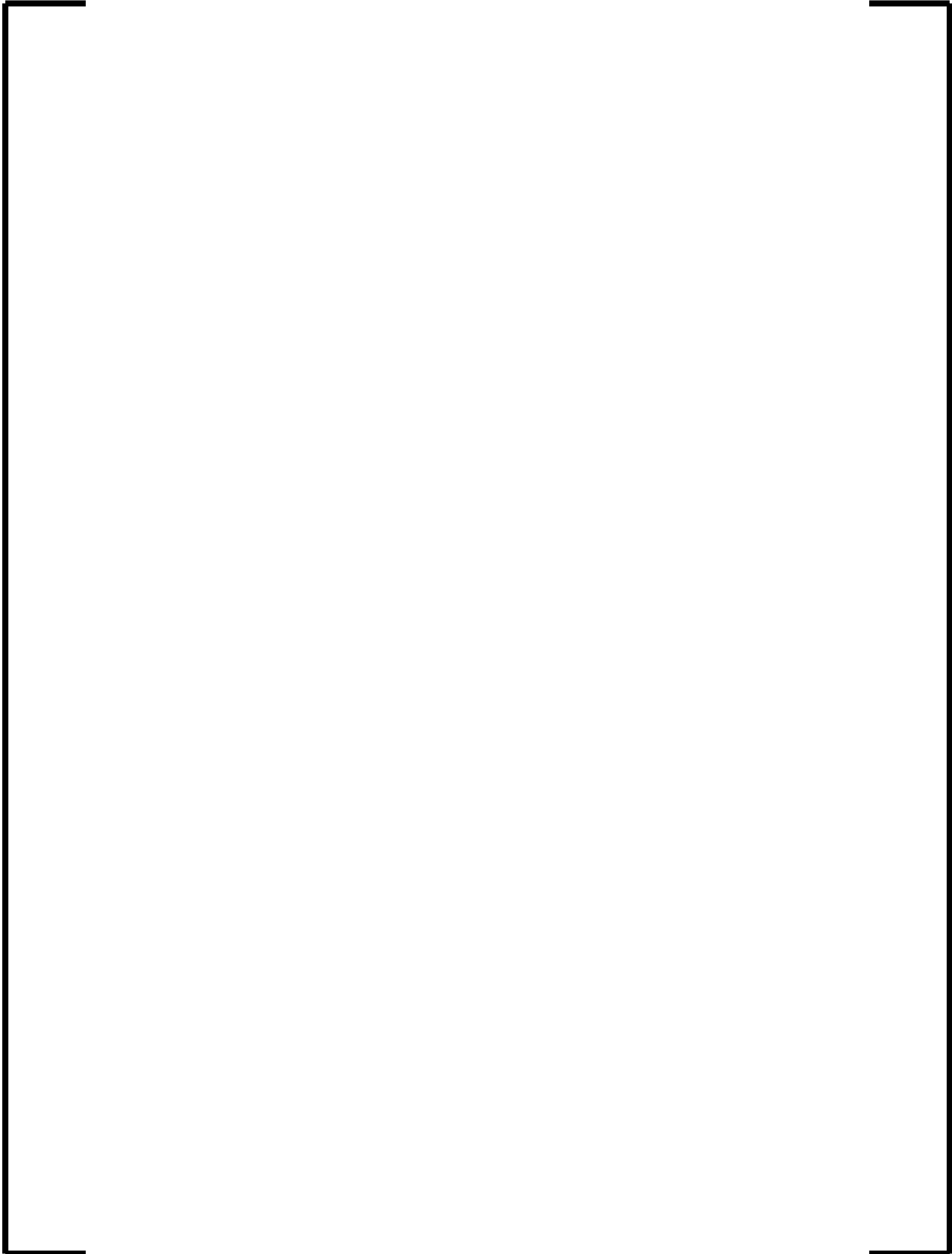
The self-adjusting characteristic further correlates the retention time with the time required to accumulate the core melt. In particular, if the first melt pour released into the cavity consists of a high fraction of the inventory, then the time to collect the residual melt is likely less than for low fractions. This effect is beneficial for defining the thickness of the sacrificial layer (Reference B-4).

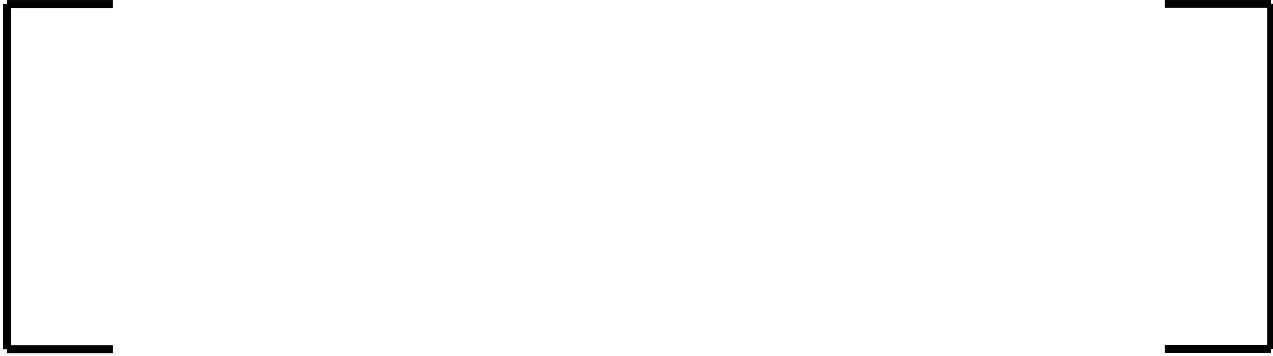
The ACE and MACE tests show that melt temperatures slightly decrease during the duration of the tests which indicates that the MCCI involves a low melt viscosity and thus establishes favorable conditions for melt spreading. These experiments tested concrete of different compositions (e.g., siliceous concrete vs. limestone concrete). This indicates that this phenomenon is independent of concrete composition. For application to severe accident mitigation, this characteristic is desirable since it broadens the possible concrete compositions that can be studied in the search for preferred concrete mixtures meeting the objectives of the temporary melt retention.

A principal objective of melt retention is the desire to minimize mass and energy release. Gas generation by MCCI constitutes an additional source for mass and energy release into the containment and thus must be considered for the design of measures that mitigate containment loads. Consequently, the selection of concrete must also take this issue into account, in addition to the issues of melt accumulation and melt conditioning.

***B.3 Composition and Mechanical Properties of the Sacrificial Concrete***

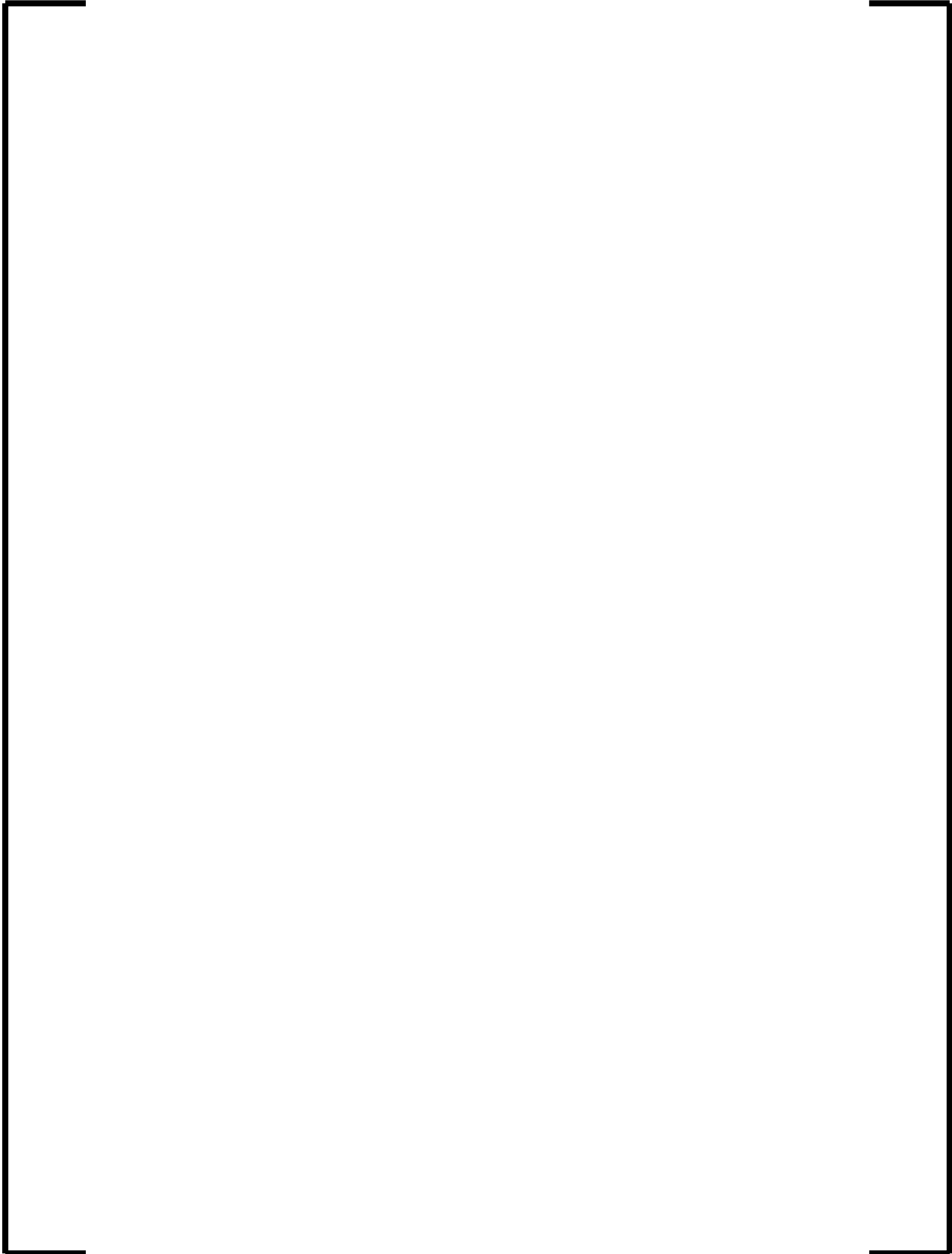


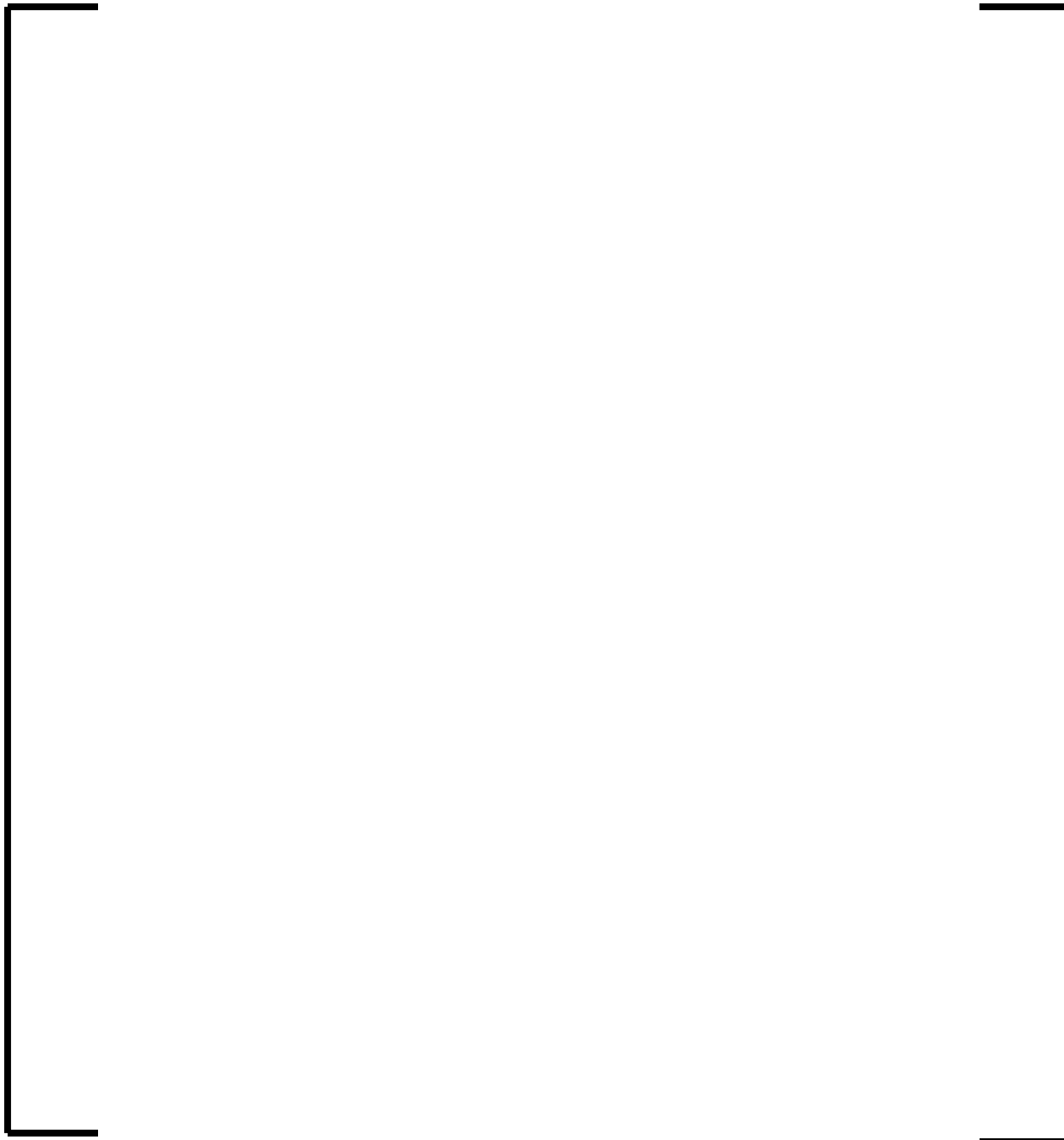




**Table B-1 Chemical composition of sacrificial siliceous concrete FeSi/PZ15/8**

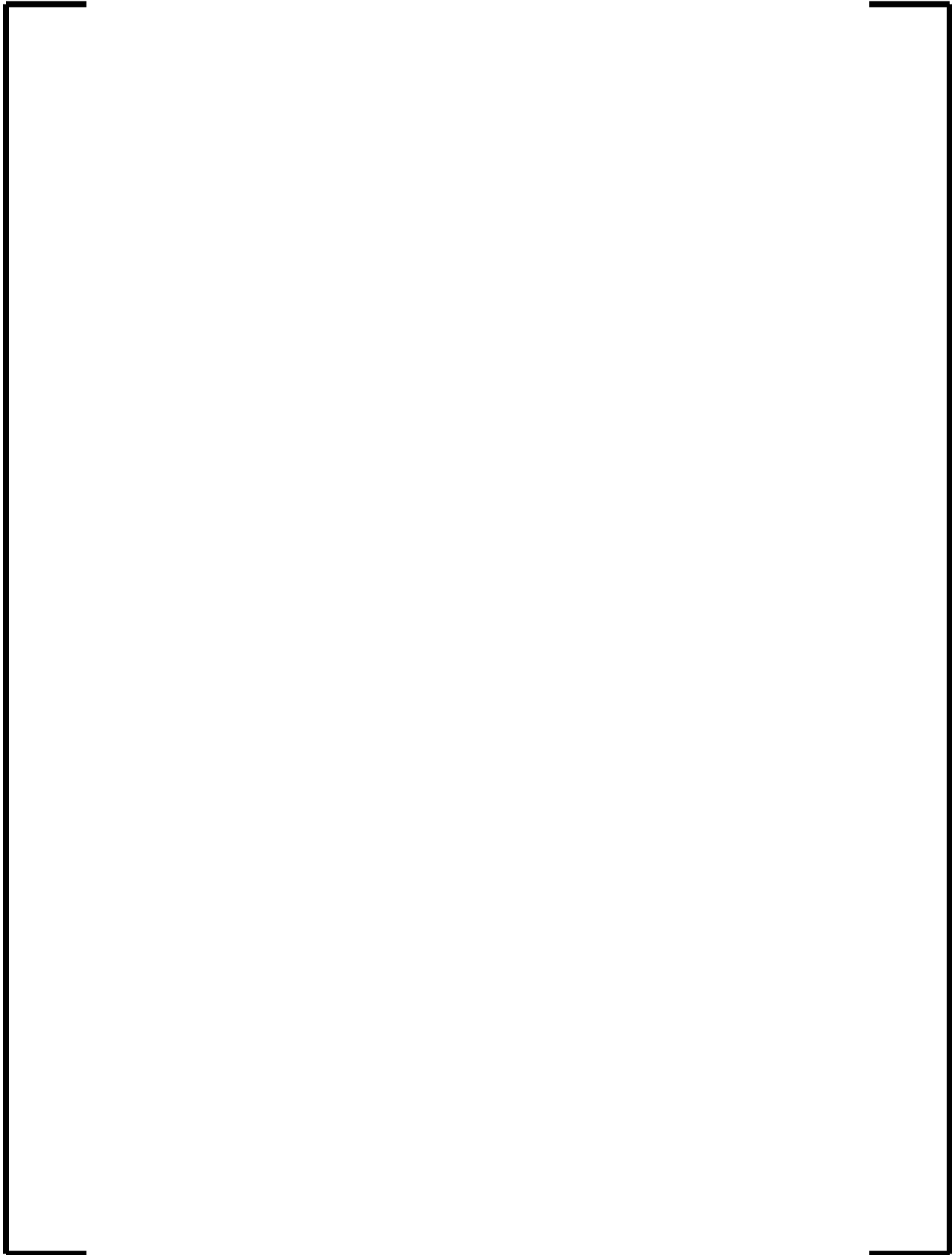
A large, empty rectangular box with a thick black border, occupying the lower half of the page. It is positioned directly below the caption and appears to be a placeholder for the data table described in the caption.





**Figure B-1 Volumetric solid fraction and decomposition enthalpy vs. temperature**





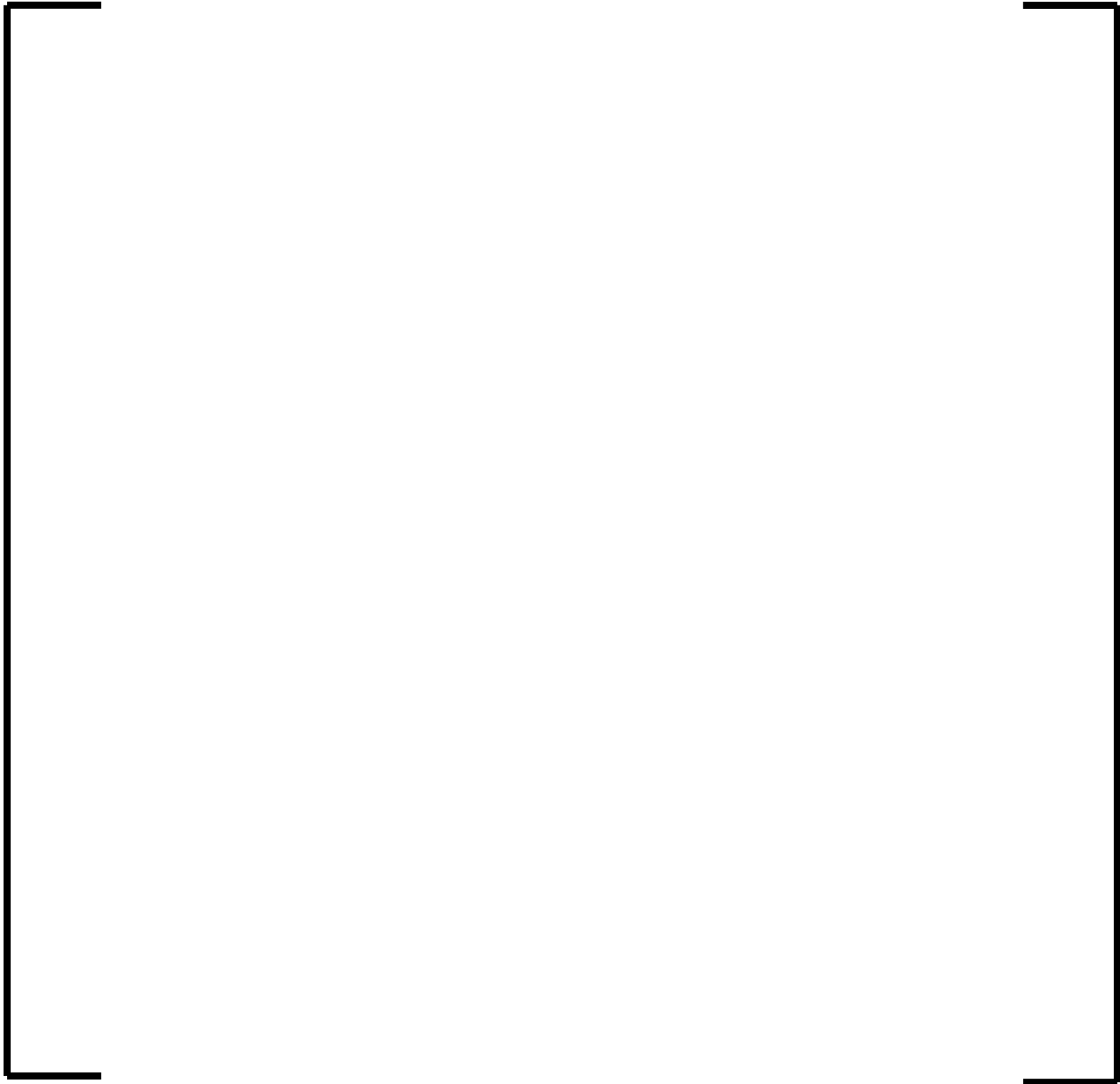


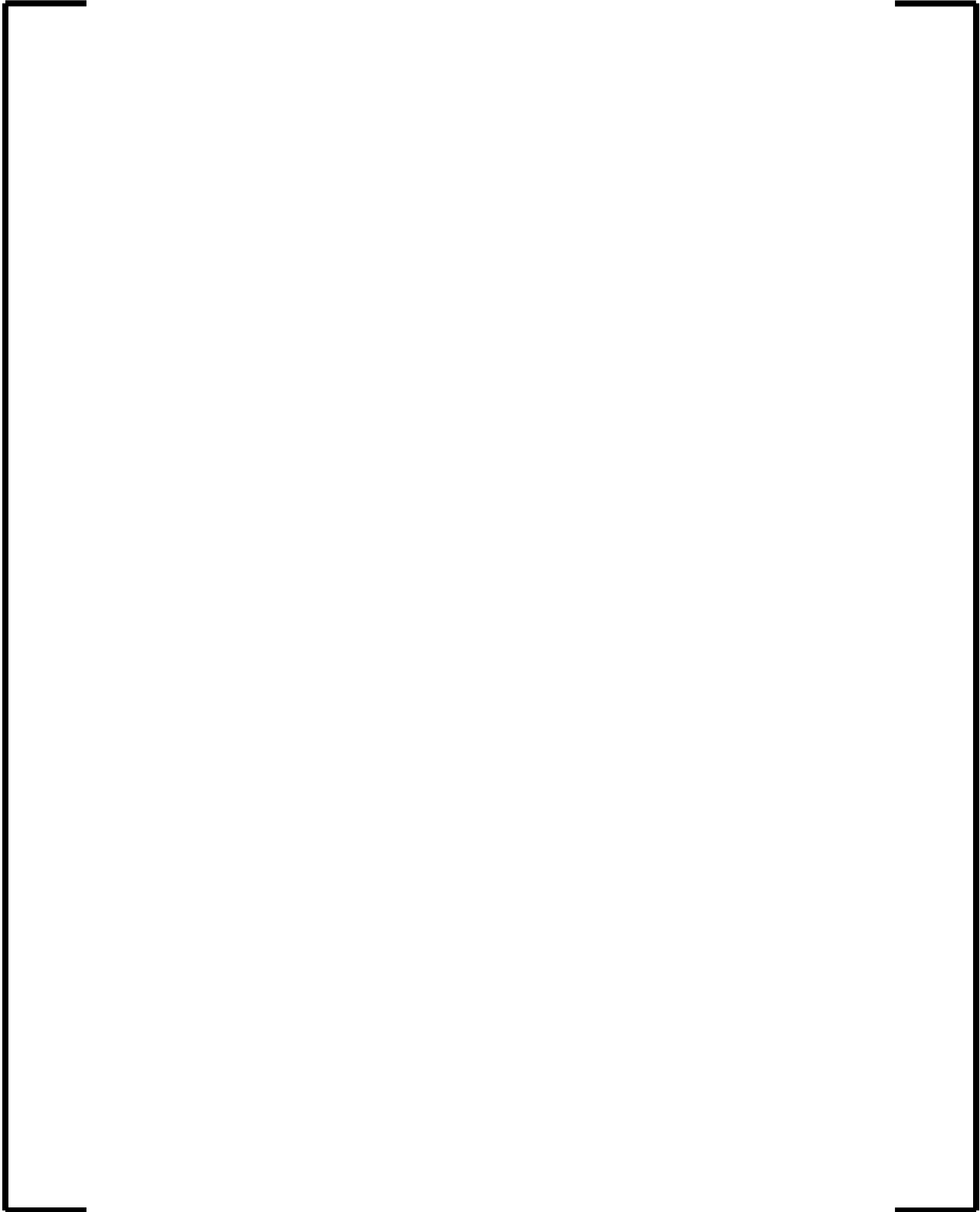


**Figure B-2: Skull-Melting Facility with HF Generator and Steel Vessel Containing the Cold Crucible and the Induction Coil**



**Figure B-3: Ablation Velocity Versus Power at the Melt/concrete Interface**

***B.5 Summary and Conclusions***





**B.6 References**

- B-1. Thompson, D.G., et al., "Compilation, analysis and Interpretation of ACE Phase C and MACE experimental data – MCCI Thermohydraulic results," ACEX TR-C-14, Vol. 1; Argonne Nat. Lab. Nov. 1997.
- B-2. Farmer, M.T. et al, "Mace Test M3b Data Report Volume 1," MACE-TR-D13, EPRI TR-108806, November 1997.
- B-3. Farmer, M.T. et al, "Mace Test M4 Data Report," MACE-TR-D16, August 1999.
- B-4. Nie, M. Fischer, M., "Use of Molten Core Concrete Interactions in the Melt Stabilization Strategy of the EPR," Proceedings, ICAPP 06, RENO, NV, USA, June 4-8, 2006.
- B-5. Farmer, M. T., Lomperski, S., Kilsdonk, D. J., Aeschlimann, R. W., "CCI-2 Test Results," Presented at the 6th OECD-MCCI Program Review Meeting, Argonne National Laboratory, 3-5 November, 2004.
- B-6. Nie, M., Fischer, M., Koller, M. 'Status of interpretation of selected transient MCCI experiments conducted in the frame of the CORESA R&D project', Proceedings of Jahrestagung Kerntechnik, Stuttgart, Germany, 14.-16. May 2002.
- B-7. Nie, M., "Temporary Melt Retention in the Reactor Pit of the European Pressurized Water Reactor (EPR)," Dissertation, Universität Stuttgart, Institut für Kernenergetik und Energiesysteme, February 2005.

## **Appendix C MELCOR 1.8.6 Model of the U.S. EPR**

To support benchmark studies of the U.S. EPR severe accident performance predicted using MAAP4, an integral MELCOR model of the plant was developed. This section provides a brief description of MELCOR 1.8.6, applicability to severe accident phenomena possible in the U.S. EPR, and the development of the MELCOR model of the U.S. EPR.

### ***C.1 Description of MELCOR 1.8.6***

MELCOR is a fully integrated, engineering-level computer code that models the progression of severe accidents in light water reactor (LWR) nuclear power plants. MELCOR has been developed at SNL for the U.S. Nuclear Regulatory Commission (NRC) as a second-generation, plant risk-assessment tool and the successor to the Source Term Code Package. A broad spectrum of severe accident phenomena in both boiling and pressurized water reactors is treated in MELCOR in a unified framework. These include: thermal-hydraulic response in the reactor coolant system (RCS); reactor cavity, containment, and confinement buildings; core heatup, degradation, and relocation; core-concrete attack; hydrogen production, transport, and combustion; fission product release and transport behavior. Current uses of MELCOR include estimation of severe accident source terms and their sensitivities and uncertainties in a variety of applications.

The MELCOR code is composed of an executive driver and a number of major modules, or packages, that together model the major systems of a reactor plant and their generally coupled interactions. Reactor plant systems and their response to off-normal or accident conditions include:

- Thermal-hydraulic response of the RCS, the reactor cavity, the containment, and the confinement buildings.
- Core uncovering (loss of coolant), fuel heatup, cladding oxidation, fuel degradation (loss of rod geometry), and core material melting and relocation.

- Heatup of reactor vessel lower head from relocated fuel materials and the thermal and mechanical loading and failure of the vessel lower head, and transfer of core materials to the reactor vessel cavity.
- Core-concrete attack and ensuing aerosol generation.
- In-vessel and ex-vessel hydrogen production, transport and combustion.
- Fission product release (aerosol and vapor), transport and deposition.
- Behavior of radioactive aerosols in the reactor containment building, including scrubbing in water pools and aerosol mechanics in the containment atmosphere such as particle agglomeration and gravitational settling.
- Impact of engineered safety features on thermal-hydraulic and radionuclide behavior.

The various code packages have been written using a modular structure with well-defined interfaces between them. This allows the exchange of complete and consistent information among them so that all phenomena are explicitly coupled at every step. The structure also facilitates maintenance and upgrading of the code.

Like MAAP4.07, MELCOR has been developed to address a broad range of severe accident phenomena occurring in an integral manner. The applicability of MELCOR 1.8.6's phenomenological models to the U.S. EPR severe accidents is summarized in Table C-1.

**Table C-1 MELCOR Severe Accident Phenomena Modeling Capability**

Phenomena	MELCOR 1.8.6
1. Fuel rod degradation	Yes
2. Melt progression/ablation through surrounding core structure	Yes
3. Core melt relocation to lower head	Yes
4. In-vessel fuel-coolant interaction	No
5. In-Vessel Oxide/Metal separation	Yes <sup>(1)</sup>
6. Crust formation and failure	Yes <sup>(2)</sup>
7. In-vessel debris formation	Yes
8. RCS/RPV failure modes	Yes
9. Reactor Cavity Thermal Radiation	Yes
10. Melt conditioning in Reactor Cavity/MCCI	Yes
11. Melt Spreading in Spreading compartment	No
12. MCCI in Spreading compartment	Yes
13. Ex-vessel Oxide/Metal separation	Yes
14. Basemat Cooling	Yes
15. Melt Flooding and Quenching	Yes
16. Steam/Hydrogen Transport	Yes
17. Hydrogen Recombination	Yes
18. In-containment Hydrogen Combustion	Yes
19. Long-term heat removal from the containment.	Yes
20. Fission Product Transport in containment.	Yes

<sup>(1)</sup> Modeling of molten pools within the vessel is a new capability with MELCOR 1.8.6.

<sup>(2)</sup> Modeling of heat transfer from molten pool through a crust within the vessel is a new capability with MELCOR 1.8.6.

## **C.2 Description of U.S. EPR Model**

### **C.2.1 Reactor Coolant System**

The U.S. EPR model of the reactor coolant system was modeled with the Control Volume Hydrodynamics, Flow Path, Heat Structure, Core, Decay Heat, Radionuclide, Material Properties, Non-Condensable Gas, Tabular Function and Control Function Packages of MELCOR 1.8.6. The reactor coolant system was modeled with conventional nodalization based on the MELCOR Zion model nodalization, with additional detail as necessary to model U.S. EPR-specific features, most notably the steam generators.

The four main coolant loops and associated reactor coolant pumps and steam generators of the U.S. EPR were lumped into two loops: the single loop contains the

pressurizer and any breaks that are initiated and the triple loop models the three remaining intact loops.

**C.2.1.1 Main Coolant Lines**

The nodalization of the single loop of the main coolant lines is shown in Figure C-2. The triple loop mirrors the single loop with volumes and flow areas adjusted appropriately.

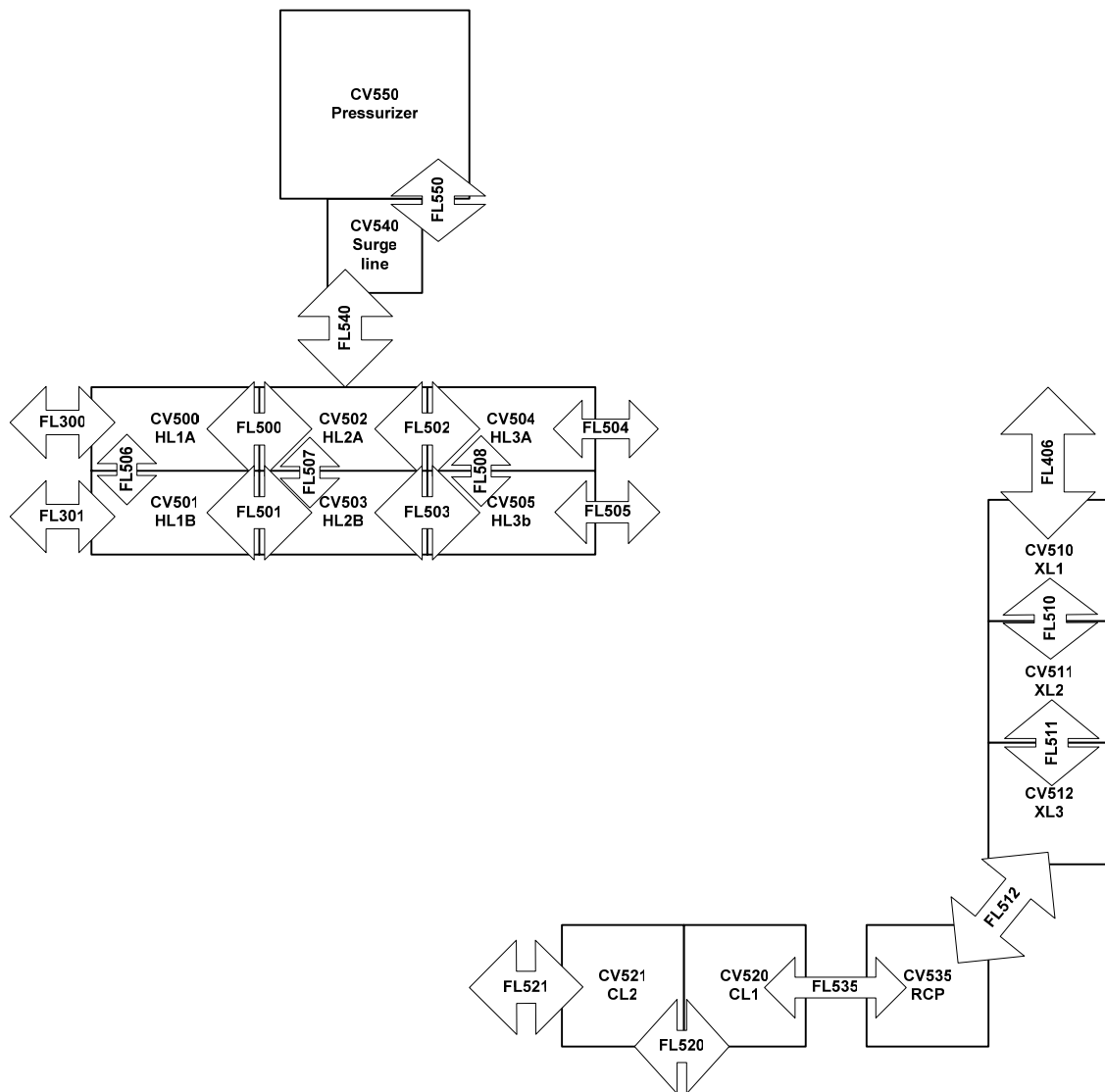


**Figure C-2 Single Loop Main Coolant Line Nodalization**

The single and triple loops of the main coolant lines are each modeled by twelve control volumes. The hot leg nodalization is subdivided to model the top and bottom of each

hot leg segment by separate control volumes to approximate natural circulation flow during high pressure accidents.

The main coolant lines are modeled as heat structures with adiabatic outer surfaces to simulate perfect insulation around the piping.

The RCPs were modeled with homologous pump models to provide the steady state and coast down pressure rises across the pump. The RCPs trip when the reactor scrams, a user-input time is reached, or offsite power is lost; time delay for signal processing is not modeled.

### **C.2.1.2 Reactor Pressure Vessel**

Above the lower plenum, the RPV structure was modeled using cylindrical heat structures with adiabatic outer surfaces to simulate perfect insulation. The RPV head was modeled as a hemispherical heat structure with an adiabatic outer surface; the heat transfer area was not conserved.

The RPV lower head was treated by MELCOR's Core Package. The lower head was modeled by 10 segments, each with 17 temperature nodes, giving mesh intervals on the order of 0.4 in (1 cm). Creep rupture parameters appropriate to the lower head carbon steel were input to MELCOR through modification of the appropriate sensitivity coefficients. Other default carbon steel properties in MELCOR were considered appropriate for the U.S. EPR lower head. Insulation on the lower head was not modeled.

### **C.2.1.3 Reactor Core**

The reactor core, downcomer, lower plenum, upper plenum and dome regions were modeled by 34 control volumes as shown in Figures C-3 and C-4. Twenty control volumes model the core region between the lower core support plate and upper core plate. These control volumes model a two-dimensional, axisymmetric core with four axial levels and five radial rings with appropriate grid-like connections. The control volume axial heights in the core region are less than 4.1 ft. There are ten control volumes in the upper plenum, two levels of five rings.

There are two bypass control volumes and additional flow paths to model the bypass between reactor nozzles, bypass to the upper head, bypass through the heavy reflector, bypass between the heavy reflector and core barrel, bypass through guide tubes, and bypass between the core and heavy reflector. These bypass control volumes and flow paths are shown in Figure C-5.

MELCOR's Core package also models the fluid volume from the lower plenum to the upper core plate, within the core barrel. The core cells are divided into seventeen axial levels, four in the lower plenum and ten in the active core region. The three remaining levels model the lower core support plate region, immediately above and below the active fuel. Core cell height in the active core is 1.4 ft. In the core region, the core cells are divided into five radial rings, as are the control volumes. In the lower plenum, a sixth ring is added to be consistent with the curved lower head modeling in MELCOR 1.8.6.

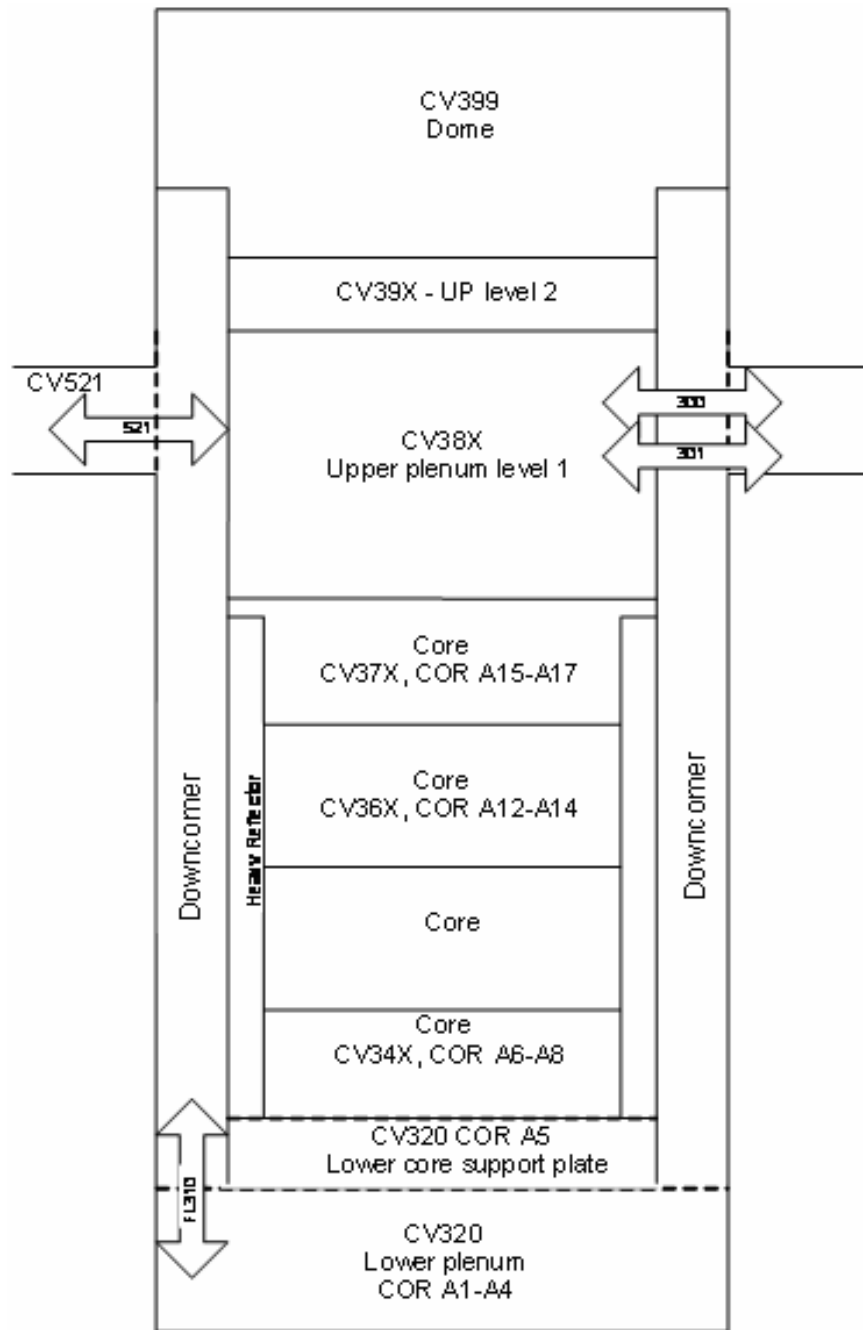


**Figure C-3 Reactor Pressure Vessel Nodalization, General View**

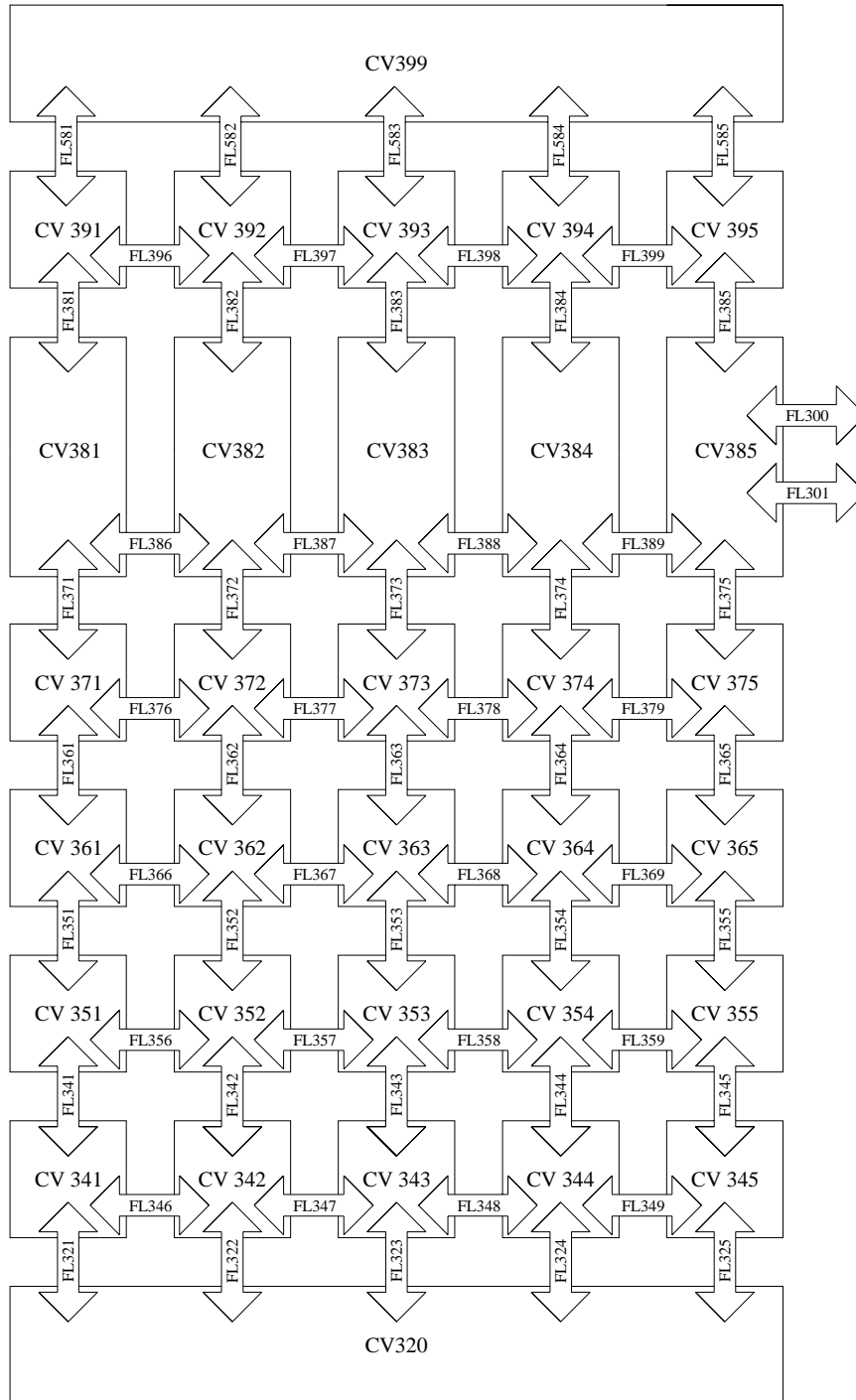


**Figure C-4. Reactor Core and Upper Plenum and Dome  
Control Volume Nodalization**

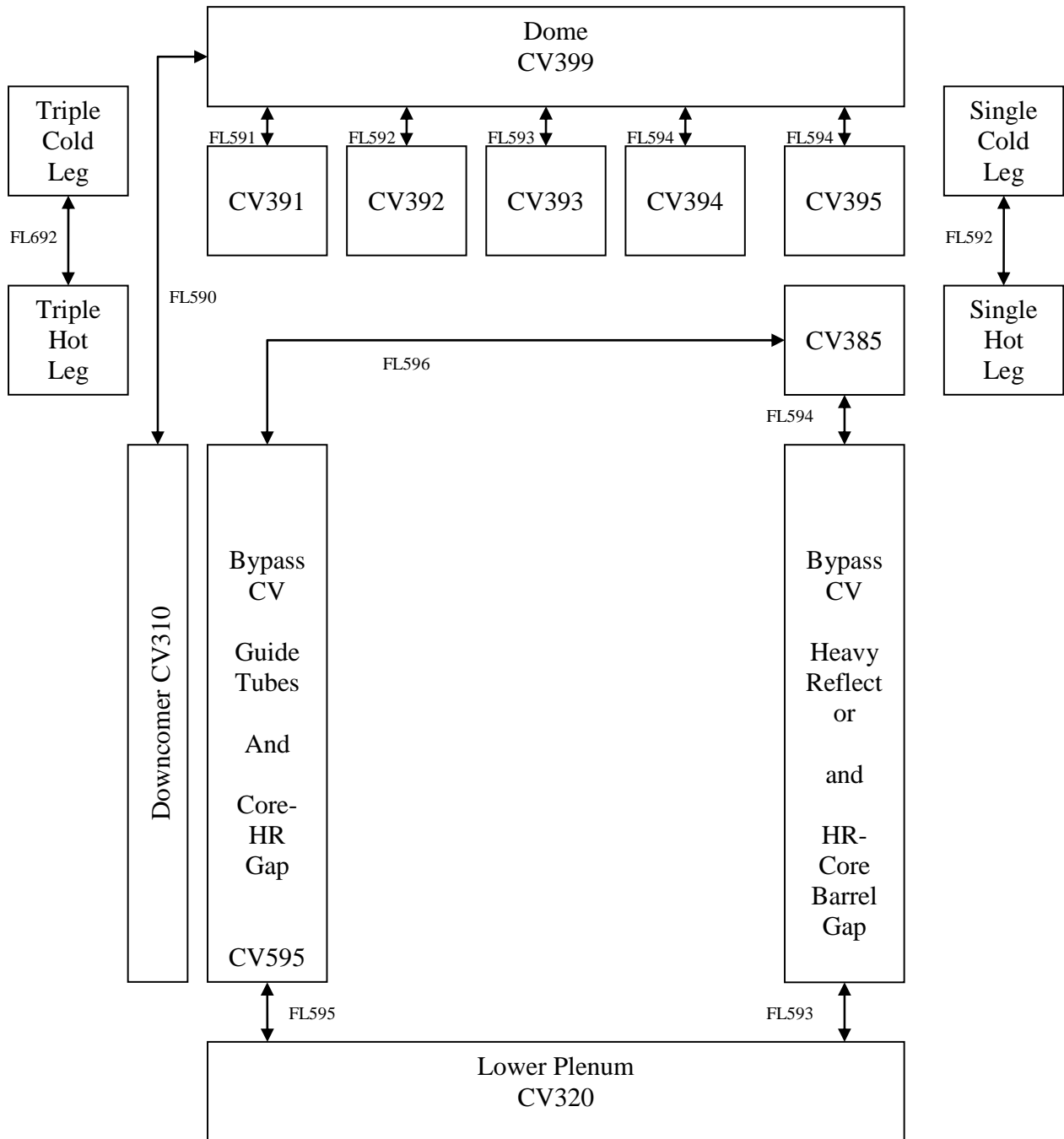


**Figure C-5. Nodalization for Bypass Flows**

Reactor vessel internal structures in the lower plenum up to the upper core plate within the core barrel are modeled by the Core Package. The control poison material is modeled in the reactor pressure vessel as if the control rods are fully inserted.

Structures modeled by the Core Package are:

- Lower core support plate
- Fuel
- Cladding
- Mixing and end grids
- Top and bottom fuel assembly nozzles
- Guide tubes
- Control rods
- Heavy reflector

Reactor vessel internal structures above the upper core plate and outside of the heavy reflector are modeled by heat structures. Structures modeled by heat structures are:

- Upper core plate
- Control rod guide assemblies
- Support columns
- Instrumentation tubes
- Upper core support plate
- Core barrel

The reactor fission power is calculated by control function from the nominal operating power and the steady state decay heat level. The decay heat was calculated as a function of time after reactor trip from the ANS 1979 standard with heavy actinide contribution (Reference C.1). Decay heat is modeled out to ten days after reactor trip.

The reactor will trip instantly if one of the following criteria is met:

- Loss of power at a user-input time

- Low pressurizer pressure
- High pressurizer pressure
- Low steam generator water level
- High steam generator water level

The reactor trips instantaneously; time for signal delay and control rod insertion are neglected. Residual fission power is also neglected; when the reactor trips the fission power drops to 0.0 W and the decay heat remains.

Radionuclide package input allows tracking of fission products and other radionuclides and their associated decay heat through the primary system, core melt stabilization system and containment during a severe accident. The initial fission product inventories and associated decay heat for each class of radionuclides were input from ORIGEN calculations for the U.S. EPR. The total radionuclide decay heat is normalized to the total decay heat to ensure the correct amount of heat generation in the system.

#### **C.2.1.4 Safety Injection Systems**

The U.S. EPR's passive and active safety injection systems are modeled: accumulator injection, medium head safety injection and low head safety injection.

Accumulator injection was modeled with control function input to calculate the rate at which liquid is delivered to the single and triple loops until the initial accumulator liquid mass is exhausted. Injection of nitrogen after the accumulator liquid has been emptied was not modeled.

The active safety injection systems were modeled for the single and triple loops. If the safety injection systems are available, as set by the user, the rate of injection is based on the cold leg pressure. Liquid is removed from the IRWST at the same rate at which it is injected by the safety injection systems. The temperature of the injected liquid was set to the IRWST temperature; the heat exchangers in the safety injection systems were not modeled. The user may activate the safety injection systems upon restart of a MELCOR calculation to model late reflood.

### **C.2.1.5 Pressurizer**

The pressurizer and surge line nodalization are shown on Figure C-2. The surge line from the single hot leg to the pressurizer was modeled with a single control volume with a detailed altitude/volume table. The pressurizer was modeled by a single control volume and provides a constant pressure and temperature boundary condition to the system during the steady state initialization. Flow paths with appropriate control logic were used to model the depressurization system.

### **C.2.1.6 Reactor Coolant System Depressurization**

The reactor coolant system depressurization system was modeled with flow path input connecting the pressurizer to the containment. Three safety valves and two severe accident valves are modeled by separate flow paths. The safety valves open and close corresponding to their designed pressure setpoints. The severe accident valves are modeled to open and remain open after the vapor temperature in the hot legs exceeds a user-input criterion.

The depressurization valves allow primary coolant to empty directly to the pressurizer compartment of the containment nodalization; the PRT is not separately modeled.

### **C.2.1.7 Steam Generators**

The steam generator nodalization is very fine in order to obtain the heat transfer performance of the U.S. EPR steam generators. Figure C-6 shows the steam generator lower plenum and tube bundle nodalization. The tube bundle was modeled by two equivalent tubes to allow natural circulation flow. Figure C-7 shows the secondary side nodalization of the steam generators. Ten control volumes model each of the separator boiler regions.

The tube bundle was modeled by cylindrical heat structures to conserve the total heat transfer area; the heat structures were divided as necessary for the control volume nodalization. The tube bundle was modeled as Inconel 690 using a user-defined material property table.

Other components of the steam generator modeled as heat structures are:

- Tube sheet
- Lower plenum shell
- Outer shell
- Bundle wrapper
- Double wrapper
- Divider plate
- Separators

The lower plenum shell and outer shell of the steam generator were modeled as heat structures with adiabatic outer surfaces to model perfect insulation on these components.

The steam generator feedwater was modeled as a constant temperature source of liquid water in the cold downcomer. By default, the feedwater is lost when the reactor trips but partial feedwater after trip can be modeled. Emergency feedwater is not modeled separately.

The steam generator secondary side pressure and temperature boundary condition is fixed (defined at the exit of the steam generators to the steam lines). The steam lines are not explicitly modeled.



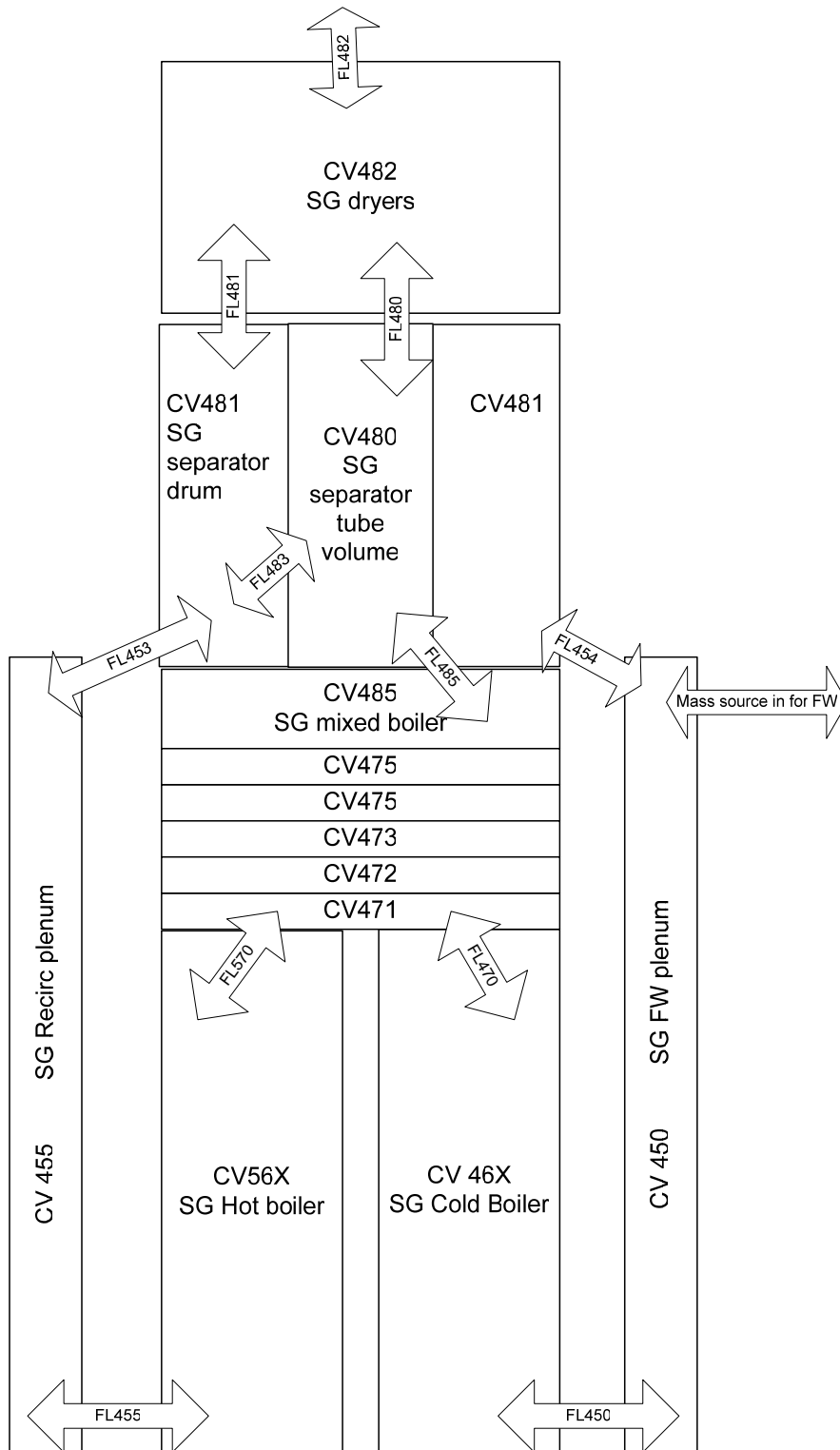


**Figure C-7. Steam Generator Secondary Side Nodalization**

### C.2.2 Core Melt Stabilization System

The core melt stabilization system (CMSS) was modeled in MELCOR using the Control Volume Hydrodynamics, Flow Path, Heat Structure, Cavity, Control Function, Tabular Function, Non-Condensable Gas, and Radionuclide packages. Non-condensable gas package input allowed initial specification of atmospheric conditions in the appropriate control volumes. Radionuclide package input was developed as necessary to allow tracking of radionuclides and associated decay heat outside of the primary system.

Figure C-8 shows the nodalization of the CMSS and the SAHRS.

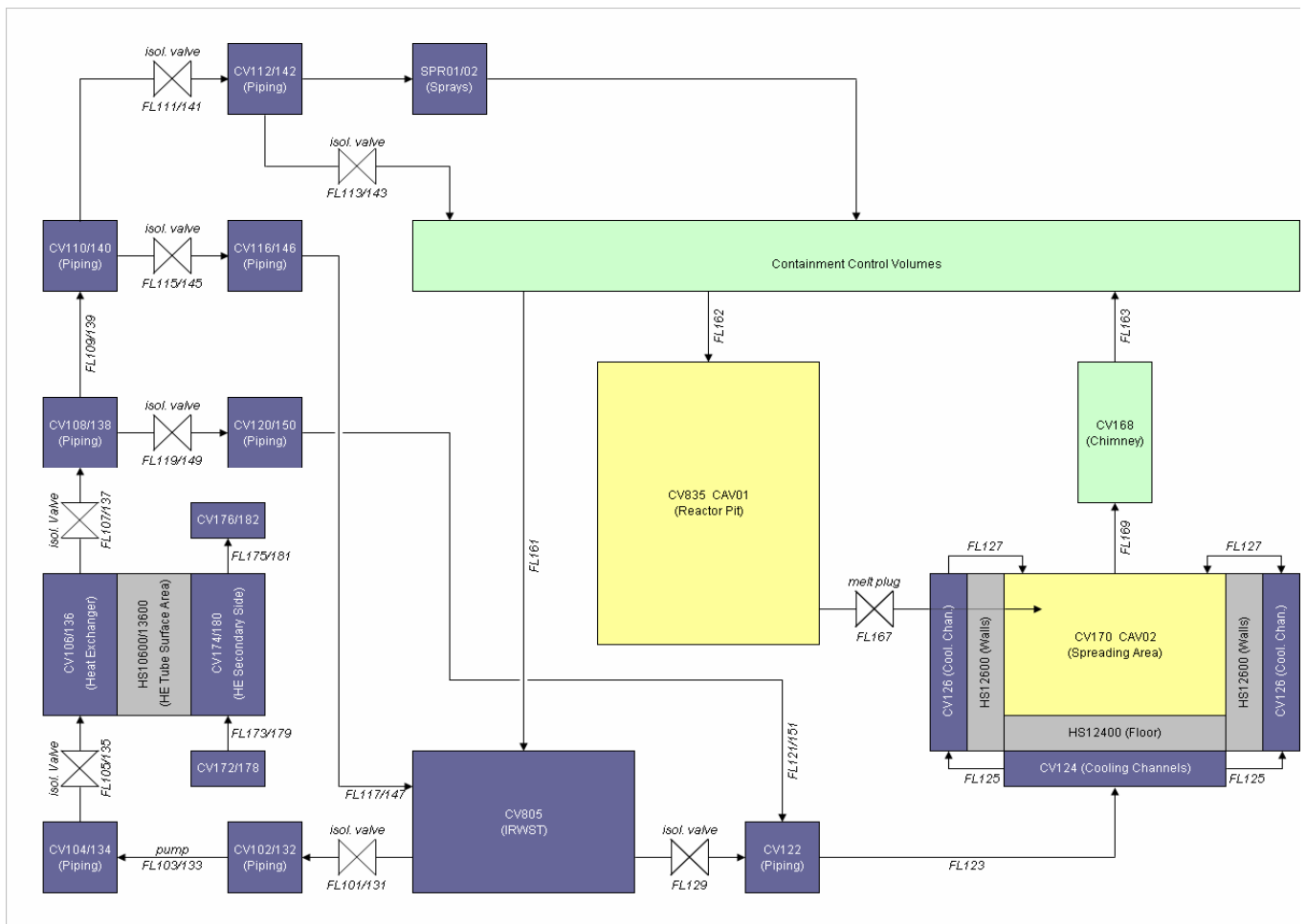


Figure C-8. CMSS/SAHRS Nodalization

### **C.2.2.1 Reactor Cavity**

The fluid volume of the reactor cavity and the volume around the RPV were modeled by a single control volume. The concrete present in the reactor cavity was modeled by Cavity input. Gate material and the zirconia protective material were not modeled.

Corium debris is transferred into the reactor cavity from the Core package when the RPV lower head fails, as determined by the Core package. Control functions were developed to allow the transfer of corium from the reactor cavity to the spreading area when the thickness of concrete in the cavity has been ablated and a user-set time to allow for gate failure and non-uniform ablation has passed.

Flow paths connect the reactor cavity control volume to the rest of the containment, allowing some fluid to enter the reactor cavity and condense before vessel failure; breaks close to the RPV empty the primary fluid into the reactor cavity.

### **C.2.2.2 Spreading Compartment**

The spreading compartment fluid area is modeled by a control volume; another control volume models the steam chimney which connects the spreading compartment to the bulk of the containment. The sacrificial concrete of the spreading compartment was modeled through Cavity package input. The melt transferred to the spreading area cavity is instantly spread over the entire available area.

The cooling channels below the sacrificial concrete and on the sides of the spreading compartment were modeled by bottom and side control volumes with associated flow paths and heat structures. The bottom cooling channel structures were modeled as a slab heat structure; the mass of the structure was conserved.

Due to limitations of the MELCOR Cavity package, bottom cooling of the melt cannot be modeled explicitly. In order to model the fluid conditions in the bottom cooling channels, the temperature at the top of the bottom cooling channel heat structure was set to the maximum corium temperature in the spreading area; the insulating effect of any remaining concrete was neglected.

The cooling channels on the side of the spreading compartment are modeled by a second slab heat structure whose boundary conditions are determined by the fluid conditions in the side cooling channel control volume and the spreading compartment.

### **C.2.2.3 Severe Accident Heat Removal System**

The SAHRS was modeled in MELCOR using the Control Volume Hydrodynamics, Flow Path, Heat Structure, Spray, Control Function, Tabular Function, Non-Condensable Gas, and Radionuclide packages. Non-condensable gas package input allowed initial specification of atmospheric conditions in the appropriate control volumes. Figure C-8 shows the SAHRS nodalization.

The SAHRS has three modes of operation. The passive flooding and containment spray modes are modeled; active recirculation is not modeled.

### **C.2.2.4 Passive Flooding**

When corium melt is transferred to the spreading area, control logic is used to open the passive flooding valve, allowing water to flow out of the IRWST, into the cooling channel control volumes, and overflowing into the spreading compartment, covering the molten corium. The flow path input was developed to limit the flooding rate to the design value.

The Cavity package/Control Volume Hydrodynamics package interface in MELCOR allows the hot corium to be top cooled by the passive flow from the IRWST. Steam and non-condensable gases generated from concrete ablation are released from the spreading area into the steam chimney and to the remainder of the containment.

### **C.2.2.5 Containment Spray**

The containment sprays are activated if the containment dome pressure exceeds the user-input limiting pressure for spray activation. Two spray lines are modeled. When the containment sprays are activated, fluid is pumped from the IRWST through the SAHRS heat exchanger and to the spray headers located in the containment dome. The secondary side of the SAHRS heat exchangers is modeled by fluid sources and sinks to model the energy removed to the ultimate heat sink. The containment spray volumetric flow rate is constant after the sprays have been activated.

### **C.2.2.6 Active Recirculation**

The containment sprays can be activated by the user, as needed, to model the long-term containment heat removal. Two recirculation lines were modeled but are initially isolated by setting the flow area of the recirculation path to zero when the containment sprays are active. When the long-term recirculation is activated, fluid is pumped from the IRWST through the SAHRS heat exchanger and to the spreading compartment cooling structure inside the containment. The secondary side of the SAHRS heat exchangers was modeled by fluid sources and sinks to model the energy removed to the ultimate heat sink.

### **C.2.3 Containment**

The U.S. EPR containment was modeled in MELCOR using the Control Volume Hydrodynamics, Flow Path, Heat Structure, Passive Autocatalytic Recombiner, Burn, Control Function, Tabular Function, Non-Condensable Gas, and Radionuclide packages.

Non-condensable gas package input allowed initial specification of atmospheric conditions in the appropriate control volumes. Radionuclide package input was developed as necessary to allow tracking of radionuclides and associated decay heat outside of the primary system.

#### **C.2.3.1 General Arrangement**

The containment was modeled by 28 control volumes divided by the logical geometry and connectivity of the containment compartments, as shown in Figure C-9. The control volumes were assembled in a grid-type arrangement. Multiple flow paths connect the control volumes for modeling open areas between adjacent compartments. Control logic was used to determine whether doors and other pressure-dependent connections are open, based on the pressure in the control volumes on either side of the boundary, and adjust the appropriate flow paths accordingly. All control volumes in the containment initially contain nitrogen and oxygen at atmospheric pressure and temperature.

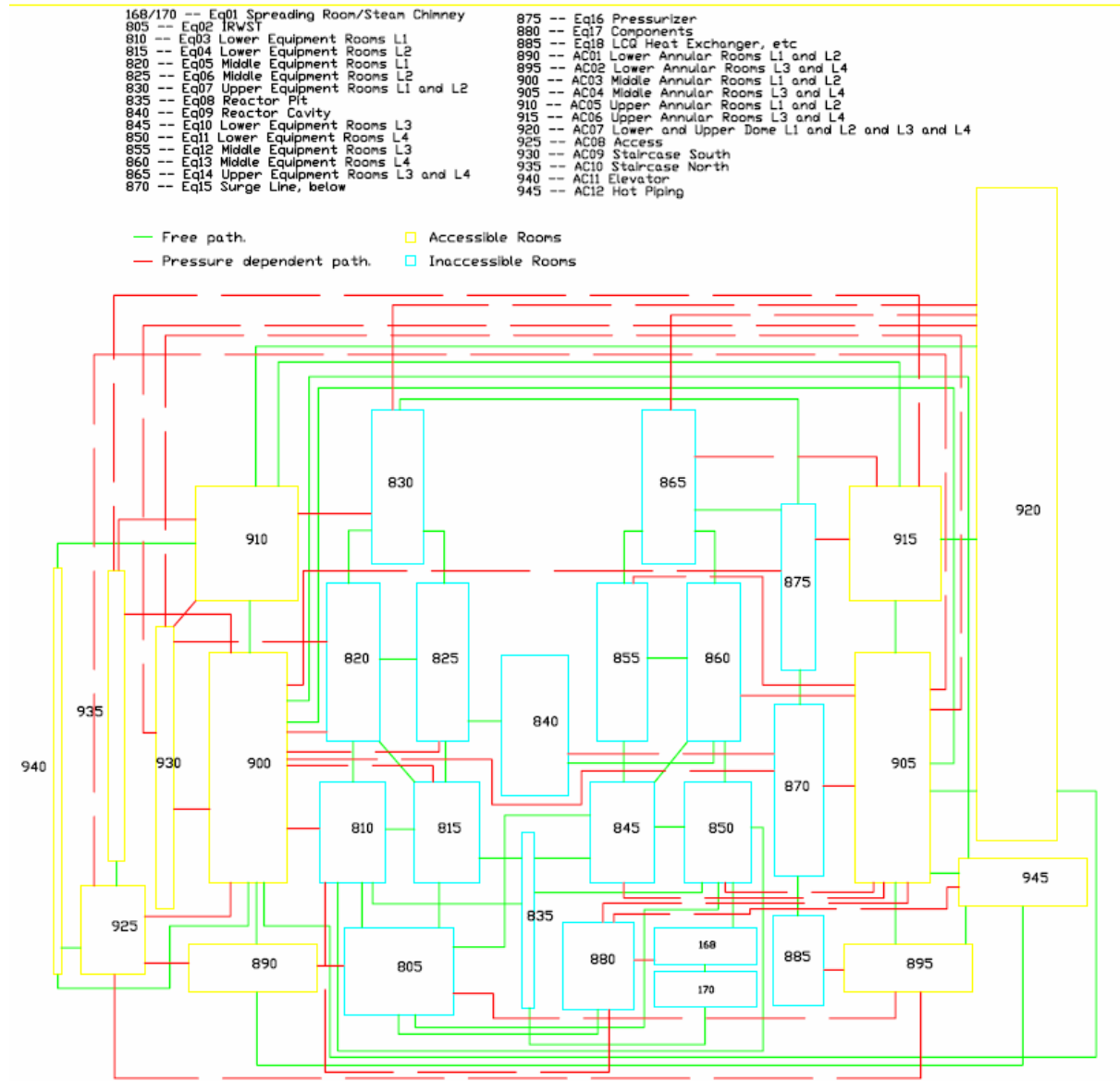


**Figure C-9. Containment Nodalization**

**C.2.3.2 Heat Sources/Sinks**

The containment walls, floors, and other structures were modeled by steel or concrete rectangular heat structures as appropriate. These heat structures, particularly the masses of concrete in the containment and forming the containment walls act as passive heat sinks during accident conditions.

The containment shell is modeled by heat structures with adiabatic outer surfaces. The annulus area between the double containment shells and heat transfer to the

environment are not modeled. Heat is ultimately removed from the containment through the containment spray system and transfer of heat from the IRWST liquid in the SAHRS heat exchangers.

### **C.2.3.3 Combustible Gas Control**

The Burn package was activated to model combustion of hydrogen gas and carbon monoxide if the default conditions were met in a control volume. By default the Burn package examines all control volume in the model to determine if conditions for combustions are met.

The MELCOR Passive Autocatalytic Recombiner package was used to model the 47 passive hydrogen recombiners placed in the containment. The default recombination rate, characteristic heat up time of the recombiners, and minimum hydrogen mole fractions required for startup were modified to reflect the U.S. EPR recombiner design.

## **C.3 References**

- C.1. ANSI/ANS-5.1-1979, "American National Standard for Decay Heat Power in Light Water Reactors," approved August 29, 1979.